NASA Technical Paper 1552

Aerodynamic Characteristics of a Hypersonic Research Airplane Concept Having a 70° Swept Double-Delta Wing at Mach Numbers From 0.80 to 1.20, With Summary of Data From 0.20 to 6.0

Jim A. Penland, James B. Hallissy,
and James L. Dillon

DECEMBER 1979

NASA

NASA Technical Paper 1552

Aerodynamic Characteristics of a Hypersonic Research Airplane Concept Having a 70° Swept Double-Delta Wing at Mach Numbers From 0.80 to 1.20, With Summary of Data From 0.20 to 6.0

Jim A. Penland, James B. Hallissy,
and James L. Dillon
Langley Research Center
Hampton, Virginia

NASA
National Aeronautics
and Space Administration

**Scientific and Technical
Information Branch**

1979

SUMMARY

The data of the present report are divided into three areas. The first area includes the results of a wind-tunnel investigation of the static longitudinal, lateral, and directional stability characteristics of a hypersonic research airplane concept having a 70° swept double-delta wing. The force tests were conducted in the Langley 8-foot transonic pressure tunnel for Mach numbers from 0.80 to 1.20, for a Reynolds number (based on fuselage length) range of 6.30×10^6 to 7.03×10^6, at angles of attack from about -4° to 23°, and at angles of sideslip of 0° and 5°. The configuration variables included the wing planform, tip fins, the center vertical tail, and scramjet engine modules. The second area is a summary of the variations of the more important aerodynamic parameters with Mach number for Mach numbers from 0.20 to 6.0. The third area is a state-of-the-art example of theoretically predicting performance parameters and static longitudinal and directional stability over the Mach number range.

The model with tip fins had more linear lift curves than models with the center vertical tail but showed more tendency to pitch up and had less lateral and directional stability at the higher angles of attack at low and transonic speeds. The forward delta wing decreased the longitudinal stability and maximum lift-drag ratio but enhanced the positive dihedral effect. The highest maximum lift-drag ratio was measured at the lowest subsonic speed, and the lowest lift-drag ratio at Mach number 6. The model scramjet engine had only small positive effects on the lateral and directional stability over the wide Mach number test range. Adequate preliminary predictions of performance and static longitudinal stability may be expected from presently available theories on models having body fineness ratios of about 7, but nonempirical predictions of directional stability are either unsatisfactory or are beyond the state of the art at subsonic and supersonic speeds and are overly optimistic at hypersonic speeds.

INTRODUCTION

Present jet airplanes are cruising at speeds of Mach 2 to 3 (refs. 1 to 3), and it appears that the Mach number limit for aircraft utilizing conventional petroleum-based fuels is about 5 (i.e., turbojets to about 3.5 and ramjets to about 5, ref. 4). Some unique problems associated with Mach numbers of 5 and above include the development of new propulsion systems which use nonpetroleum-derived fuels such as liquid hydrogen (ref. 5). Some of these new propulsion systems include cryogenic-fueled turbojets for low speeds,

ramjets (subsonic combustion) for moderate supersonic speeds, and scramjets (supersonic combustion ramjets) for high supersonic and hypersonic speeds. New structural concepts must be developed which can provide cooled airframes and engine surfaces for protection from high aerodynamic heating as well as insulated tankage for cryogenic fuels such as liquid hydrogen.

One industry study (refs. 6 to 9) concluded that only through the use of both ground facilities and flight vehicles could these major required advancements in technology be made. These findings were in accord with previous NACA-NASA experience with the various research airplane projects from the X-1 to the X-15, each of which resulted in an extensive technology advancement at a minimum expenditure of cost and time (ref. 10). In addition to the unique problems previously outlined, correlation of ground test data (forces, moments, and aerodynamic heating all measured at relatively low Reynolds numbers in mixed laminar-turbulent boundary layers) with flight test data is required for future efficient design. A need thus exists for comprehensive flight research in the range of Mach numbers from 3 to 5 and for detailed exploration to Mach 8.

The present configuration is one of several research airplane concepts under study at the NASA Langley Research Center (refs. 11 to 14) that meets the requirements envisioned as necessary to provide a technology base for future high-speed aircraft. This configuration was the result of a preliminary design study utilizing computerized aerodynamic, structural, and weight and balance programs. The requirements of large-volume fuel tanks for the low-density liquid hydrogen fuel and sufficient depth between the airstream surfaces and the tanks and primary structure for thermal protection insulation resulted in the low-fineness-ratio fuselage of about 7 and the 5- to 6-percent thick wing. Wing planform area was based on landing criteria, and vertical-tail design on hypersonic directional stability requirements. Such a research airplane would be air launched from a B-52 or C-5 and would have a length of 15.24 to 24.38 m (50 to 80 ft), a flight time of up to 800 sec with a nominal 40-sec cruise at a Mach number of about 7 on the scramjet engine, and a return to base for a dead-stick landing. In-flight tests would include powerless glides, rocket-boosted flights, and combined rocket-scramjet boost-cruise experiments.

The data of the present report are divided into three areas. The first area includes the results of a study designed to experimentally investigate the longitudinal, lateral, and directional stability and control of a large-fuselage, 70° swept double-delta wing configuration at transonic speeds. Studies of this same design concept at subsonic, supersonic, and hypersonic speeds (refs. 15 to 21) have also been completed. This study was conducted at Mach numbers of 0.80 to 1.20 and a Reynolds number (based on fuselage length) range of 6.30×10^6 to 7.03×10^6 in the Langley 8-foot transonic pressure tunnel. The angle-of-attack range was from about -4° to 23°, with angles of sideslip of 0° and 5°.

The tests were parametric in nature and included configuration buildup and variations in wing planform, longitudinal control, and roll control. The second area of this paper summarizes the variations of the more important aerodynamic parameters from previous tests (refs. 15 to 21) with Mach number for Mach numbers from 0.20 to 6.0. The third area presents a state-of-the-art example of theoretically predicting performance parameters and static longitudinal and directional stability over the Mach number test range.

SYMBOLS

The longitudinal characteristics are presented about the stability axes, and the lateral-directional characteristics are presented about the body axes. The body and stability axis systems are illustrated in figure 1. The moment reference point was at the design center-of-gravity location which was at a longitudinal station 64.5 percent of the fuselage length and at a vertical station 1.25 percent of the fuselage length below the vehicle reference line. Values are given in both SI and U.S. Customary Units. The measurements and calculations were made in U.S. Customary Units.

A reference area, area of 70° delta wing including fuselage intercept, 0.043 m^2 (67.2 in^2)

b wing span, 0.217 m (8.542 in.)

$C_{A,b}$ base axial-force coefficient, $\frac{\text{Base axial force}}{q_\infty A}$

C_D drag coefficient, $\frac{D}{q_\infty A}$

C_L lift coefficient, $\frac{L}{q_\infty A}$

C_{L_α} rate of change of C_L with angle of attack, per degree

C_l rolling-moment coefficient, $\frac{M_X}{q_\infty Ab}$

C_{l_β} rate of change of C_l with angle of sideslip, per degree

$C_{l_{\delta_H}}$ rolling-moment coefficient due to roll control, per degree

C_m pitching-moment coefficient, $\frac{M_Y}{q_\infty A \ell}$

C_{m_α} rate of change of C_m with angle of attack, per degree

$\partial C_m / \partial C_L$ rate of change of C_m with lift coefficient, longitudinal stability parameter

$\left(\partial C_n / \partial C_Y\right)(b/\ell)$ rate of change of C_n with side-force coefficient, directional stability parameter

C_n yawing-moment coefficient, $\frac{M_Z}{q_\infty A b}$

C_{n_β} rate of change of C_n with angle of sideslip, per degree

$C_{n_{\delta_H}}$ yawing-moment coefficient due to roll control, per degree

C_Y side-force coefficient, $\frac{F_Y}{q_\infty A}$

C_{Y_β} rate of change of C_Y with angle of sideslip, per degree

$C_{Y_{\delta_H}}$ side-force coefficient due to roll control, per degree

c.g. design center of gravity, moment reference

D drag, $F_N \sin \alpha + F_A \cos \alpha$

F_A axial force along X-axis (positive direction is -X)

F_N normal force along Z-axis (positive direction is -Z)

F_Y side force along Y-axis (positive direction is +Y)

L	lift, $F_N \cos \alpha - F_A \sin \alpha$
L/D	lift-drag ratio
ℓ	length of model fuselage, 0.508 m (20.0 in.), reference length
M	Mach number
M_X, M_Y, M_Z	moments about X-, Y-, and Z-axes
q_∞	free-stream dynamic pressure
R	Reynolds number based on fuselage length
X,Y,Z	reference axes
α	angle of attack, degree
β	angle of sideslip, degree
δ_e	elevon deflection angle, positive when trailing edge is down, degree
δ_H	differential elevon deflection, positive to provide positive roll, $\left(\delta_{H,left} - \delta_{H,right}\right)$, degree

Subscripts:

max	maximum
min	minimum
o	condition at zero lift
S	stability axis system
t	trim condition, $C_m = 0$

Model nomenclature:

B	body with high profile nose
E	model scramjet engine
F_D	forward delta wing
V_C	center vertical tail
V_T	tip fins, vertical
W	wing

MODEL

A photograph of a model of the winged hypersonic airplane configuration is shown in figure 2(a). The test model was of modular design, as shown in figure 2(b), to allow the buildup of variations of the basic model from components consisting of the body, a forward delta wing, a 70° swept clipped-delta wing, vertical tip fins, a center vertical tail, and an engine. Geometric details of the model are shown in figure 3 and are given in table I. The model design rationale was primarily based on the stability and control requirements at the design hypersonic cruise Mach number range up to 8. The forward delta wing was included in the design to help decrease the rearward shift of the aerodynamic center with increasing Mach number. The tip fins (fig. 3(b)) were designed with a 7.5° toe-in and were located outboard of the fuselage flow field to enhance the directional stability at hypersonic speeds. A center vertical tail (fig. 3(c)) having a wedge airfoil section and the same total planform area as the sum of the tip fins was tested to assess the difference in directional stability between it and the tip fins. Elevons having a combined area equal to 10.64 percent of the reference area could be deflected from -20° to 5° in 5° increments. A model scramjet engine (fig. 3(d)) was used to complete the configuration buildup. The engine consisted of six clustered modules of the concept described in reference 22, each having outside dimensions, angles, and areas to scale, but with the inside fuel struts and compression surfaces designed to provide an internal contraction ratio of approximately 2 (compared with about 4 for the flight engine). This increased internal area was provided to partly account for the relatively low Reynolds number and the resulting thick boundary layer of this test. Details of these model engine inlet flow fields and boundary layers may be found in references 23 and 24.

APPARATUS AND TESTS

Tunnel

The investigation was conducted in the Langley 8-foot transonic pressure tunnel. The test section of this tunnel is 2.164 m (7.1 ft) square in cross section, with longitudinal slots in the upper and lower walls to permit changing the test section Mach number continuously from 0 to over 1.20, with negligible effects of choking and blockage. The span of the present small model was only 1/11 the tunnel diameter, and no wall corrections were required. The sting diameter was 0.0254 m (1.00 in.).

Test Conditions

Tests were made at Mach numbers from 0.80 to 1.20, at a stagnation pressure of 1 atm (1 atm = 101.3 kPa), and at a stagnation temperature of 322 K. The Reynolds number and dynamic pressures of the investigation are presented in the following table:

M	R	q_∞	
		N/cm^2	psia
0.80	6.30×10^6	2.99	4.33
.90	6.63	7.16	4.94
.95	6.77	3.59	5.21
.98	6.83	3.69	5.35
1.10	7.00	4.02	5.83
1.20	7.03	4.22	6.12

The tunnel air was dried sufficiently to avoid condensation effects. The angle-of-attack range was from about -4° to 23° for angles of sideslip of 0° and 5°. In order to insure a turbulent boundary layer, 0.159-cm (0.063-in.) wide strips of No. 150 carborundum grains were applied 1.0 cm (0.394 in.) streamwise aft of the leading edges of the wings and the tail surfaces; a 0.159-cm (0.063-in.) wide strip of No. 150 carborundum grains was applied at the nose at a station 3.0 cm (1.181 in.) streamwise from the apex (refs. 25 and 26).

Measurements and Corrections

The aerodynamic forces and moments were measured by means of a six-component strain-gage balance which was housed within the model fuselage. Balance-chamber pressure was measured with pressure tubes located in the vicinity of the balance.

Angles of attack and sideslip have been corrected for the deflection of the balance and sting due to aerodynamic loads. The angle of attack was corrected for tunnel flow angularity. The drag coefficients were corrected to the condition of free-stream static pressure in the balance chamber. The base perimeter of the model was internally feathered to equalize the pressure over the base. Typical variations of base axial-force coefficient measured during the tests are presented in figure 4 for the BWV_TF_DE and BWV_TF_D models at the various Mach numbers tested. No correction was made to the drag data for flow through the model scramjet engine.

PRESENTATION OF RESULTS

The results of the wind-tunnel investigation in the Langley 8-foot transonic pressure tunnel are presented in the following figures:

A summary of the variation of the more important aerodynamic parameters with Mach numbers is presented in the following figures for M = 0.20 to 6.0:

A comparison of theoretical estimates and various experimental longitudinal and directional parameters on the WBV_T configuration at $M = 0.20$ to 6.0 is presented in the following figures:

RESULTS AND DISCUSSION

All the basic data presented in this paper were machine plotted from the computational tape, and the data points were machine faired using the cubic spline method. Because of the preliminary nature of this study, individual curves such as L/D plotted against C_L were not given detailed cross-checks against polar plots of C_L plotted against C_D.

Static Longitudinal Aerodynamics

Component buildup of model with tip fins.- Variations of the longitudinal characteristics with component buildup are presented in figure 5 for the six transonic Mach numbers tested. A comparative study of these data shows a trend of increasing C_{m_o} from a negative value at $M = 0.80$ to a positive value at $M = 0.95$ and above for all variations of the configurations tested, from the basic body-wing to the complete model with engine. This positive increase in C_{m_o} was accompanied by a positive shift in the angle for zero lift. All configurations exhibited a small increase in longitudinal stability with increasing subsonic Mach number.

As expected, the drag increases with subsonic Mach number, reaches a maximum for the present data at $M = 0.98$, and then decreases with supersonic Mach number. The lift-drag ratio is highest at the lowest test Mach number of 0.80 and inversely follows the trends of the drag due in part to the nearly constant lift-curve slope. Whereas the addition of the forward delta wing F_D to the nonfinned configurations made relatively small changes to the lift and drag, the addition of the tip fins made significant increases in both lift and drag; thus, about a 20-percent loss in lift-drag ratio resulted. The gain in lift may be attributed to an alteration of the wing-tip flow field by the tip fins acting as end plates and thereby reducing the tip losses. The increase in drag was due to skin friction and to the drag due to the 7.5° toe-in of the tip fins.

Component buildup on model with center vertical tail.- The use of a center vertical tail (fig. 6) in lieu of twin tip fins produces some trends similar to those produced with the tip fins (i.e., the C_{m_0} moves from negative to positive, α_0 increases positively, and the configurations become slightly more stable with increasing Mach number). One noticeable difference was a slight loss of lift with the addition of the center tail to the body-wing configuration, whereas there was a gain in lift with the addition of the tip fins, as previously discussed. The increase in drag with the addition of the center tail was considerably less than with the addition of the tip fins. This small increase in drag and slight loss in lift combined to produce a decrease of approximately one-half unit in maximum lift-drag ratio, as compared with a loss of about one unit for the addition of the tip fins.

Comparison of tip fins and center vertical tail.- A comparison of models equipped with tip fins and a center vertical tail is presented in figure 7 both with and without the forward delta wing. At all test Mach numbers, the models with tip fins exhibit higher lift coefficients and more linear lift curves with angle of attack than the models with the center vertical tail. The addition of the forward delta wing to either fin configuration made only small positive increases to lift as a function of angle of attack. The pitching-moment curves plotted as a function of lift coefficient for the center-tail models were slightly more linear and showed less tendency to become neutrally stable or to pitch up at the higher angles of attack. The addition of the forward delta wing increased the drag through the range of medium lift coefficients at all test Mach numbers and contributed to the consistent trend of lower maximum lift-drag ratios for those models equipped with the forward delta wing. The drag of the tip-fin models was substantially higher than the drag of the center-tail models, thus overcoming the higher lift and resulting in consistently lower maximum lift-drag ratios for the tip-fin models at all Mach numbers.

Trim Characteristics

The effect of elevon deflection on the longitudinal aerodynamic characteristics of the complete tip-fin configuration $\left(BWV_TF_DE\right)$ with scramjet engine is presented in figure 8 for all test Mach numbers and in figure 9 for the center-vertical-tail model $\left(BWV_CF_D\right)$ without engine. Data were obtained at elevon deflections of 0^o, -10^o, and -20^o for both configurations.

The longitudinal characteristics at trim are presented in figure 10 for both test configurations. The trends of the performance parameters at trim are similar for the two configurations through the transonic Mach number test range from $M = 0.80$ to 1.20, with some exceptions, one of which is the 0.5 to 1.5 loss in maximum lift-drag ratio due to the combined scramjet engine drag and trim drag required to trim the incurred incremental pitching moments. The trim angle-of-attack range is also up to 3^o greater at Mach numbers of 0.98 and higher for the complete configuration than for the center-vertical-tail model without engine. The lift-curve slopes were similar in trend and magnitude for the two tests, whereas the angle of attack for zero lift was consistently lower by about 0.5^o to 1^o for the complete tip-fin model with engine.

Both configurations were statically longitudinally stable throughout the test angle-of-attack range at the design center of gravity, with the static margin varying from about 2 percent at $M = 0.80$ to as much as 8 percent at $M = 1.20$. This high degree of stability contributed to the lower trim angle-of-attack range at the higher transonic test Mach numbers for the center-vertical-tail model without engine.

Static Lateral-Directional Stability

The variations of the static lateral-directional stability with component buildup of the tip-fin configurations are presented in figure 11. The models tested without tip fins were unstable directionally $\left(-C_{n_\beta}\right)$ but exhibited positive dihedral effect $\left(-C_{l_\beta}\right)$ at angles of attack above about 3^o for all Mach numbers tested. The installation of the tip fins provided some improvement of the dihedral effect at low angles of attack and altered the directional stability in a nonsystematic manner with both angle of attack and Mach number. The directional stability was enhanced to positive values at low and high angles of attack for all Mach numbers but was variously altered with Mach number in the range of $\alpha = 8^o$ to 12^o, from only slightly at $M = 0.80$ to neutral stability at $M = 1.20$. A decrease in directional stability at $\alpha = 8^o$ to 12^o was observed at $M = 0.20$ (ref. 19) on this same configuration, but instability did not occur. The exact cause of this region of tip-fin ineffectiveness is not known, but it is probably a function of the vorticular flow emanating from the fuselage nose section and the wing leading edge. Before these tip fins can be used with confidence, this region of reduced effectiveness must be explored and the

design altered to eliminate the deficiency. The addition of the model scramjet engine to the BWV_TF_D model improved both the directional stability and positive dihedral effect.

The variations of the static lateral-directional stability with component buildup of the center-tail configurations are presented in figure 12. The installation of the center tail greatly improved both the positive dihedral effect and the directional stability at all angles of attack and at all test Mach numbers. The positive dihedral effect increased with angle of attack for all Mach numbers. The directional stability remained positive for all Mach numbers but decreased with increasing angle of attack for the higher Mach numbers.

A comparison of the lateral-directional stability characteristics of the tip-fin and center-tail configurations is presented in figure 13. The center tail not only provides a greater level of positive dihedral effect but a higher degree of directional stability than the tip fins at all angles of attack and at all test Mach numbers. The addition of the forward delta wing enhanced both stability derivatives.

Roll Control

The results of tests to determine the roll-control characteristics with 5° of differential aileron deflection are presented in figure 14 for the complete tip-fin configuration with engine. The data indicate that the configuration had positive roll control at all test conditions. However, some adverse yaw or cross coupling of yaw due to roll control occurred at the higher angles of attack for $M = 0.80$ and 0.90 at all angles of attack for $M = 0.95$ to 1.20.

SUMMARY OF DATA WITH MACH NUMBER FROM 0.20 TO 6.0

The present paper is the last of a series of reports that give details of wind-tunnel tests made on the 70° swept double-delta wing research airplane concept over the Mach number range of 0.20 to 6.0. These reports include subsonic studies (refs. 15 and 19), transonic studies (present report), supersonic studies (ref. 16), hypersonic studies (ref. 17), and hypersonic heat-transfer studies (refs. 20 and 21). A summary of the more important aerodynamic parameters as they vary with Mach number will be presented in this section. Summaries of data variation with Mach number for other research airplane configurations may be found in reference 18.

Tests

Reynolds number.- The variation of test Reynolds number with the test Mach number as used in the various wind tunnels is presented in figure 15. The widest range of test Reynolds numbers (based on fuselage length), 2.2×10^6 to 19.7×10^6, was made in

the Langley low-turbulence pressure tunnel at $M = 2.0$ with free transition. The majority of tests at $M = 0.20$ were made at a constant Reynolds number of 10×10^6 with fixed transition (ref. 19). Transonic tests were made with fixed transition at a constant stagnation pressure in the Langley 8-foot transonic pressure tunnel, thus accounting for variations in Reynolds number with increasing Mach number, as discussed in the section entitled "Test Conditions." Supersonic tests were made with fixed transition at $M = 1.50$ to 2.86 in the Langley Unitary Plan wind tunnel at a constant Reynolds number of 3.3×10^6 (ref. 16). Hypersonic tests were made at $M = 6$ with free transition in the Langley 20-inch Mach 6 tunnel at a constant Reynolds number of 10.5×10^6 (ref. 17). The summary of data presented herein is plotted as received from the tunnels, with no corrections made for variations in Reynolds number or for grit drag for the fixed transition tests.

Angles of attack for lift coefficient of 0 and 0.2.- The variation of angle of attack with Mach number at lift coefficients of 0 and 0.2 is presented in figure 15. These data are shown for two typical configurations to give a better understanding of subsequent figures of longitudinal and lateral-directional stability presented at $C_L = 0$ and 0.2. The value of $C_L = 0.2$ was selected because it was the highest value of lift coefficient available for all the Mach numbers utilized in the test program. It should be noted that the angles of attack for $C_L = 0$ varied by about $\pm 2^\circ$ from $M = 0.20$ to 6.0 and that angle of attack for $C_L = 0.2$ varied from about 8° for the body-wing (BW) model to 8.5° for the complete $\left(BWV_TF_DE\right)$ model. This relatively wide spread in angle of attack to obtain $C_L = 0.2$ is an illustration of the decrease in lifting efficiency that occurs with increasing Mach number.

Buildup of Tip-Fin Models

Minimum drag.- The minimum drag coefficients of the various configurations used in the buildup of the tip-fin model are presented in figure 16 for the various test Mach numbers. It should be noted that all of the faired data have been corrected for base pressure and that only the flagged symbols at $M = 0.20$ are uncorrected. The minimum drag coefficients at the low Mach number of 0.20 increased to a maximum at $M \approx 1$ and are about the same as those at $M = 6$. The addition of the forward delta wing made only minor drag variations, but the tip fins increased the minimum drag as much as 78 percent at low speeds. The values of minimum drag coefficient shown without base pressure correction are higher by as much as 83 percent and, when corrected for Reynolds number, are considered as good engineering estimates of full-scale flight values at low subsonic Mach numbers. This large base-drag contribution illustrates the purpose of reducing base area to a minimum, particularly on aircraft that operate subsonically.

Maximum lift-drag ratio.- The maximum lift-drag ratio for the various tip-fin buildup models is presented in figure 16 over the Mach number test range. The maximum lift-drag ratio decreases rapidly with higher subsonic and transonic speeds but, once supersonic, appears to level out and remain above 3 up to $M = 6$. Each addition to the basic (BW) configuration decreased the lift-drag ratio substantially at subsonic speed, but the forward delta wing has considerably less effect than the tip fins at supersonic and hypersonic speeds.

Pitching moment at zero lift.- The variation of pitching-moment coefficient with Mach number at zero lift is presented in figure 17 for the tip-fin model buildup. The C_{m_o} of all configurations increase up to $M \approx 1$ and exhibit the undesirable characteristics of negative C_{m_o} at low speeds, with the tip-fin models having the most negative values. The tip fins tend to act as end plates and increase the local lift coefficients near the wing trailing edge, thus contributing to the negative pitching moments. The C_{m_o} values for all models at all speeds above about $M = 0.95$ exhibit positive C_{m_o} as desired. The C_{m_o} is adversely affected by the addition of the tip fins at low speeds but is favorably affected at all supersonic speeds. The addition of the forward delta wing produces a desirable positive increment in C_{m_o} at all test speeds.

Lift-curve slope.- The variation of the lift-curve slope with Mach number for the tip-fin model buildup is presented in figure 17. There was a general decrease in C_{L_α} with Mach number for all configurations. The addition of the tip fins had a marked positive effect on the C_{L_α} at low speeds but little effect at supersonic and hypersonic speed. The addition of the forward delta wing in conjunction with the tip fins produced the highest subsonic lift-curve slope.

Longitudinal stability.- The variation of longitudinal stability with Mach number of the buildup of the tip-fin models is presented in figure 18 for lift coefficients of 0 and 0.2. A general trend for all configurations is a sharp increase in stability from low subsonic speeds to $M \approx 1$ and a more gradual decrease in stability with increasing Mach number. The stability may be expected to become neutral or negative at a sufficiently high Mach number for any given fixed configuration. The addition of the tip fins increased the longitudinal stability at all Mach numbers and lift coefficients. As expected, the addition of the forward delta wing deteriorated the longitudinal stability at all Mach numbers for all configurations tested.

Lateral-directional stability.- The variation of lateral-directional stability with Mach number of the tip-fin buildup configurations is presented in figure 19. The configurations without tip fins were directionally unstable at all Mach numbers at both lift coefficients and exhibited negative dihedral effect at $C_L = 0$ through a range of Mach numbers from 0 to 1.20 and from 2.86 to 6.0. The addition of tip fins provided positive directional

stability for both configurations at Mach numbers up to at least 2.36 at $C_L = 0$ and 0.2, and it also provided positive dihedral effect below $M = 2.86$ at $C_L = 0$. The lateral-directional stability was unaffected by the addition of the forward delta wing.

Effect of Addition of Model Scramjet Engine

Minimum drag.- The variation of the minimum drag with Mach number due to the addition of the model scramjet engine is presented in figure 20. At low speeds, the minimum drag was increased more than 100 percent, excluding base pressure, and increased about 64 percent when the base pressure is included. The increment of minimum drag coefficient was relatively constant for speeds up to about $M = 1$ (as discussed in ref. 18 for other research airplane configurations), but gradually decreases thereafter as Mach number increases.

Maximum lift-drag ratio.- The losses in maximum lift-drag ratio due to the installation of the scramjet engine are presented in figure 20. The largest loss occurred at low subsonic speeds and where decreases in L/D could be least tolerated (ref. 18). The incremental reduction in $(L/D)_{max}$ with Mach number due to engine addition decreases to only about 0.3 at cruising speed. It may be seen that base pressure further contributes to the low subsonic $(L/D)_{max}$ ratios.

Pitching moment at zero lift.- The effect of the addition of the model scramjet engine on the pitching moment at zero lift is presented in figure 21. There is a beneficial effect up to $M = 2.36$ and only a small undesirable decrease in positive C_{m_o} at Mach numbers up to 6.0.

Lift-curve slope.- The variation of the slope of the lift curve at zero lift with the installation of the model scramjet engine is presented in figure 21. A loss in C_{L_α} was experienced at subsonic speeds, but a gain was measured at the design cruise Mach number of 6.0.

Longitudinal stability.- The effects of the addition of the model scramjet engine on the longitudinal stability variation with Mach number are presented in figure 22 at lift coefficients of 0 and 0.2. No variations may be seen that exceed 0.01 except at transonic speeds, and there the decrease in stability was desirable.

Lateral-directional stability.- The results of tests to determine the variations in lateral-directional stability with the installation of the model scramjet engine are presented in figure 23. The addition of the model engine was either favorable or nondetrimental on the lateral-directional stability at $C_L = 0$ and 0.2 except at $M = 6.0$ for $C_L = 0$.

Buildup of Center-Vertical-Tail Models

Minimum drag.- The variation of the minimum drag with model buildup of the center-vertical-tail configurations is shown in figure 24. The positive increment in drag due to the center-vertical-tail addition was nearly constant with Mach number, with the base pressure corrected to free-stream static pressure. It should be noted that the base area of the center vertical tail was not included in this correction. The addition of the forward delta wing had only a very small effect on the minimum drag coefficients.

Maximum lift-drag ratio.- The largest loss of maximum L/D was at low subsonic speeds with the addition of the center vertical tail (fig. 24). The wedge airfoil section contributed to the large losses in $(L/D)_{max}$ and would not normally be used at subsonic or low supersonic speeds. The addition of the forward delta wing made a favorable contribution to $(L/D)_{max}$ only at $M > 3$.

Pitching moment at zero lift.- Both the center vertical tail and the forward delta wing contributed to the positive increases of C_{m_o} (fig. 25). The low-speed C_{m_o} remained negative for the complete configuration and may compromise the pitch control and increase the trim drag.

Lift-curve slope.- The variation of the lift-curve slope with Mach number at zero lift for the buildup of the center-vertical-tail model is shown in figure 25. The addition of the center vertical tail and the forward delta wing made only small nonsystematic changes in the variation of lift-curve slope with Mach number.

Longitudinal stability.- The variation of longitudinal stability with Mach number for the configuration buildup on the center-vertical-tail configuration is presented in figure 26. With the exception of the increase in stability at $M = 0.20$ for $C_L = 0$, the addition of the center vertical tail either made little change in the longitudinal stability or decreased it, as expected. The installation of the forward delta wing decreased the stability as expected at both lift coefficients throughout the Mach number test range.

Lateral-directional stability.- The addition of the center vertical tail had a major positive effect on both the directional stability and the dihedral effect (fig. 27). The directional stability parameter C_{n_β} was increased from unstable negative values to stable positive values at all Mach numbers and lift coefficients except for $M = 6$ at $C_L = 0.2$. The positive dihedral effect $\left(-C_{l_\beta}\right)$ was increased at all conditions. The installation of the forward delta wing improved the directional stability at the higher speeds for the higher lift coefficient, thereby showing more effect in conjunction with the center vertical tail V_C than with the tip fins V_T.

Theoretical Estimates of Configuration Aerodynamics

Estimates are presented of currently available computerized theories of performance and static stability parameters on the wing—body—tip-fin $\left(WBV_T\right)$ configuration through the Mach number test range from $M = 0.20$ to 6.0. Estimates were calculated at $M = 0.20$ by the vortex-lattice method described in references 27 and 28, with the base-pressure drag coefficient being made by methods outlined by Hoerner in reference 29. Estimates at $M = 1.20$ to 3.0 were made by the linear-theory methods presented in references 30 and 31, and at $M = 3.0$ to 6.0 by the Gentry Hypersonic Arbitrary Body Program (GHABP) of reference 32. Skin friction was calculated by the Spalding and Chi method of reference 33 with the test Reynolds numbers of figure 15, and boundary layers were assumed all turbulent. Other examples of the application of these theories on similar configurations may be seen in references 12, 18, and 34 to 38.

Estimates of the minimum drag coefficient and the maximum lift-drag ratio on the WBV_T model are presented in figure 28 for the test Mach number range. The semi-empirical values of the calculated minimum drag coefficient presented at $M = 0.20$ underestimate the experiment data by a greater percentage than those calculated for supersonic and hypersonic speeds by high-speed computer programs. The estimated drag coefficients at $M = 0.20$ combined the turbulent flat-plate skin-friction coefficients modified by empirical form factors for body fineness ratios and wing thickness ratios with the base pressure coefficients determined from the empirical correlations with the body skin friction of reference 29. Possible sources of error were that no component interference effects were included and that no estimate of possible separated flows was made over the lower model afterbody.

The viscid estimates of minimum drag coefficient are satisfactory for Mach numbers of 2.0 and above, but those at transonic speed are low by about 20 percent. The discontinuity in the viscid curve for $M = 1$ to 1.20 is due to the sharp increase in test Reynolds number (fig. 15).

A comparison of estimates of the maximum lift-drag ratio on the WBV_T model with experimental data in figure 28 shows adequate predictions except at high subsonic Mach numbers. The estimates at Mach numbers up to 3.0 were made by using linear theory with the predicted values of minimum drag coefficient and lift-curve slope. For Mach numbers from 3.0 to 6.0, the GHABP was used.

A comparison of measured lift coefficients and lift-curve slopes with calculated estimates is presented in figure 29 for $\alpha = 0^{\circ}$. The theoretical model for the low-speed vortex-lattice calculations and the supersonic linear-theory calculations was an uncambered flat surface; thus, a C_L value of zero resulted at $\alpha = 0^{\circ}$. The slope of the lift curve, however, was well predicted with this simplified theoretical model. The GHABP,

utilizing a three-dimensional input model, predicted the lift coefficient poorly for $\alpha = 0^{\circ}$ at $M = 3$, but predicted well at $M = 6$. The lift-curve slope was well predicted by the GHABP.

The calculated static longitudinal and directional stability parameters at zero lift are compared in figure 30 with experimental data for the WBV_T configuration. The predictions of the longitudinal stability by the vortex-lattice method and the GHABP are good at low subsonic and hypersonic speeds, respectively, but are less than desirable by linear theory at supersonic speeds. The linear theory conservatively predicted the approximate level of positive longitudinal stability but showed a fortuitous trend with Mach number. This trend is partly due to the effects of the tip fins and the low body fineness ratio, neither of which was accounted for by the linear theory.

A comparison of the static directional stability with the GHABP is presented in figure 30. For this plot, the directional stability parameter $\partial C_n / \partial C_Y$ was referenced to body length by the factor b/ℓ to make it parallel to the previous discussion of longitudinal data. No present vortex-lattice or linear-theory method addresses the prediction of directional stability; thus, only the prediction from the GHABP is shown. It may be seen that the hypersonic theory overestimates the experimental data by a substantial amount, due in part to the inability of the program to take into account local variations in dynamic pressure and flow direction.

It should be noted that none of the prediction methods discussed herein give completely satisfactory estimates of the aerodynamic characteristics of configurations with the model scramjet engine installed. These inadequacies are due in part to the inability of the programs to handle internal flows with the converging walls, the external spillage of flow not swallowed by the inlet, and the resulting interference effects.

It may be concluded that good preliminary predictions of performance and static longitudinal stability can be expected across the speed range with the vortex-lattice, linear, and hypersonic theories on configurations with body fineness ratios of about 7. Predictions of directional stability are beyond the scope of these methods at subsonic and supersonic speeds and are grossly optimistic at hypersonic speeds.

CONCLUSIONS

An analysis of the experimental data for a hypersonic research airplane concept having a 70° double-delta wing at Mach numbers from 0.20 to 6.0 for a range of Reynolds numbers (based on fuselage length) from about 3.3×10^6 to 10.5×10^6 leads to the following conclusions:

1. Models equipped with tip fins had more linear lift curves than models with the center vertical tail.

2. Models equipped with the center vertical tail showed less tendency to pitchup and had a higher degree of directional stability and positive dihedral effect at higher angles of attack than models with tip fins.

3. At transonic speeds, a region of directional instability that was not present for the center-tail models was observed at angles of attack from 8° to 12° for the models equipped with tip fins.

4. The addition of the forward delta wing made only small changes in lift and drag but decreased maximum lift-drag ratio.

5. The forward delta wing decreased longitudinal stability as expected but enhanced the positive dihedral effect.

6. A positive increase in minimum drag coefficient, zero-lift pitching-moment coefficient, and zero-lift longitudinal stability was observed for all configurations with Mach number up to about 1.

7. The tip fins made signficant increases in lift and drag to Mach 1.20 but resulted in a net loss in maximum lift-drag ratio at all speeds, due in part to the large fixed toe-in angle.

8. Excluding base drag, the highest maximum lift-drag ratio for any one configuration occurred at the minimum subsonic test Mach number of 0.20 and the lowest lift-drag ratio at the hypersonic Mach number of 6.0.

9. The installation of the model scramjet engine either had little effect or increased directional stability and positive dihedral effect through the Mach number test range.

10. Good preliminary predictions of performance and static longitudinal stability can be expected across the speed range by use of the vortex-lattice, linear, and hypersonic theories on configurations with body fineness ratios of about 7.

11. Predictions of directional stability are beyond the scope of these methods at subsonic and supersonic speeds and are grossly optimistic at hypersonic speed.

Langley Research Center
National Aeronautics and Space Administration
Hampton, VA 23665
September 20, 1979

REFERENCES

1. Wetmore, Warren C.: Concorde Impressive in Flights. Aviat. Week & Space Technol., vol. 100, no. 25, June 24, 1974, pp. 25-28.

2. SR-71 Sets Record. Aviat. Week & Space Technol., vol. 101, no. 10, Sept. 9, 1974, p. 17.

3. SR-71 Sets Mark in New Speed Category: London-Los Angeles. Aviat. Week & Space Technol., vol. 101, no. 12, Sept. 23, 1974, p. 28.

4. Kirkham, Frank S.; Jackson, L. Robert; and Weidner, John P.: The Case for a High-Speed Research Airplane – Results From an In-House Study. AIAA Paper No. 74-988, Aug. 1974.

5. Small, W. J.; Fetterman, D. E.; and Bonner, T. F., Jr.: Potential of Hydrogen Fuel for Future Air Transportation Systems. [Preprint] 73-ICT-104, American Soc. Mech. Eng., Sept. 1973.

6. Hypersonic Research Facilities Study. Volume II, Part 1, Phase I: Preliminary Studies – Research Requirements and Ground Facility Synthesis. NASA CR-114323, 1970.

7. Hypersonic Research Facilities Study. Volume II, Part 2, Phase I: Preliminary Studies – Flight Vehicle Synthesis. NASA CR-114324, 1970.

8. Hypersonic Research Facilities Study. Volume III, Part 2, Phase II: Parametric Studies – Flight Vehicle Synthesis. NASA CR-114326, 1970.

9. Hypersonic Research Facilities Study. Volume IV, Part 1, Phase III: Final Studies – Flight Research Facilities. NASA CR-114327, 1970.

10. Becker, John V.: The X-15 Program in Retrospect. Raumfahrtforschung, Bd. XIII, Heft 2, Mar./Apr. 1969, pp. 45-53.

11. Clark, Louis E.: Hypersonic Aerodynamic Characteristics of an All-Body Research Aircraft Configuration. NASA TN D-7358, 1973.

12. Penland, Jim A.; Creel, Theodore R., Jr.; and Howard, Floyd G.: Experimental Low-Speed and Calculated High-Speed Aerodynamic Characteristics of a Hypersonic Research Airplane Concept Having a 65° Swept Delta Wing. NASA TN D-7633, 1974.

13. Penland, Jim A.; and Creel, Theodore, R., Jr.: Low-Speed Aerodynamic Characteristics of a Lifting-Body Hypersonic Research Aircraft Configuration. NASA TN D-7851, 1975.

14. Lawing, Pierce L.; and Hunt, James L.: Aerodynamic Heat Transfer to a Hypersonic Research Aircraft Model (X-24C) at Mach 6. J. Aircr., vol. 13, no. 12, Dec. 1976, pp. 1018-1020.

15. Creel, Theodore R., Jr.; and Penland, Jim A.: Low-Speed Aerodynamic Characteristics of a Hypersonic Research Airplane Concept Having a 70° Swept Delta Wing. NASA TM X-71974, 1974.

16. Penland, Jim A.; Fournier, Roger H.; and Marcum, Don C., Jr.: Aerodynamic Characteristics of a Hypersonic Research Airplane Concept Having a 70° Swept Double-Delta Wing at Mach Numbers From 1.50 to 2.86. NASA TN D-8065, 1975.

17. Clark, Louis E.; and Richie, Christine B.: Aerodynamic Characteristics at Mach 6 of a Hypersonic Research Airplane Concept Having a 70° Swept Delta Wing. NASA TM X-3475, 1977.

18. Penland, Jim A.; Dillon, James L.; and Pittman, Jimmy L.: An Aerodynamic Analysis of Several Hypersonic Research Airplane Concepts From $M = 0.2$ to 6.0. J. Aircr., vol. 15, no. 11, Nov. 1978, pp. 716-723.

19. Penland, Jim A.; Creel, Theodore R., Jr.; and Dillon, James L.: Aerodynamic Characteristics of a Hypersonic Research Airplane Concept Having a 70° Swept Double-Delta Wing at Mach Number 0.2. NASA TP-1252, 1978.

20. Johnson, Charles B.; Taylor, Allan H.; and Weinstein, Irving: Heat-Transfer and Pressure Measurements on a Simulated Elevon Deflected 30° Near Flight Conditions at Mach 7. NASA TM X-3563, 1977.

21. Lawing, Pierce L.: Configuration Heating for a Hypersonic Research Airplane Concept Having a 70° Swept Double-Delta Wing. NASA TP-1143, 1978.

22. Henry, John R.; and Anderson, Griffin Y.: Design Considerations for the Airframe-Integrated Scramjet. NASA TM X-2895, 1973.

23. Lawing, Pierce L.; and Johnson, Charles B.: Inlet Boundary-Layer Shapes on Four Aircraft Forebodies at Mach 6. J. Aircr., vol. 15, no. 1, Jan. 1978, pp. 62-63.

24. Johnson, Charles B.; and Lawing, Pierce L.: Mach 6 Flowfield Survey at the Engine Inlet of a Research Airplane. J. Aircr., vol. 14, no. 4, Apr. 1977, pp. 412-414.

25. Braslow, Albert L.; and Knox, Eugene C.: Simplified Method for Determination of Critical Height of Distributed Roughness Particles for Boundary-Layer Transition at Mach Numbers From 0 to 5. NACA TN 4363, 1958.

26. Blackwell, James A., Jr.: Preliminary Study of Effects of Reynolds Number and Boundary-Layer Transition Location on Shock-Induced Separation. NASA TN D-5003, 1969.

27. Lamar, John E.; and Gloss, Blair B.: Subsonic Aerodynamic Characteristics of Interacting Lifting Surfaces With Separated Flow Around Sharp Edges Predicted by a Vortex-Lattice Method. NASA TN D-7921, 1975.

28. Polhamus, Edward C.: A Concept of the Vortex Lift of Sharp-Edge Delta Wings Based on a Leading-Edge-Suction Analogy. NASA TN D-3767, 1966.

29. Hoerner, Sighard F.: Fluid-Dynamic Drag. Publ. by the author (148 Busteed Drive, Midland Park, New Jersey 07432), 1965.

30. Middleton, Wilbur D.; and Carlson, Harry W.: Numerical Method of Estimating and Optimizing Supersonic Aerodynamic Characteristics of Arbitrary Planform Wings. J. Aircr., vol. 2, no. 4, July-Aug. 1965.

31. Harris, Roy V., Jr.: An Analysis and Correlation of Aircraft Wave Drag. NASA TM X-947, 1964.

32. Gentry, Arvel E.: Hypersonic Arbitrary-Body Aerodynamic Computer Program (Mark III Version). Vol. I – User's Manual. Rep. DAC 61552, Vol. I (Air Force Contract Nos. F33615 67 C 1008 and F33615 67 C 1602), McDonnell Douglas Corp., Apr. 1968. (Available from DDC as AD 851 811.)

33. Spalding, D. B.; and Chi, S. W.: The Drag of a Compressible Turbulent Boundary Layer on a Smooth Flat Plate With and Without Heat Transfer. J. Fluid Mech., vol. 18, pt. 1, Jan. 1964, pp. 117-143.

34. Pittman, Jimmy L.; and Dillon, James L.: Vortex Lattice Prediction of Subsonic Aerodynamics of Hypersonic Vehicle Concepts. J. Aircr., vol. 14, no. 10, Oct. 1977, pp. 1017-1018.

35. Pittman, Jimmy L. (appendix by C. L. W. Edwards): Application of Supersonic Linear Theory and Hypersonic Impact Methods to Three Nonslender Hypersonic Airplane Concepts at Mach Numbers From 1.10 to 2.86. NASA TP-1539, 1979.

36. Dillon, James L.; and Pittman, Jimmy L.: Aerodynamic Characteristics at Mach Numbers From 0.33 to 1.20 of a Wing-Body Design Concept for a Hypersonic Research Airplane. NASA TP-1044, 1977.

37. Dillon, James L.; and Creel, Theodore R., Jr.: Aerodynamic Characteristics at Mach Number 0.2 of a Wing-Body Concept for a Hypersonic Research Airplane. NASA TP-1189, 1978.

38. Dillon, James L.; and Pittman, Jimmy L.: Aerodynamic Characteristics at Mach 6 of a Wing-Body Concept for a Hypersonic Research Airplane. NASA TP-1249, 1978.

TABLE I.- GEOMETRIC CHARACTERISTICS OF MODEL

Wing:	
Reference area (includes area projected to fuselage center line), m^2 (in^2)	0.043 (67.200)
Exposed area, m^2 (in^2)	0.023 (36.121)
Wetted area, m^2 (in^2)	0.047 (72.242)
Span, m (in.)	0.217 (8.542)
Aspect ratio	1.086
Root chord (on fuselage center line), m (in.)	0.353 (13.896)
Tip chord, m (in.)	0.085 (3.355)
Taper ratio	0.241
Mean aerodynamic chord, m (in.)	0.248 (9.779)
Sweepback angles, deg:	
Leading edge	70
25-percent chord line	64
Trailing edge	0
Dihedral angle (airfoil mean line), deg	-3.64
Incidence angle, deg	0
Airfoil section (see fig. 3(a)):	
Thickness ratio –	
Exposed root	0.05
Tip	0.06
Leading-edge radius, m (in.):	
Fuselage center-line chord	0.000508 (0.020)
Tip	0.000508 (0.020)
Elevon area (both), m^2 (in^2)	0.005 (7.161)
Forward delta wing:	
Area exposed (outside of fuselage, forward of wing leading edge), m^2 (in^2)	0.002 (3.394)
Leading-edge sweep, deg	80
Wetted area (both), m^2 (in^2)	0.0044 (6.788)
Tip fin (vertical tails):	
Area (each), m^2 (in^2)	0.0038 (5.848)
Span, m (in.)	0.069 (2.730)
Aspect ratio	1.274
Root chord, m (in.)	0.086 (3.354)
Tip chord, m (in.)	0.029 (1.135)
Taper ratio	0.336
Mean aerodynamic chord, m (in.)	0.062 (2.445)
Sweepback angles, deg:	
Leading edge, top	55.0
Leading edge, bottom	70.1
Trailing edge, top	21.3

TABLE I.- Concluded

Toe-in angle, deg	7.5
Airfoil section:	
Thickness ratio	0.067
Leading-edge radius, m (in.)	0.000508 (0.020)
Center fin (vertical tail):	
Area (exposed), m^2 (in^2)	0.007 (11.492)
Span (exposed), m (in.)	0.086 (3.380)
Aspect ratio of exposed area	0.994
Root chord (fuselage surface line), m (in.)	0.128 (5.040)
Tip chord, m (in.)	0.045 (1.760)
Taper ratio	0.349
Mean aerodynamic chord of exposed area, m (in.)	0.093 (3.664)
Sweepback angles, deg:	
Leading edge	55.0
Trailing edge	24.6
Airfoil section:	
Thickness ratio –	
Tip	0.106
Root	0.106
Leading-edge radius, m (in.)	0.000508 (0.020)
Fuselage:	
Length, m (in.)	0.508 (20.000)
Maximum height, m (in.)	0.071 (2.782)
Maximum width, m (in.)	0.073 (2.866)
Fineness ratio of equivalent round body	6.822
Planform area, m^2 (in^2)	0.026 (40.445)
Wetted area, m^2 (in^2)	0.083 (128.460)
Wetted area (with wing on), m^2 (in^2)	0.078 (120.695)
Wetted area (with wing and forward delta on), m^2 (in^2)	0.077 (118.747)
Base area, m^2 (in^2)	0.002 (3.726)
Complete model (wing and forward delta):	
Planform area, m^2 (in^2)	0.052 (79.960)
Aspect ratio of planform	0.913
Planform area (without forward delta), m^2 (in^2)	0.049 (76.566)
Aspect ratio (without forward delta)	0.953
Model scramjet engine:	
Frontal area, m^2 (in^2)	0.00084 (1.308)
Width-to-height ratio	5.23

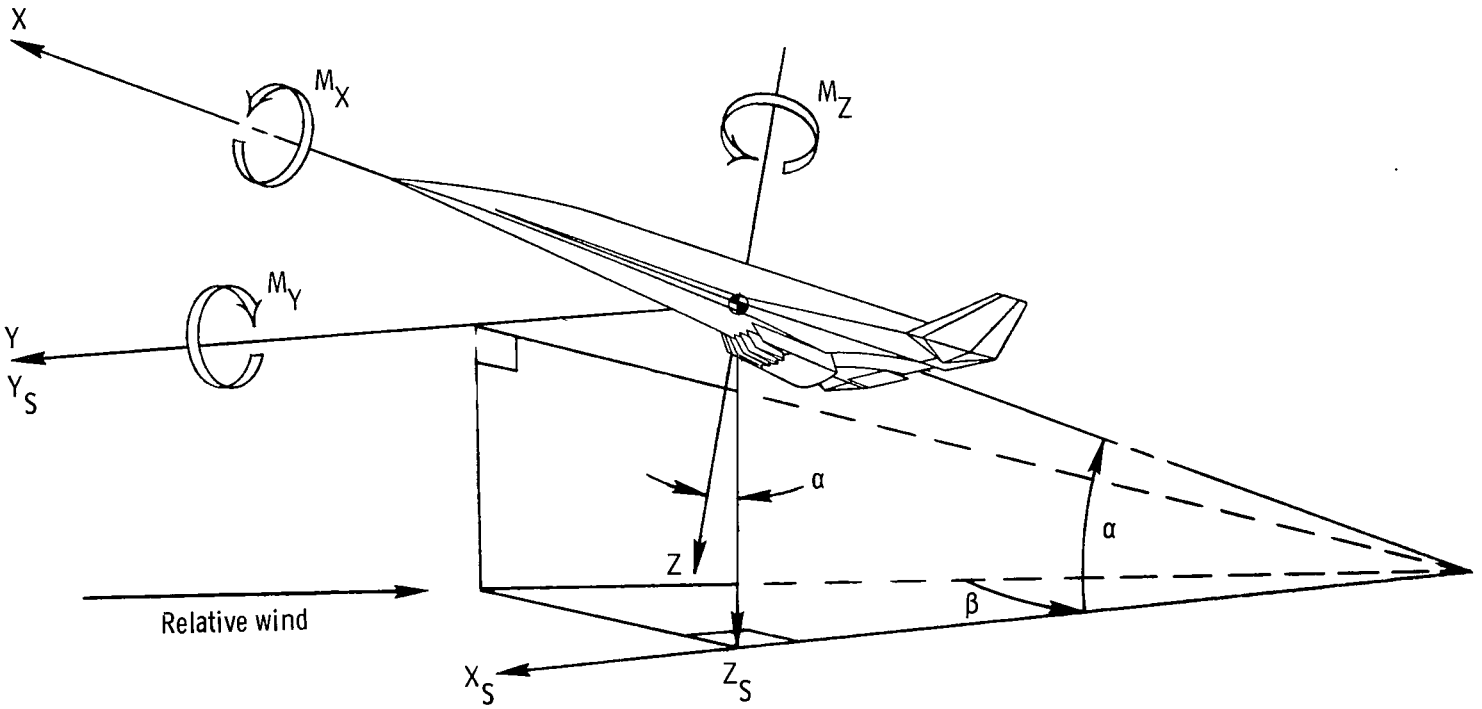

Figure 1.- Systems of reference axes; arrows indicate positive direction.

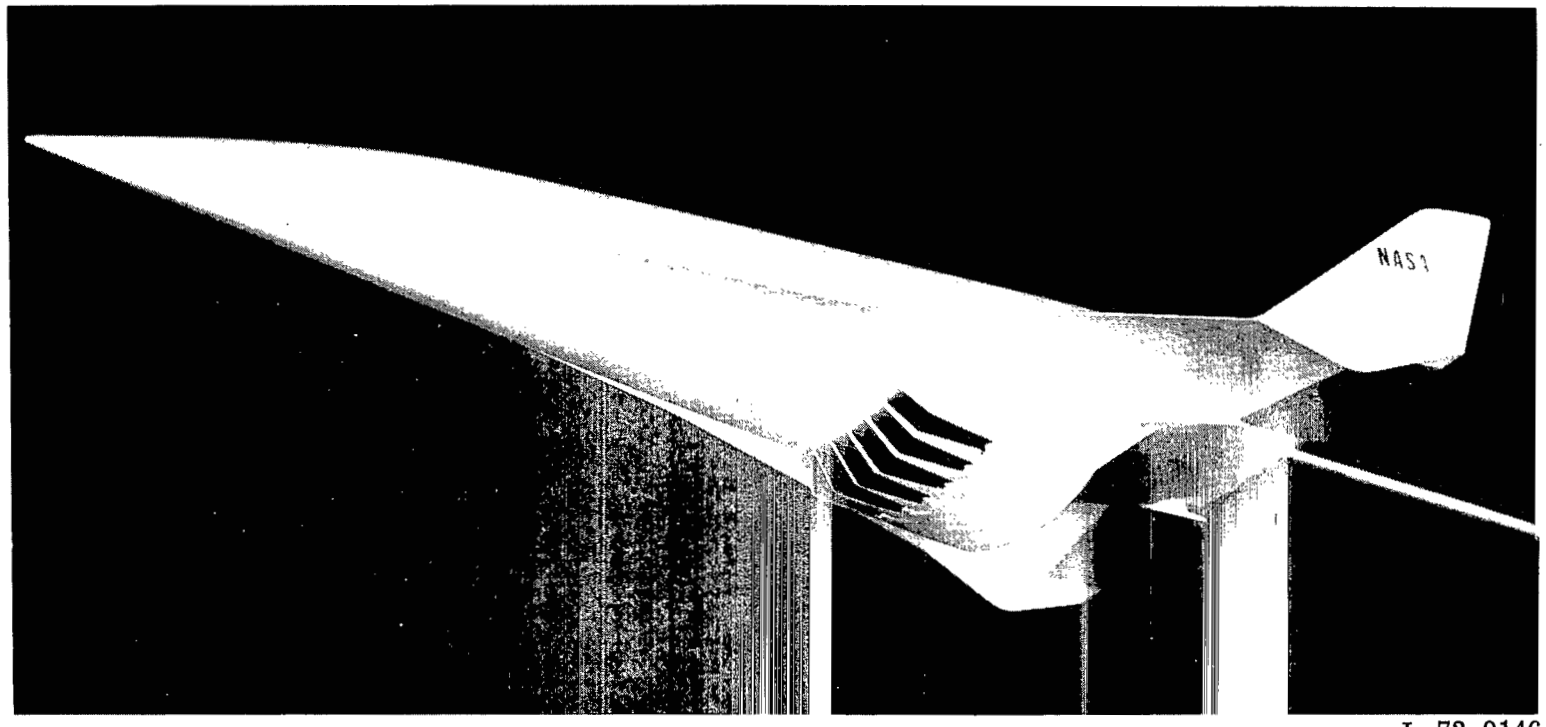

L-72-9146

(a) Configuration model.

Figure 2.- Configuration and sketch showing interchangeable parts.

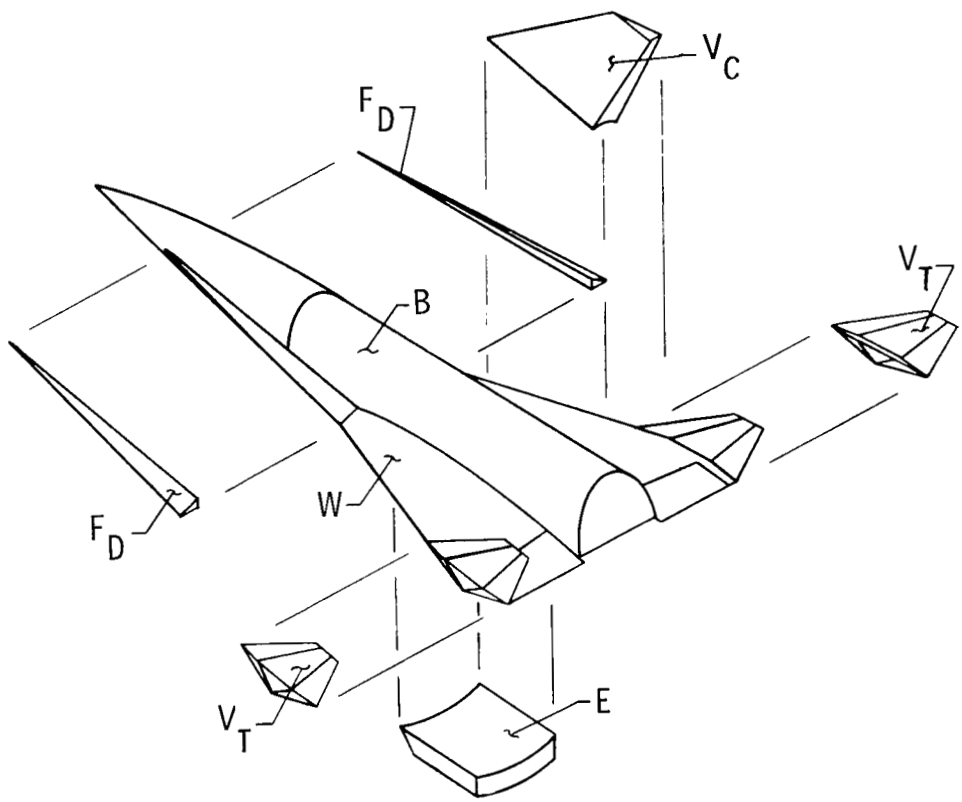

(b) Sketch showing interchangeable parts.

Figure 2.- Concluded.

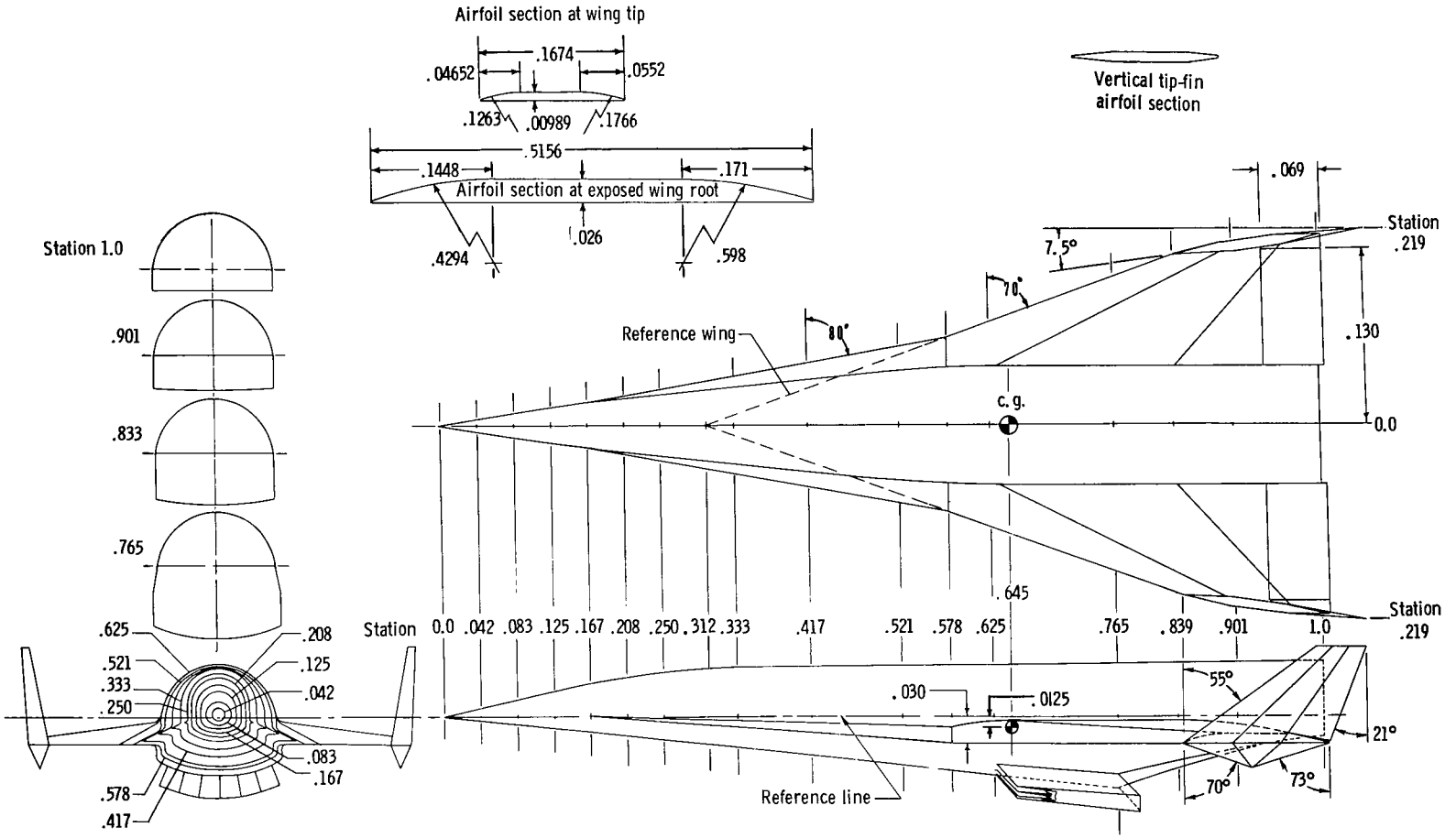

(a) Base-line configuration.

Figure 3.- Model general dimensions. All dimensions have been normalized by the body length (ℓ = 50.8 cm).

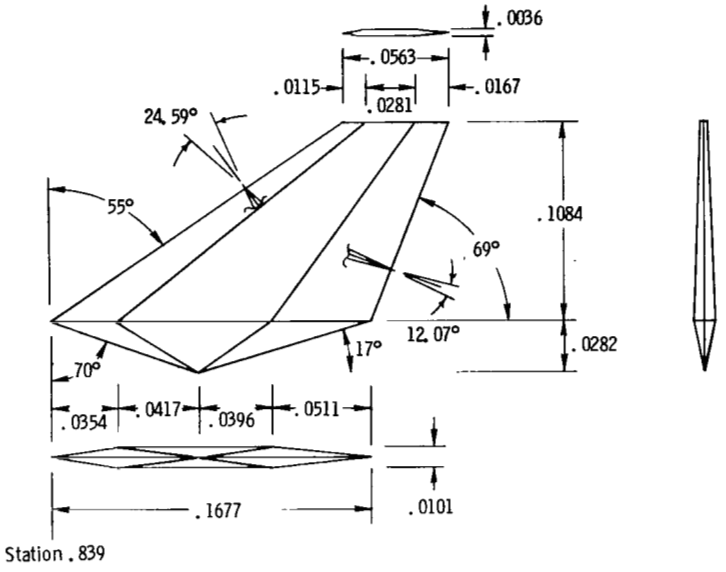

(b) Tip fin.

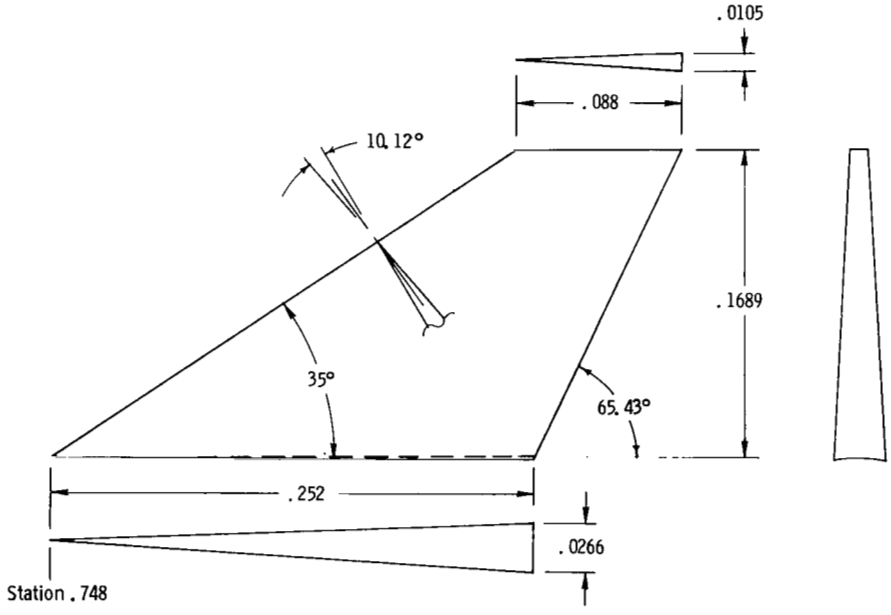

(c) Center vertical tail.

Figure 3.- Continued.

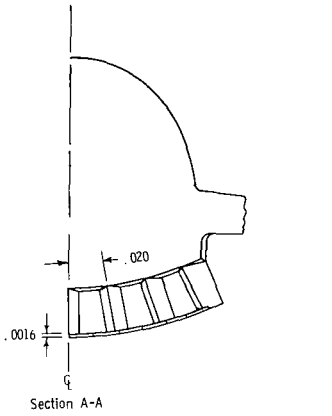

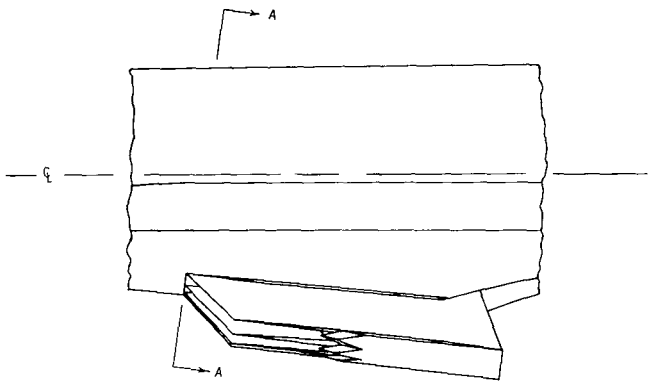

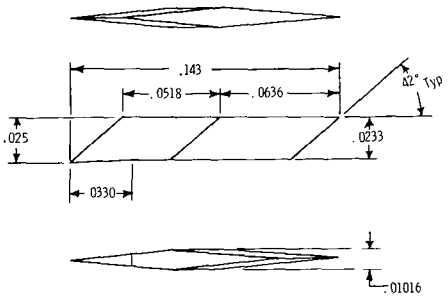

Inside splitter plate

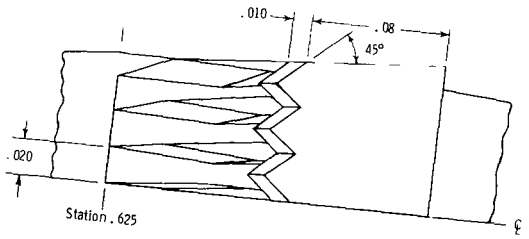

Bottom view of scramjet engine with cowl on

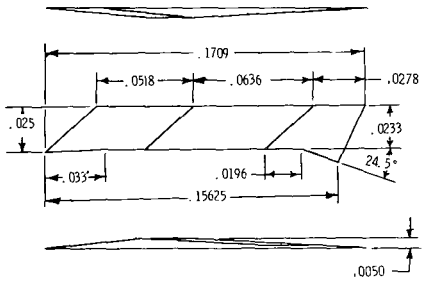

Left outside plate

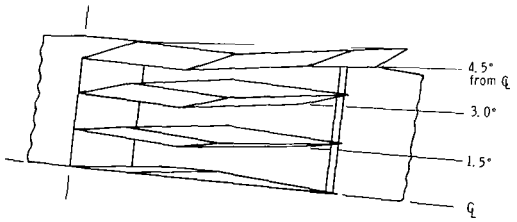

Bottom view of scramjet engine with cowl removed

(d) Scramjet engine.

Figure 3.- Concluded.

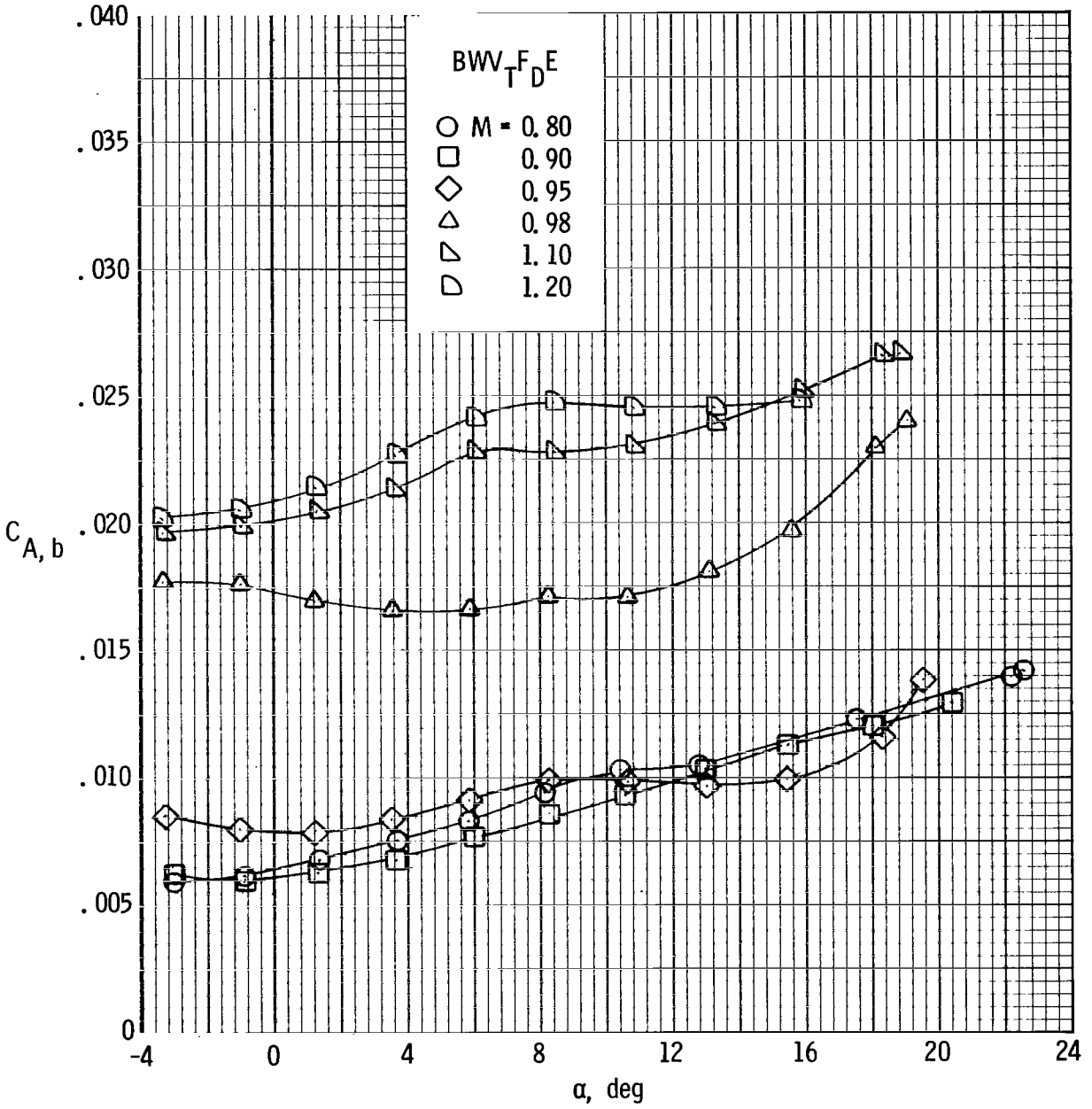

(a) BWV$_T$F$_D$E.

Figure 4.- Variation of base axial-force coefficient with angle of attack for various test Mach numbers for complete configuration with and without engine.

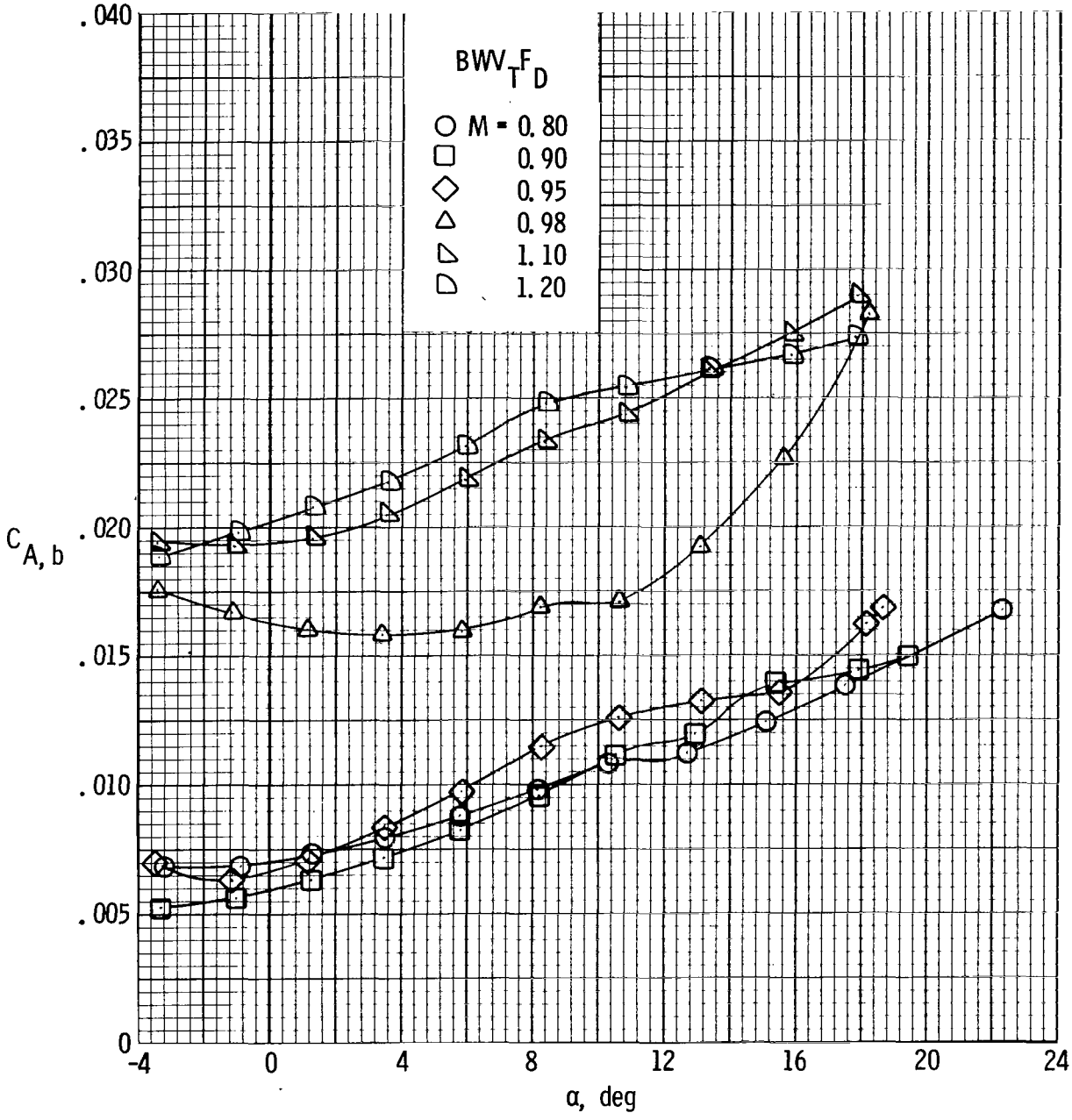

(b) BWV_TF_D.

Figure 4.- Concluded.

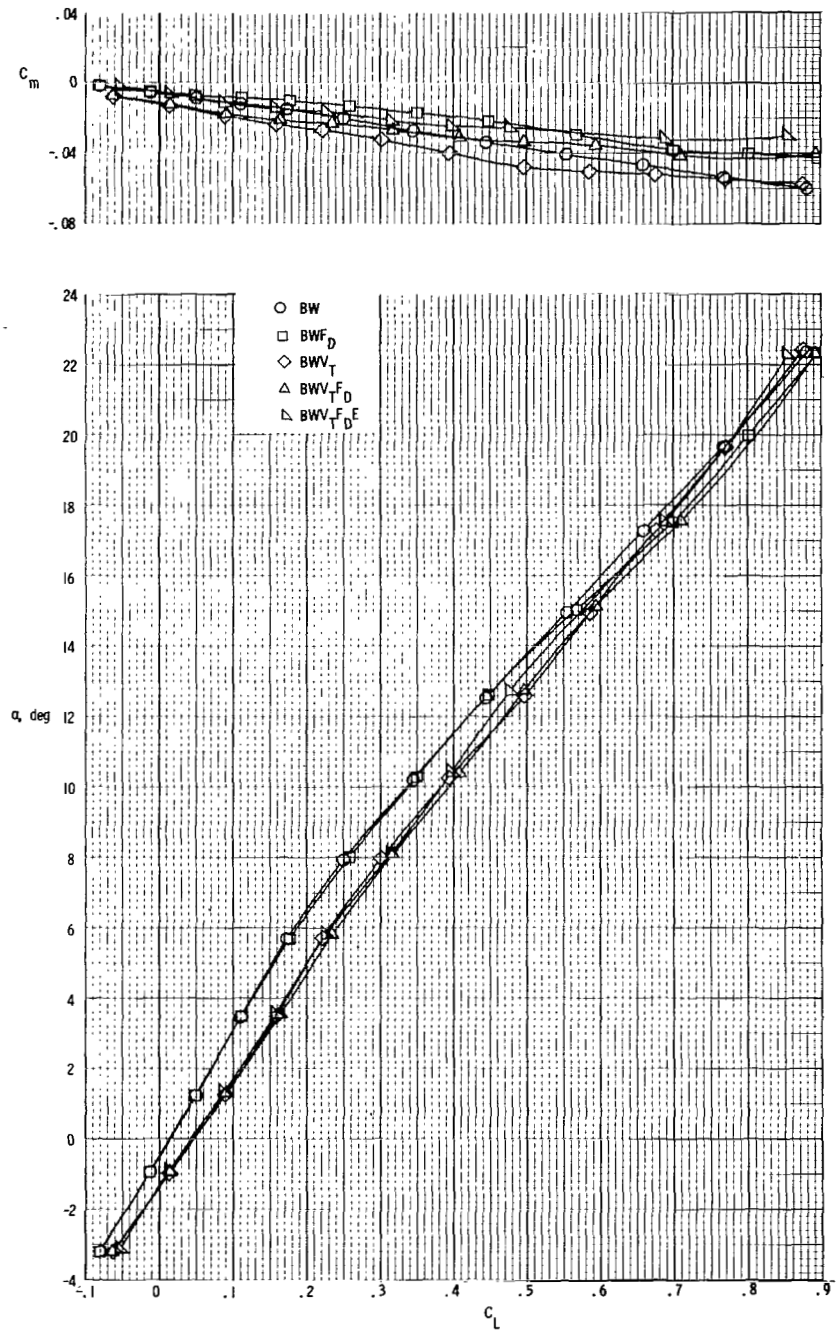

(a) M = 0.80.

Figure 5.- Longitudinal aerodynamic characteristics of body-wing configuration alone and with various forward delta, tip-fin, and engine components.

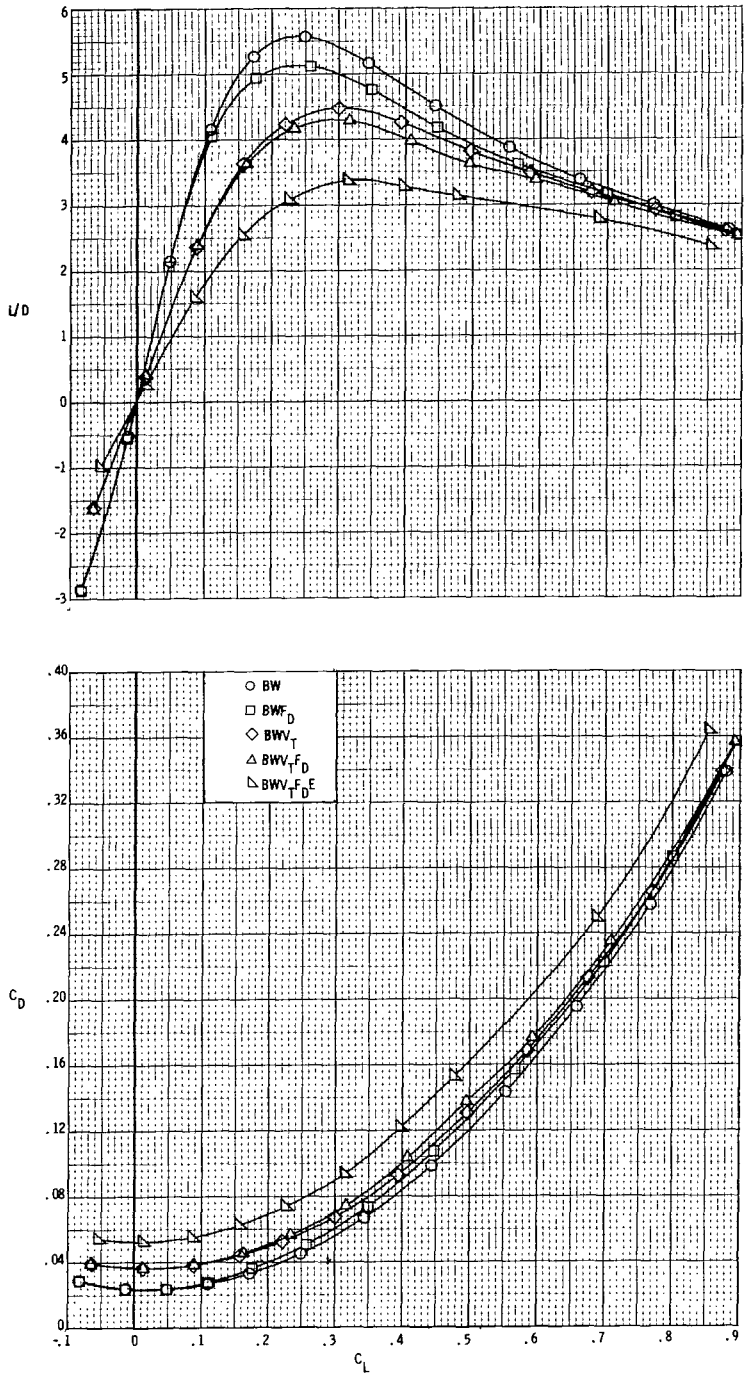

(a) Concluded.

Figure 5.- Continued.

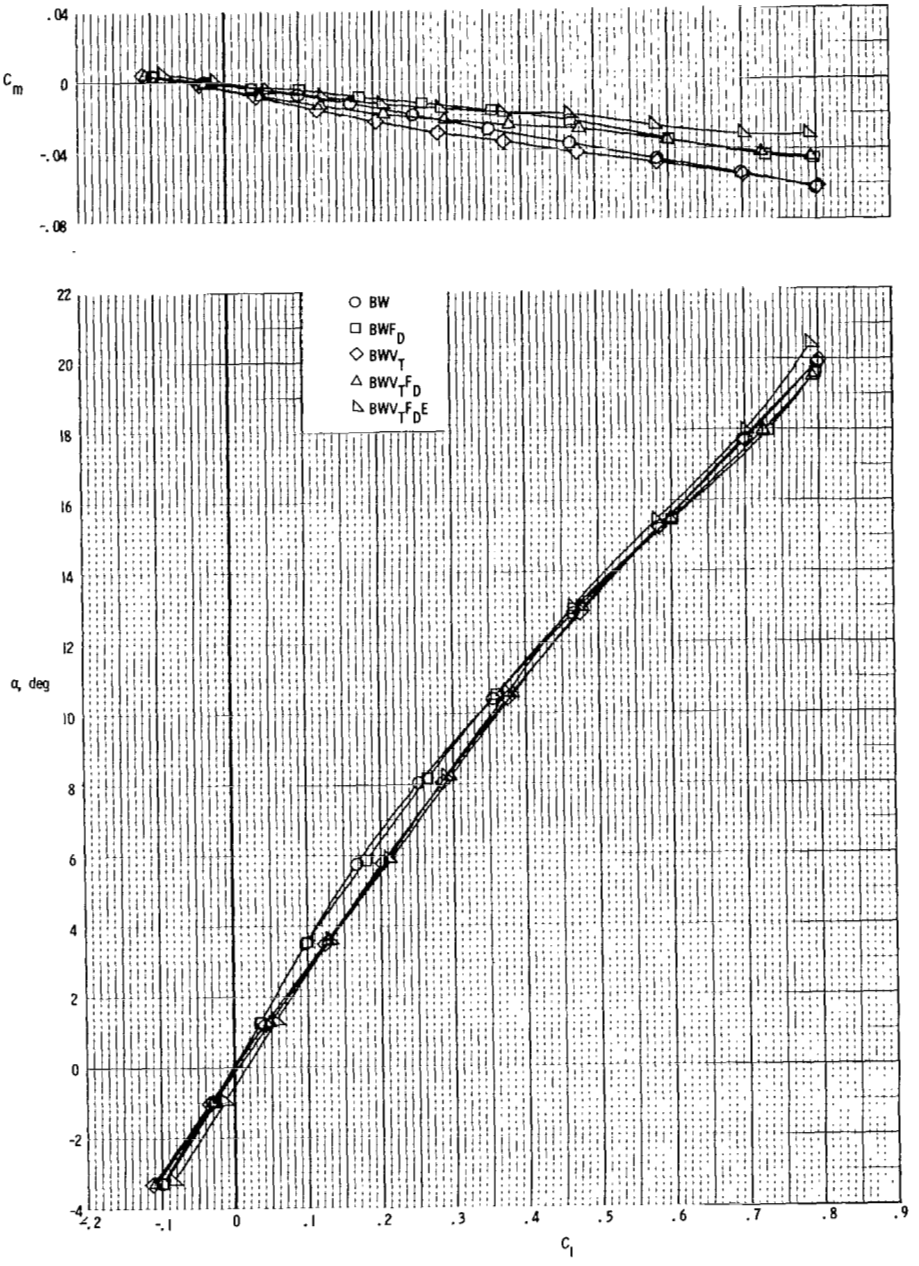

(b) M = 0.90.

Figure 5.- Continued.

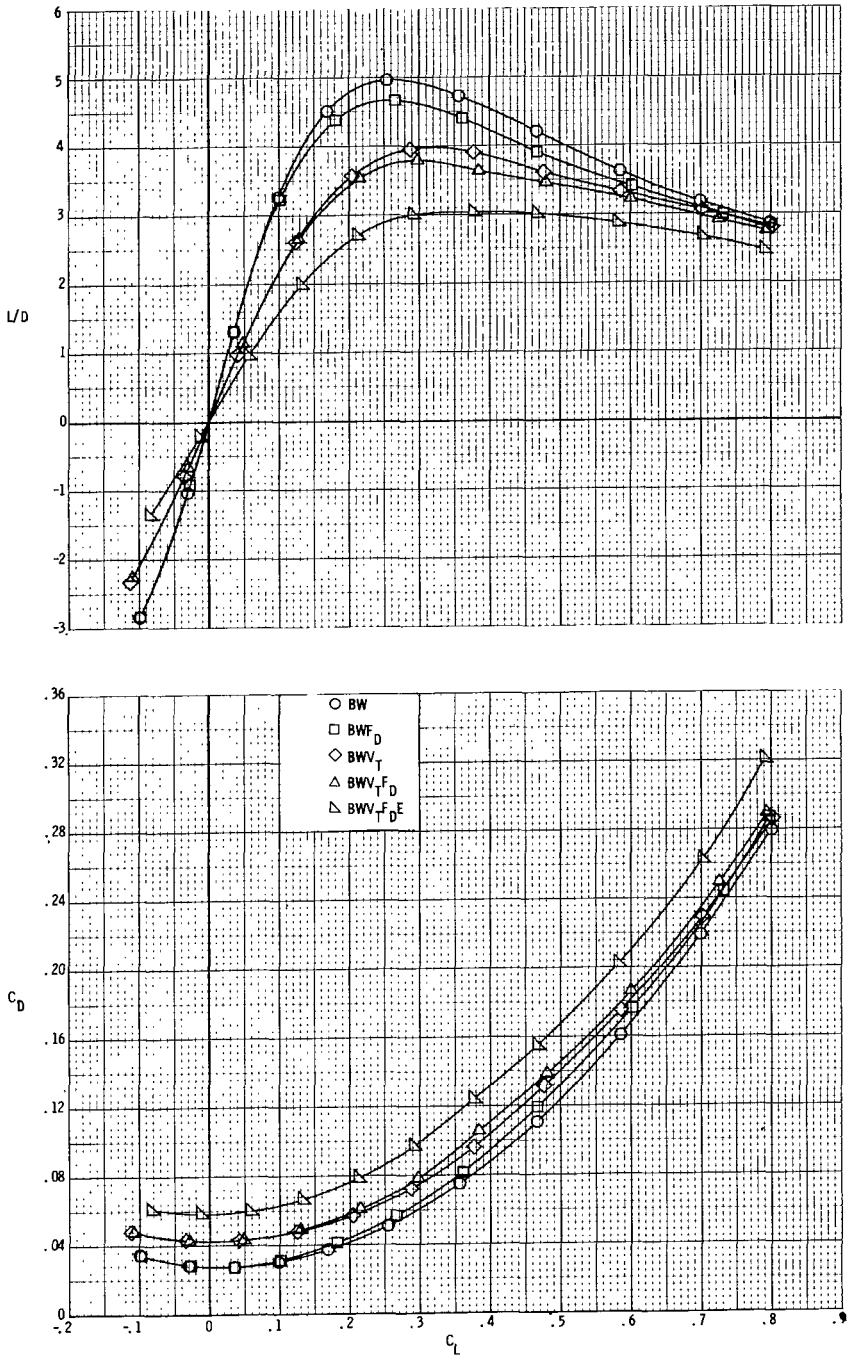

(b) Concluded.

Figure 5.- Continued.

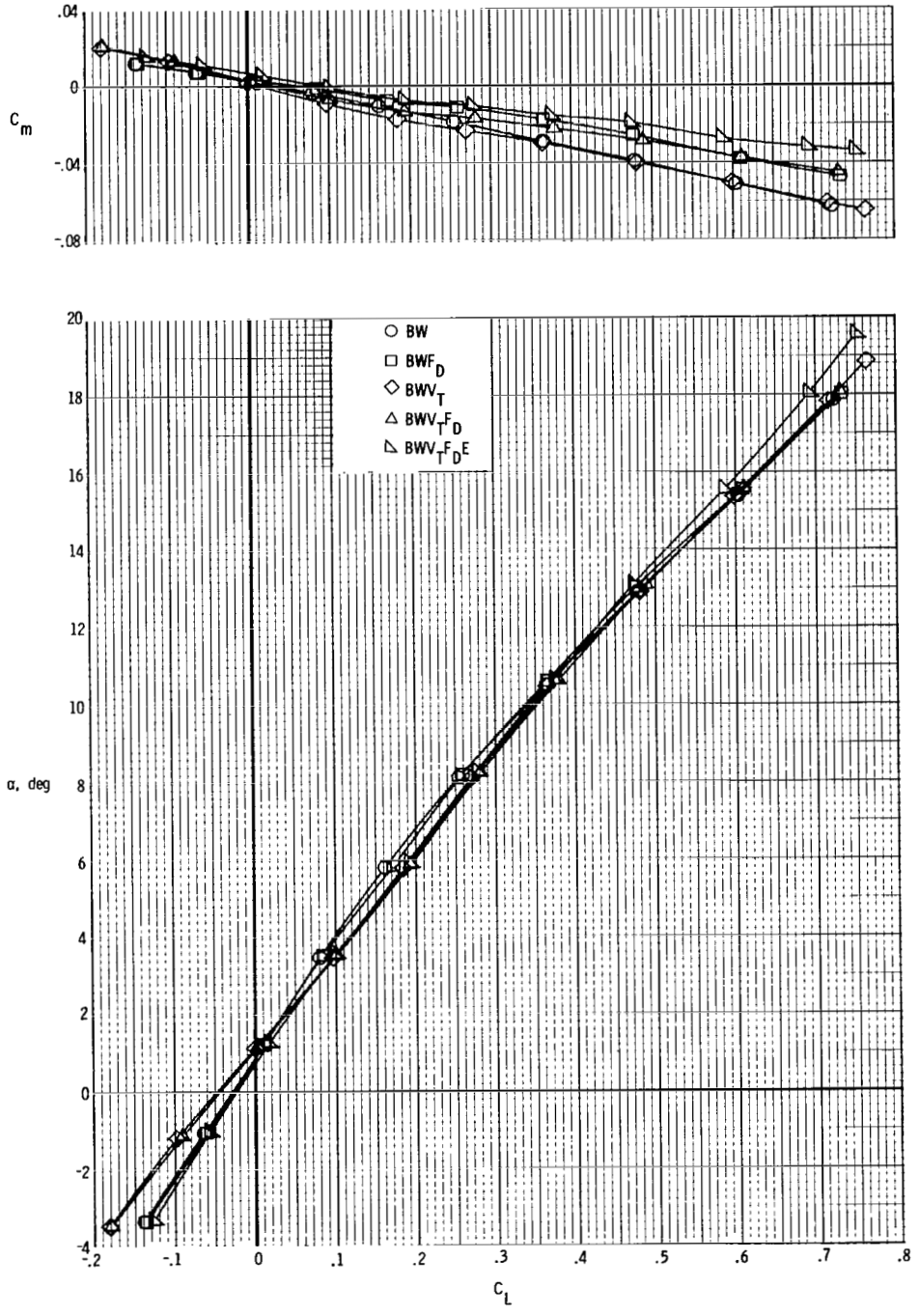

(c) M = 0.95.

Figure 5.- Continued.

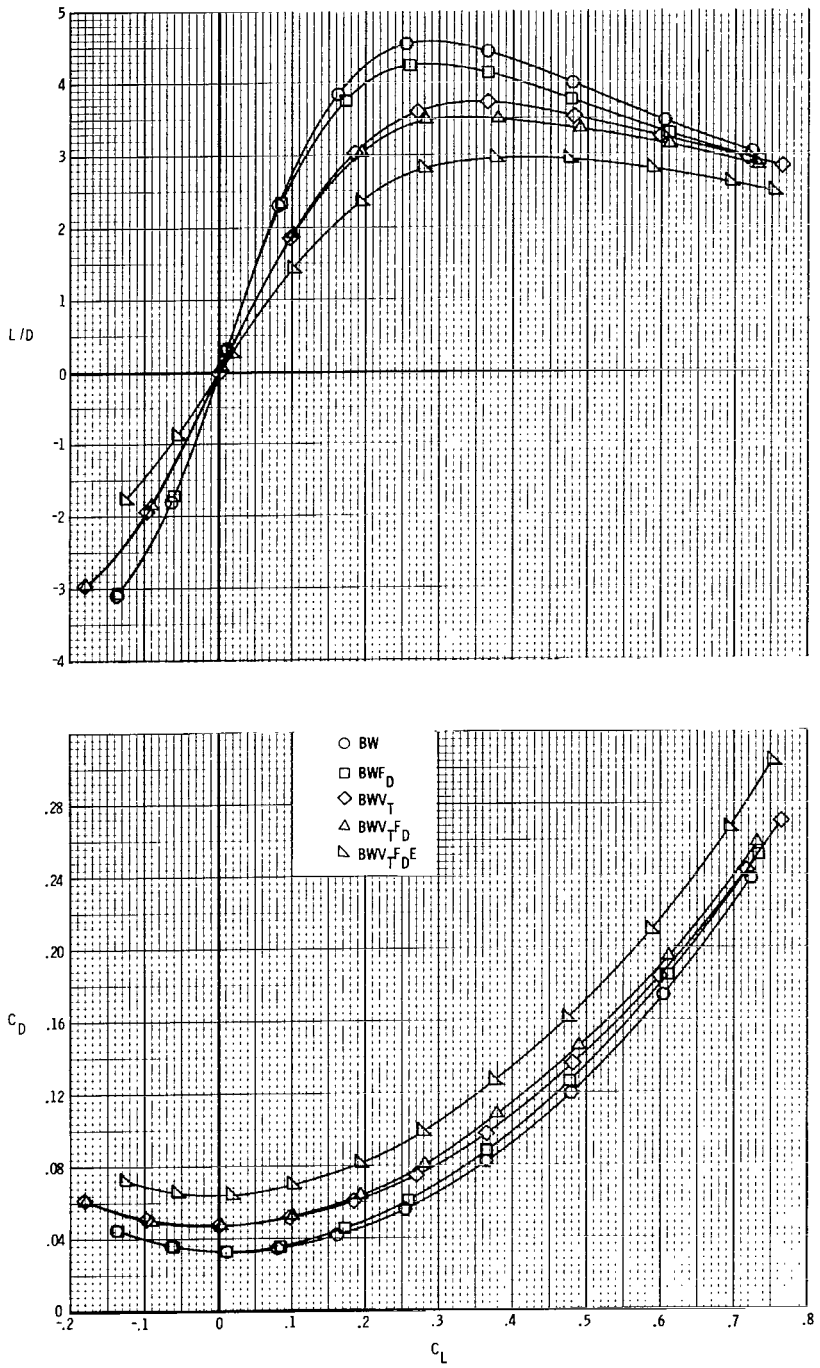

(c) Concluded.

Figure 5.- Continued.

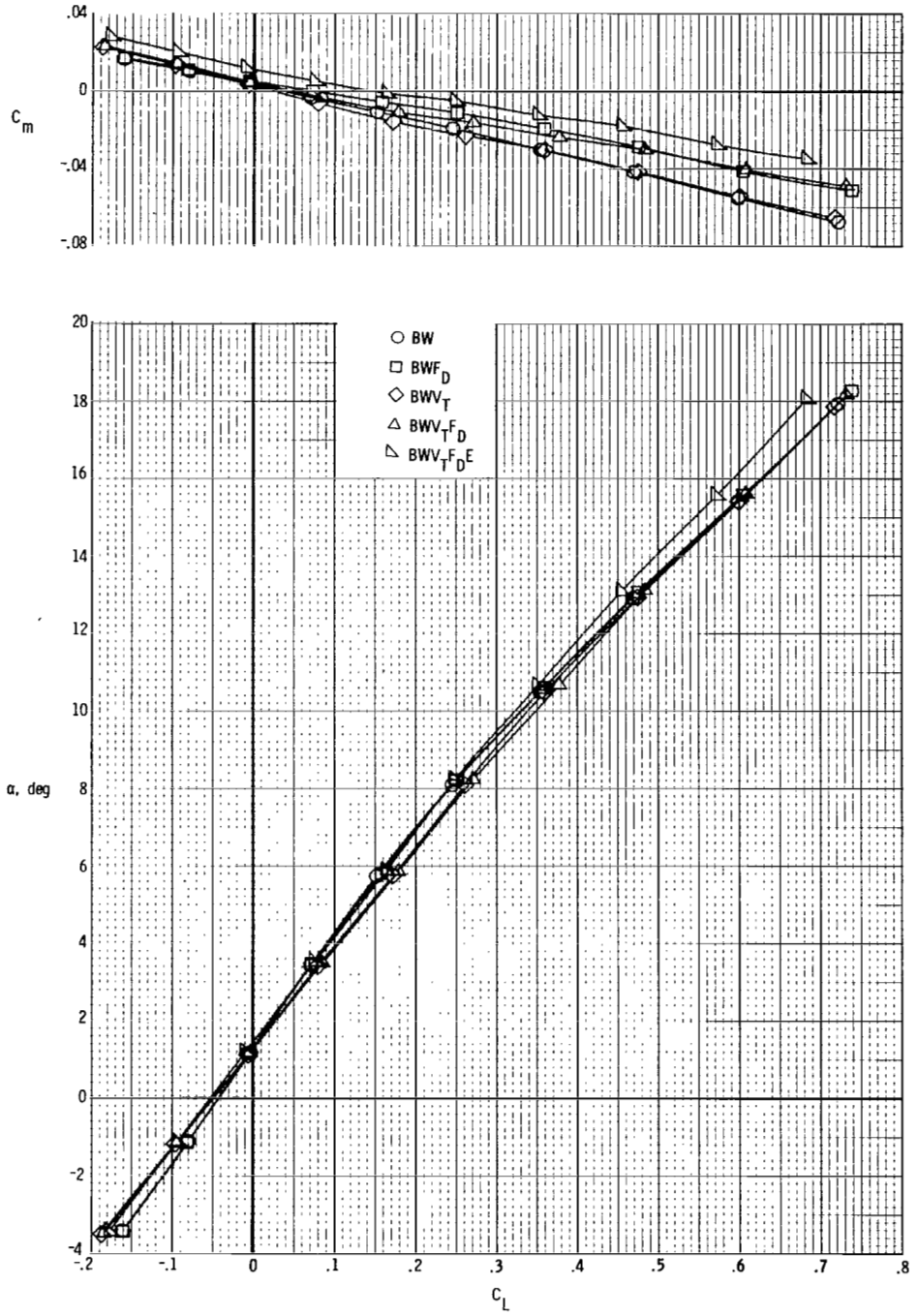

(d) M = 0.98.

Figure 5.- Continued.

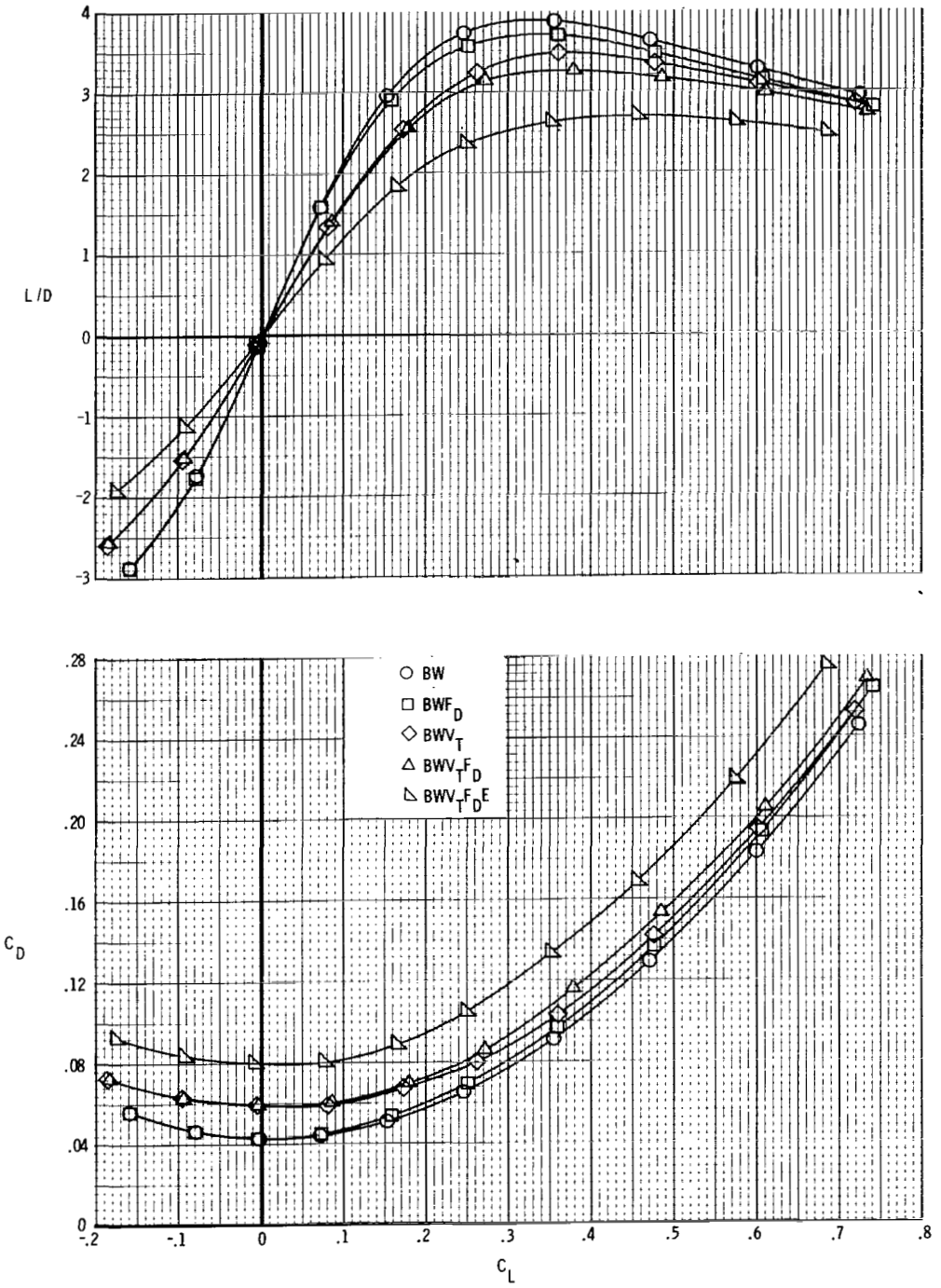

(d) Concluded.

Figure 5.- Continued.

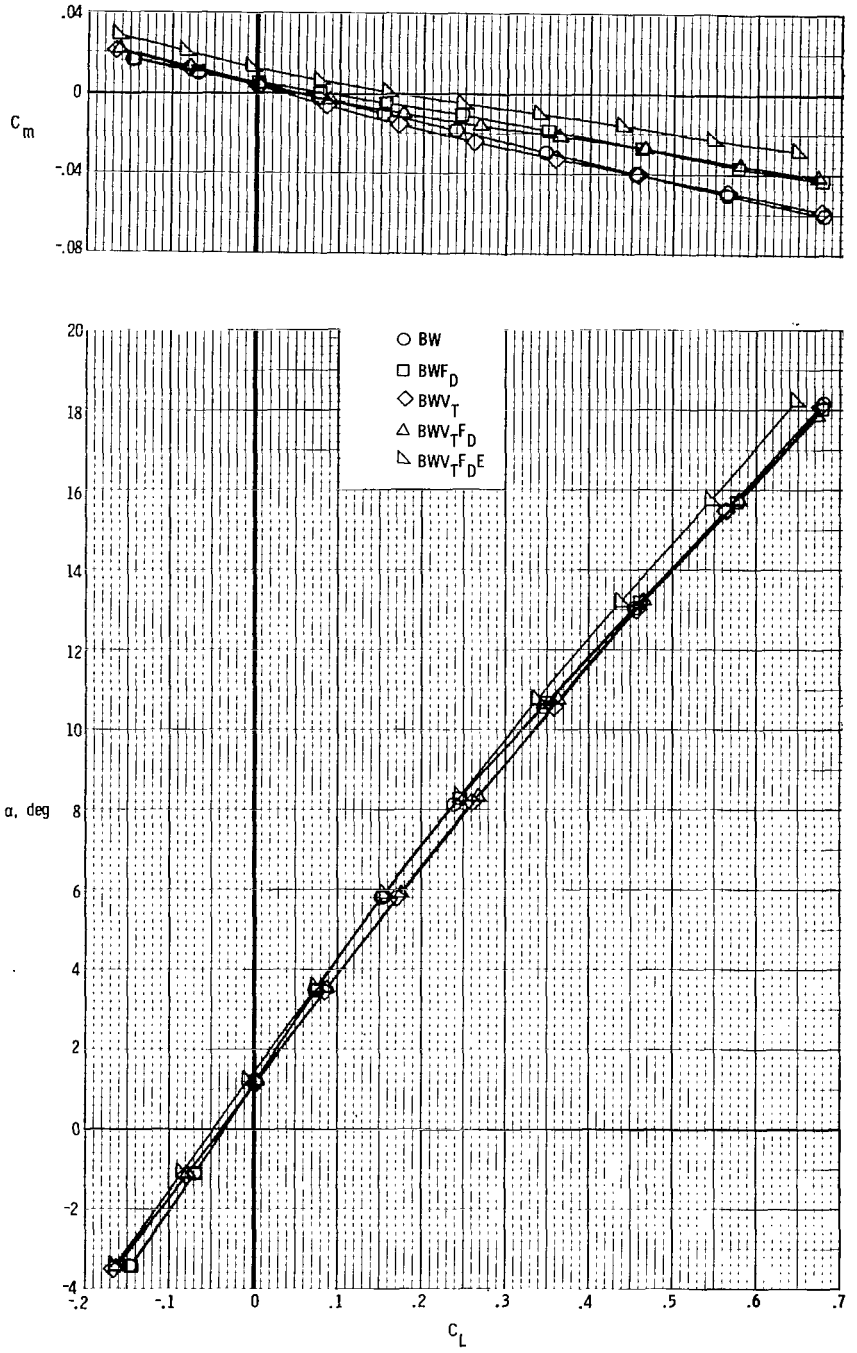

(e) M = 1.10.

Figure 5.- Continued.

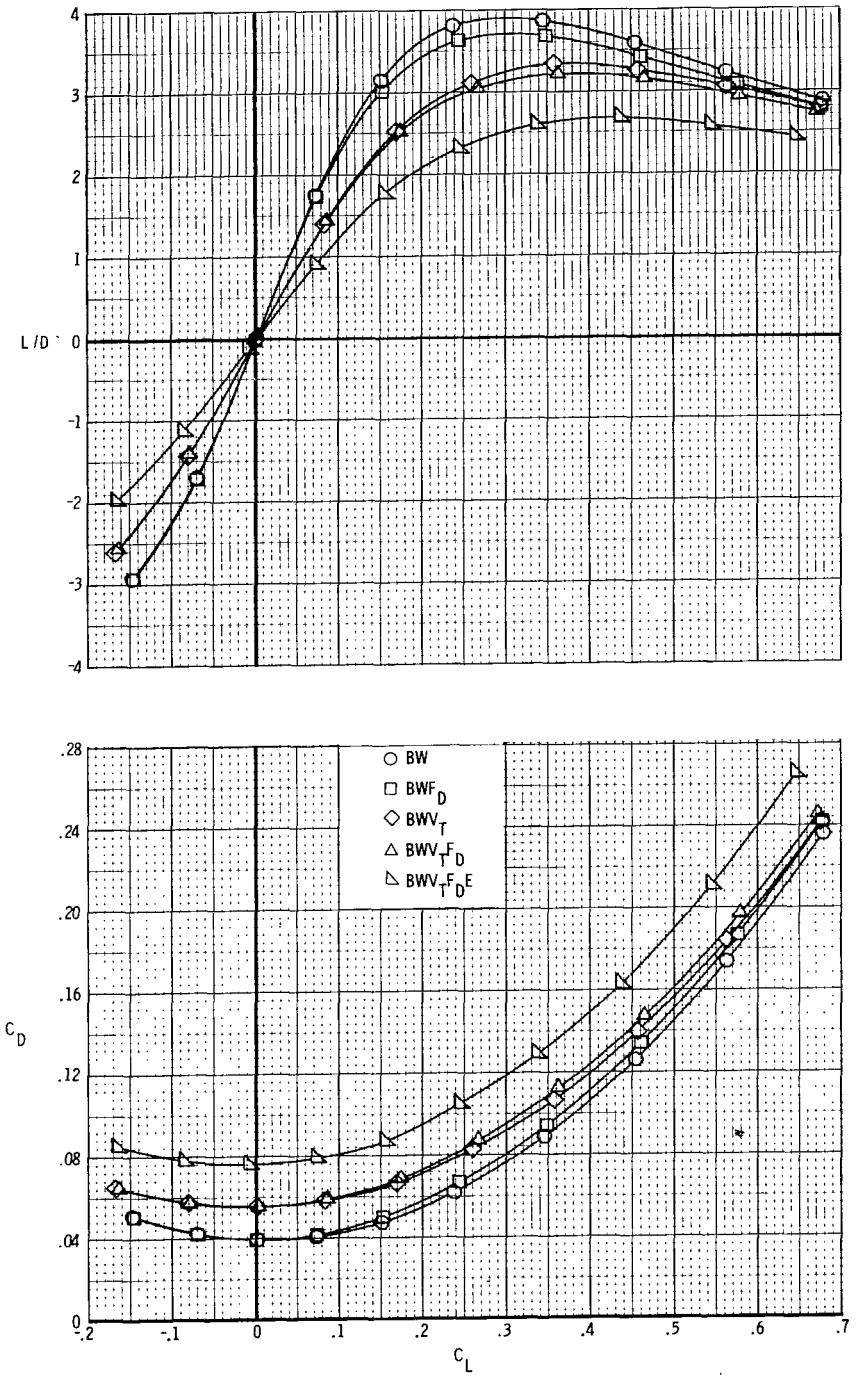

(e) Concluded.

Figure 5.- Continued.

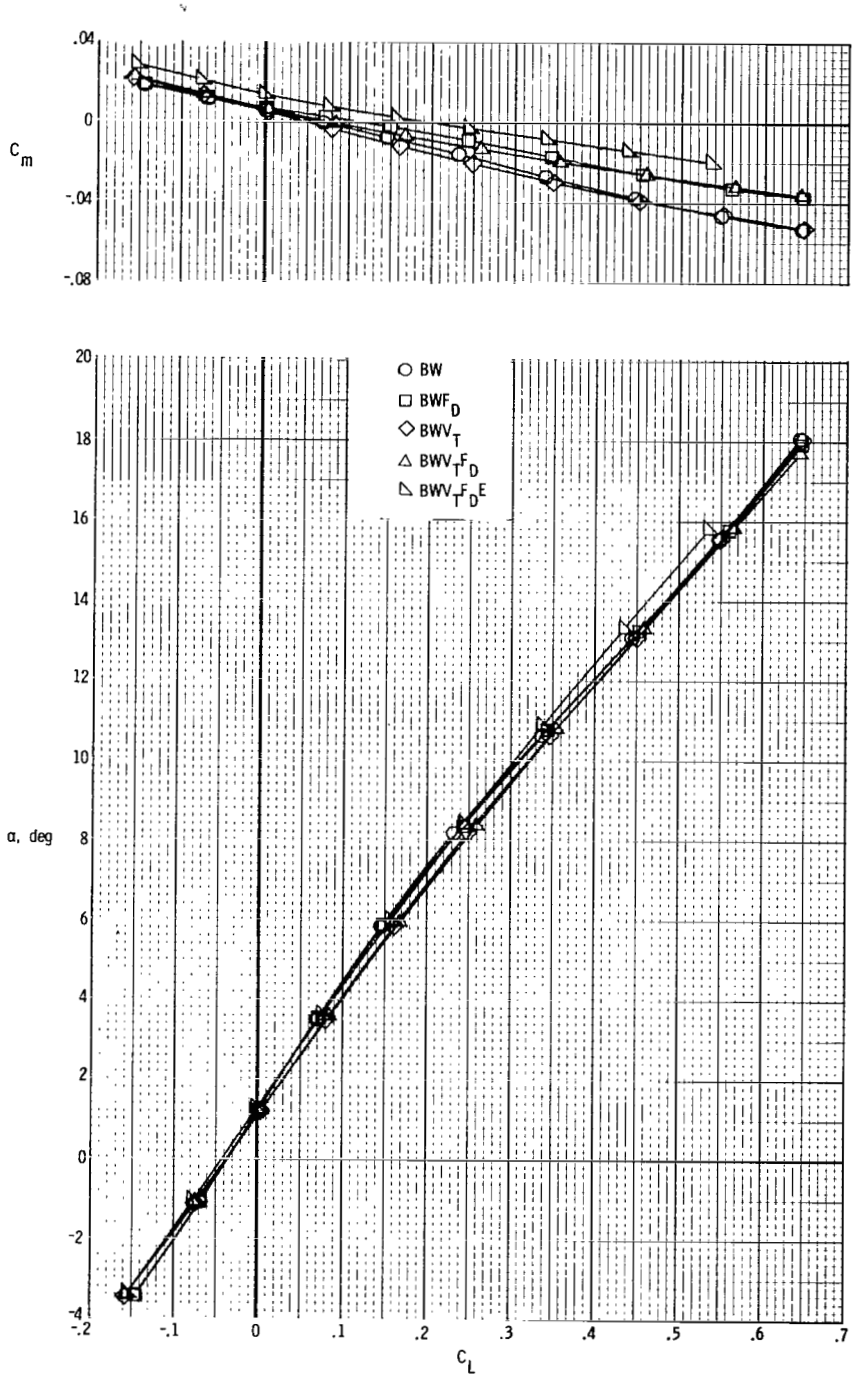

(f) M = 1.20.

Figure 5.- Continued.

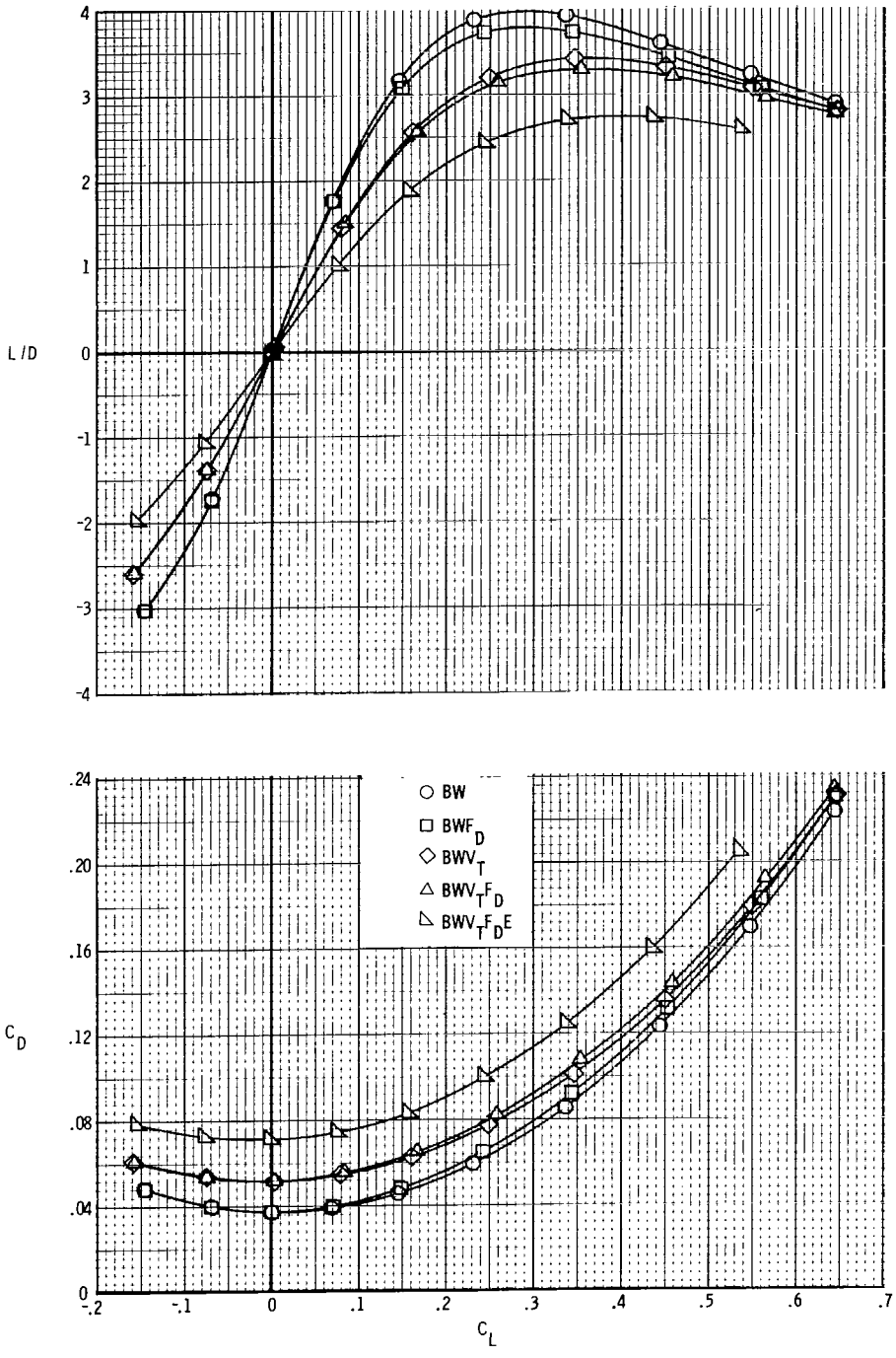

(f) Concluded.

Figure 5.- Concluded.

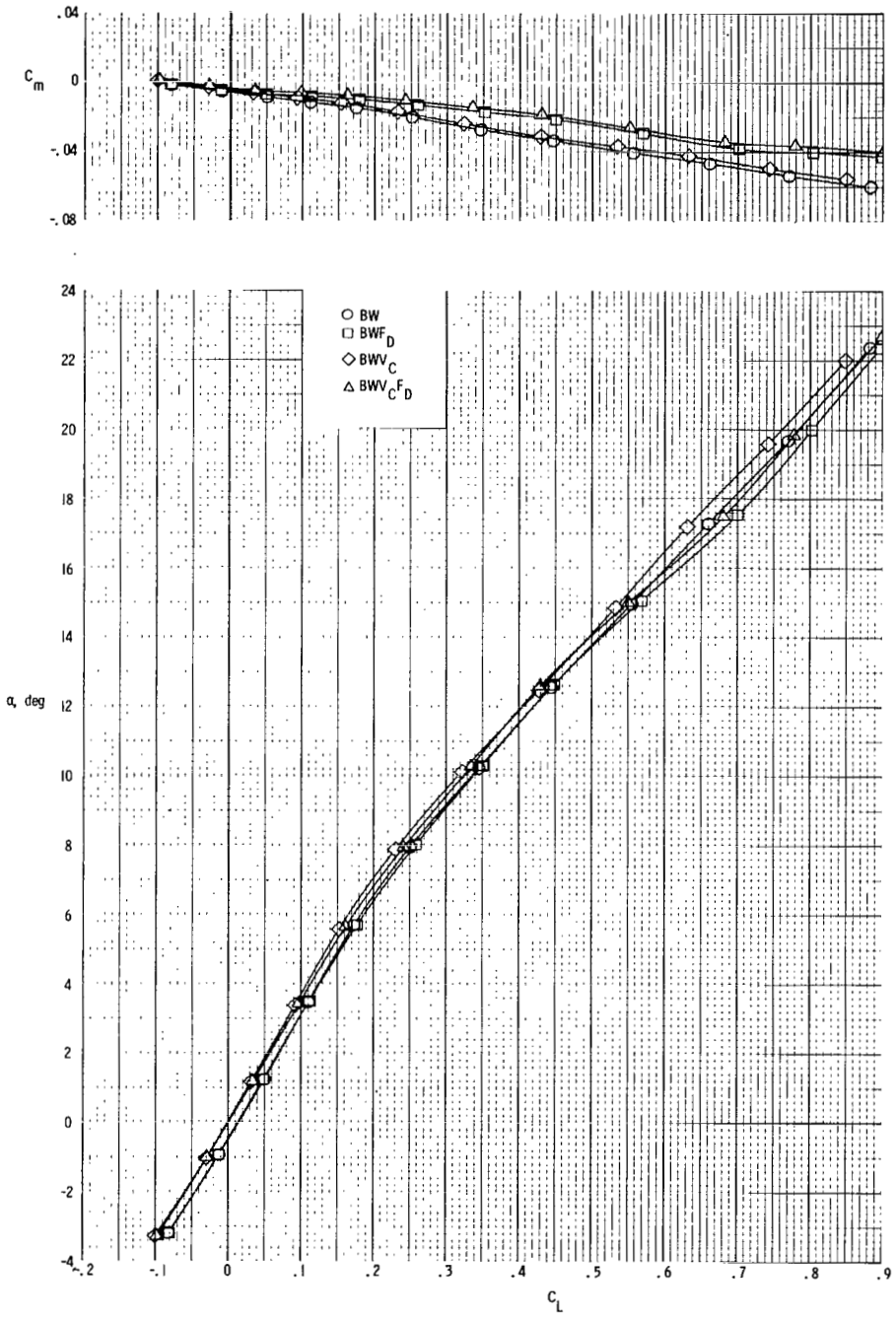

(a) M = 0.80.

Figure 6.- Longitudinal aerodynamic characteristics of body-wing configuration alone and with various forward delta and center-tail components.

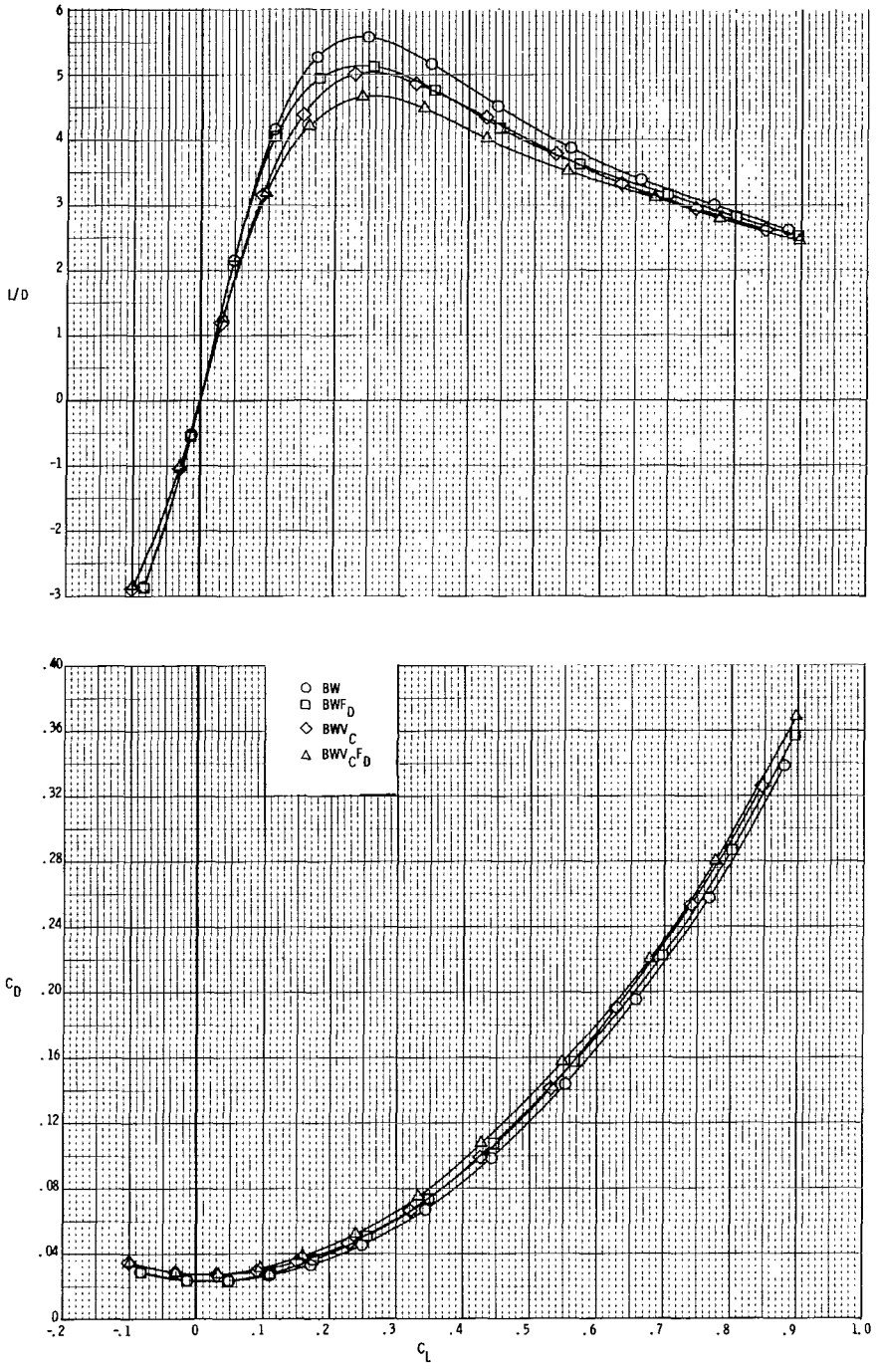

(a) Concluded.

Figure 6.- Continued.

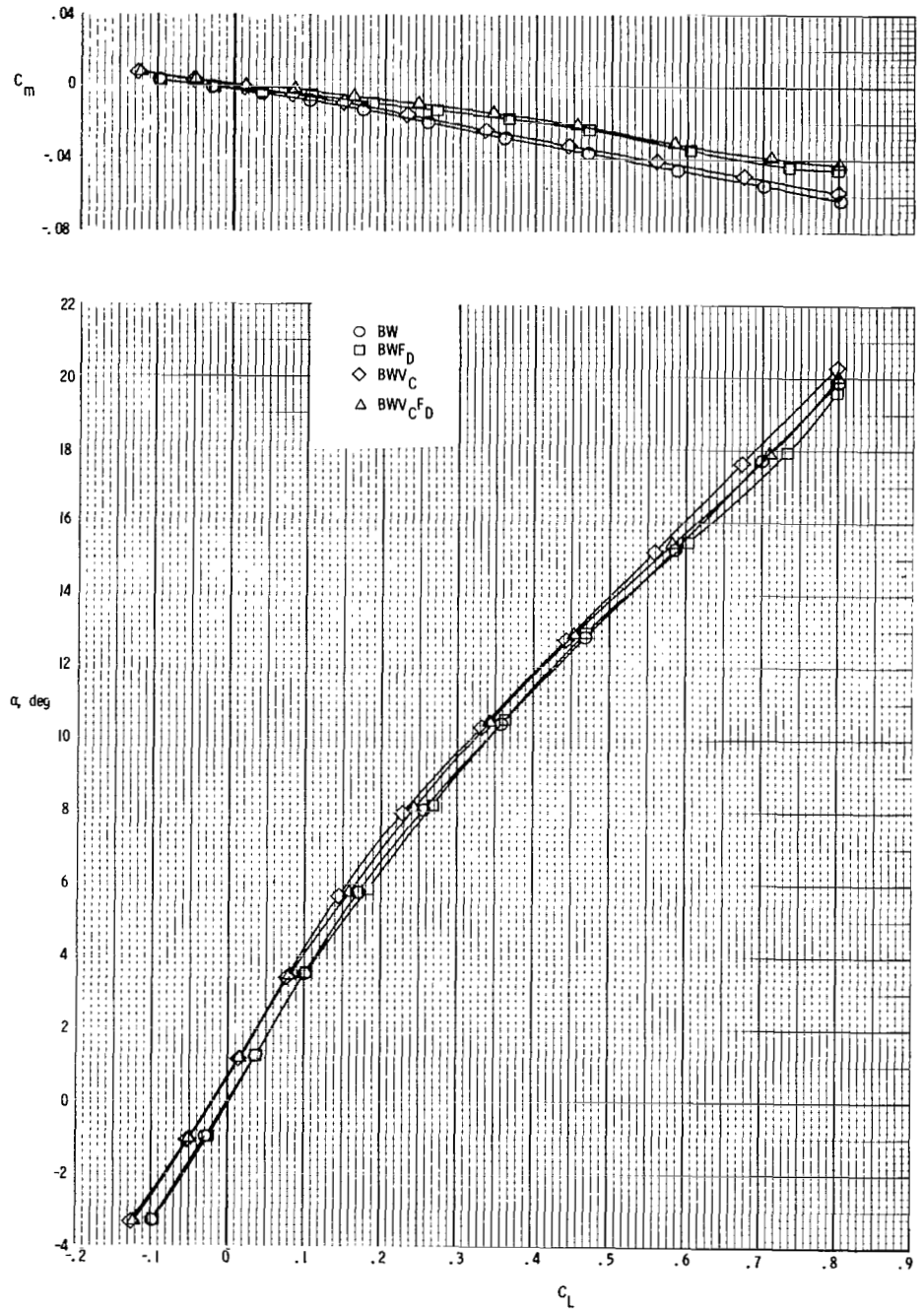

(b) M = 0.90.

Figure 6.- Continued.

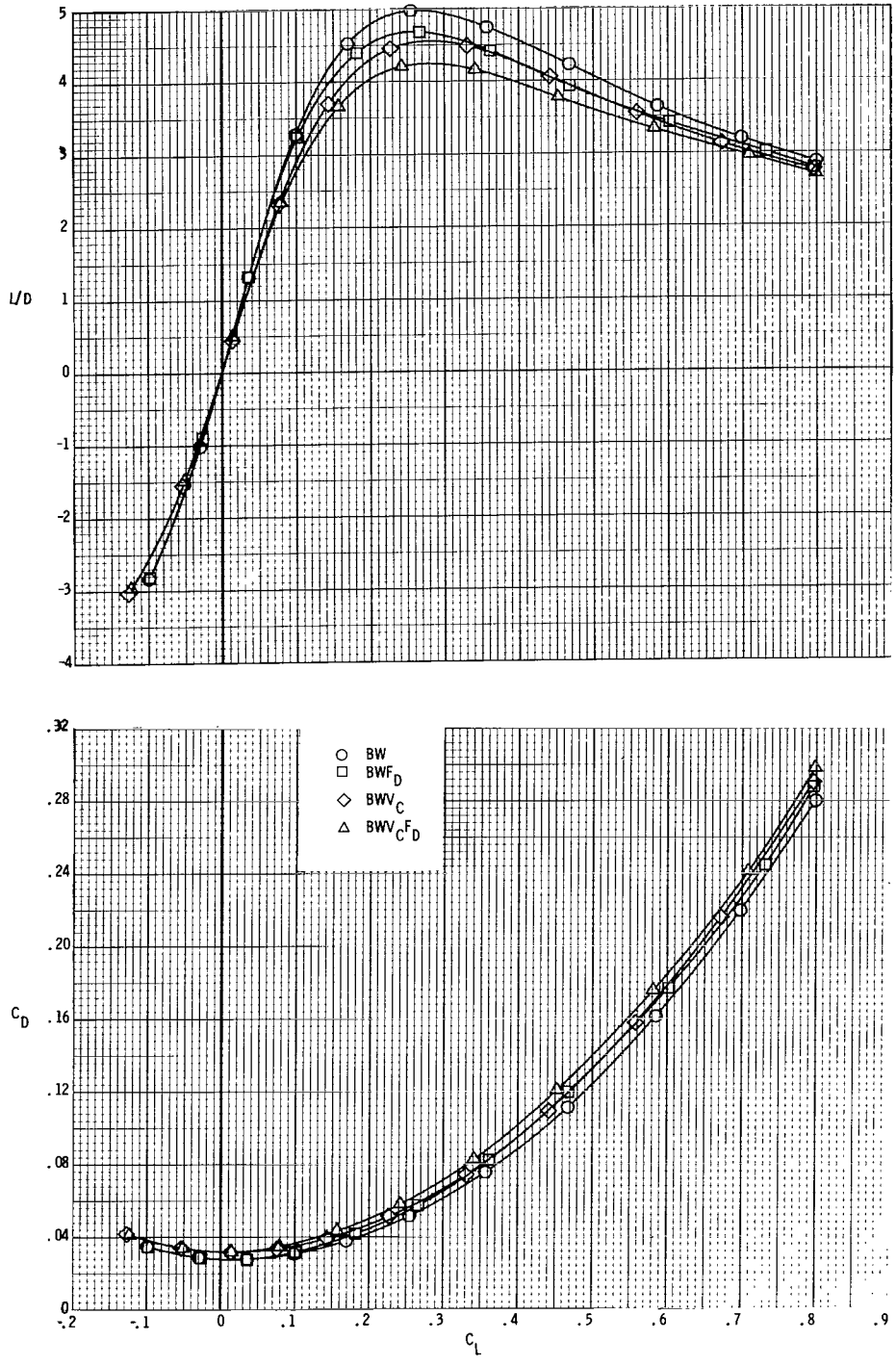

(b) Concluded.

Figure 6.- Continued.

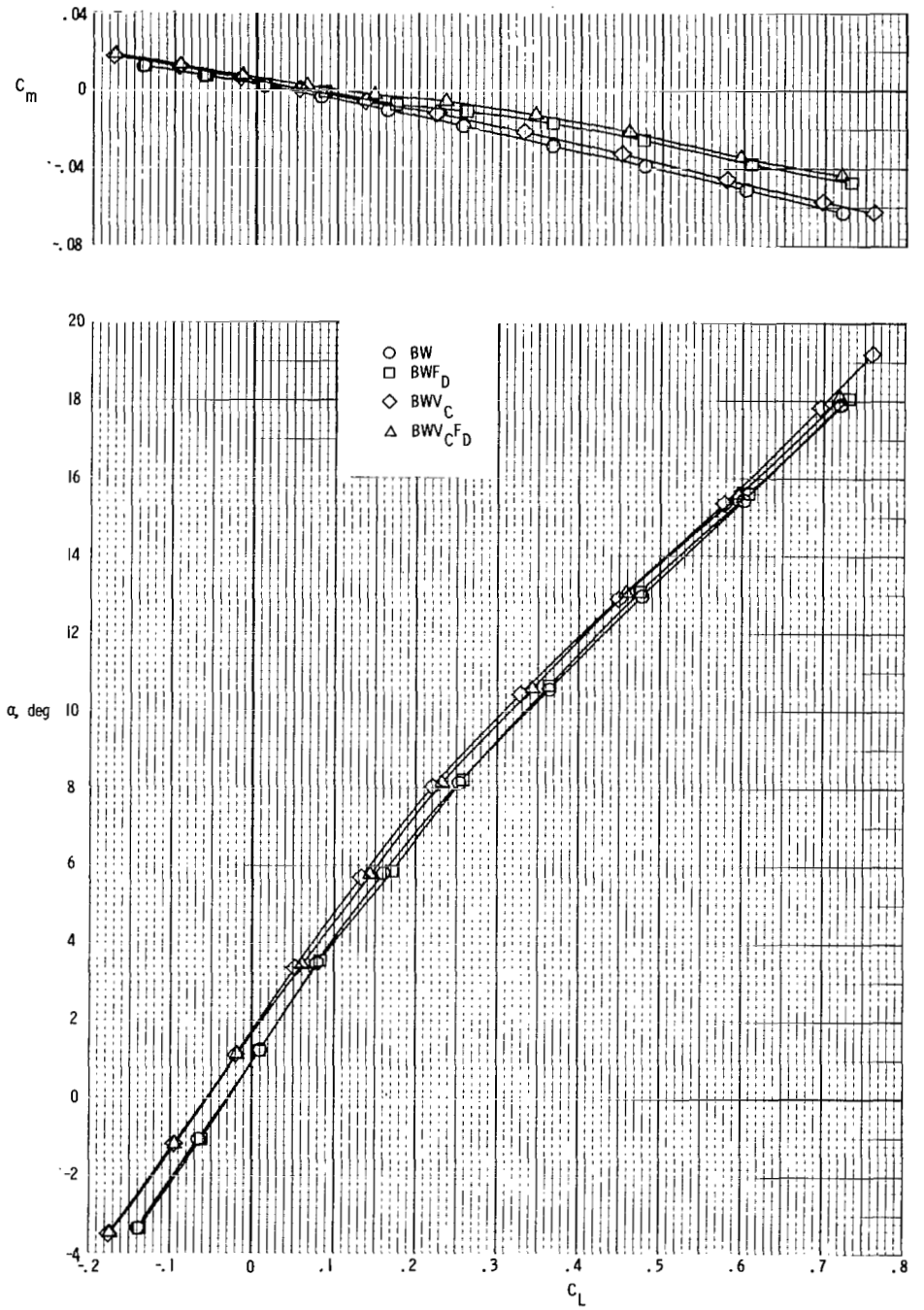

(c) M = 0.95.

Figure 6.- Continued.

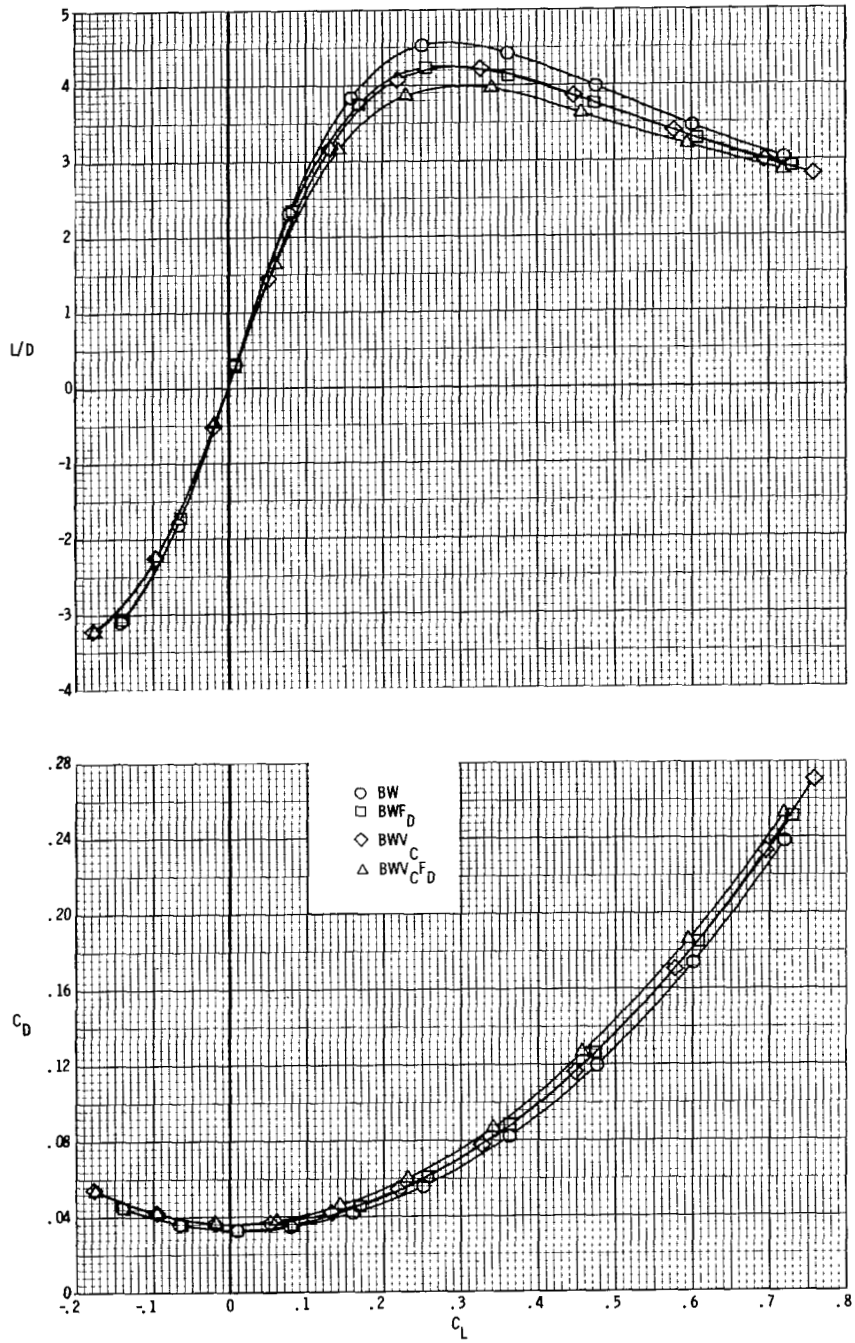

(c) Concluded.

Figure 6.- Continued.

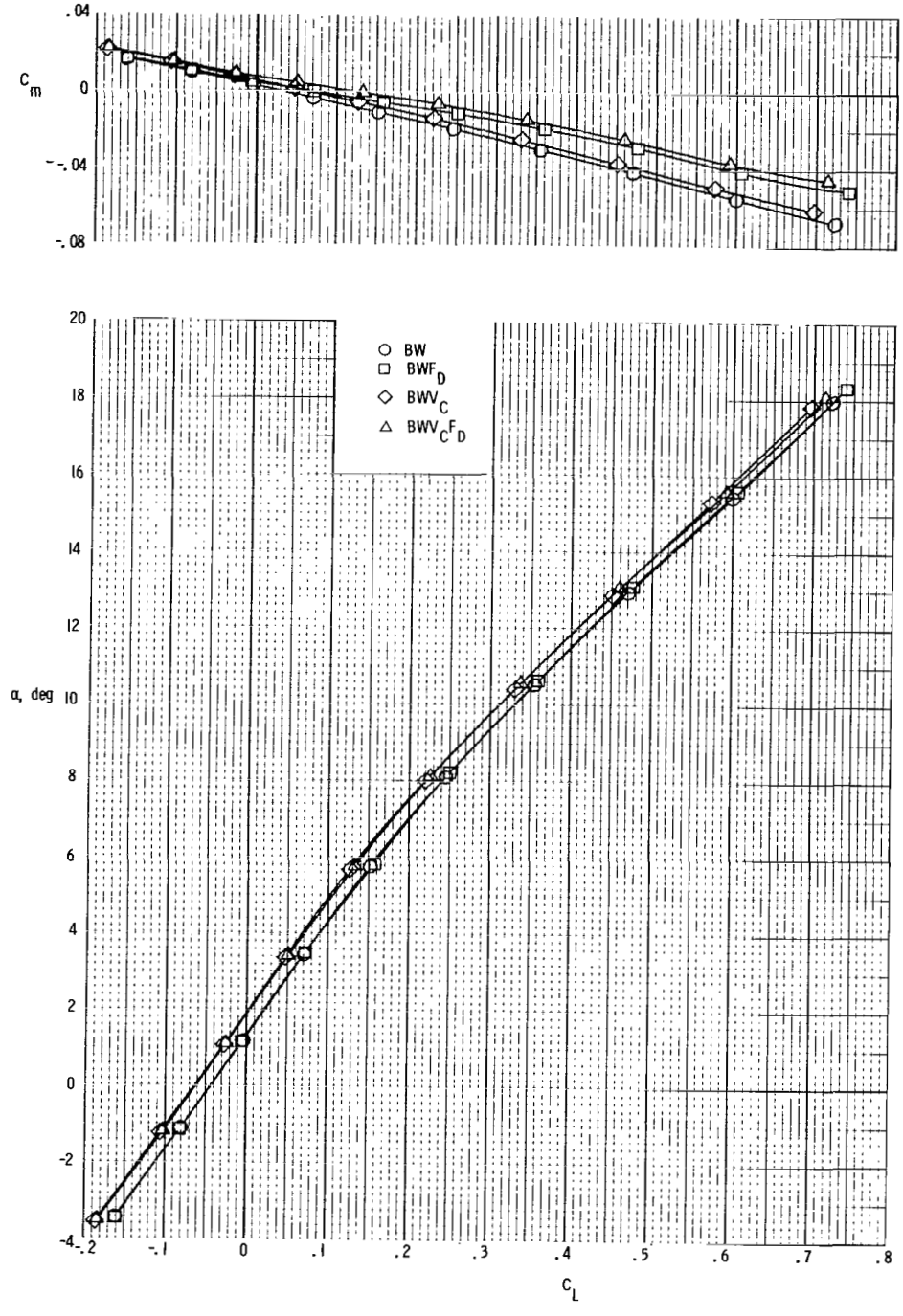

(d) M = 0.98.

Figure 6.- Continued.

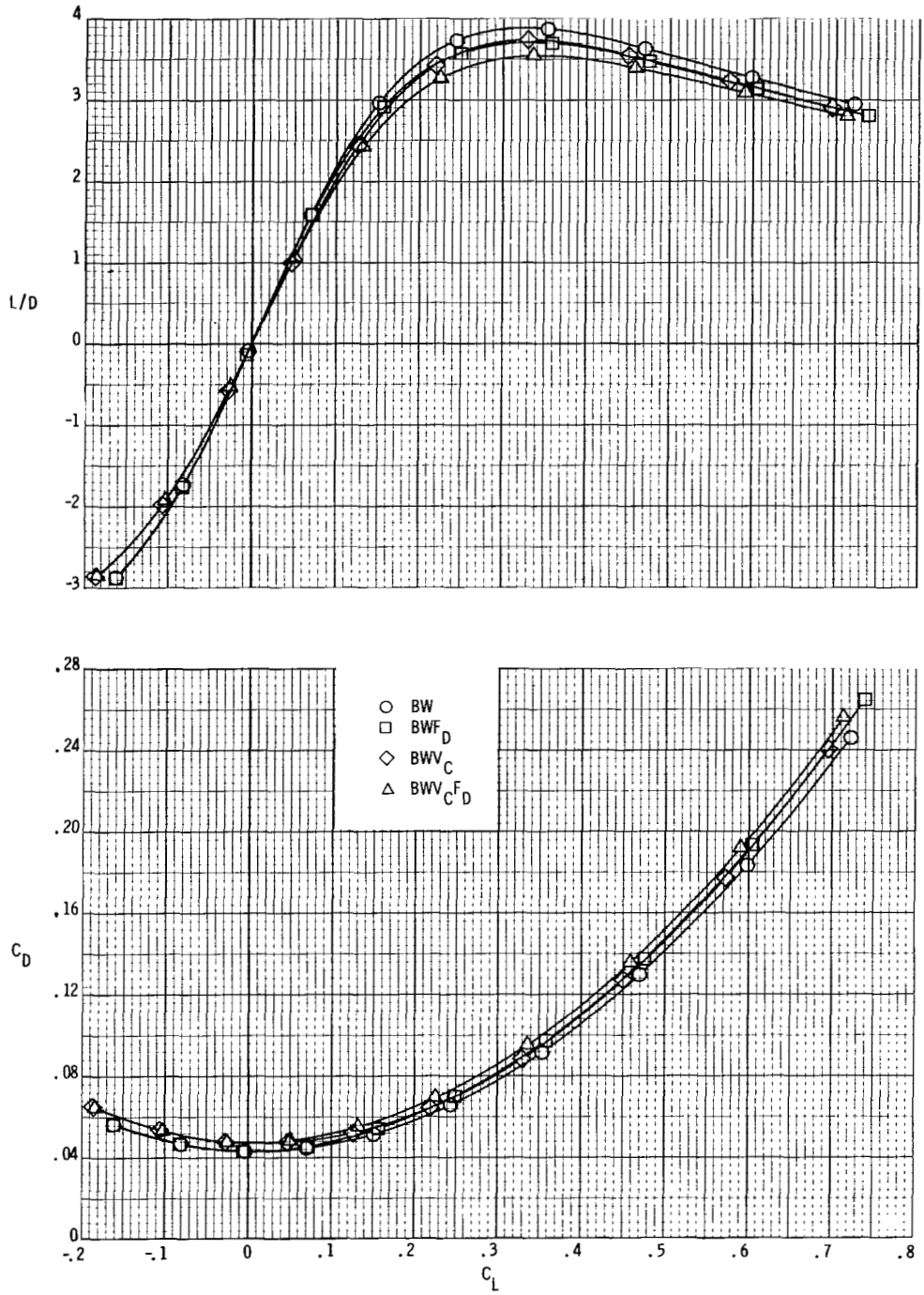

(d) Concluded.

Figure 6.- Continued.

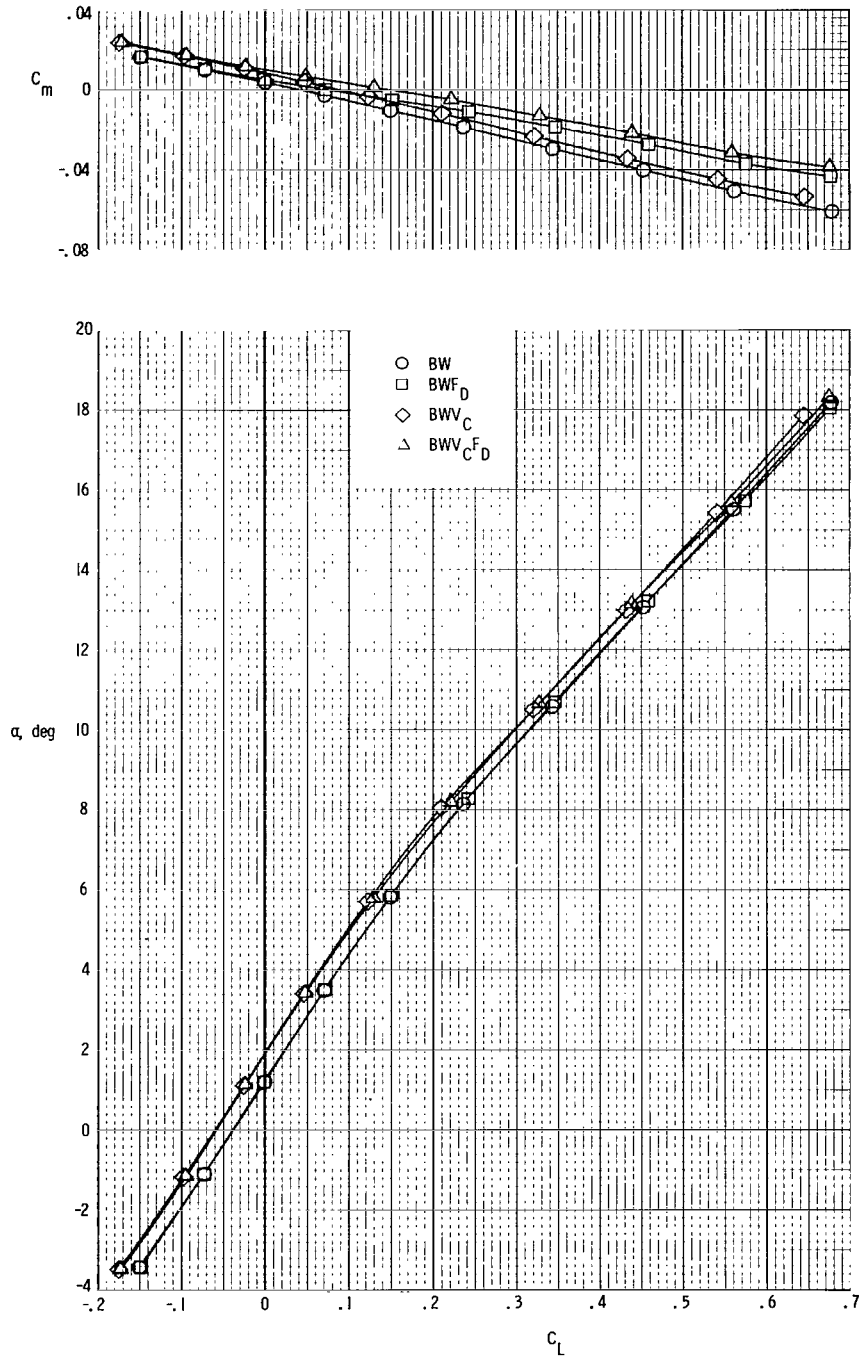

(e) M = 1.10.

Figure 6.- Continued.

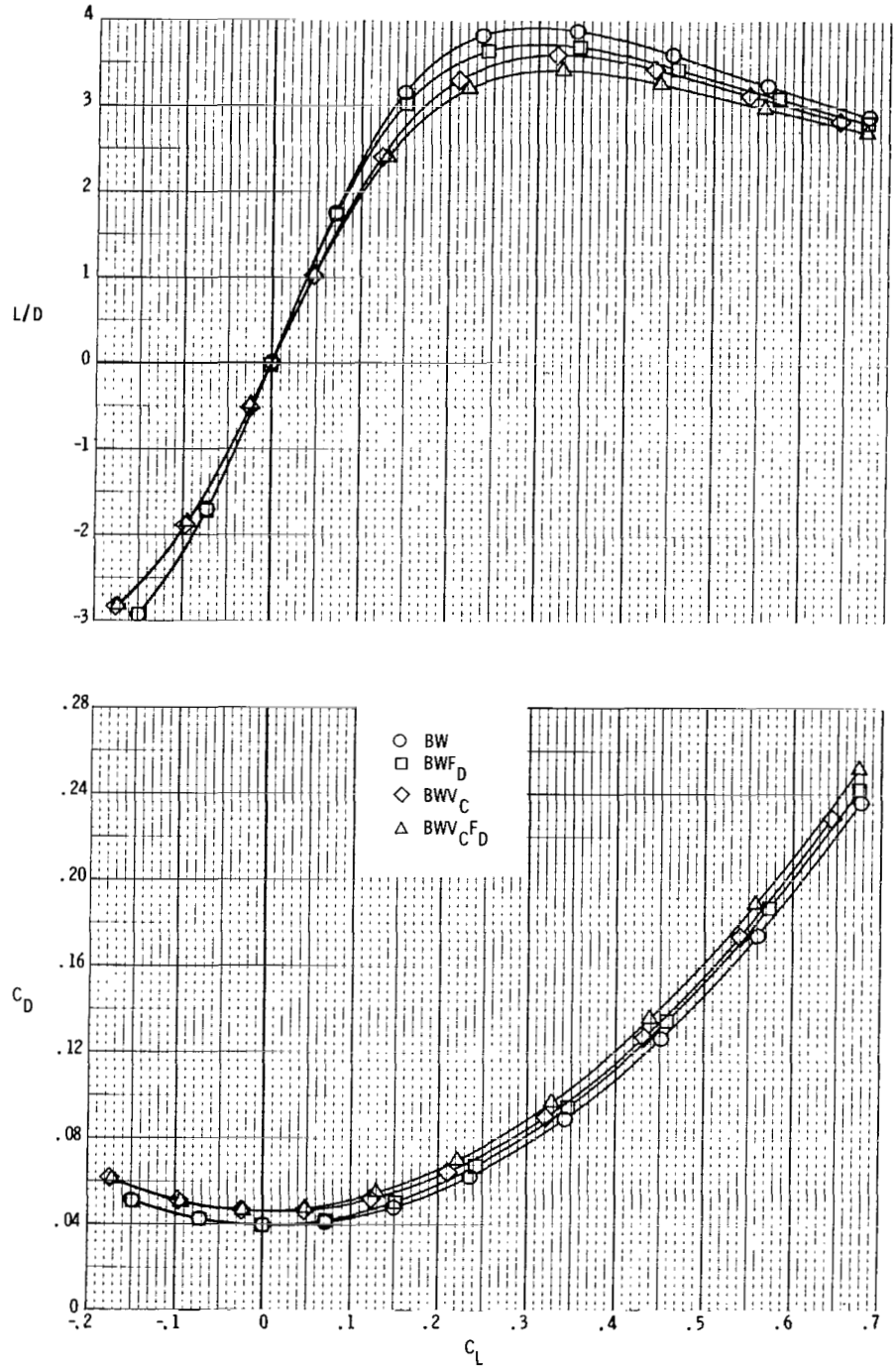

(e) Concluded.

Figure 6.- Continued.

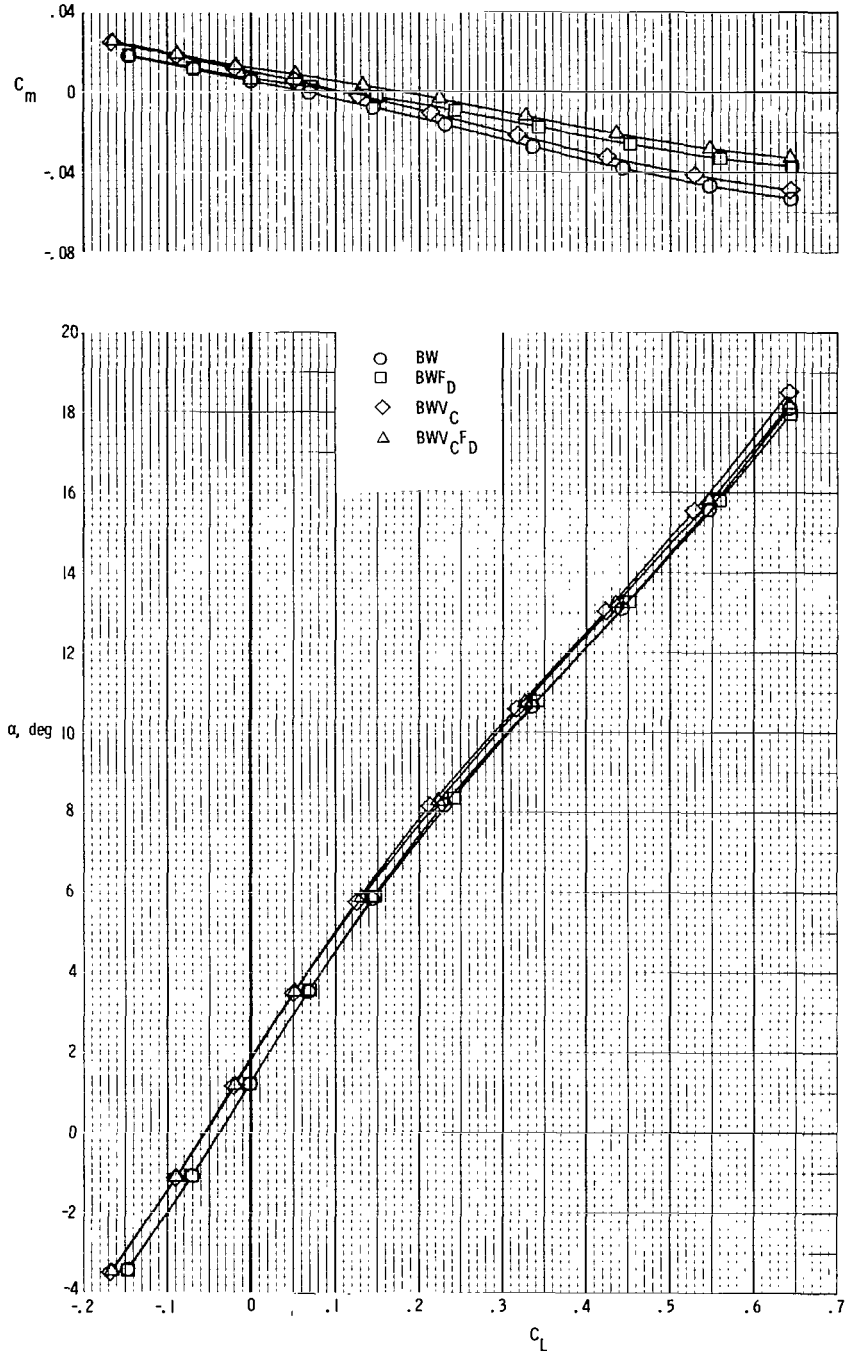

(f) M = 1.20.

Figure 6.- Continued.

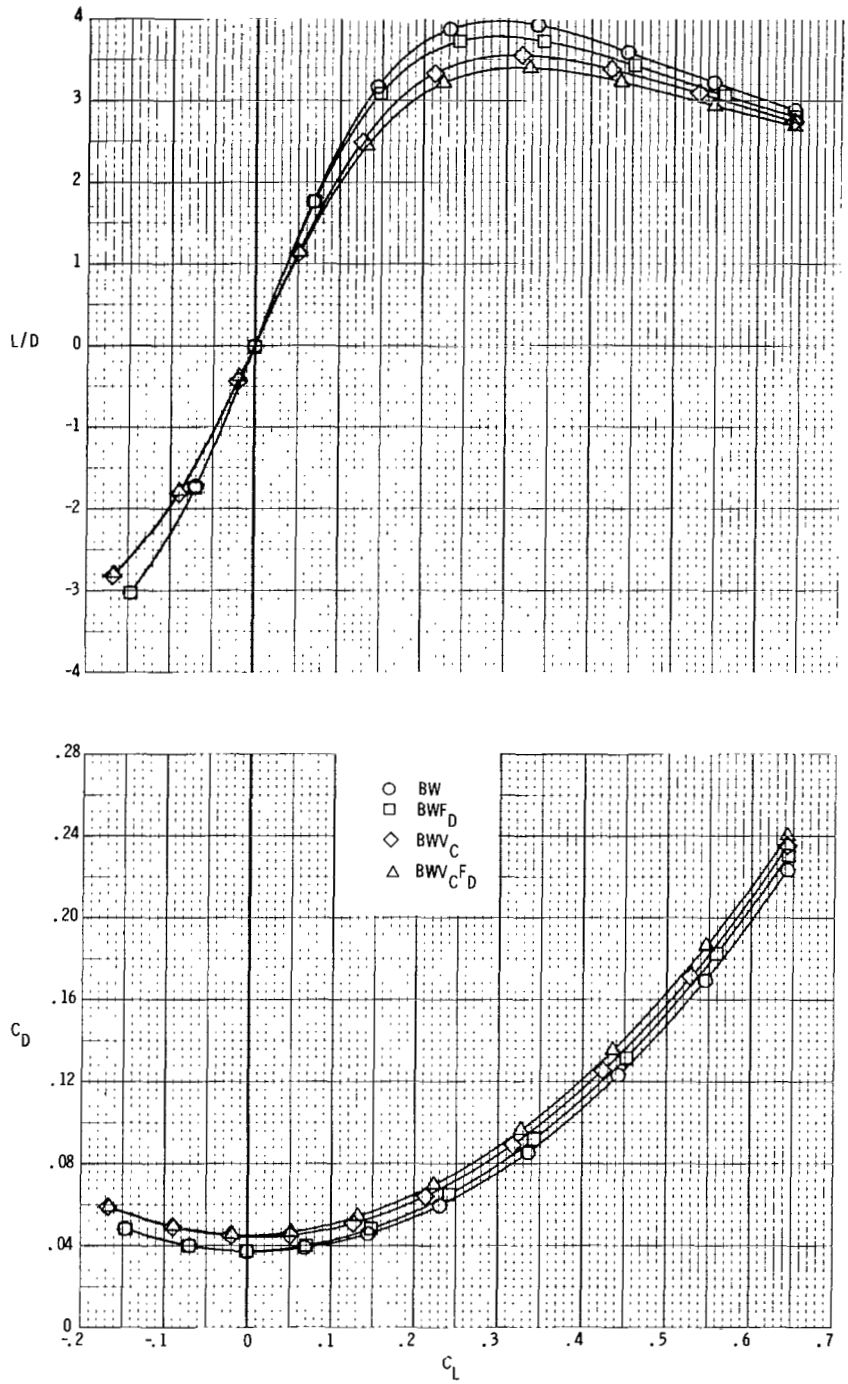

(f) Concluded.

Figure 6.- Concluded.

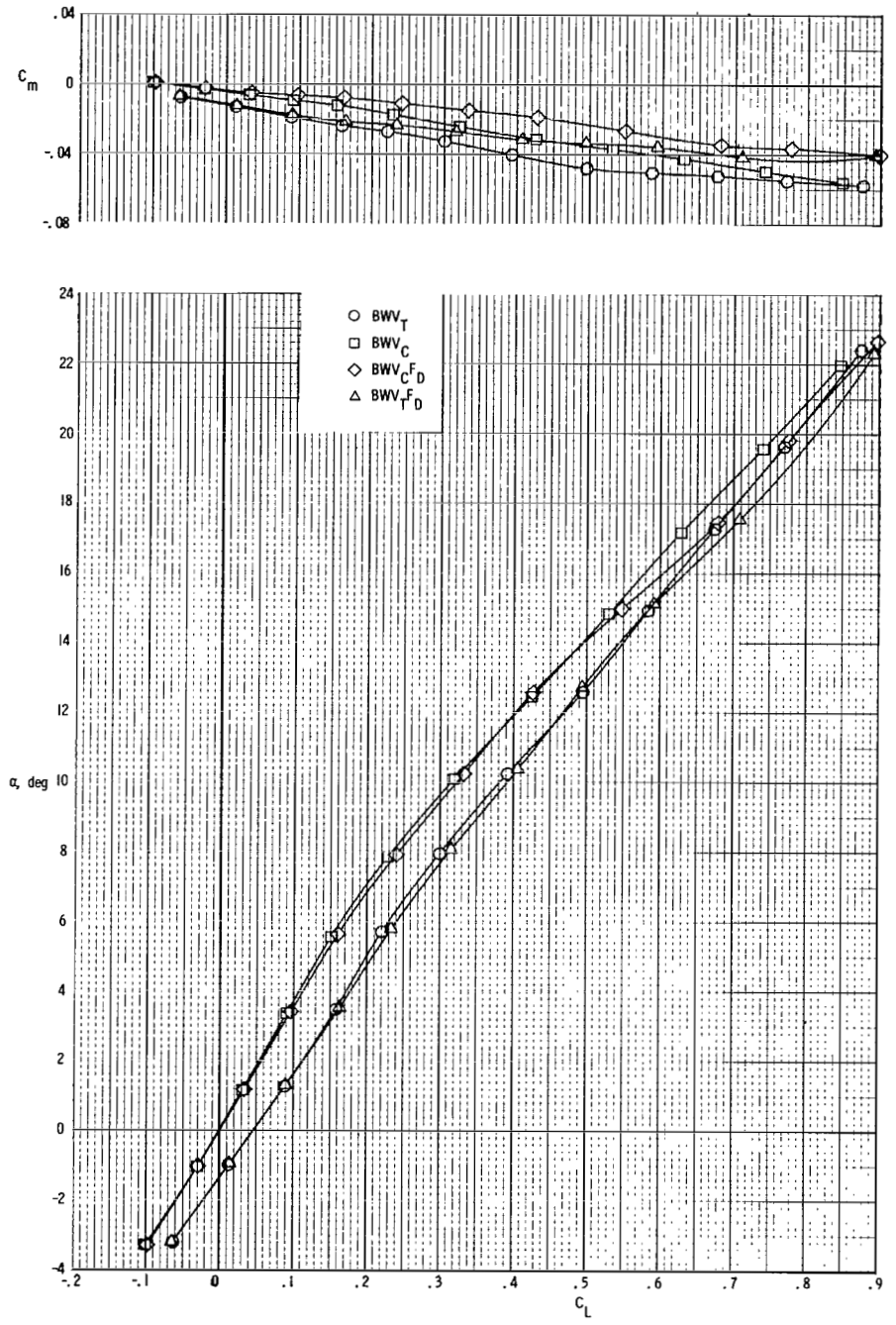

(a) M = 0.80.

Figure 7.- Longitudinal aerodynamic characteristics of tip-fin and center-tail configurations with and without forward delta.

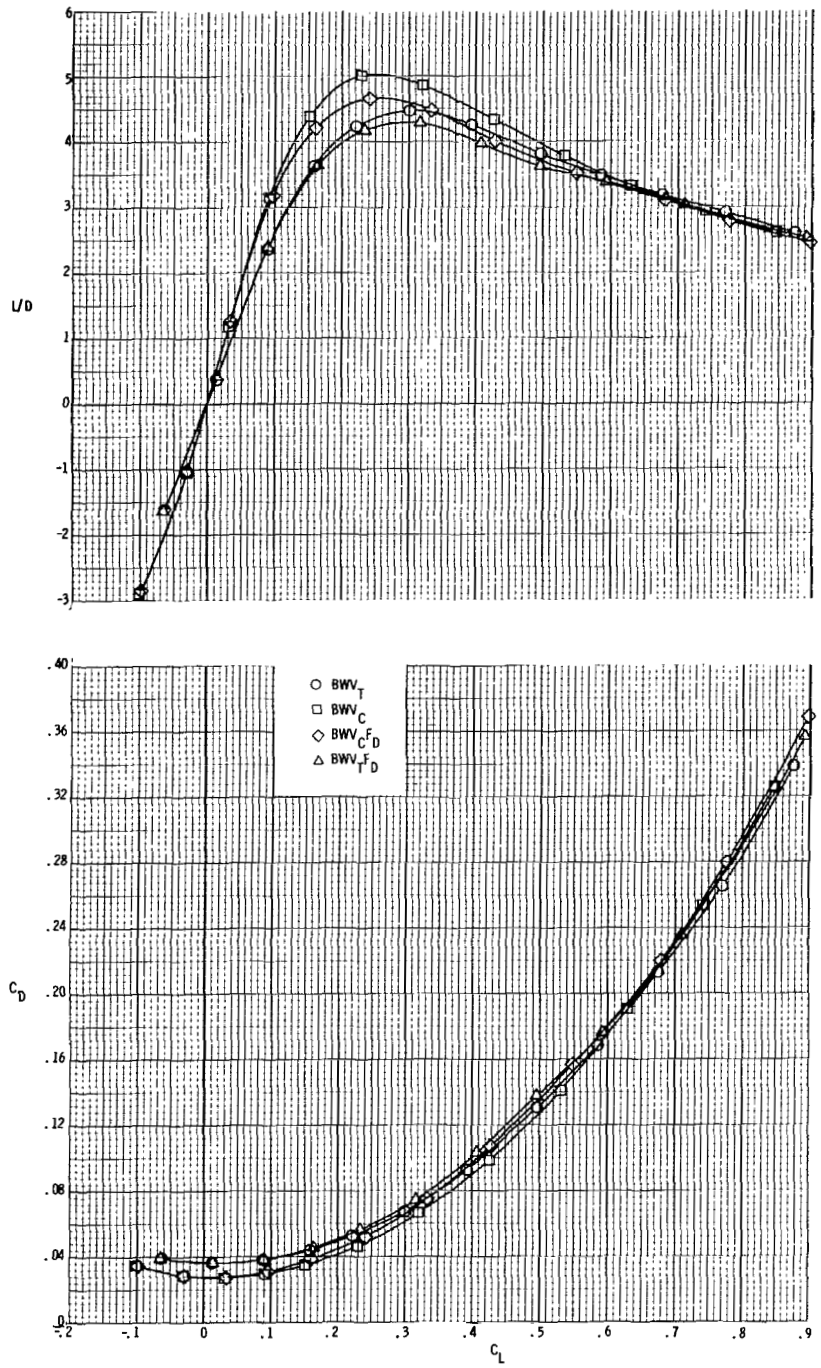

(a) Concluded.

Figure 7.- Continued.

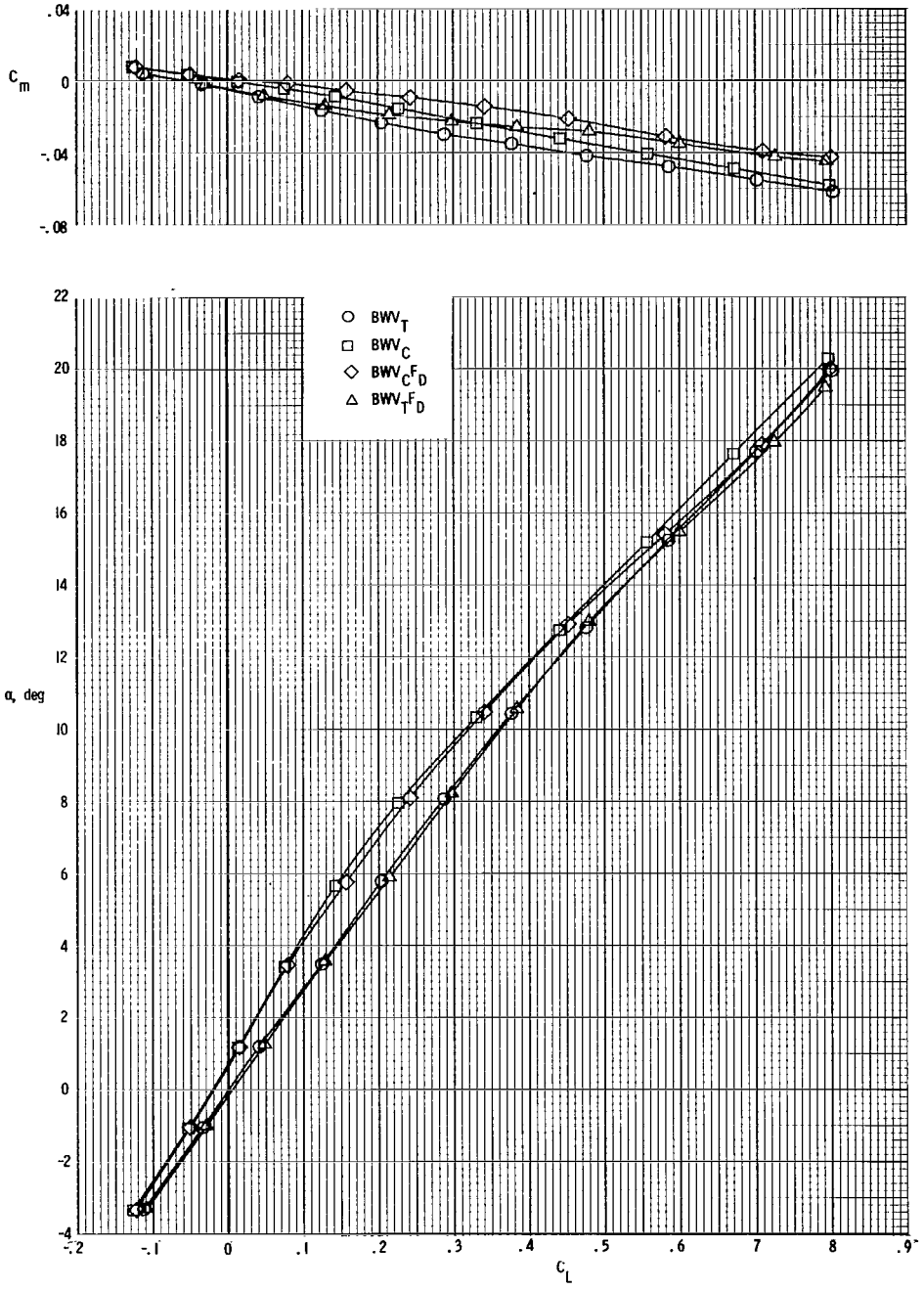

(b) M = 0.90.

Figure 7.- Continued.

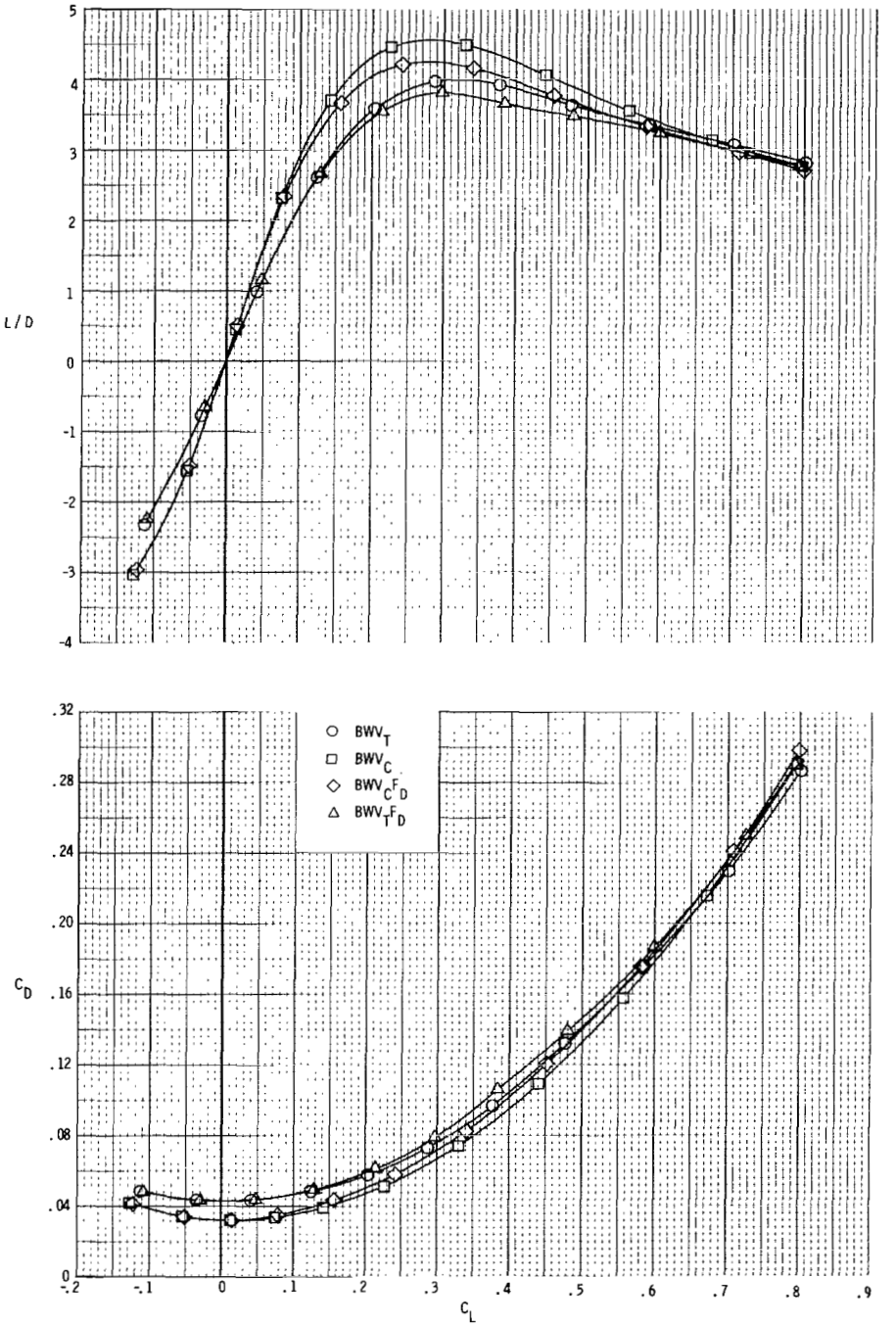

(b) Concluded.

Figure 7.- Continued.

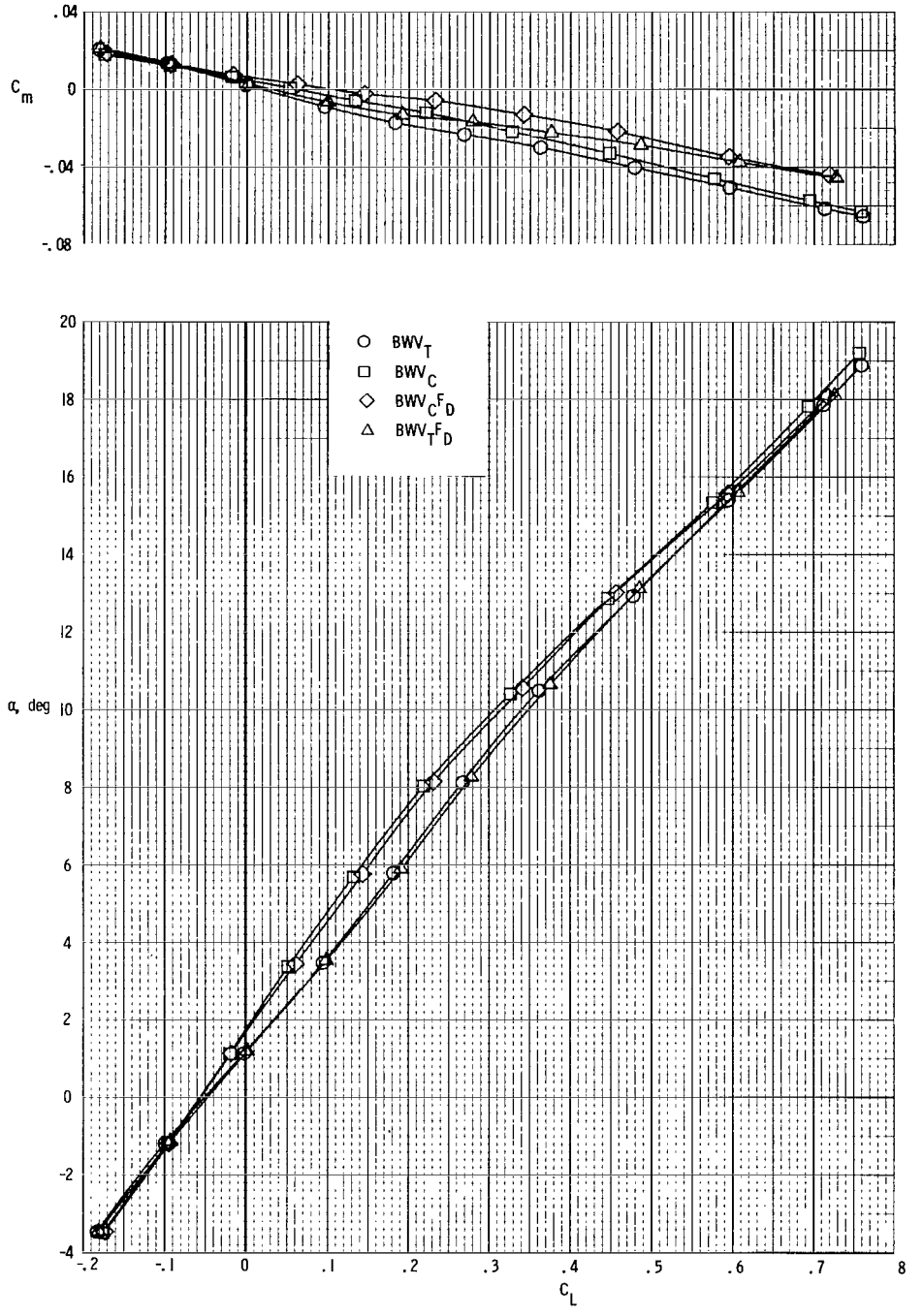

(c) M = 0.95.

Figure 7.- Continued.

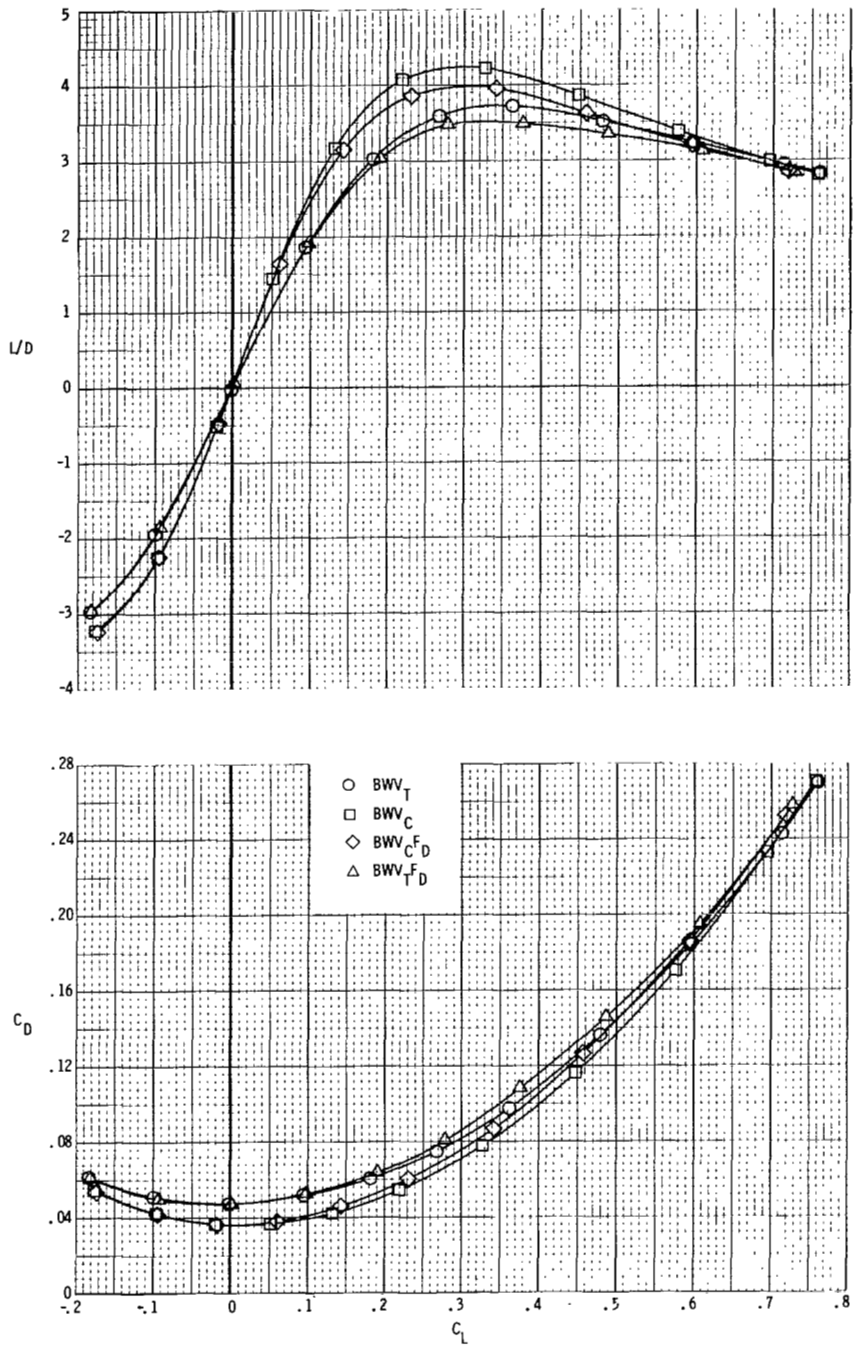

(c) Concluded.

Figure 7.- Continued.

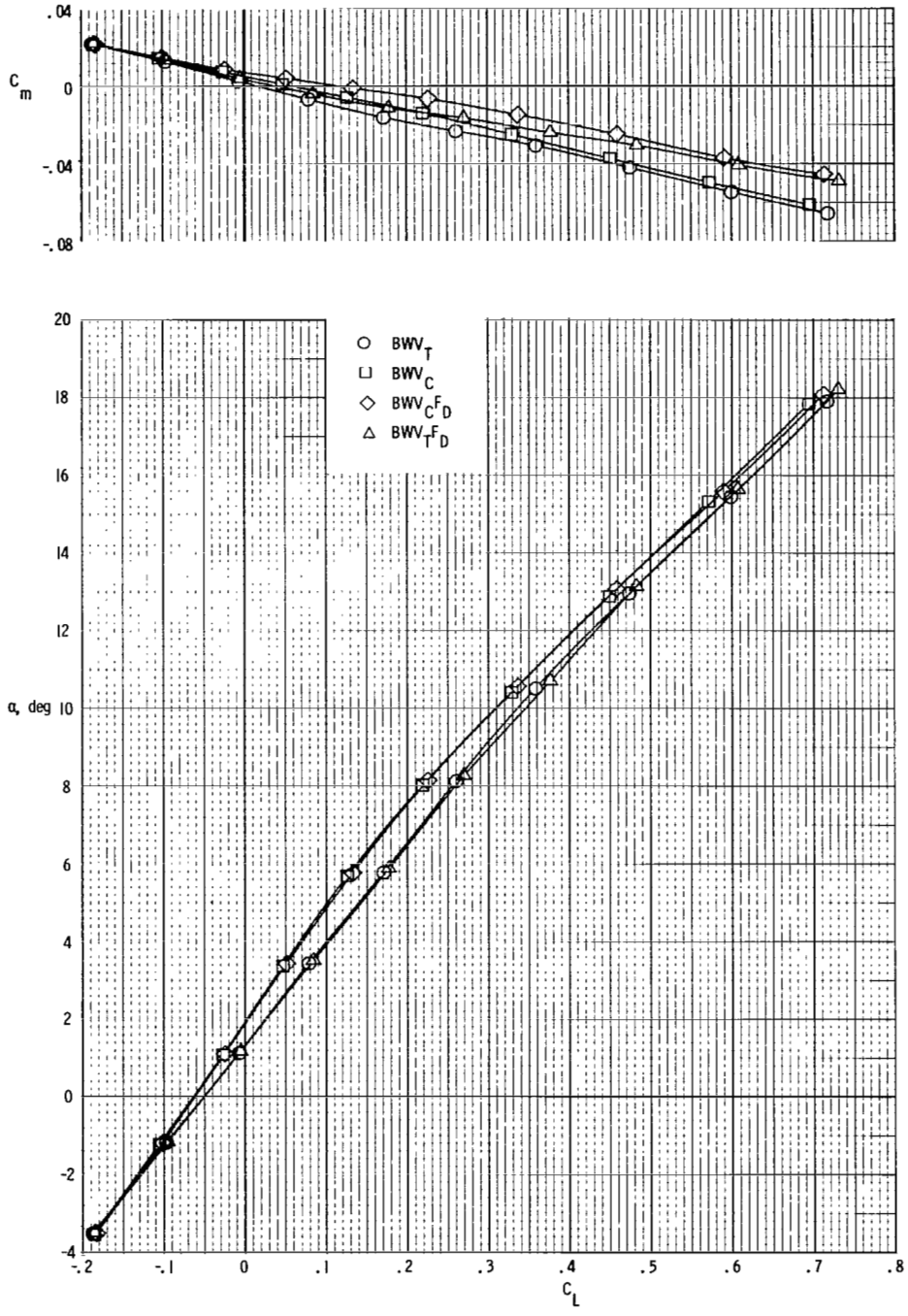

(d) M = 0.98.

Figure 7.- Continued.

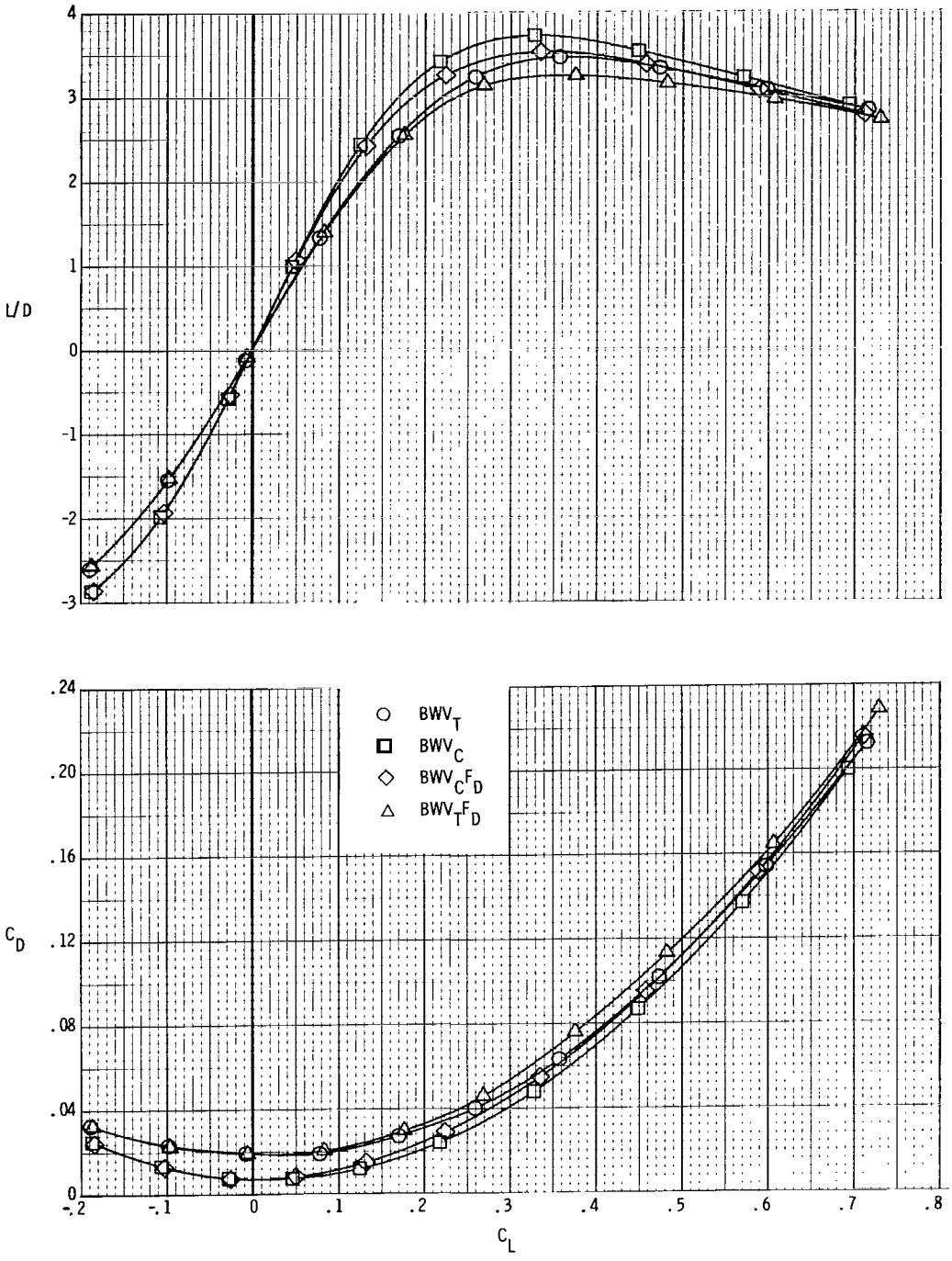

(d) Concluded.

Figure 7.- Continued.

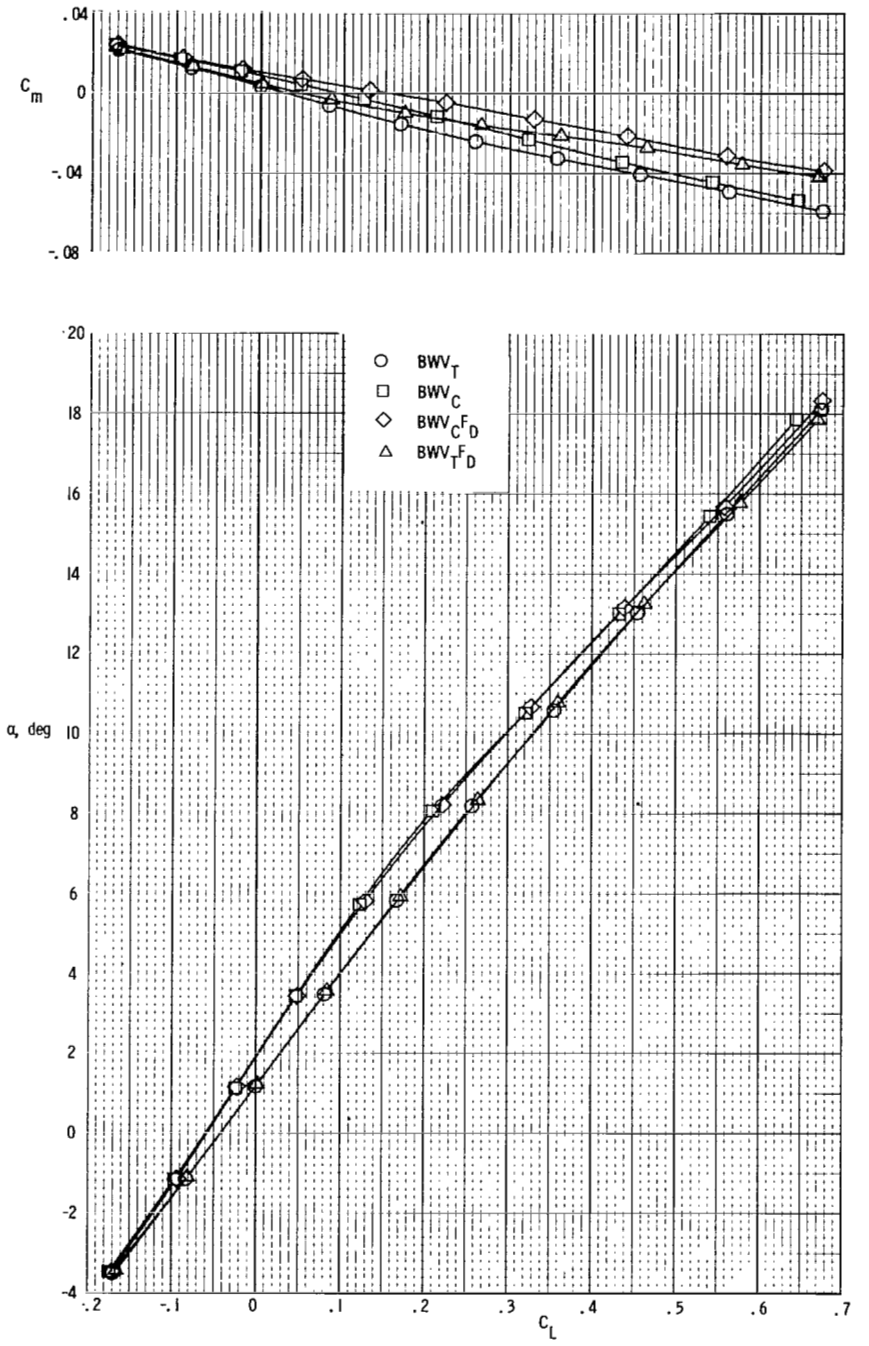

(e) M = 1.10.

Figure 7.- Continued.

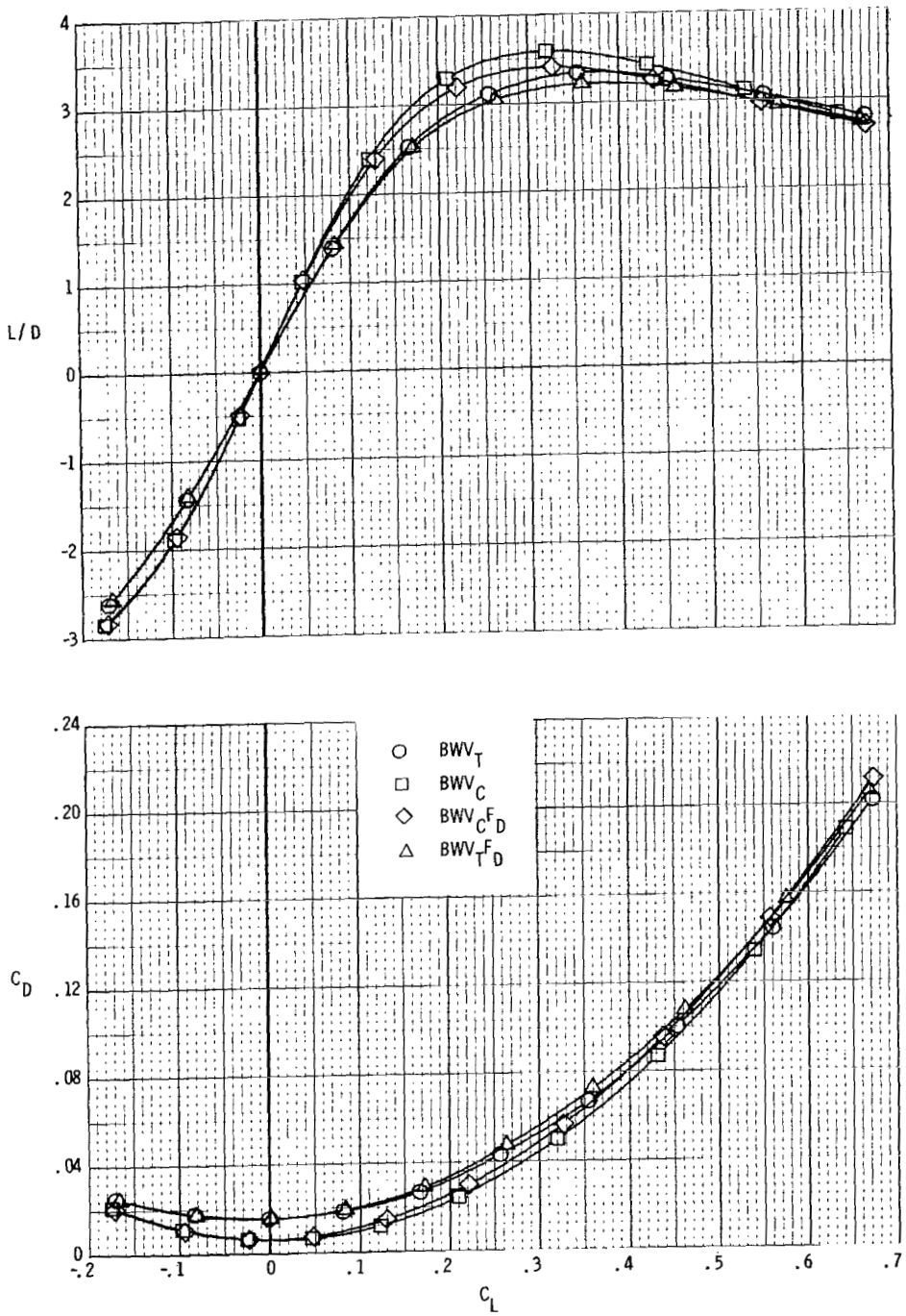

(e) Concluded.

Figure 7.- Continued.

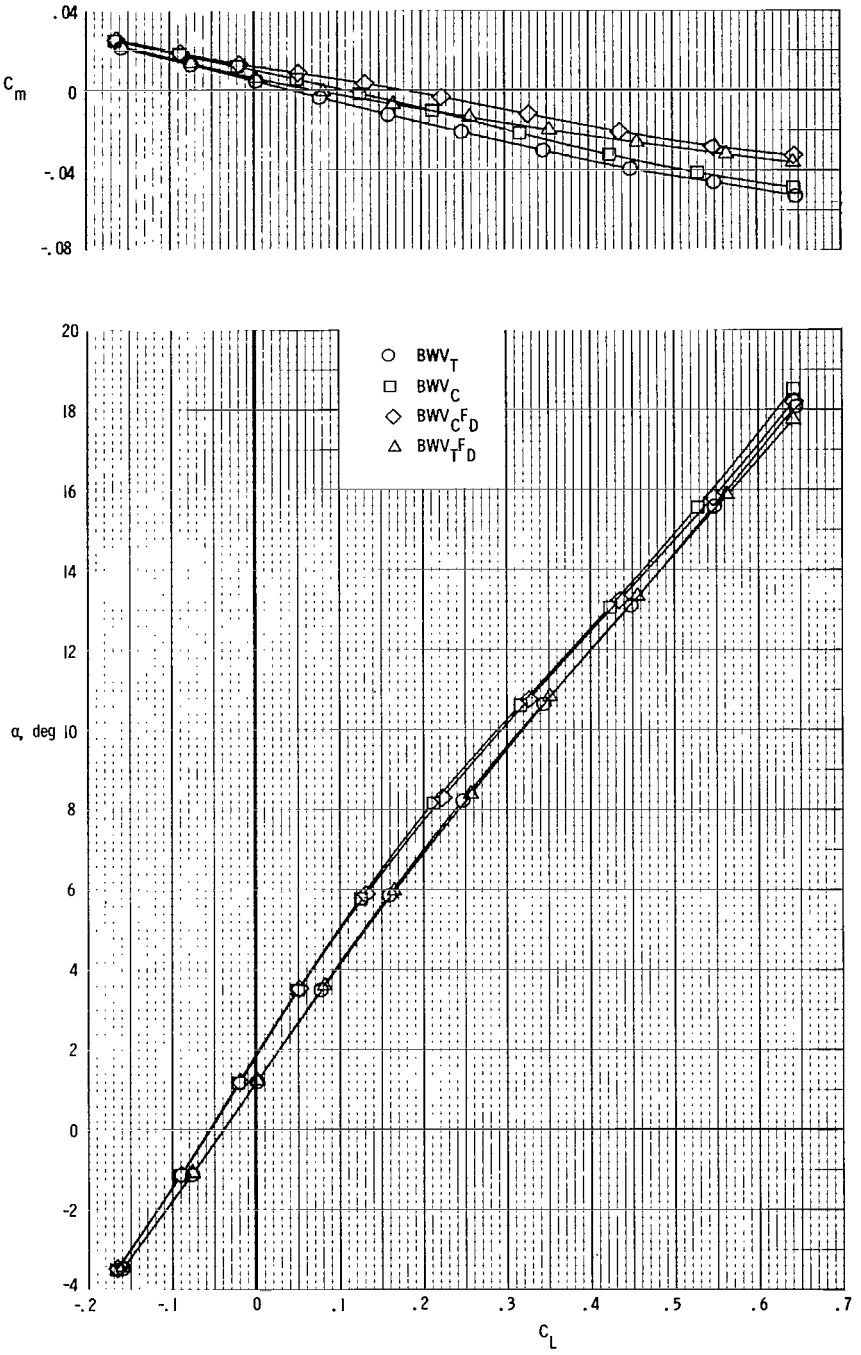

(f) M = 1.20.

Figure 7.- Continued.

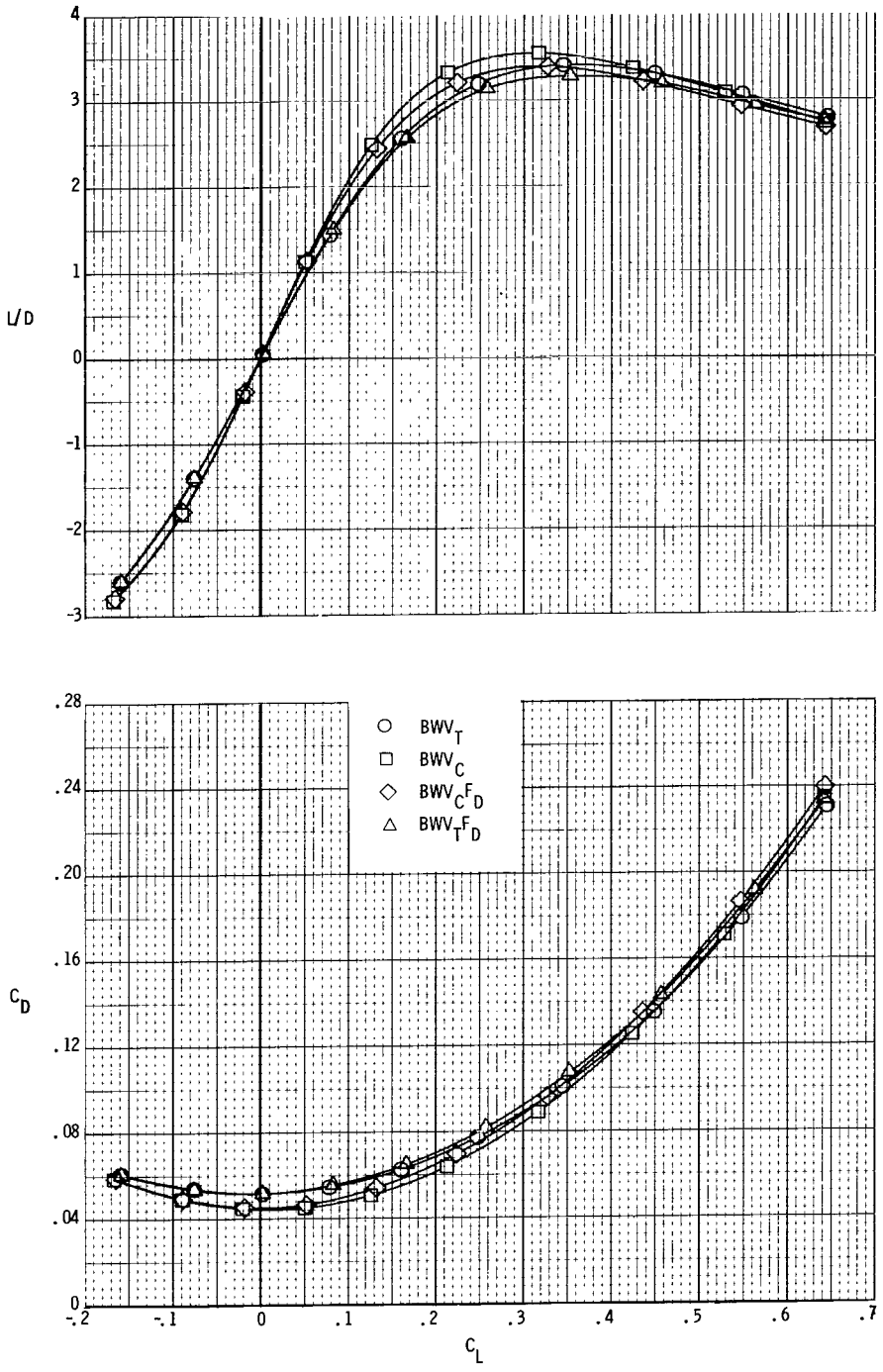

(f) Concluded.

Figure 7.- Concluded.

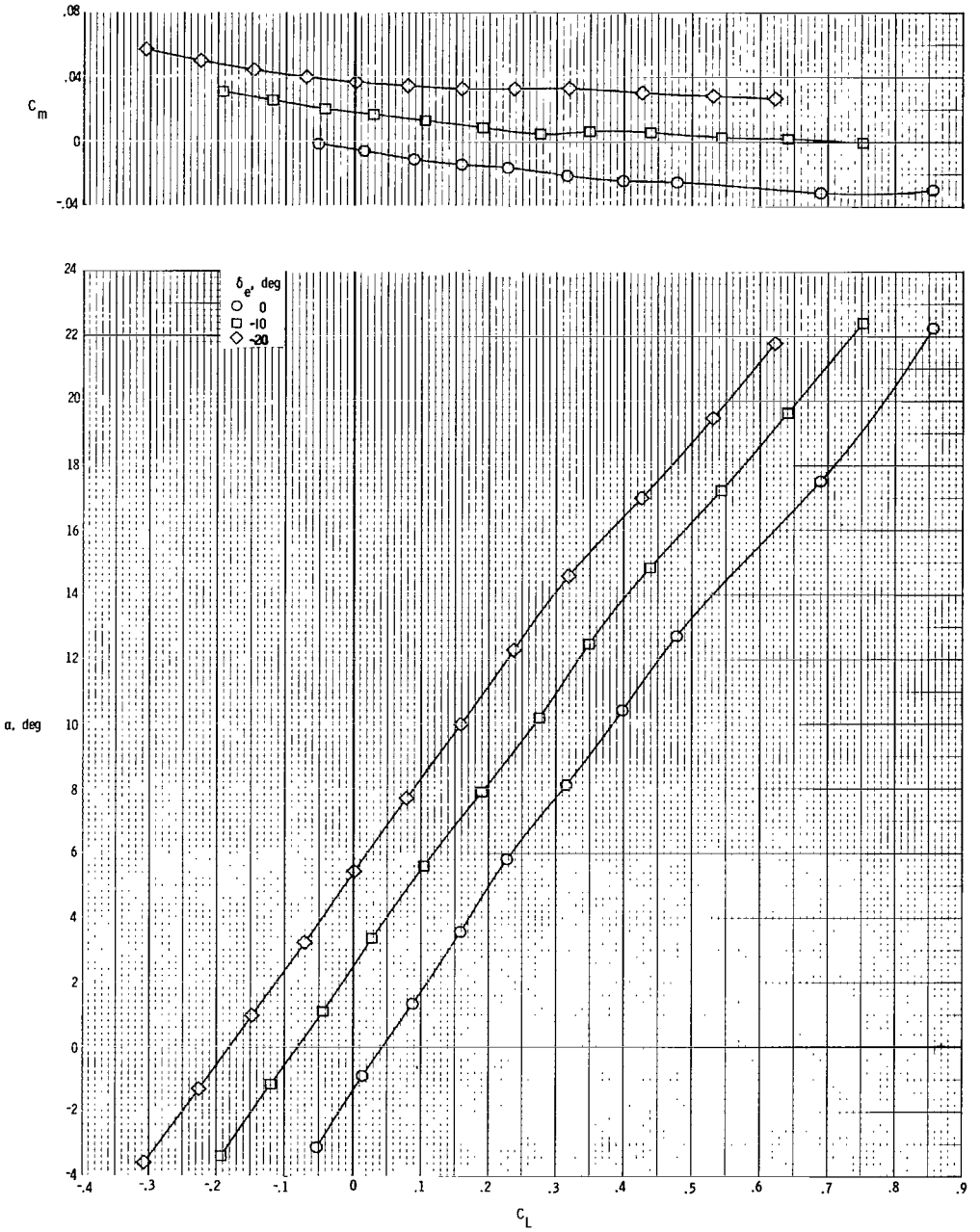

(a) M = 0.80.

Figure 8.- Elevon effects on longitudinal aerodynamic characteristics of BWV_TF_DE configuration.

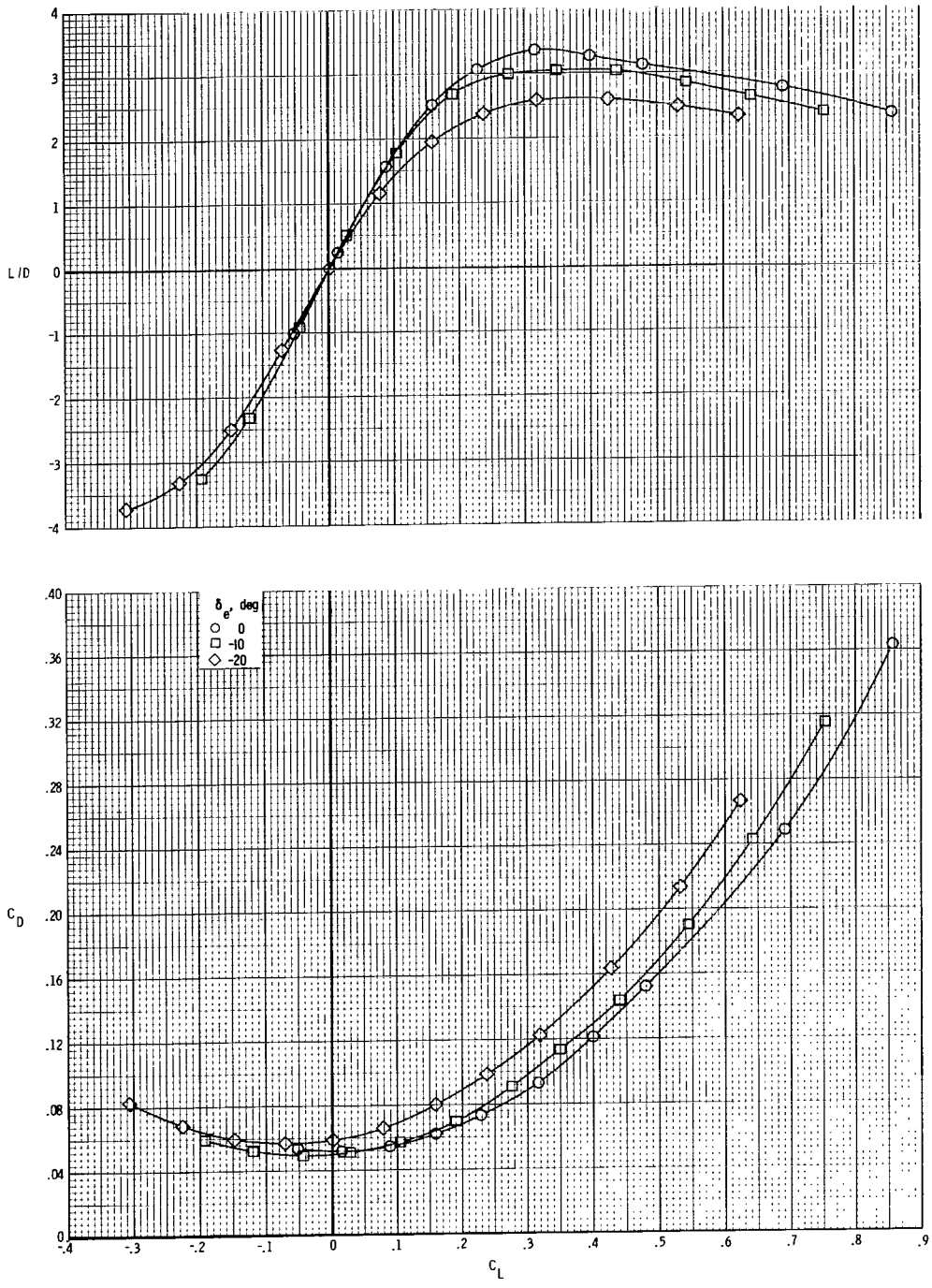

(a) Concluded.

Figure 8.- Continued.

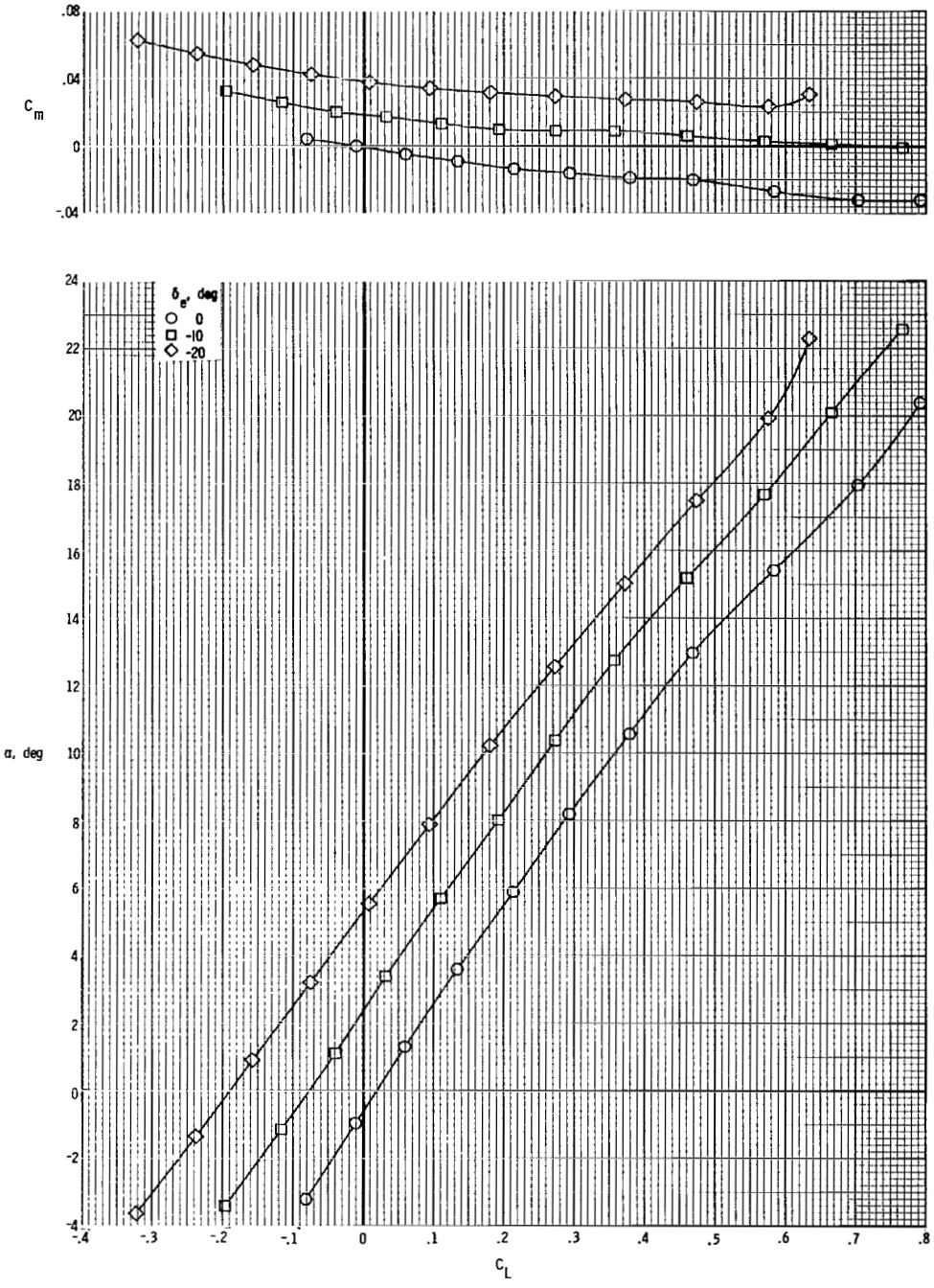

(b) M = 0.90.

Figure 8.- Continued.

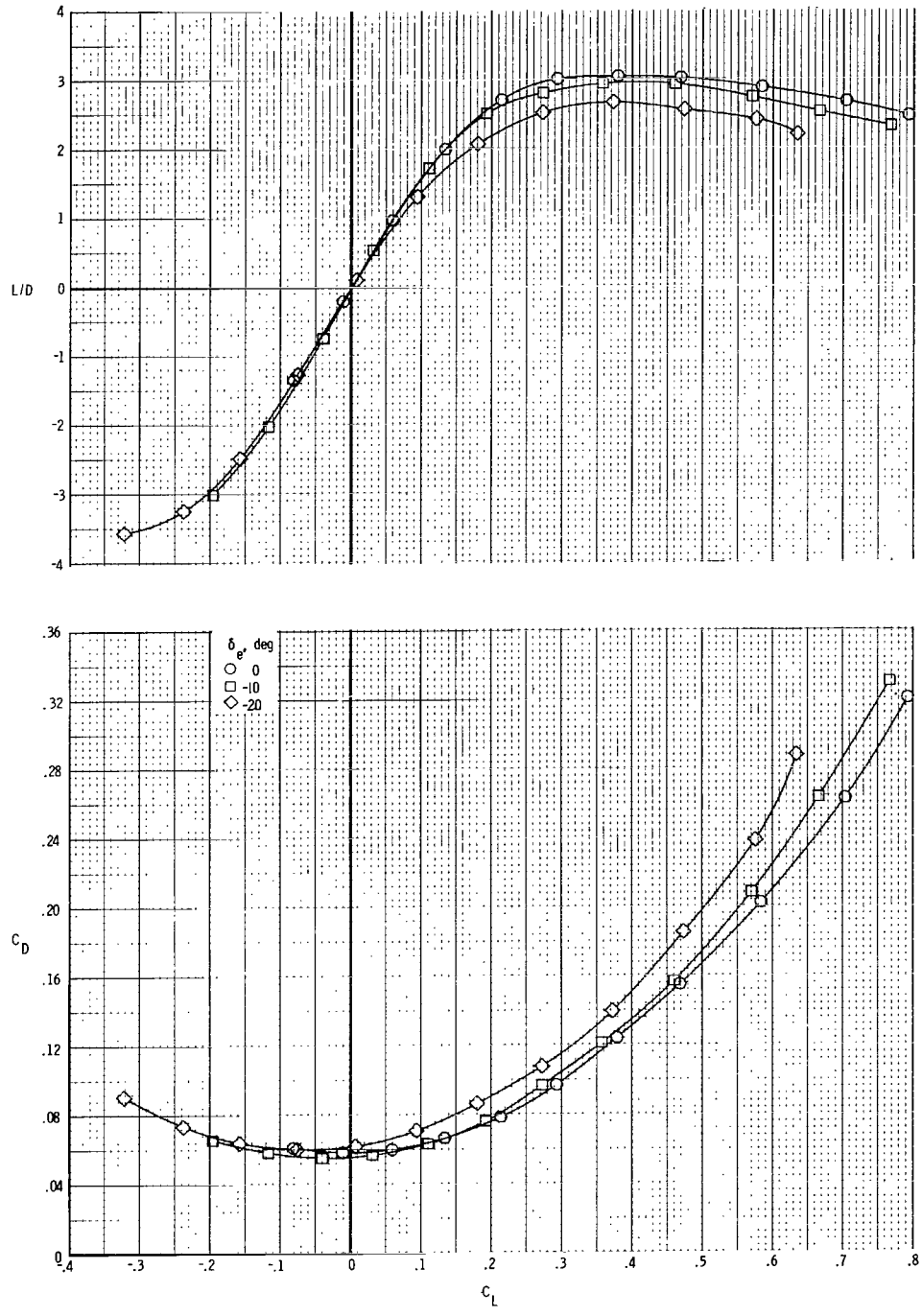

(b) Concluded.

Figure 8.- Continued.

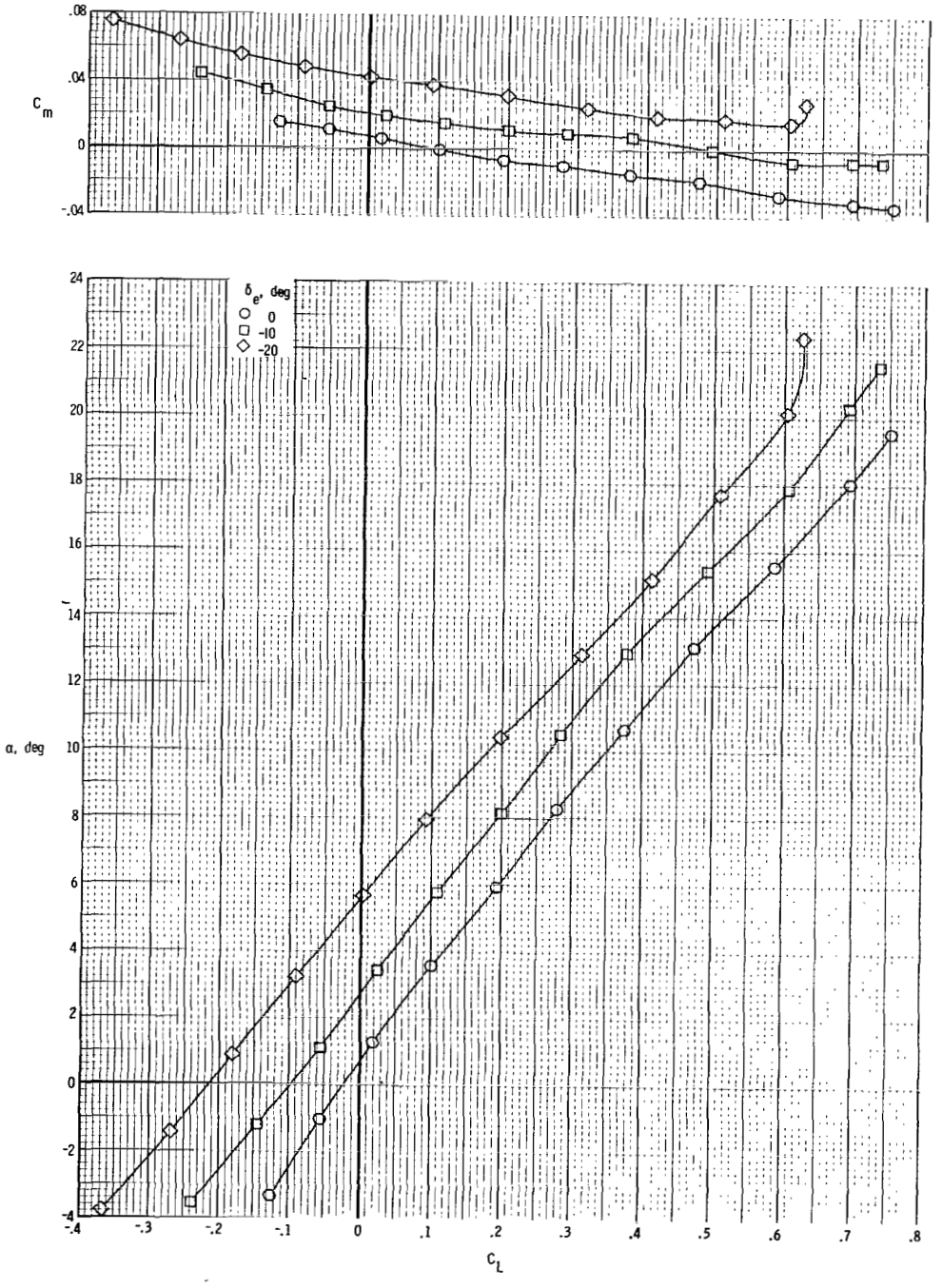

(c) M = 0.95.

Figure 8.- Continued.

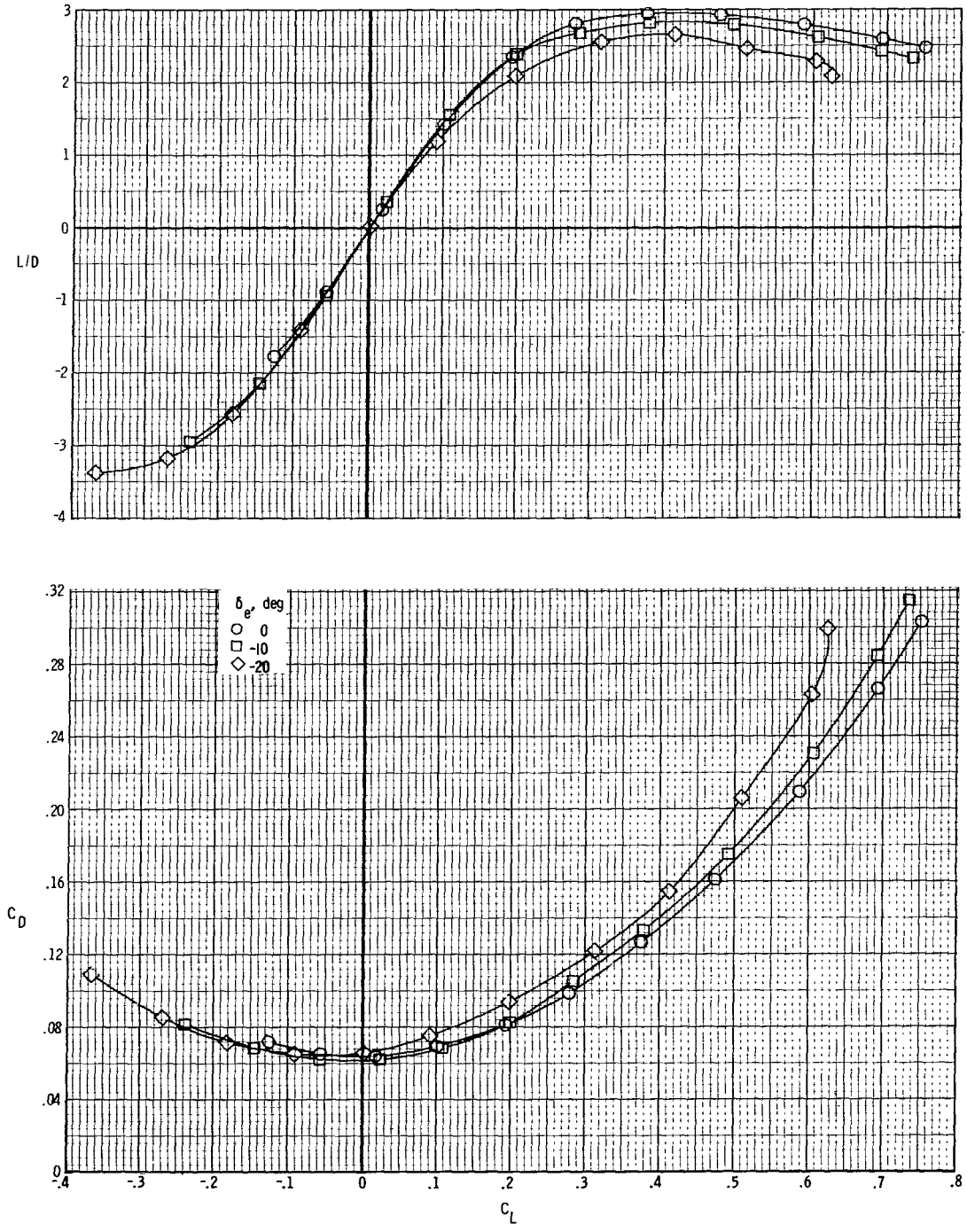

(c) Concluded.

Figure 8.- Continued.

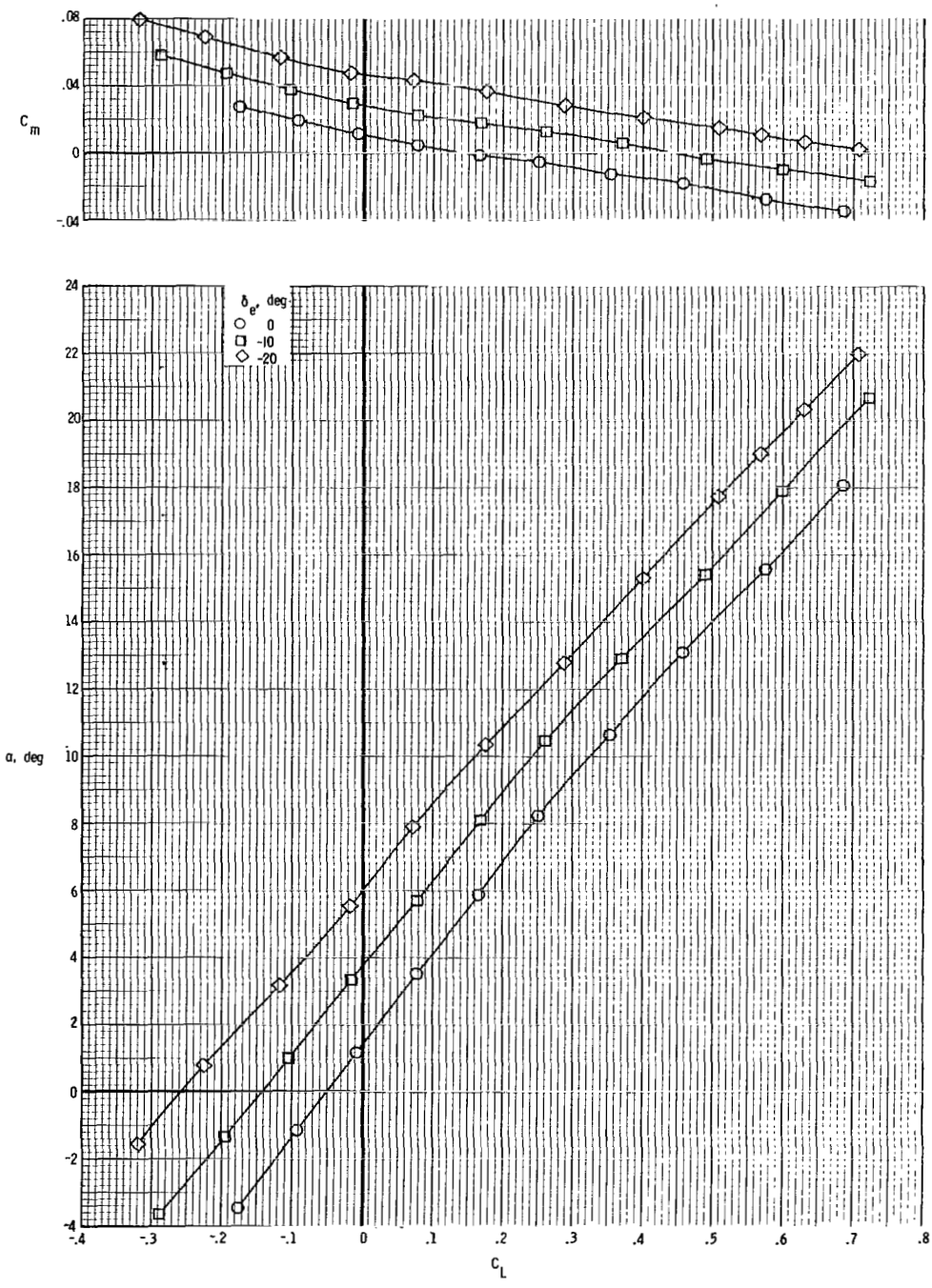

(d) M = 0.98.

Figure 8.- Continued.

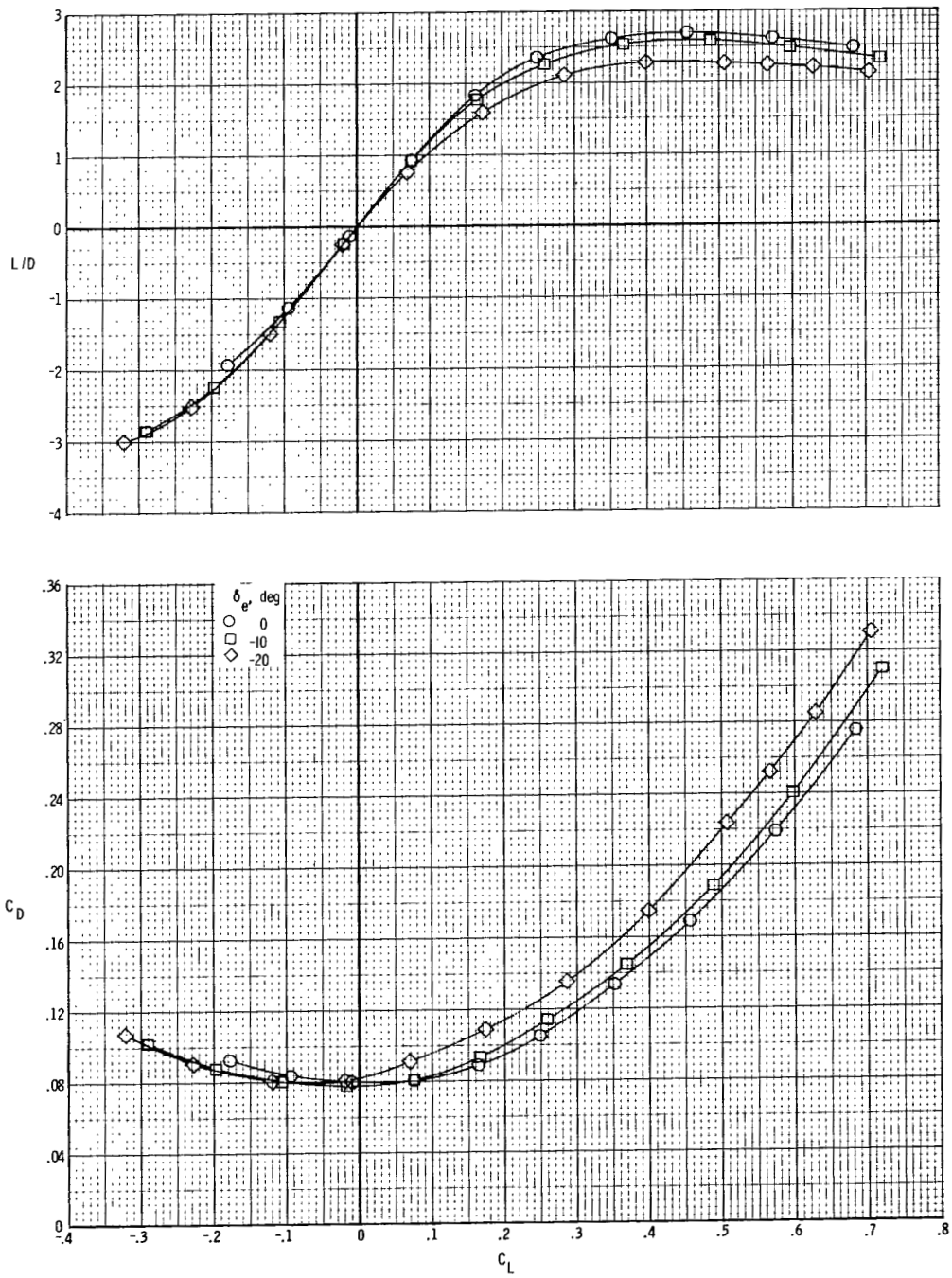

(d) Concluded.

Figure 8.- Continued.

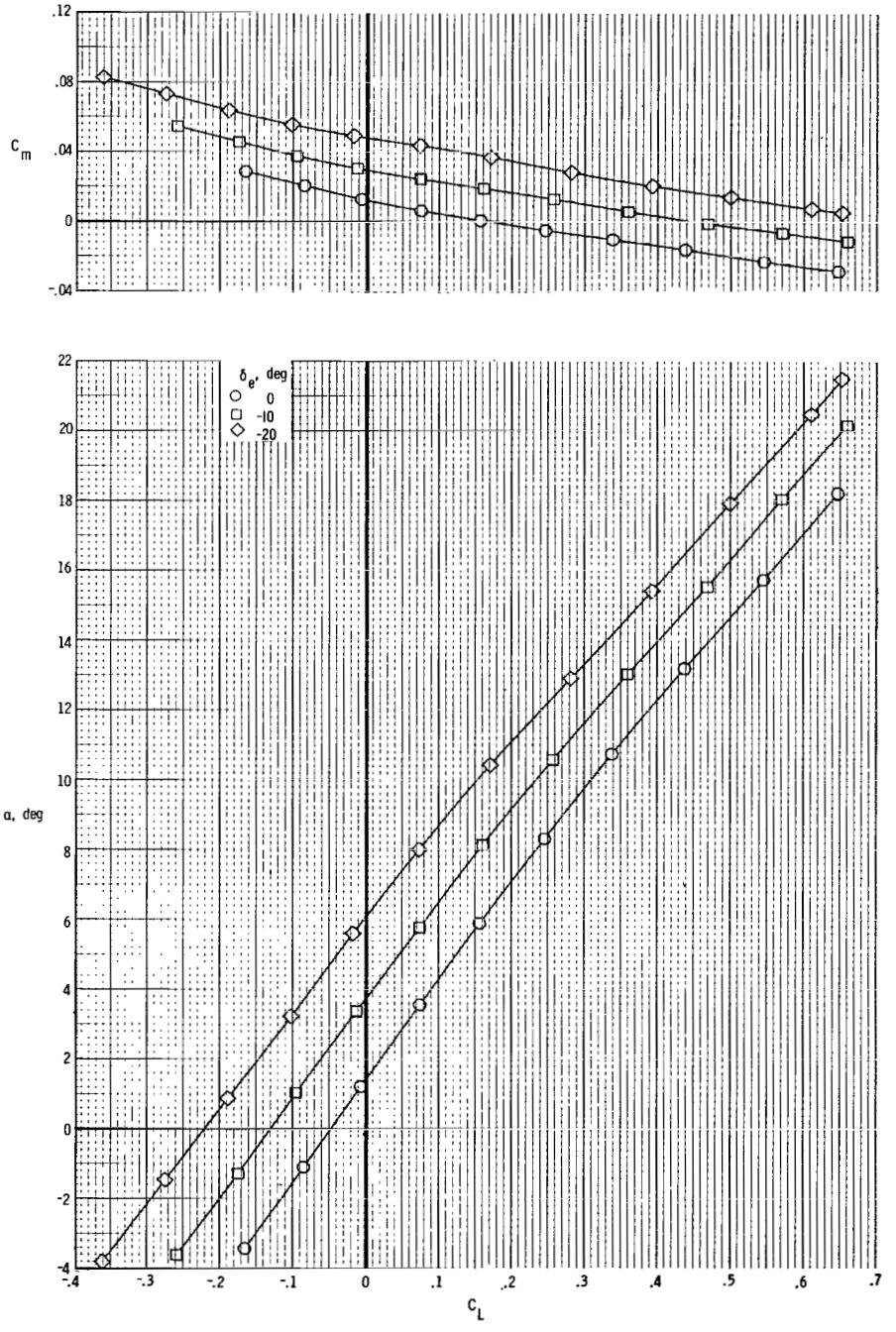

(e) M = 1.10.

Figure 8.- Continued.

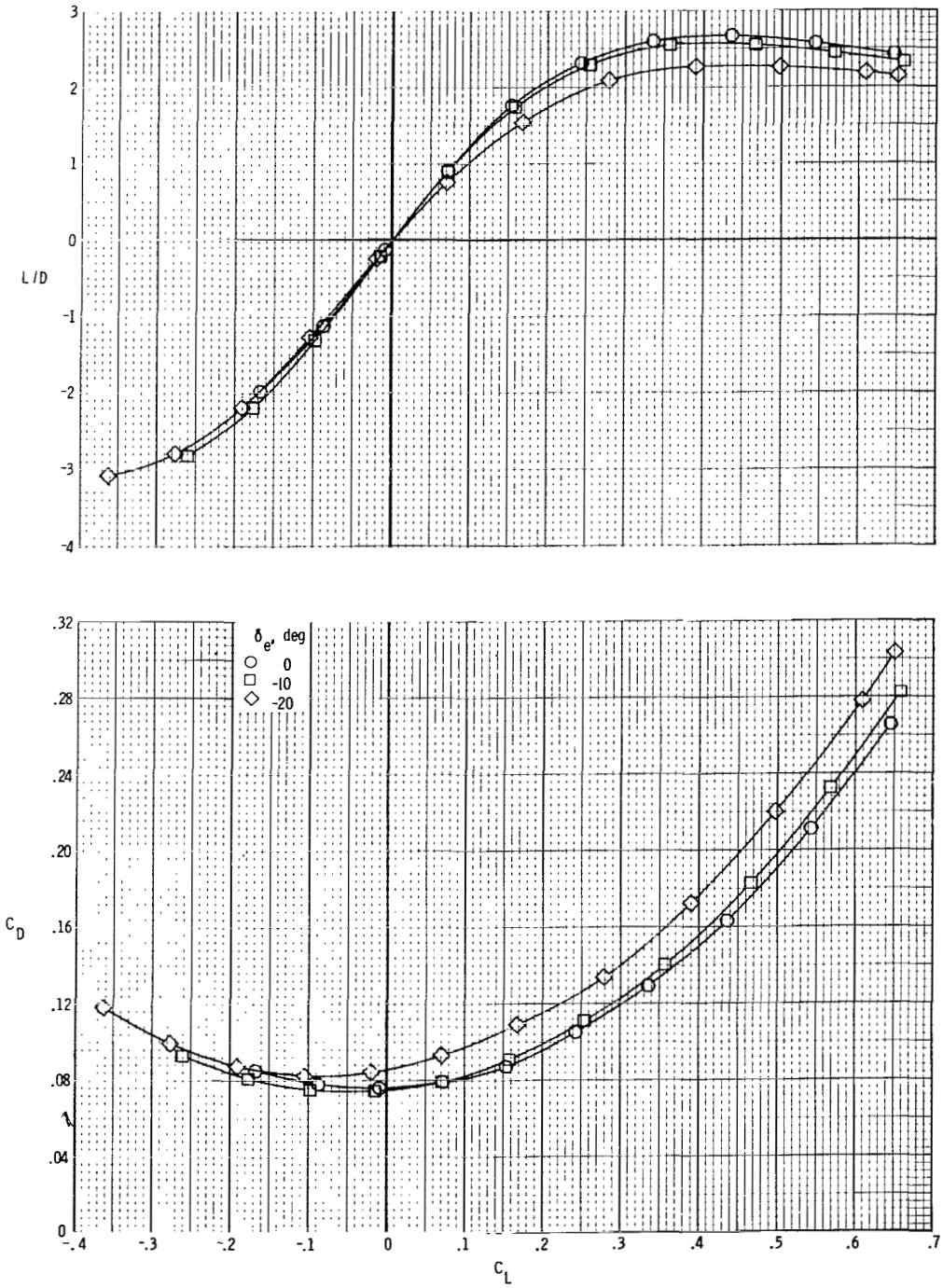

(e) Concluded.

Figure 8.- Continued.

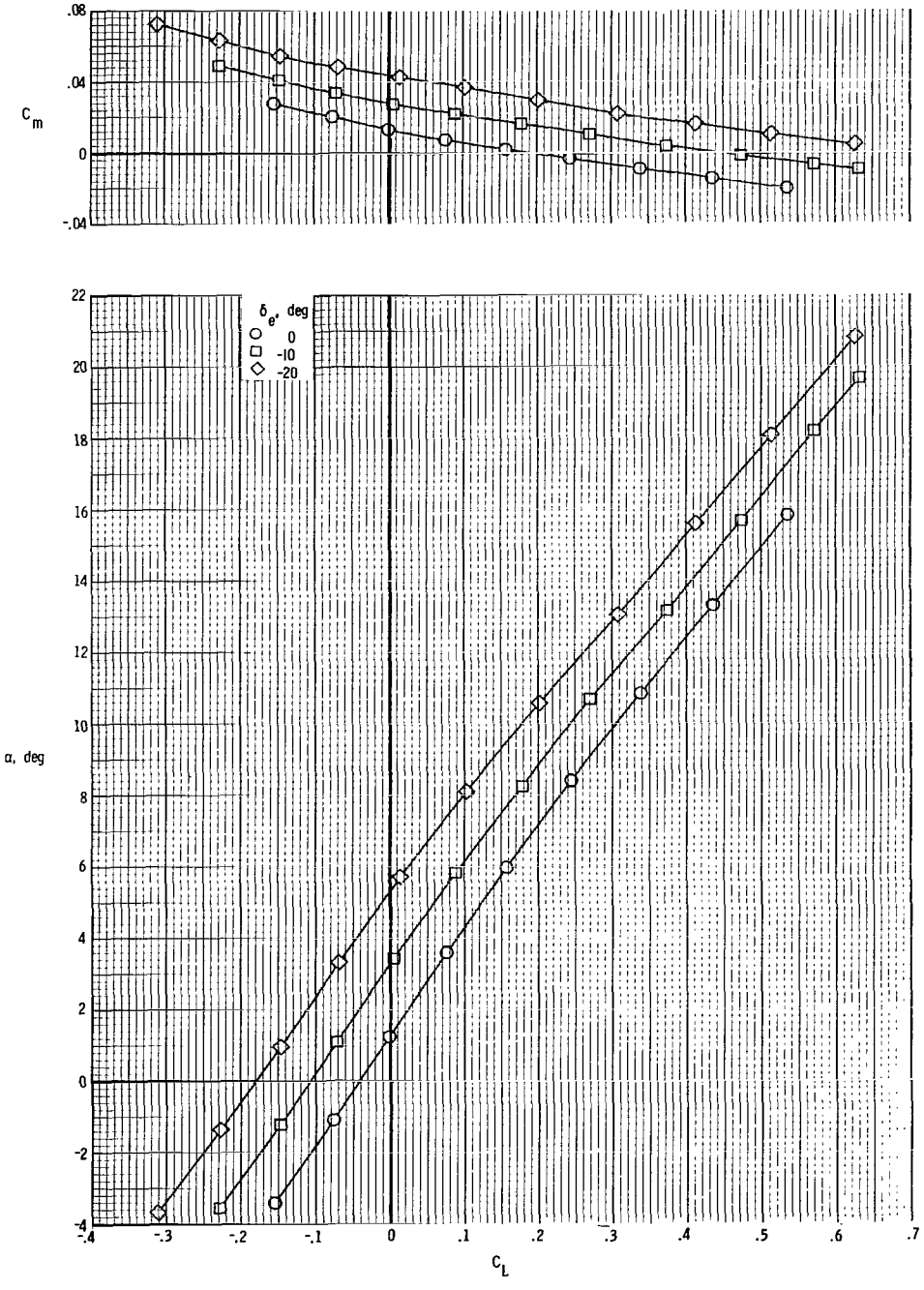

(f) M = 1.20.

Figure 8.- Continued.

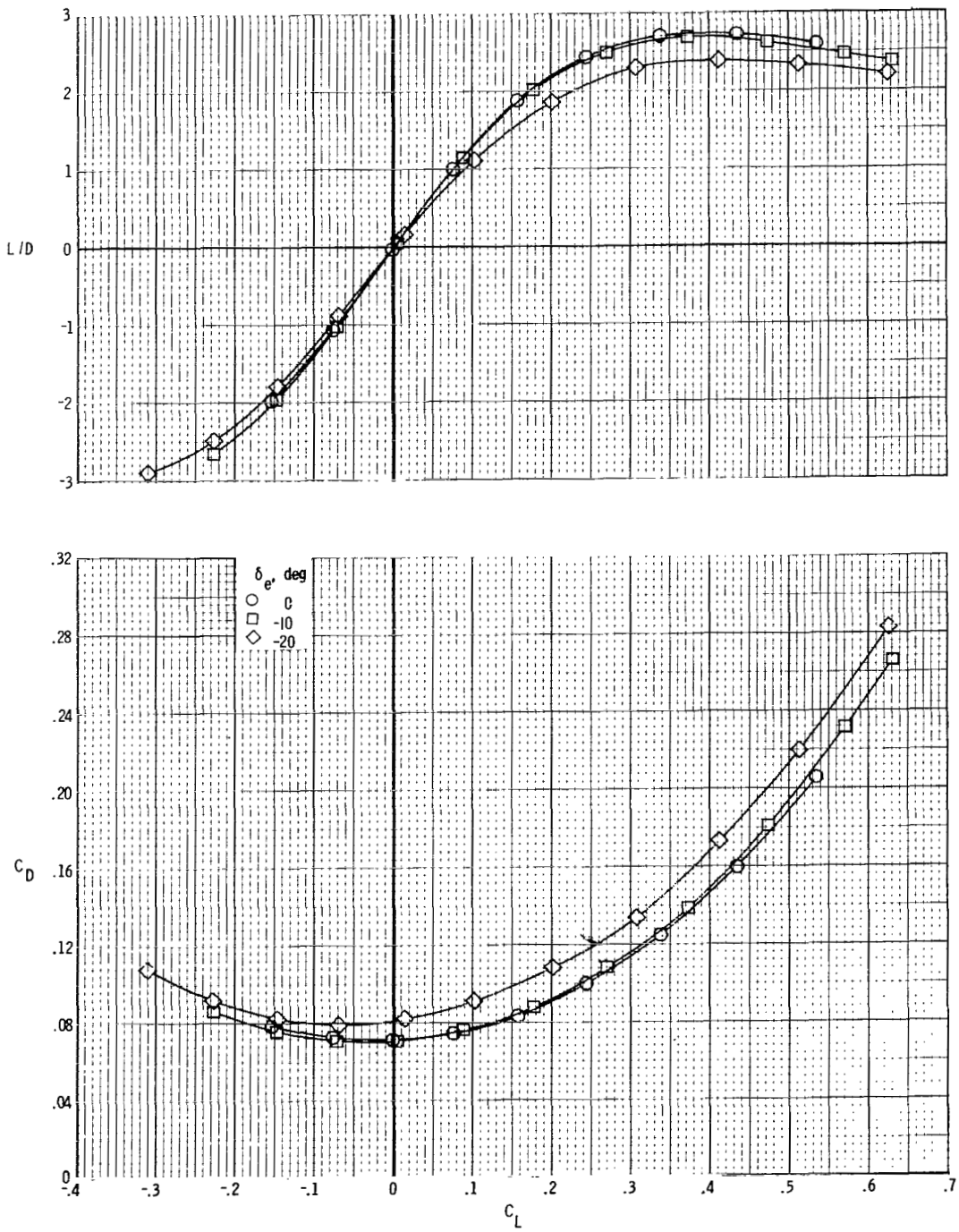

(f) Concluded.

Figure 8.- Concluded.

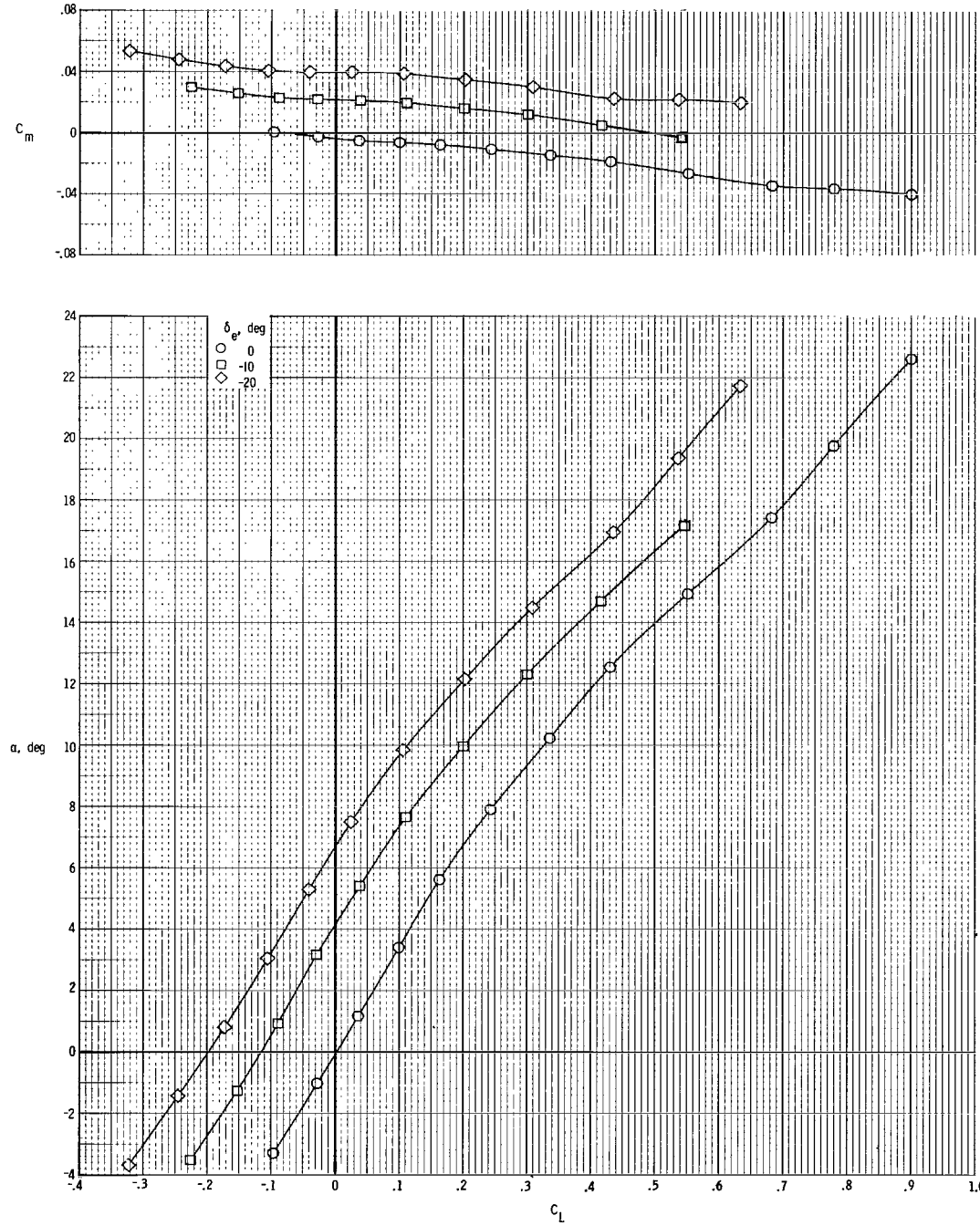

(a) M = 0.80.

Figure 9.- Elevon effects on longitudinal aerodynamic characteristics of BWV_CF_D configuration.

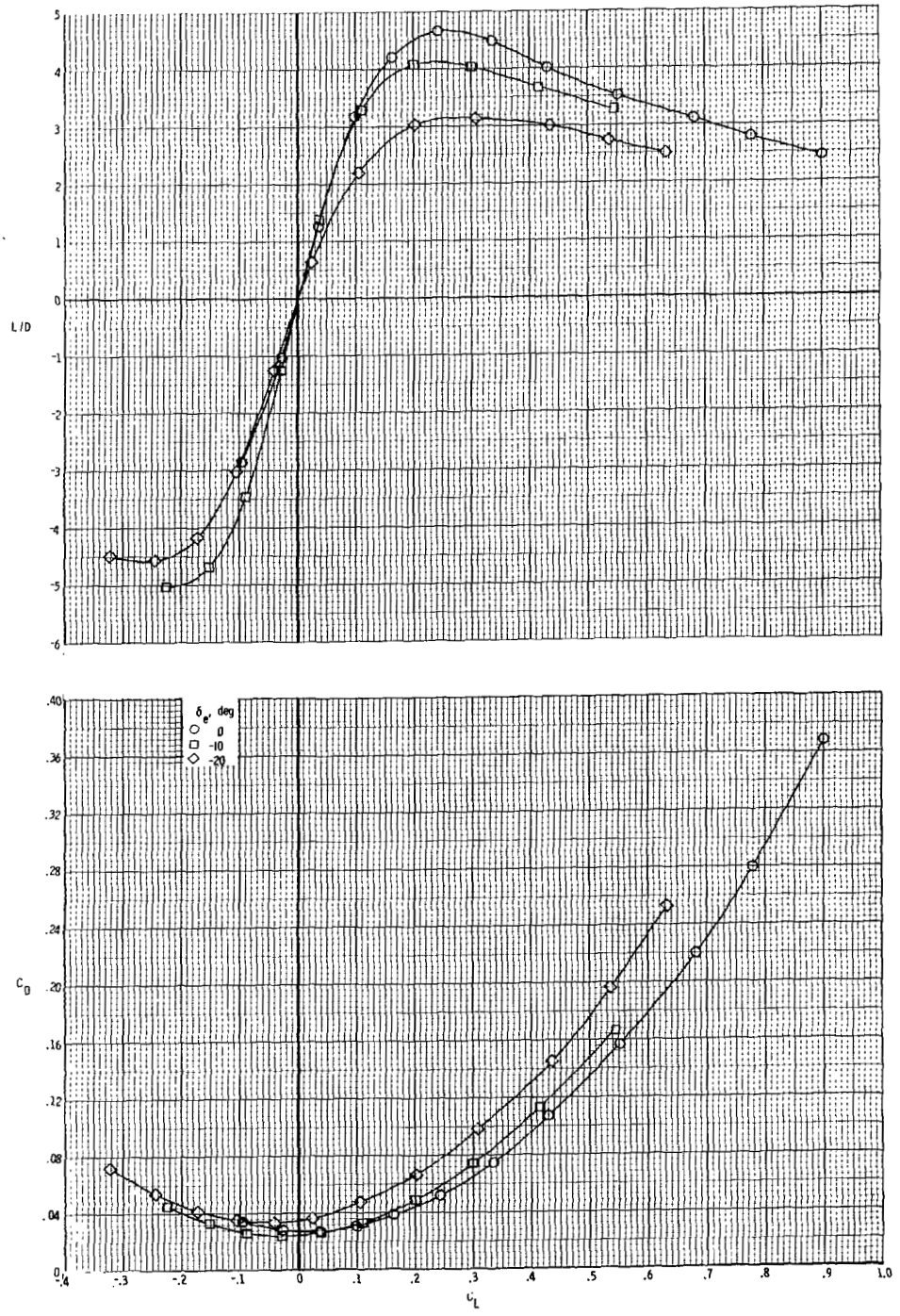

(a) Concluded.

Figure 9.- Continued.

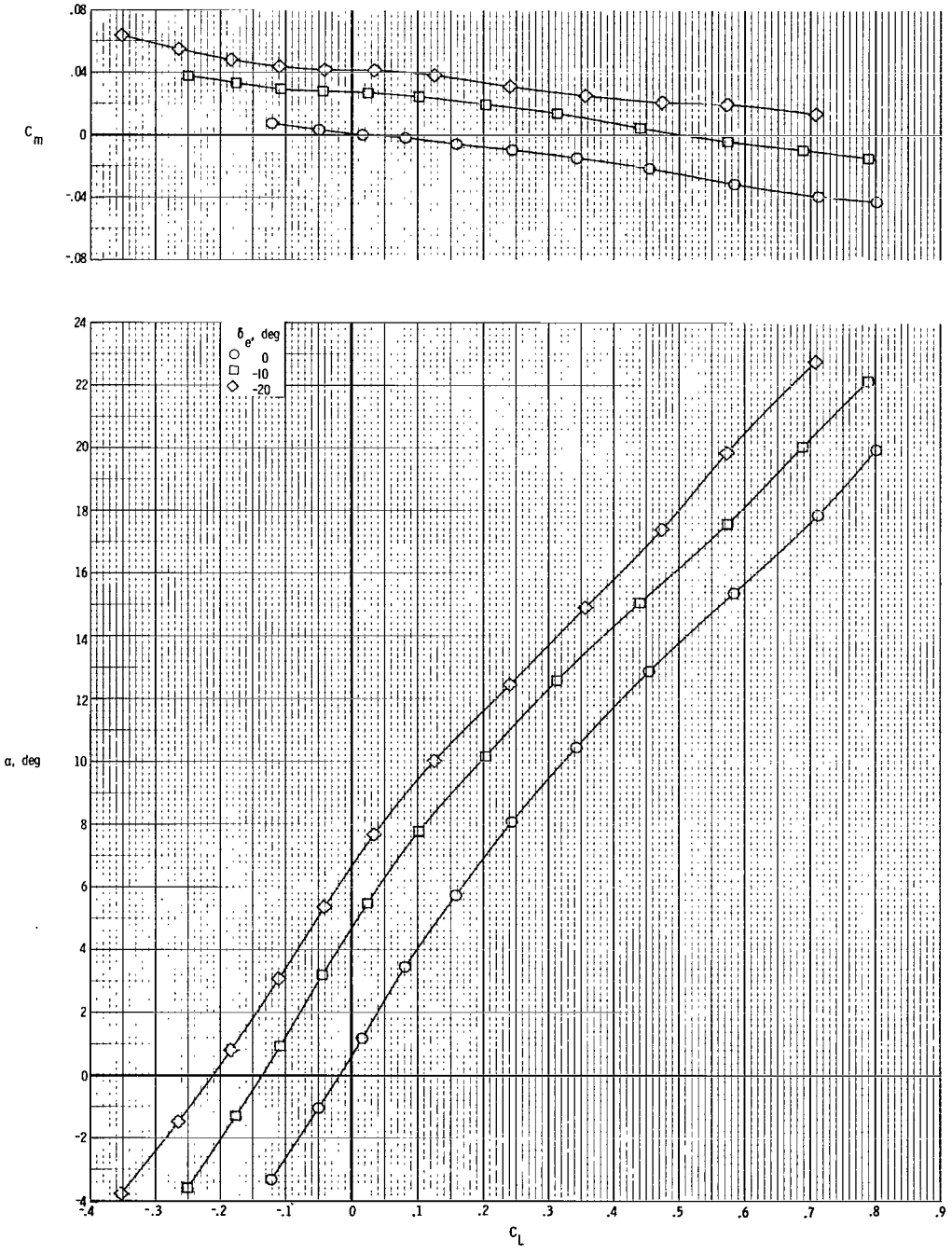

(b) M = 0.90.

Figure 9.- Continued.

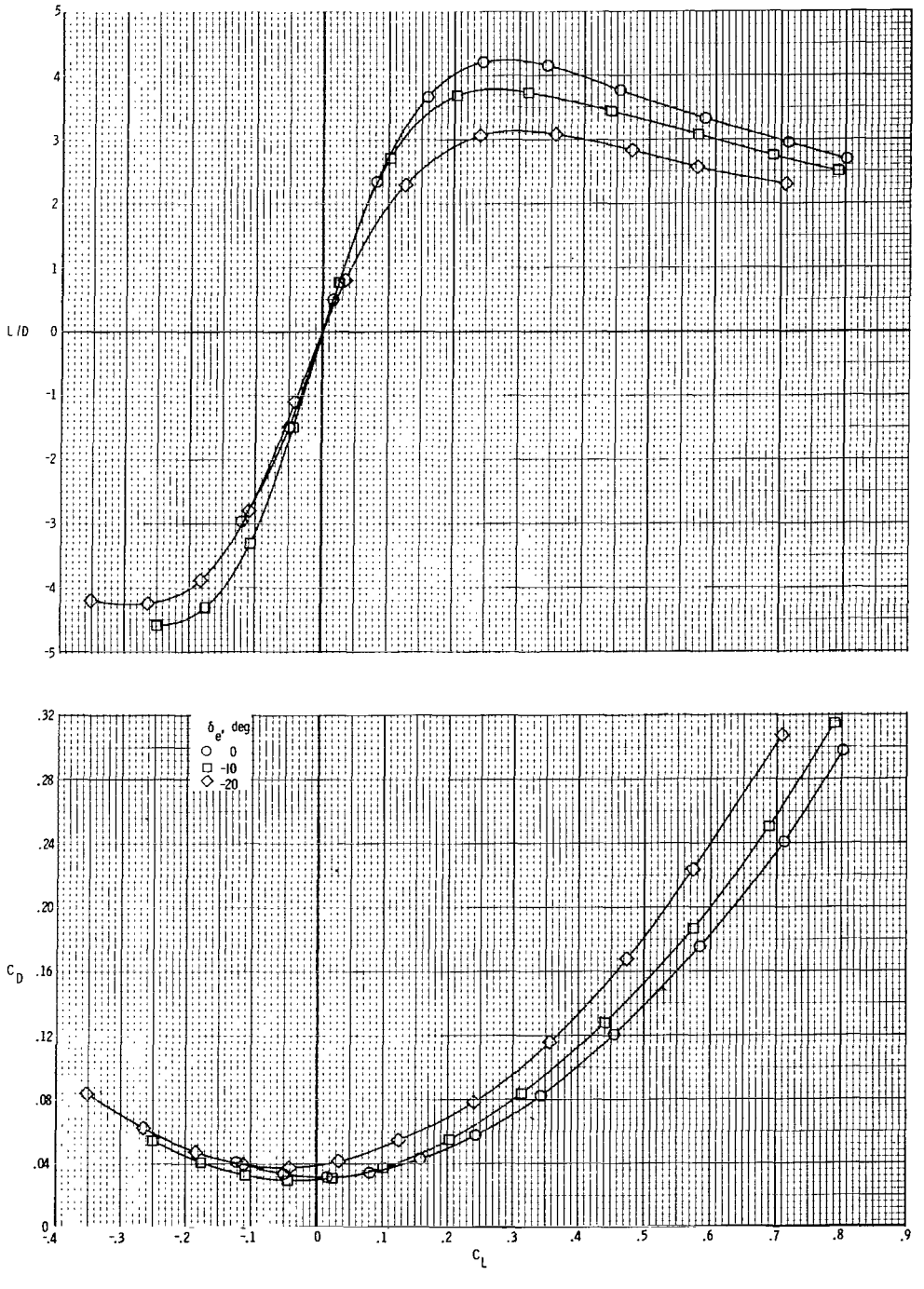

(b) Concluded.

Figure 9.- Continued.

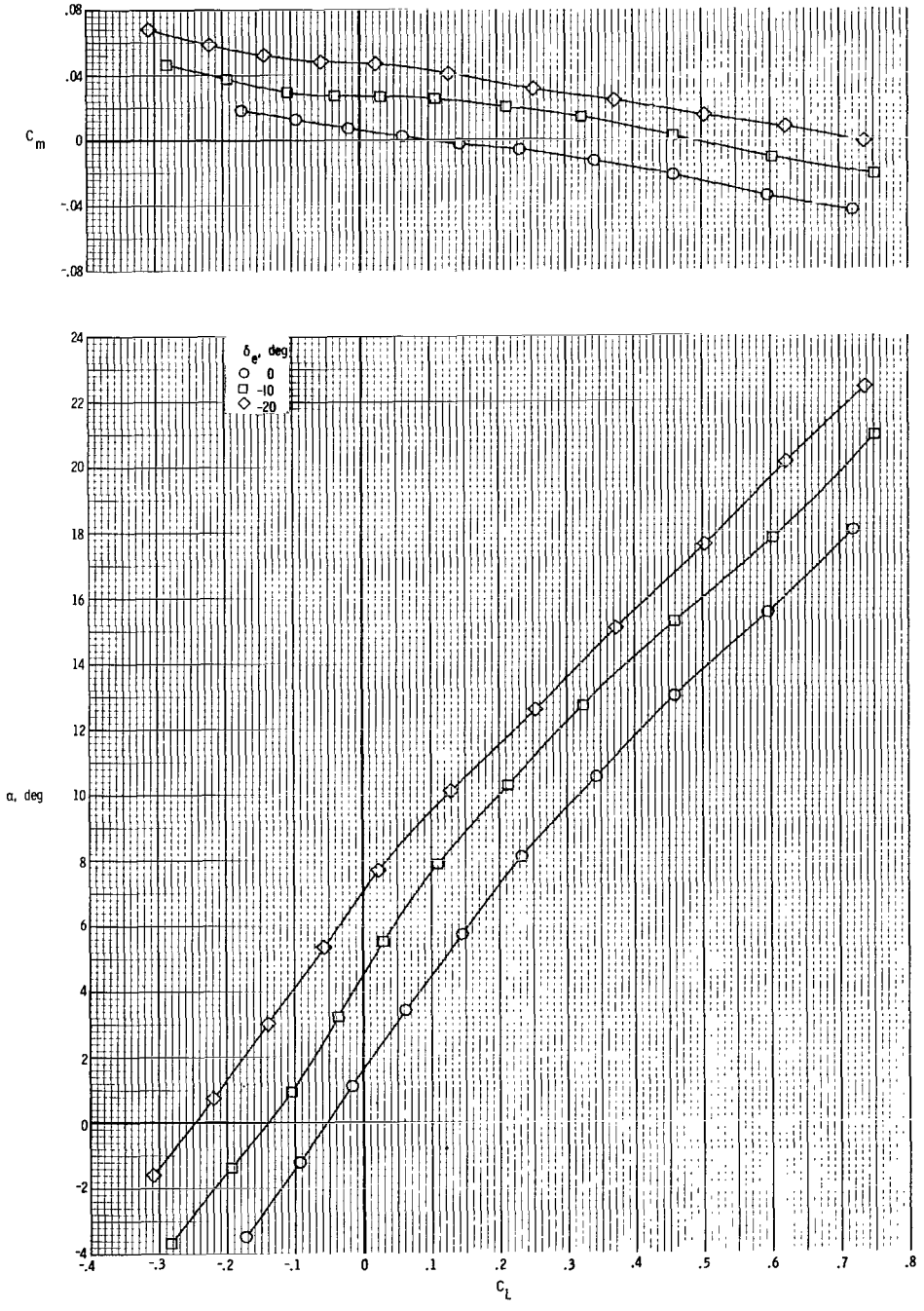

(c) M = 0.95.

Figure 9.- Continued.

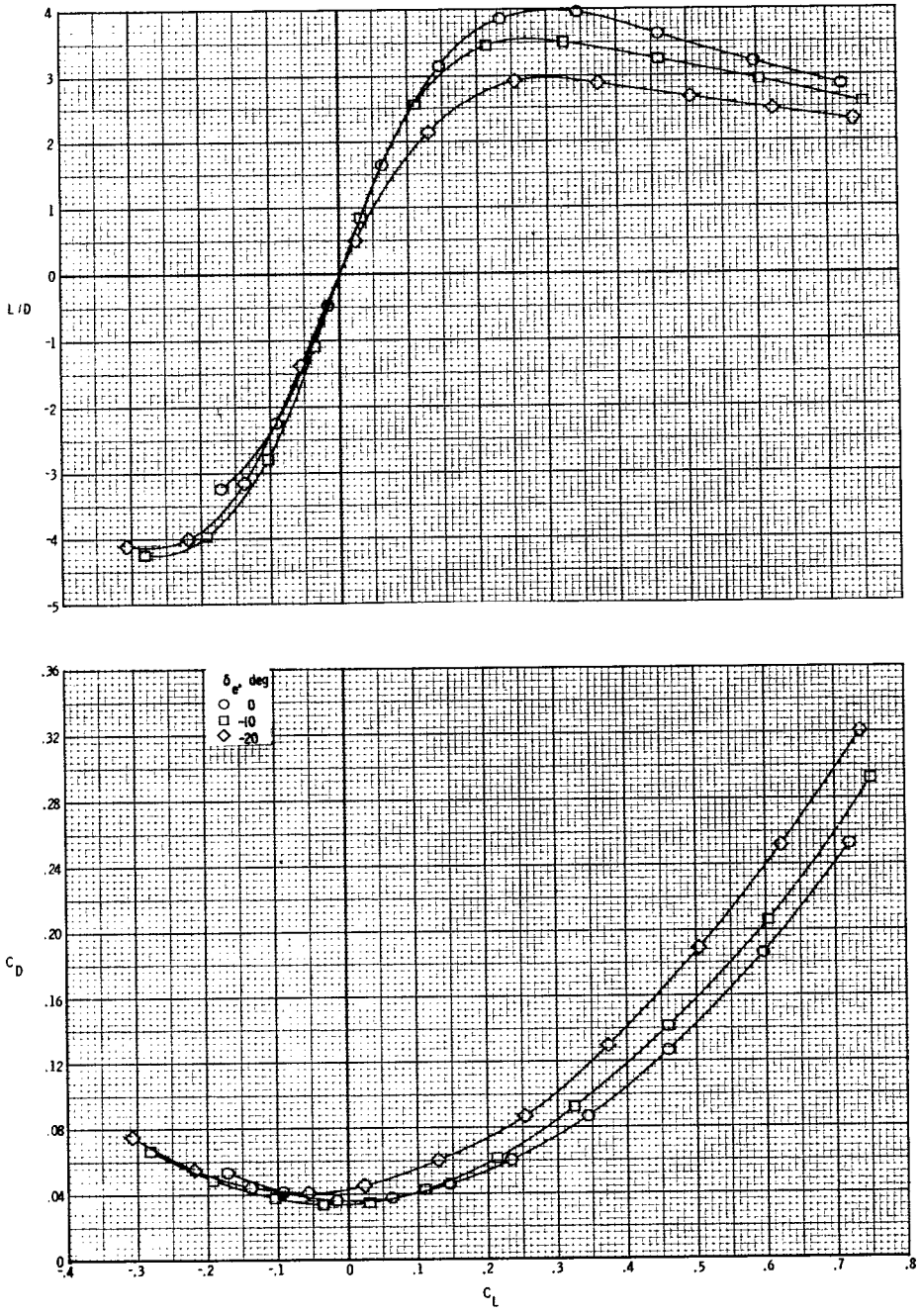

(c) Concluded.

Figure 9.- Continued.

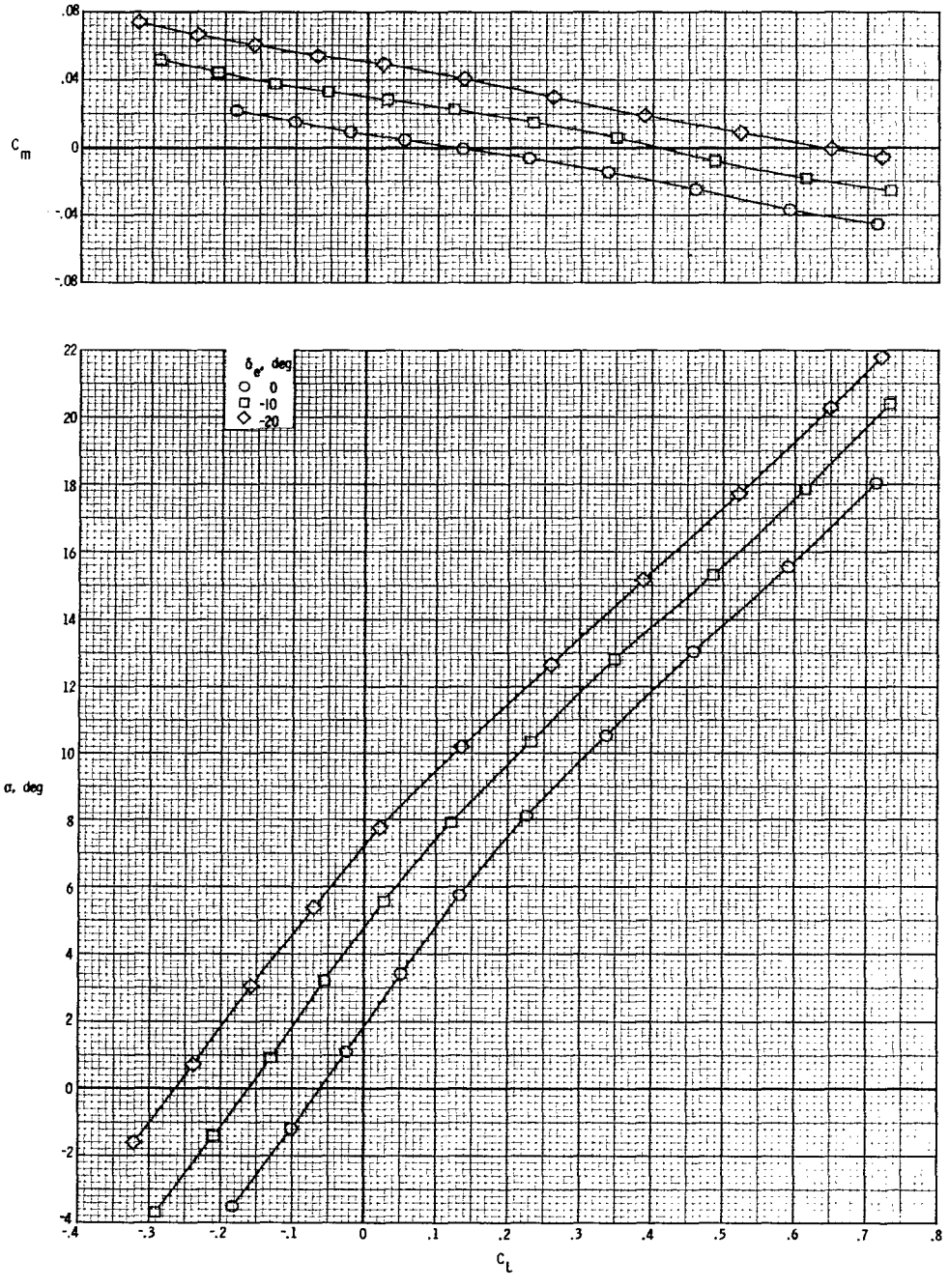

(d) M = 0.98.

Figure 9.- Continued.

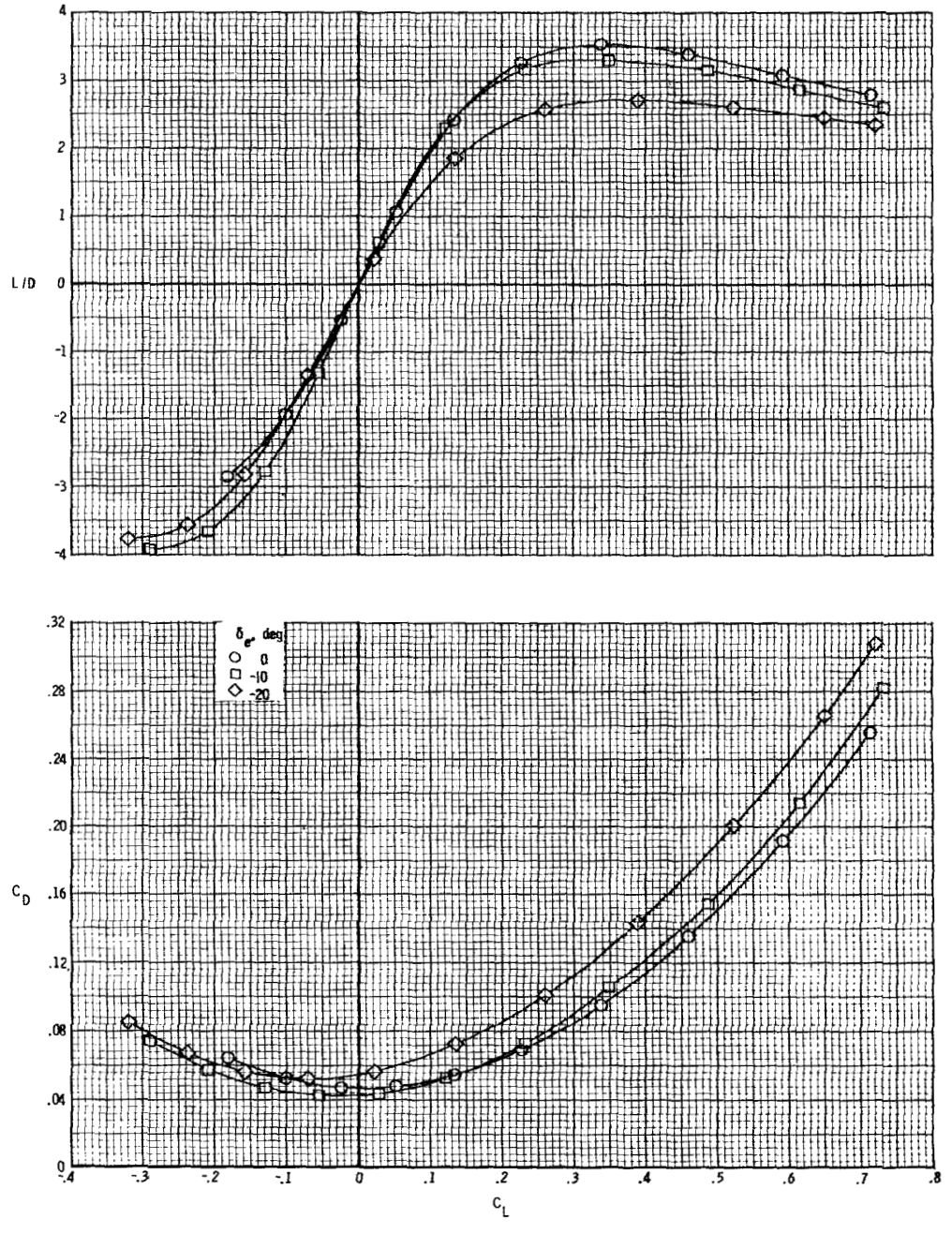

(d) Concluded.

Figure 9.- Continued.

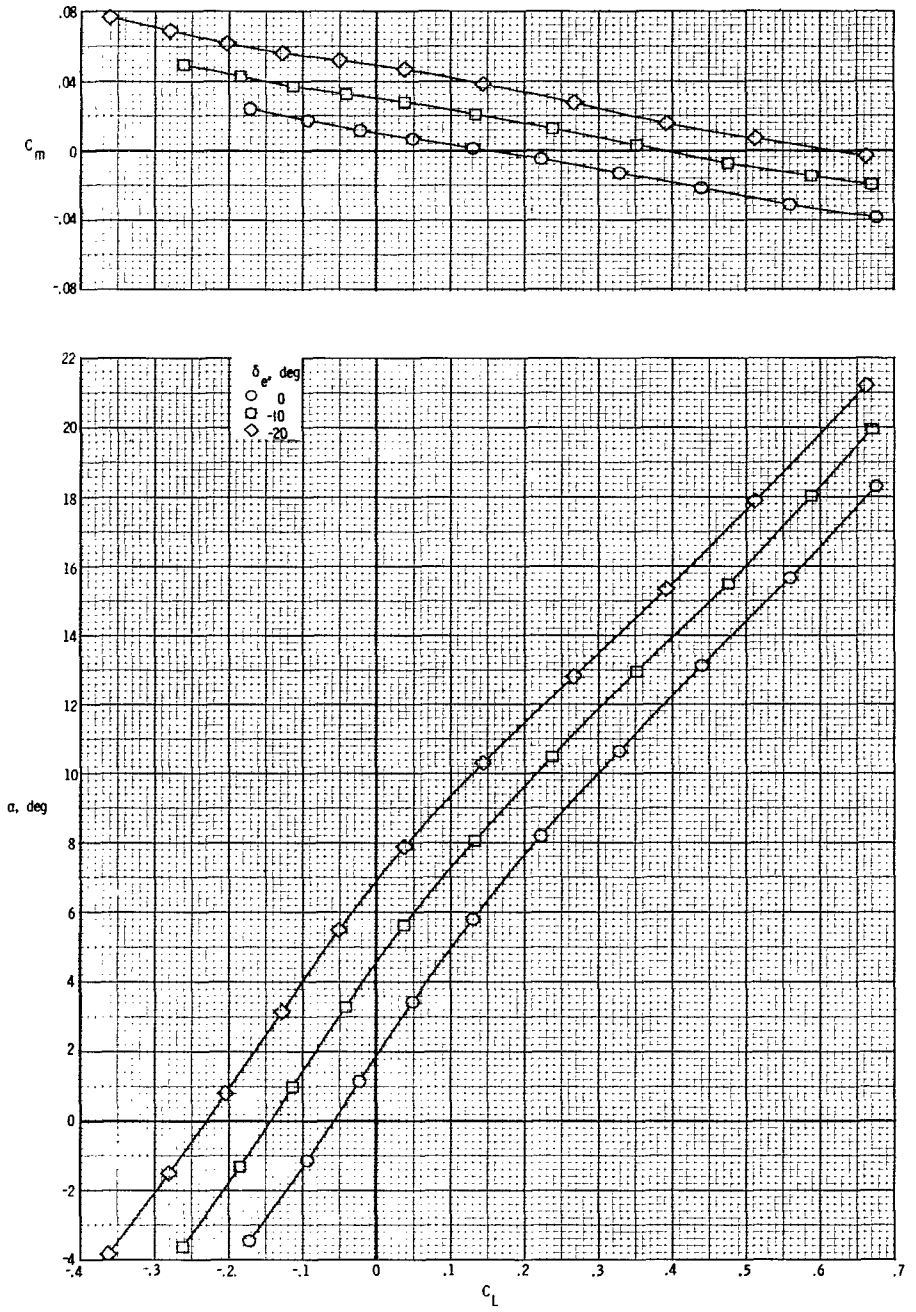

(e) M = 1.10.

Figure 9.- Continued.

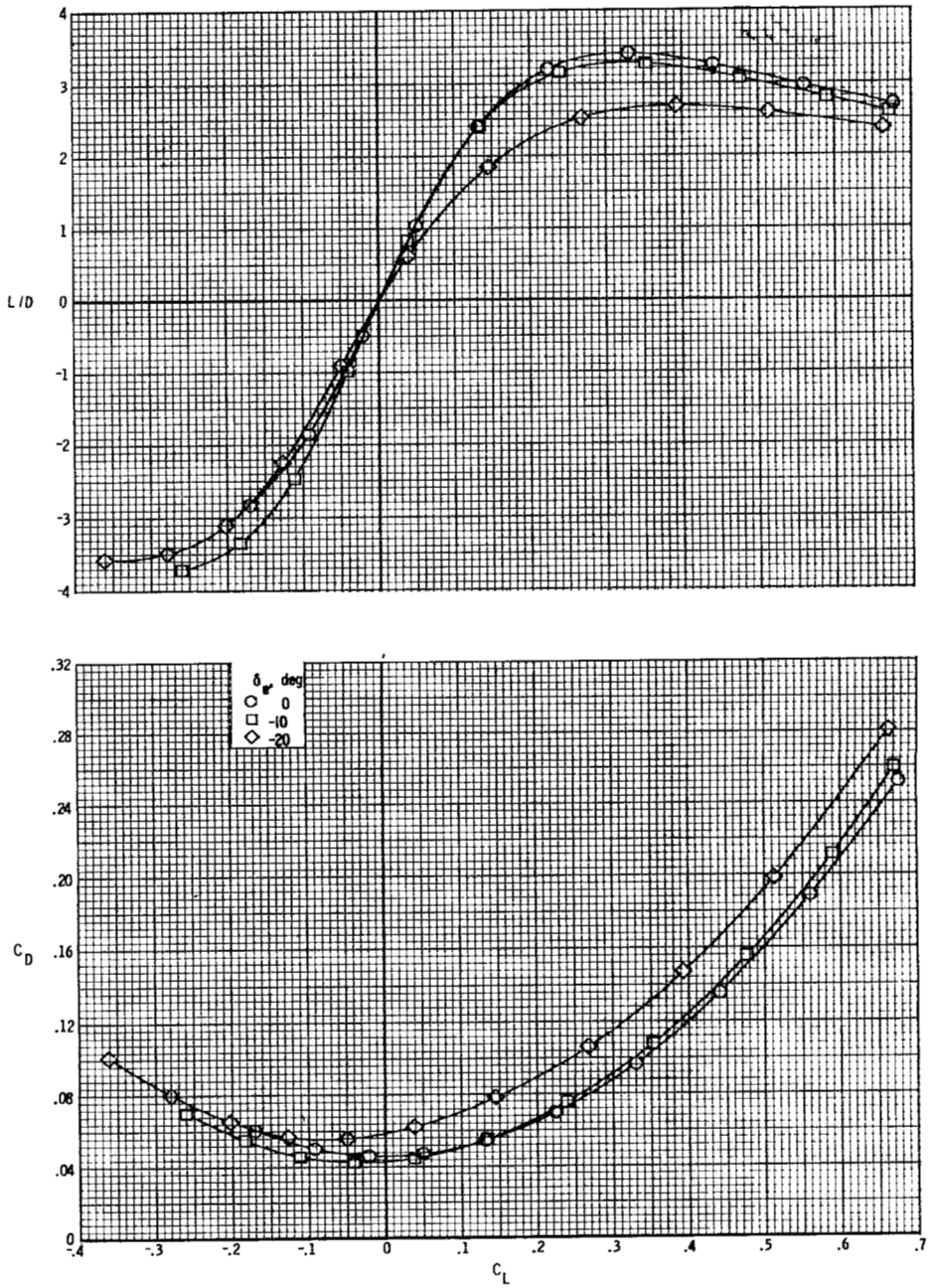

(e) Concluded.

Figure 9.- Continued.

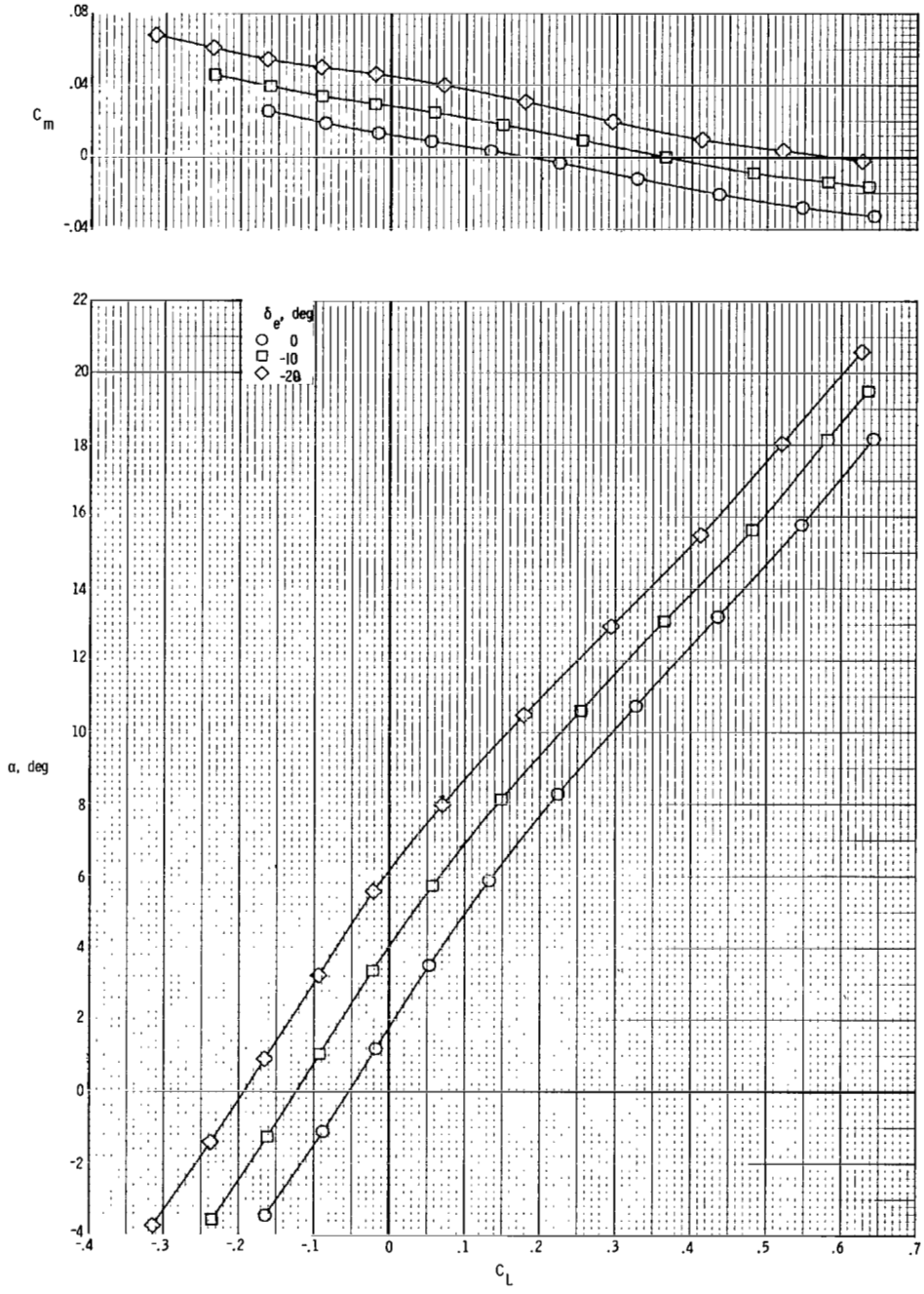

(f) M = 1.20.

Figure 9.- Continued.

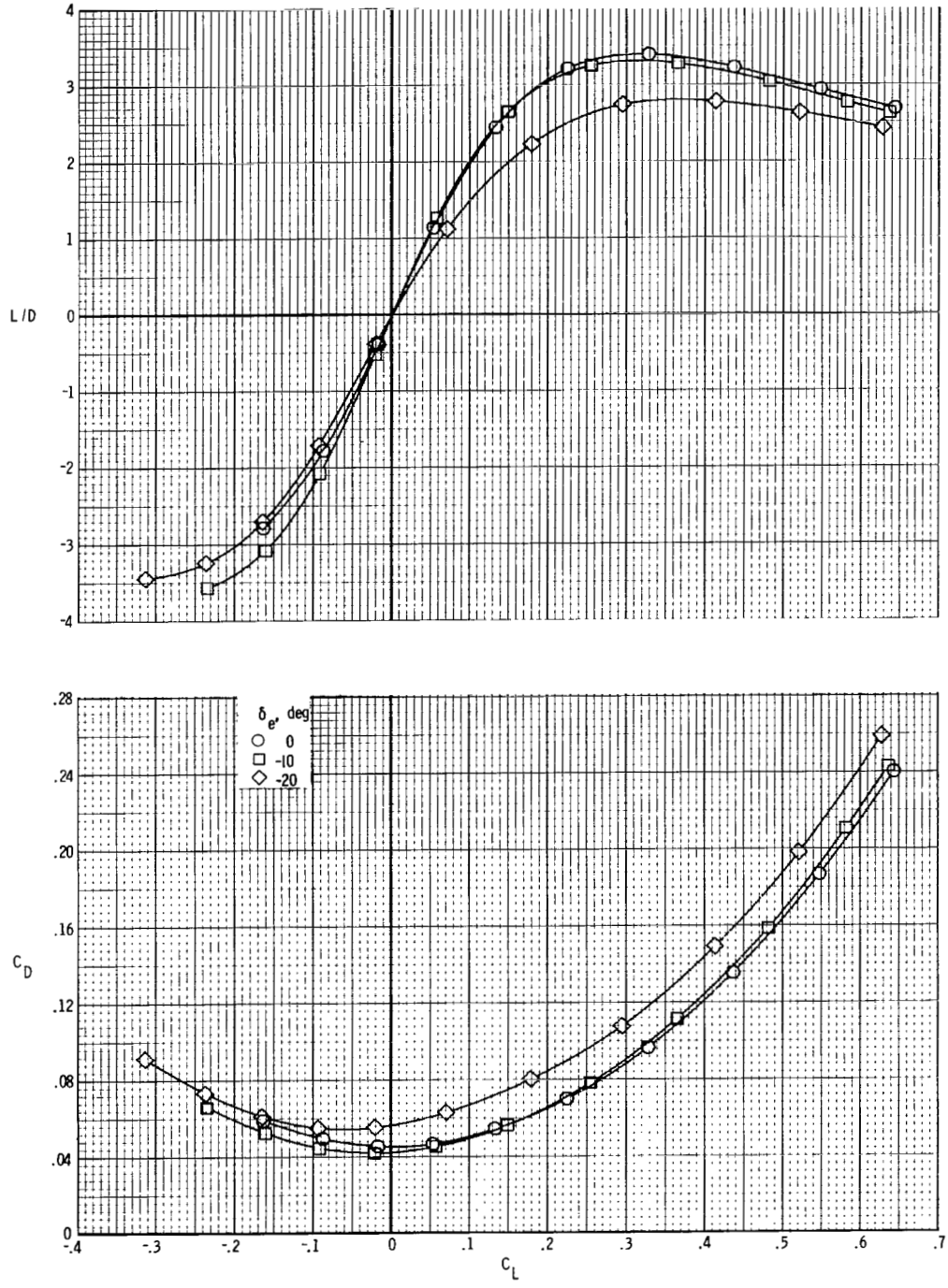

(f) Concluded.

Figure 9.- Concluded.

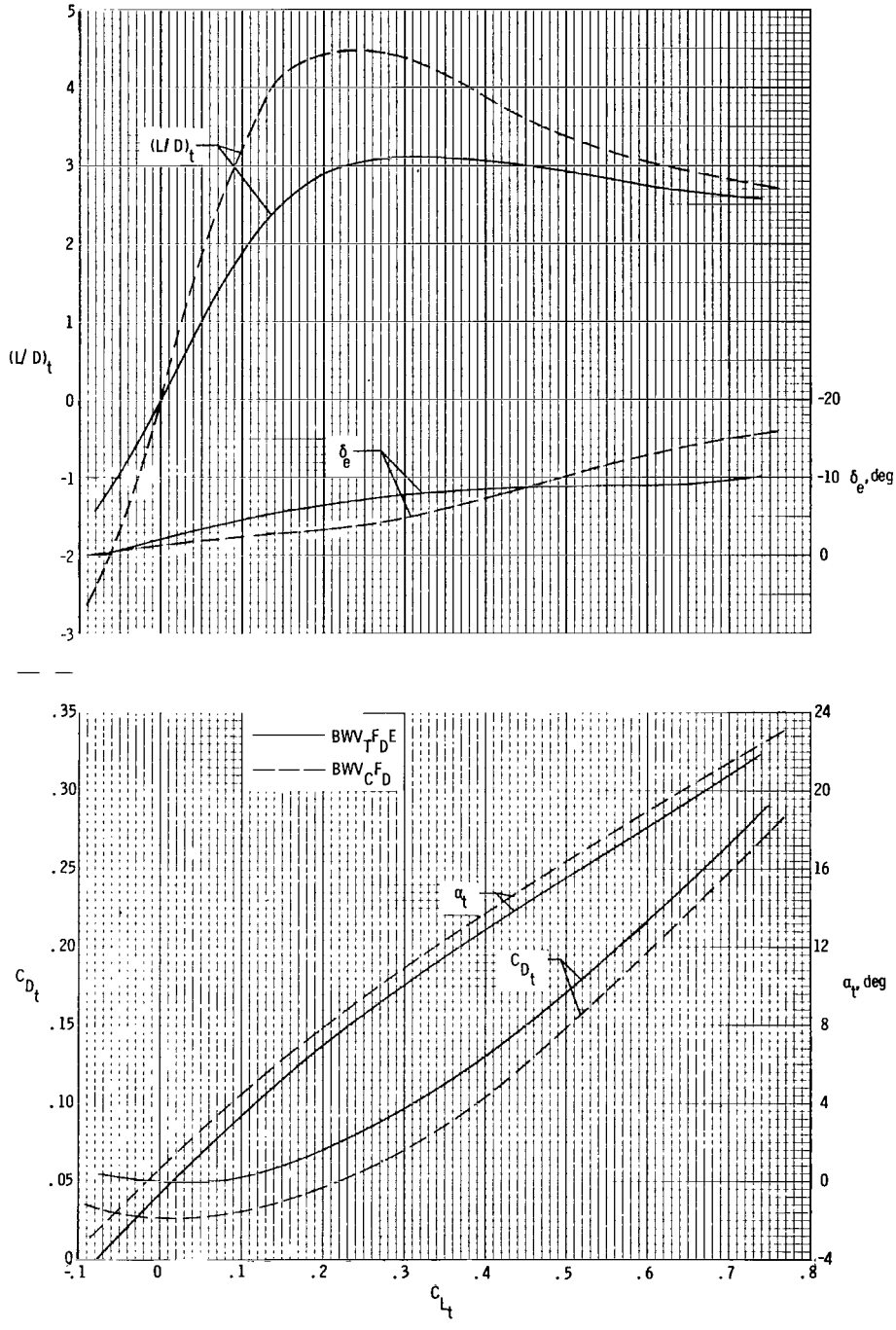

(a) M = 0.80.

Figure 10.- Longitudinal aerodynamic characteristics at trim of BWV_TF_DE and BWV_CF_D configurations.

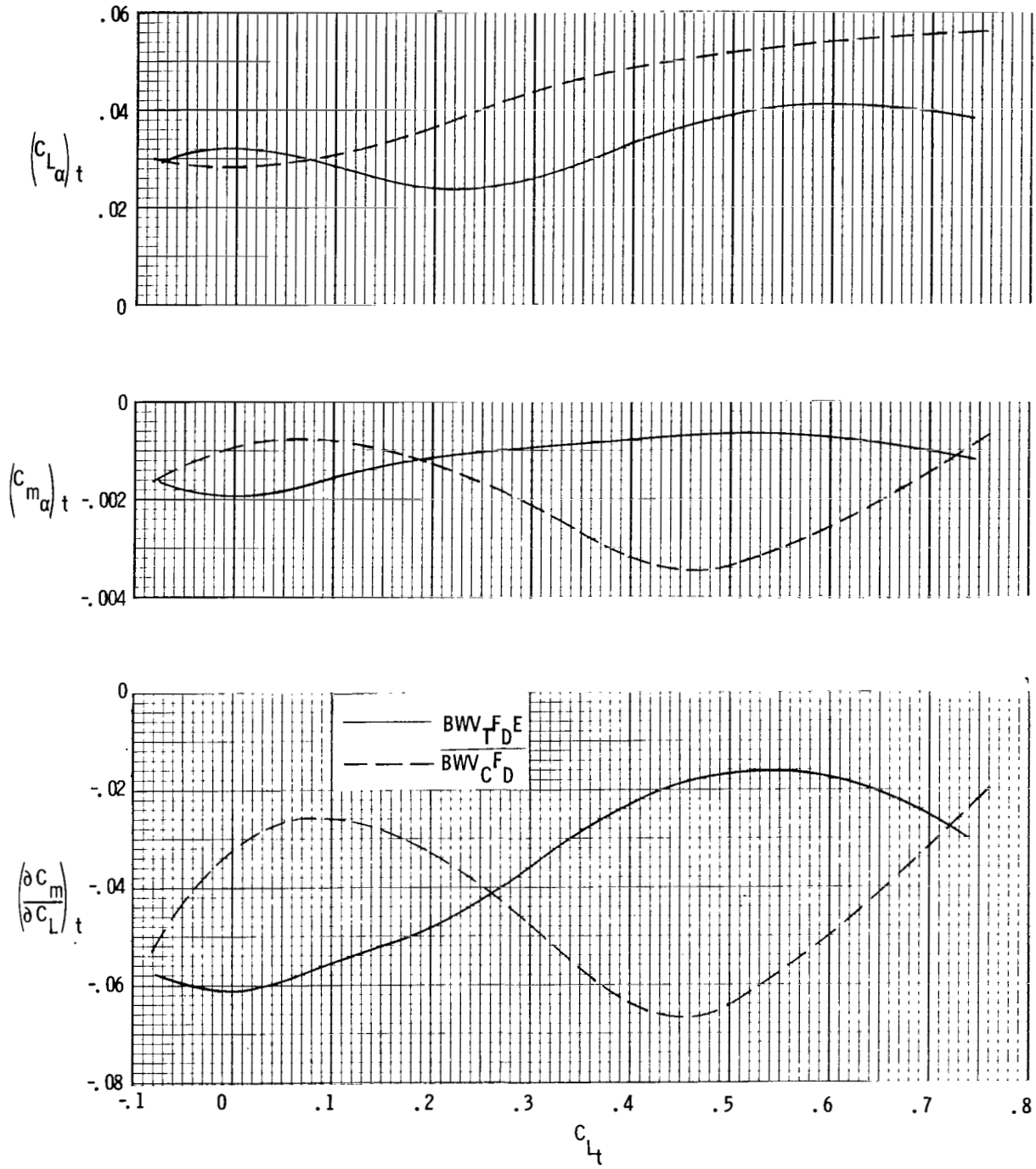

(a) Concluded.

Figure 10.- Continued.

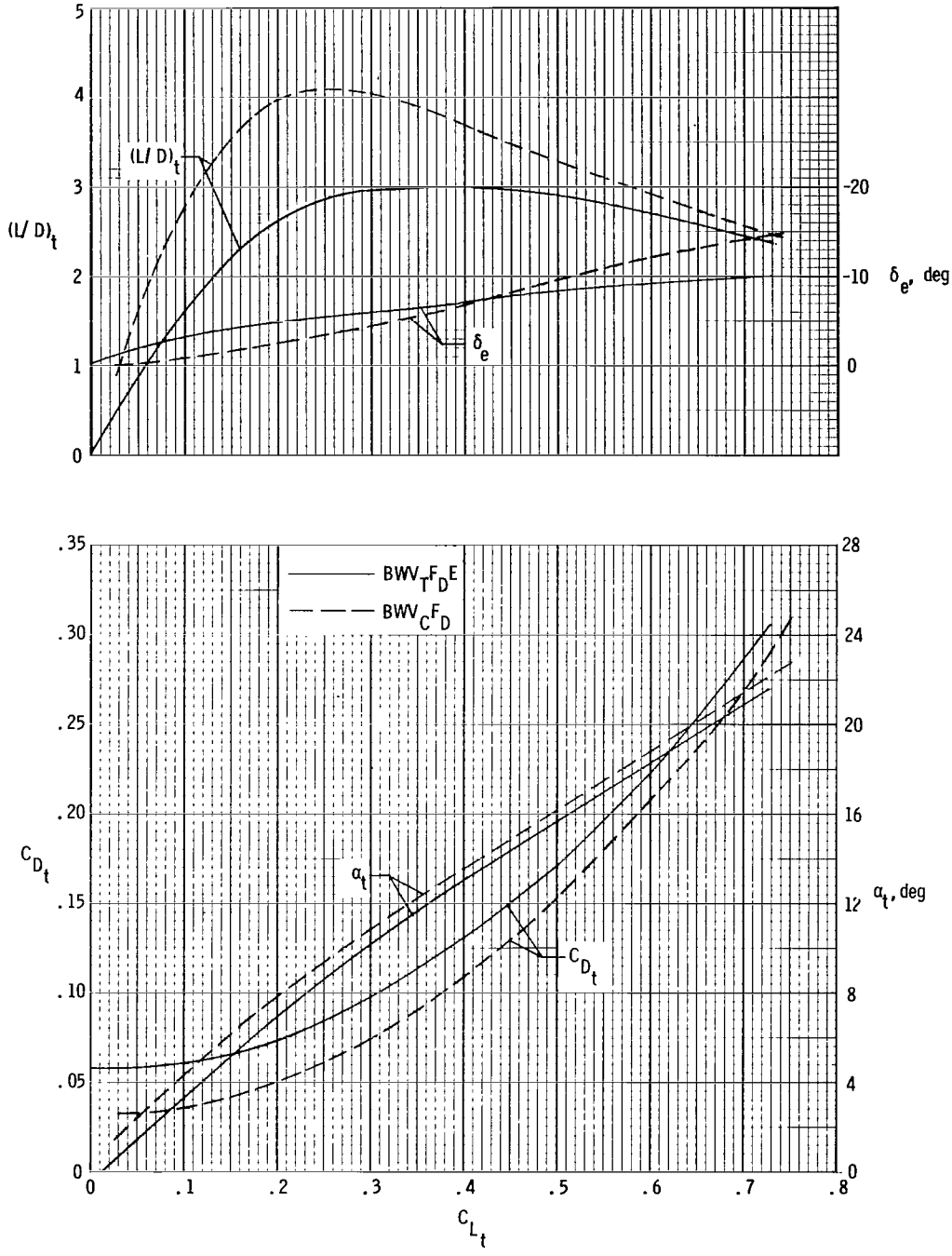

(b) M = 0.90.

Figure 10.- Continued.

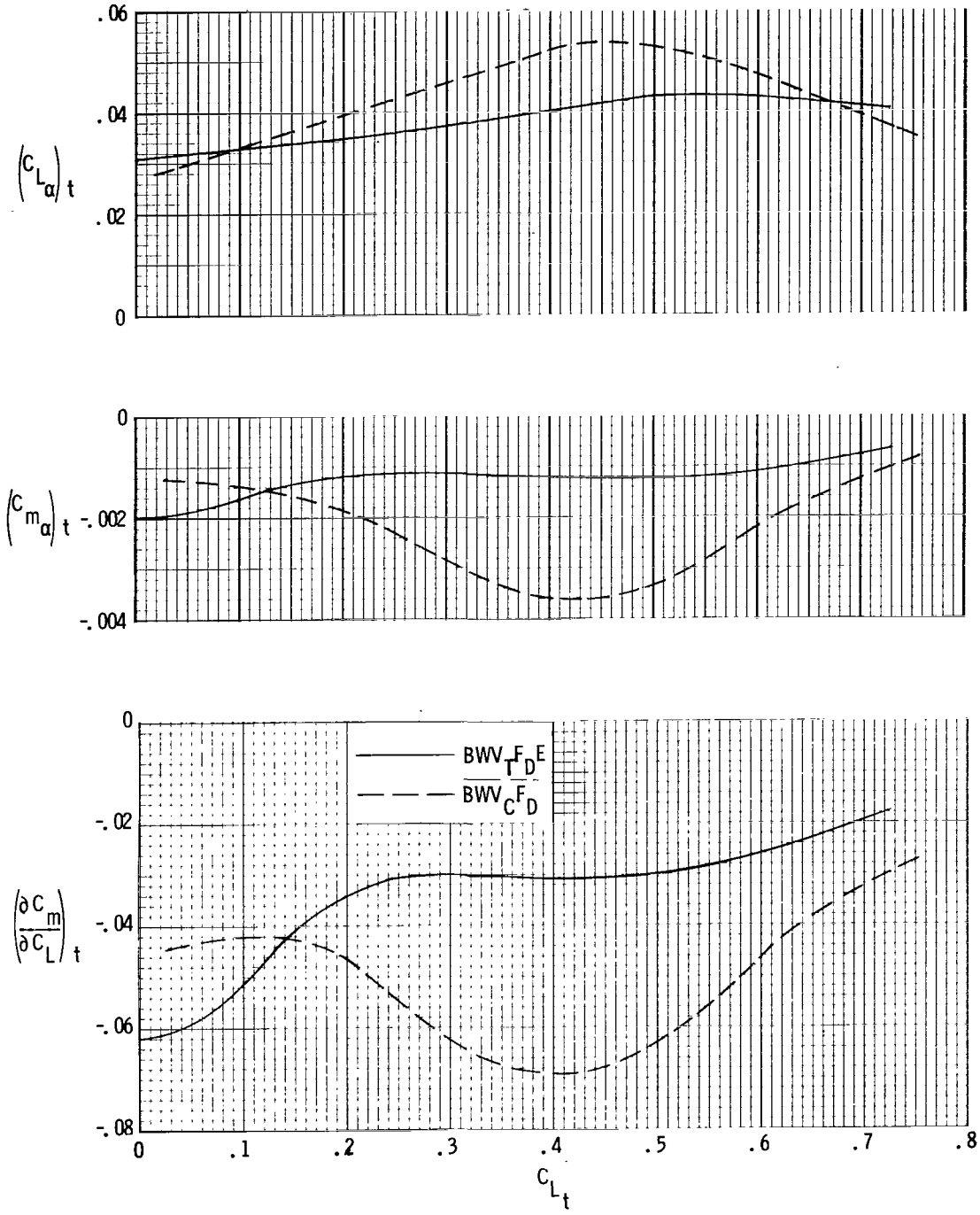

(b) Concluded.

Figure 10.- Continued.

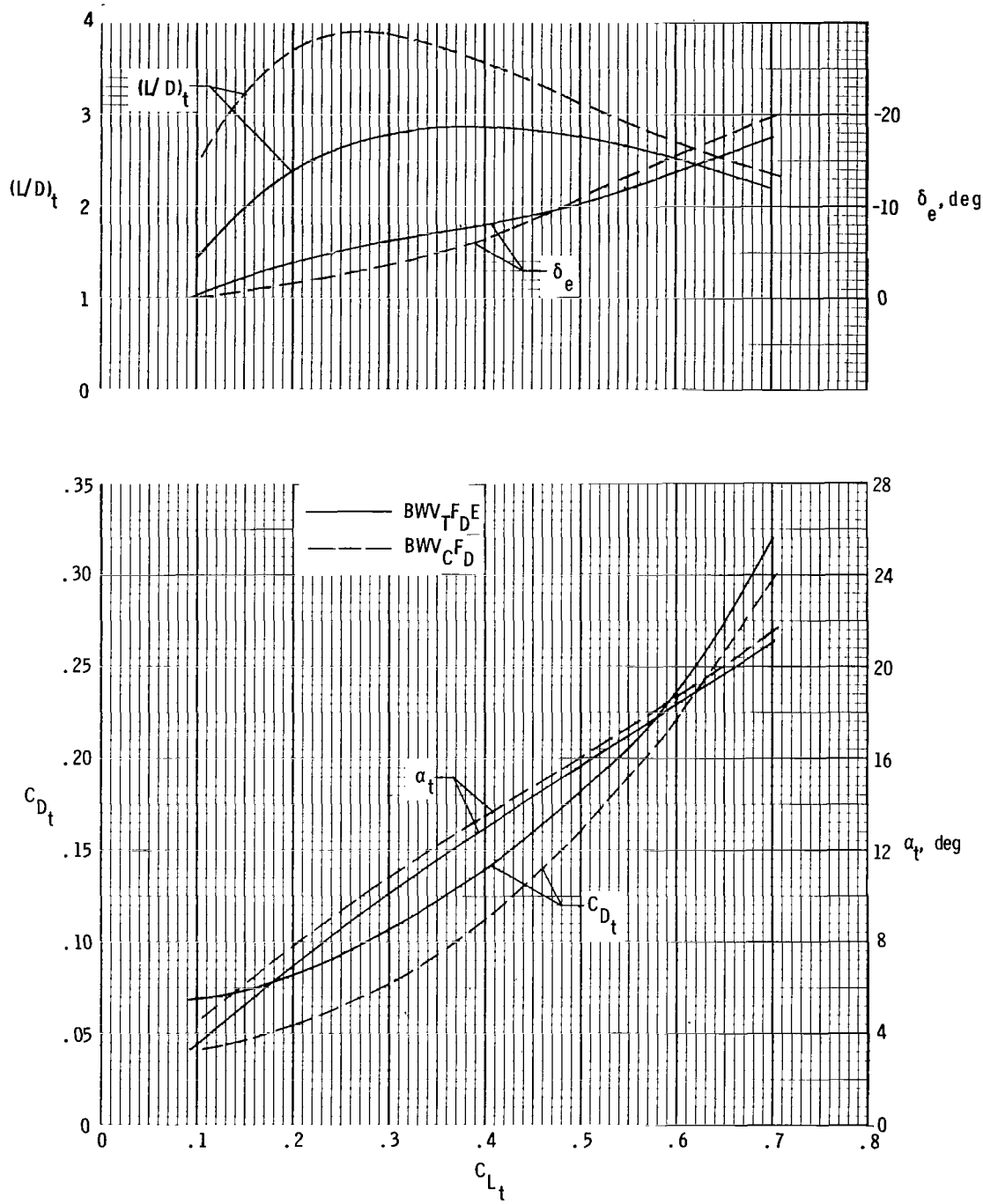

(c) M = 0.95.

Figure 10.- Continued.

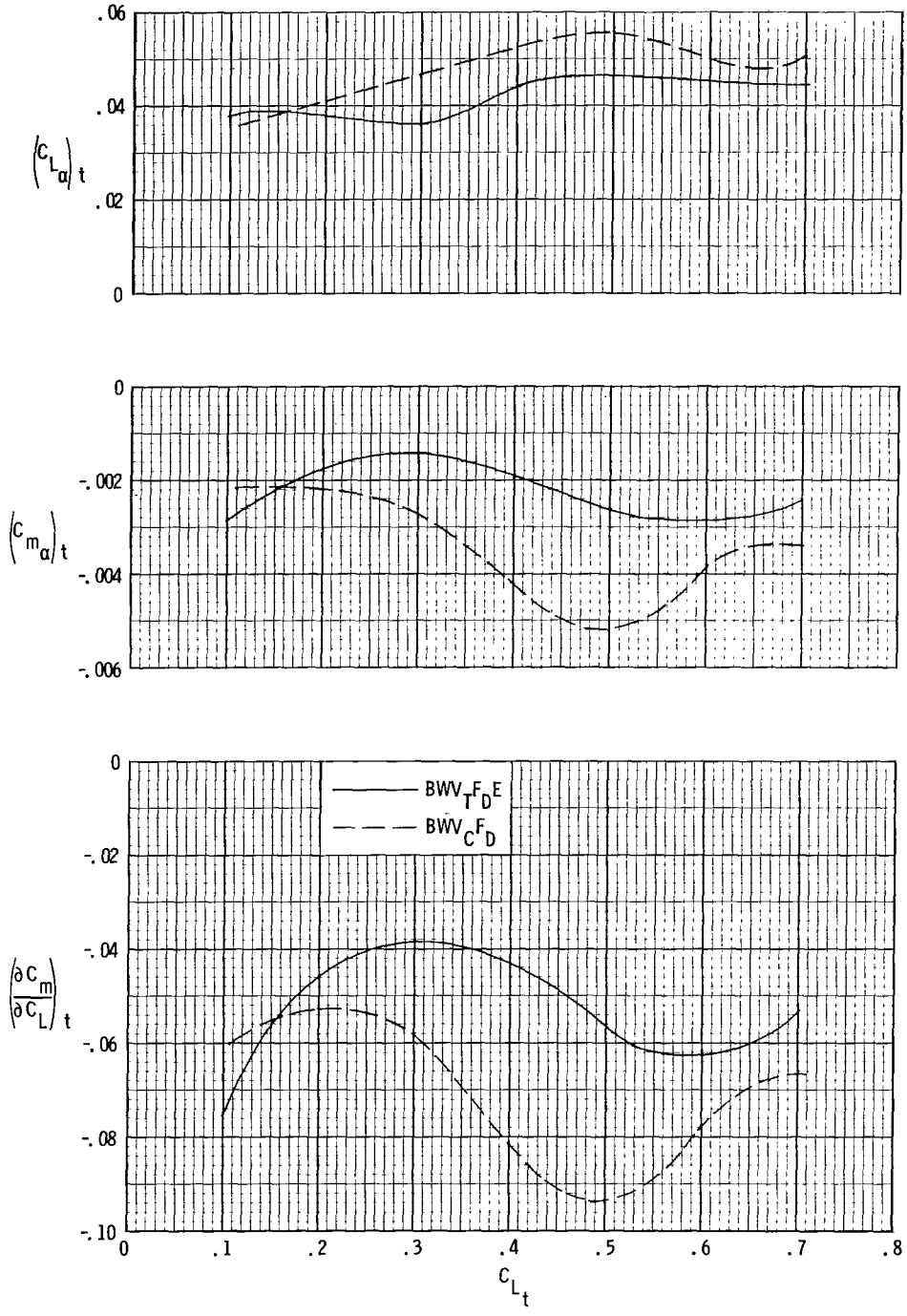

(c) Concluded.

Figure 10.- Continued.

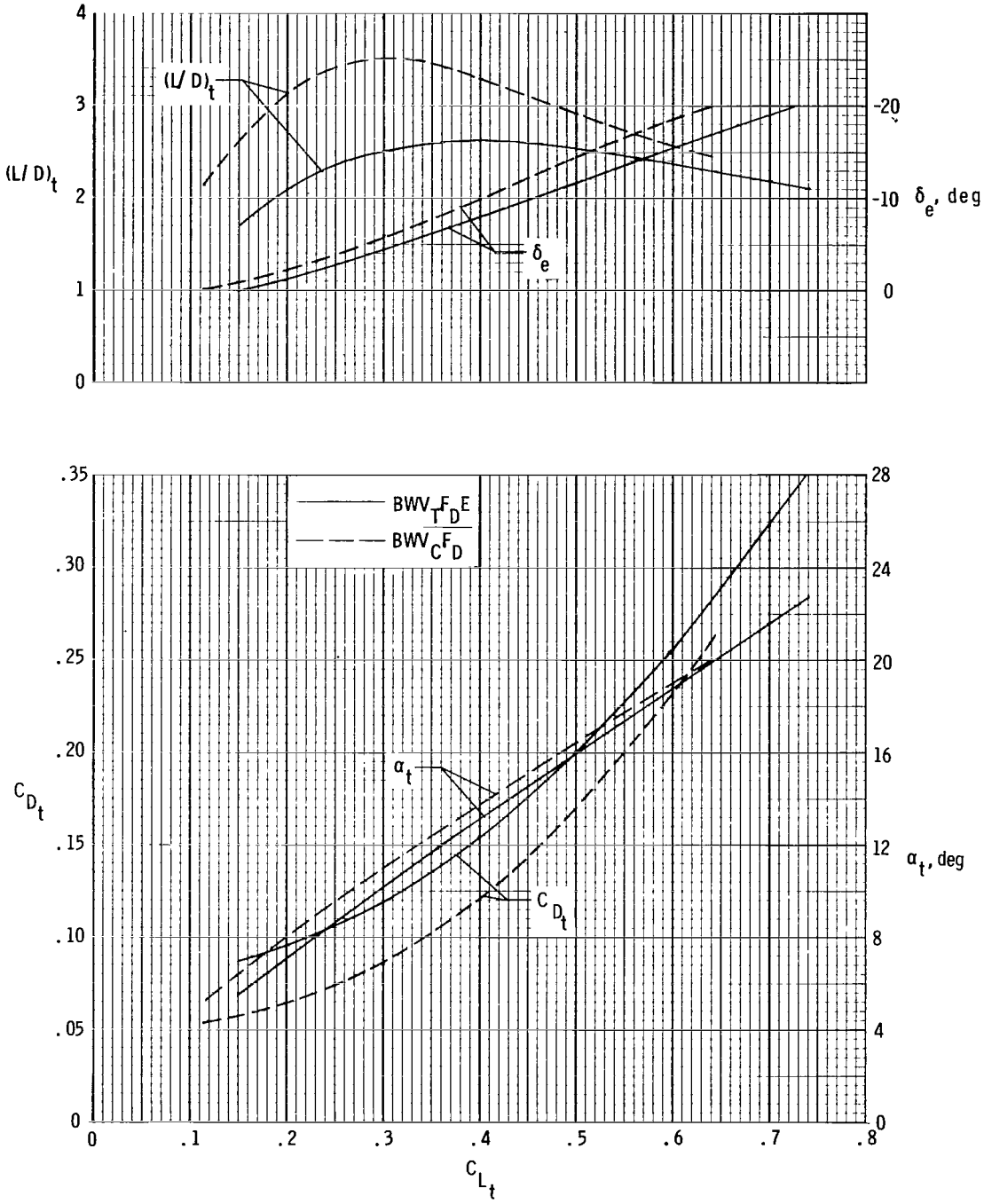

(d) M = 0.98.

Figure 10.- Continued.

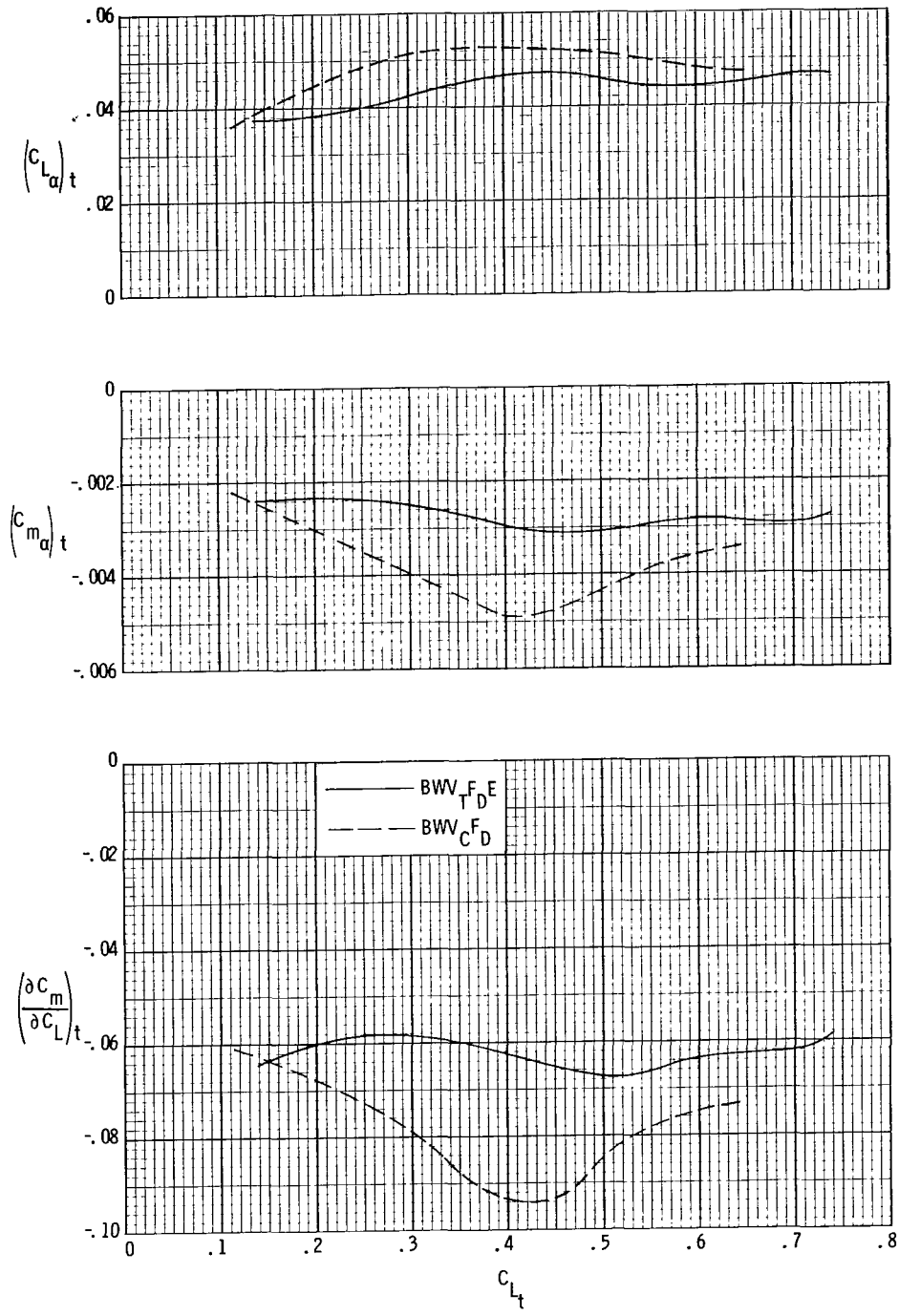

(d) Concluded.

Figure 10.- Continued.

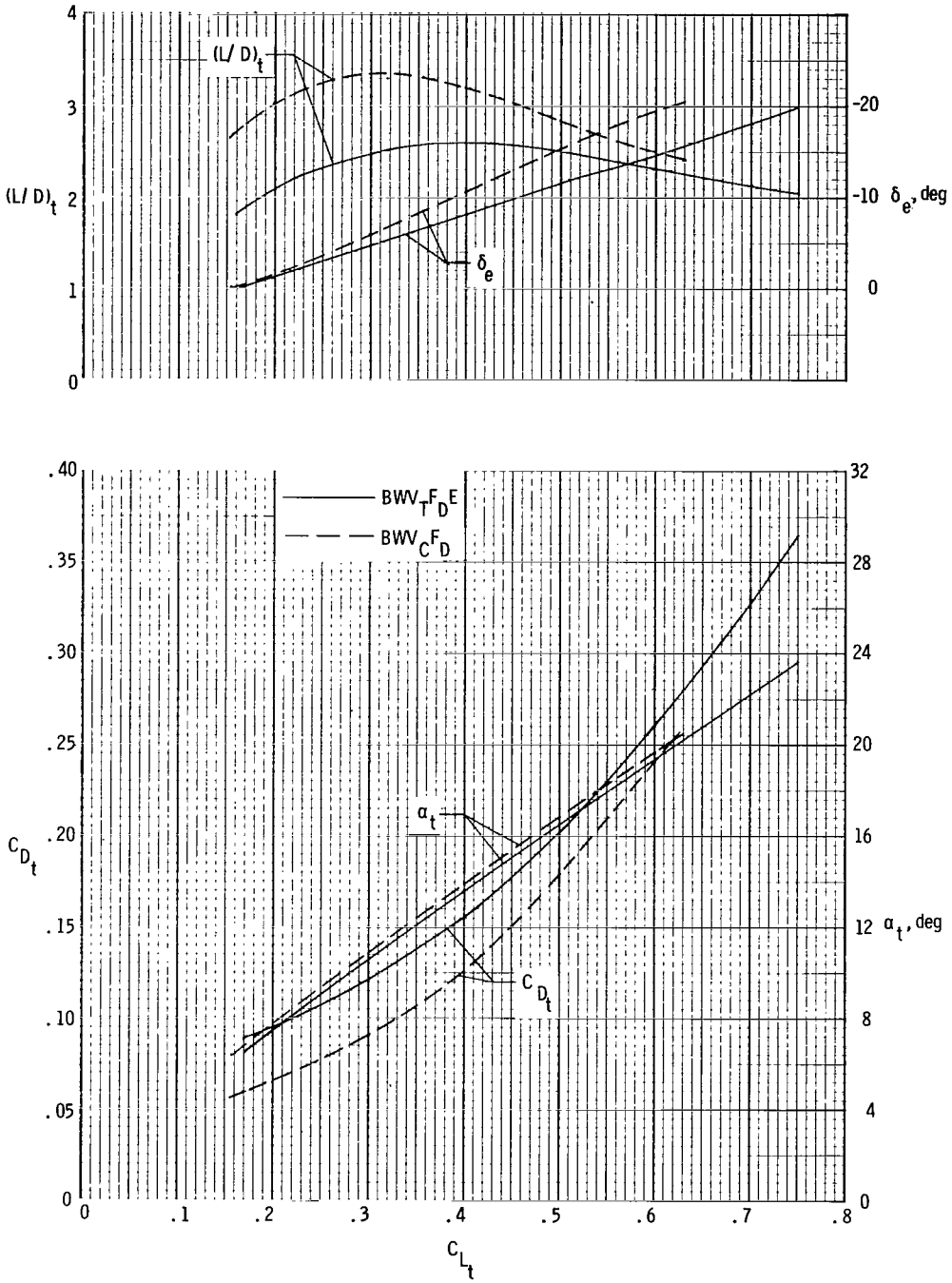

(e) M = 1.10.

Figure 10.- Continued.

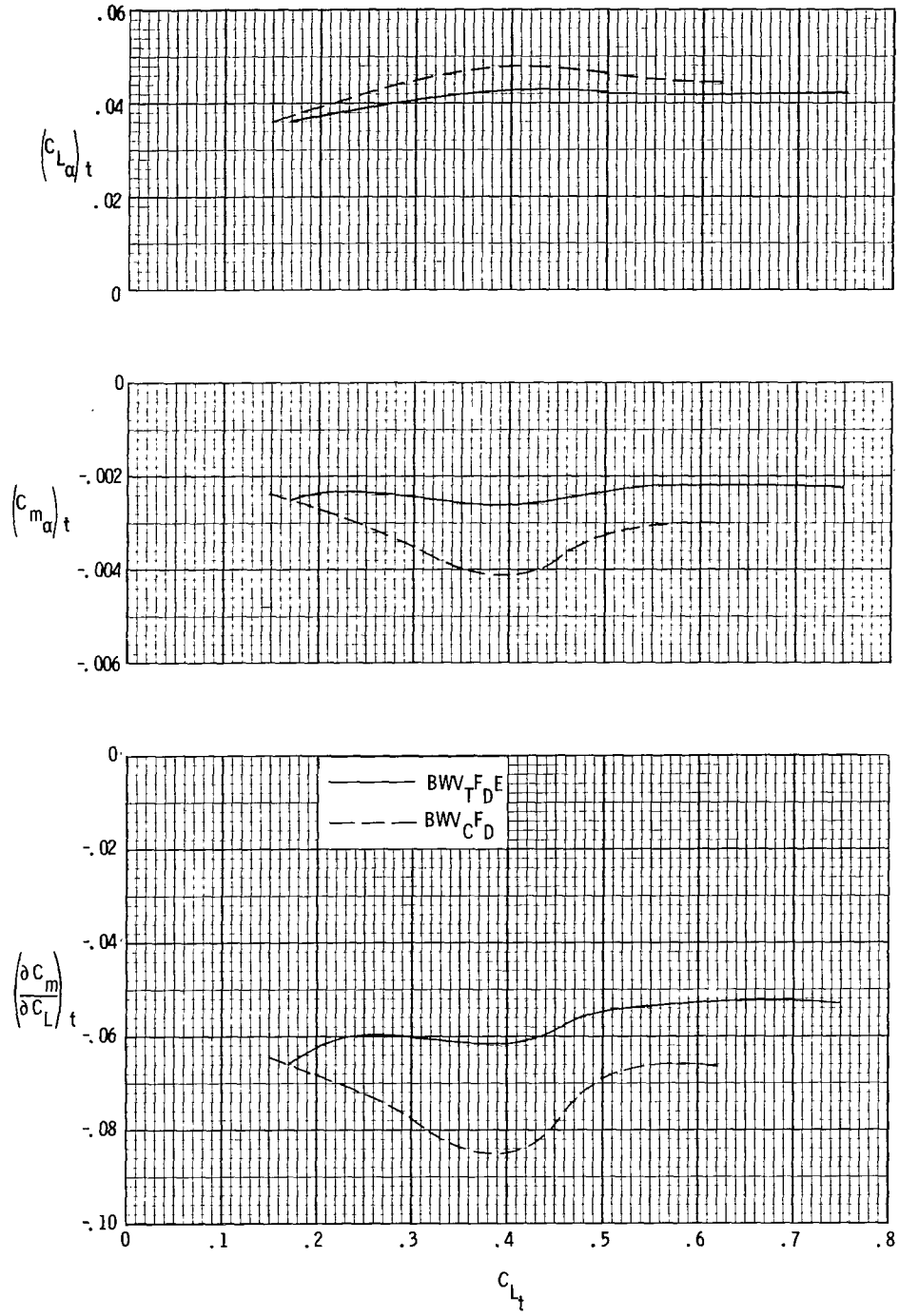

(e) Concluded.

Figure 10.- Continued.

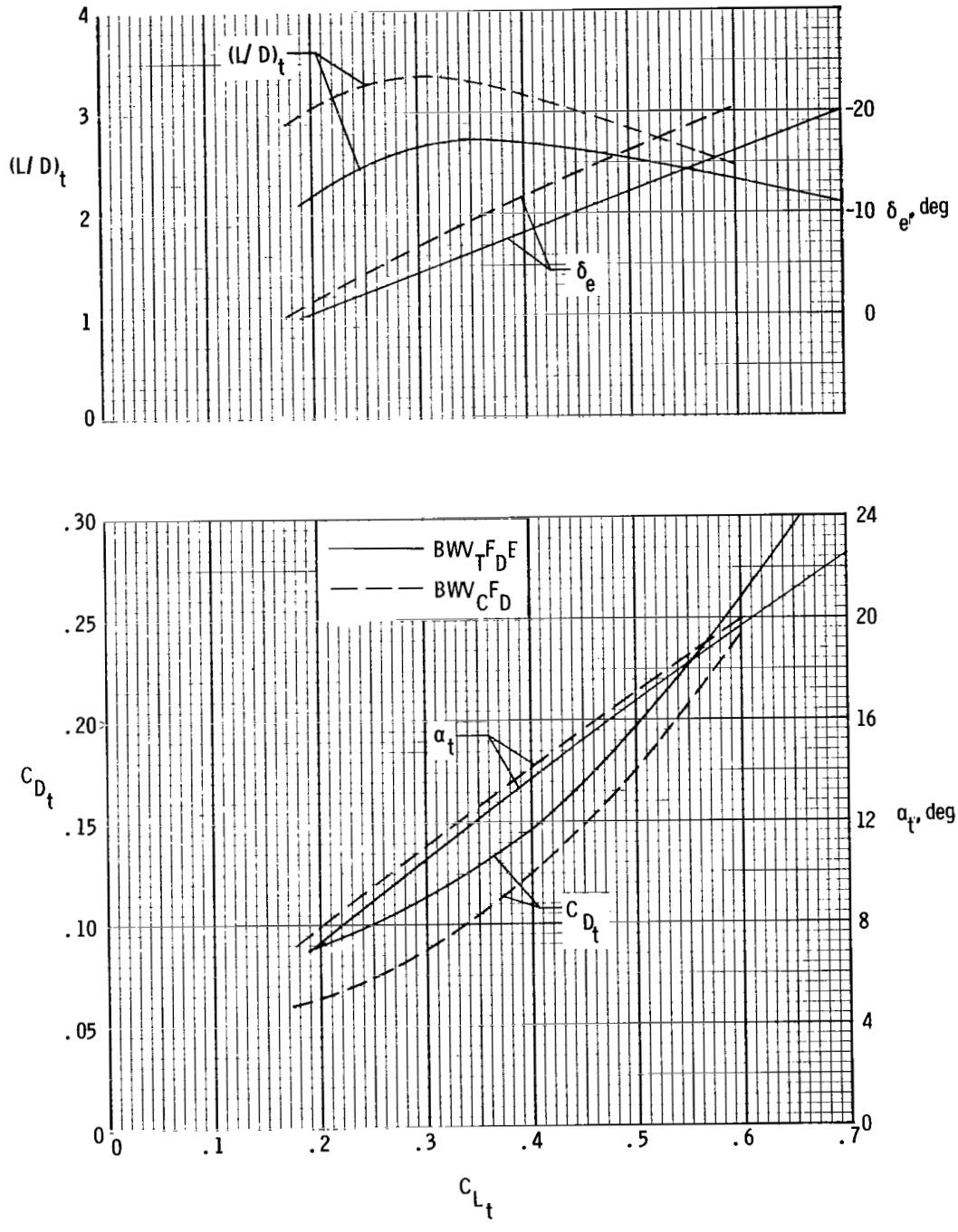

(f) M = 1.20.

Figure 10.- Continued.

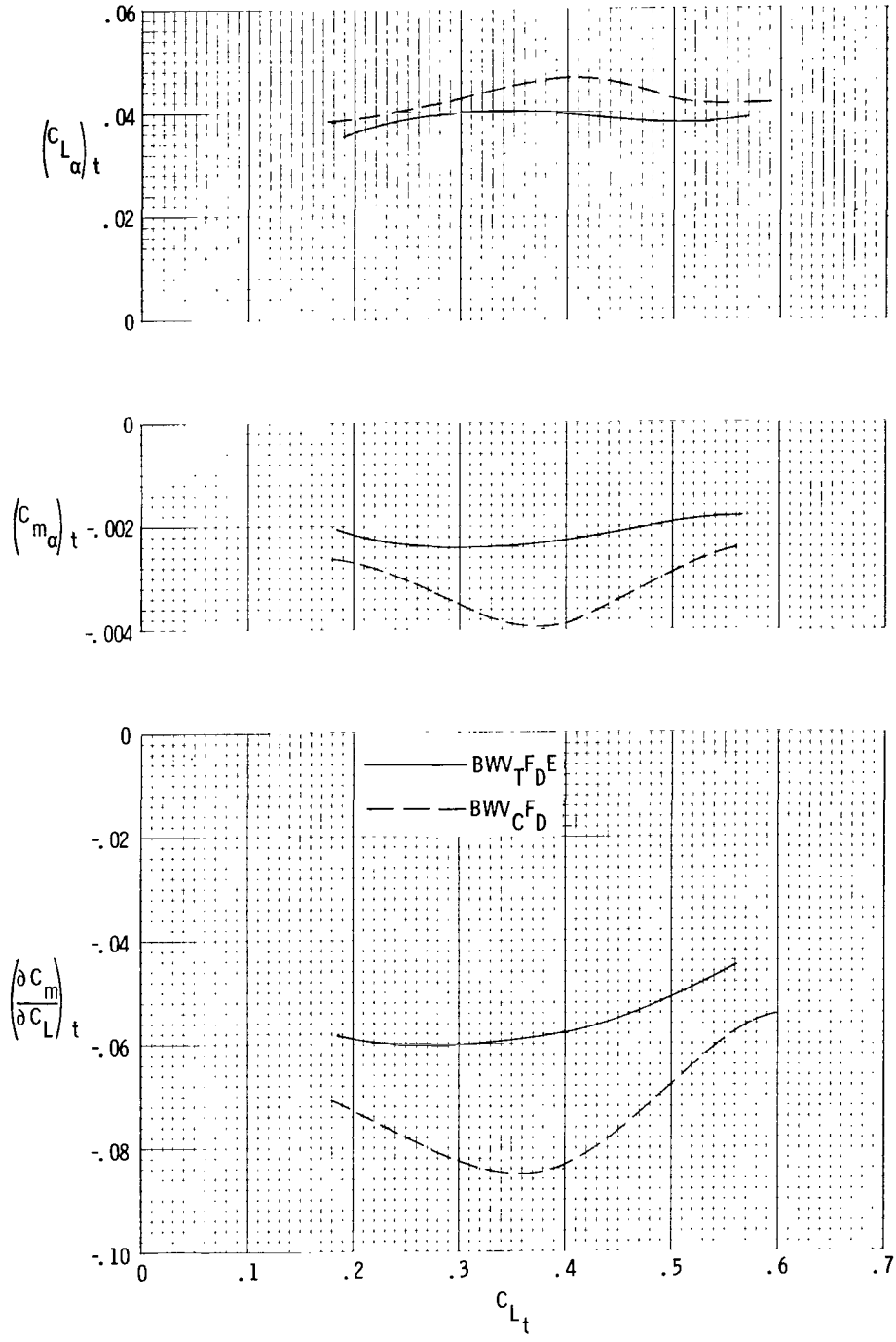

(f) Concluded.

Figure 10.- Concluded.

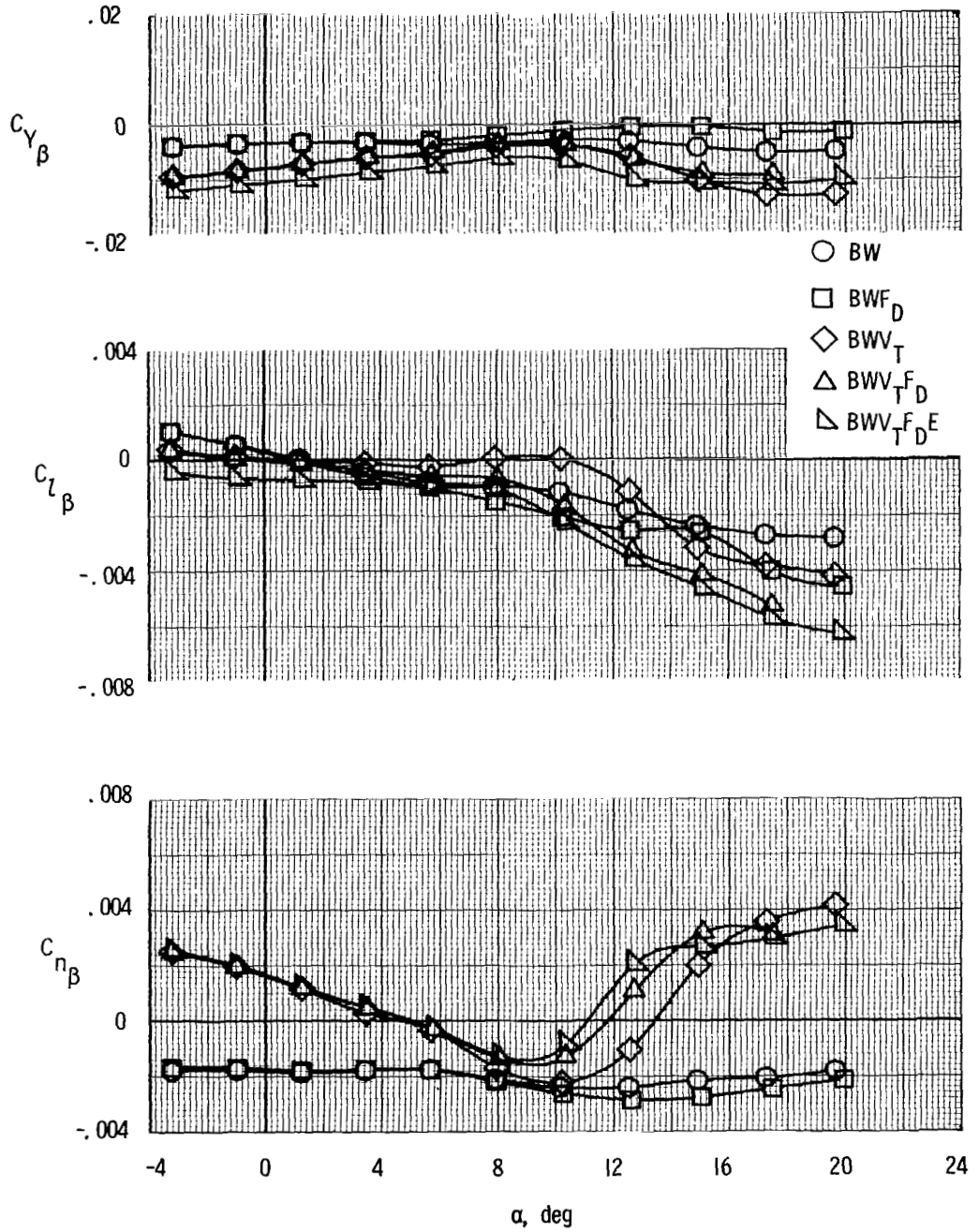

(a) M = 0.80.

Figure 11.- Lateral-directional stability characteristics of body-wing configuration alone and with various forward delta, tip-fin, and engine components.

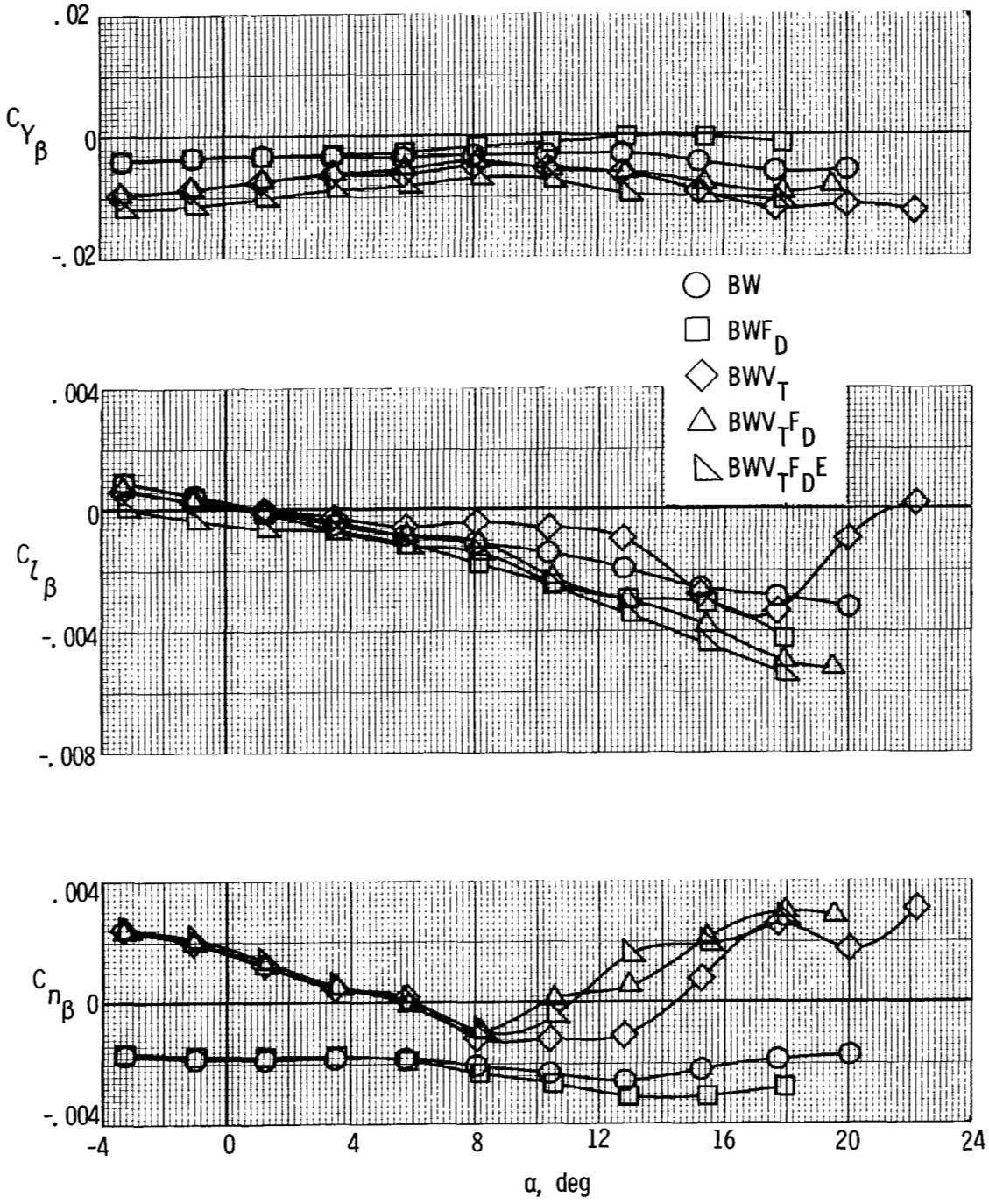

(b) M = 0.90.

Figure 11.- Continued.

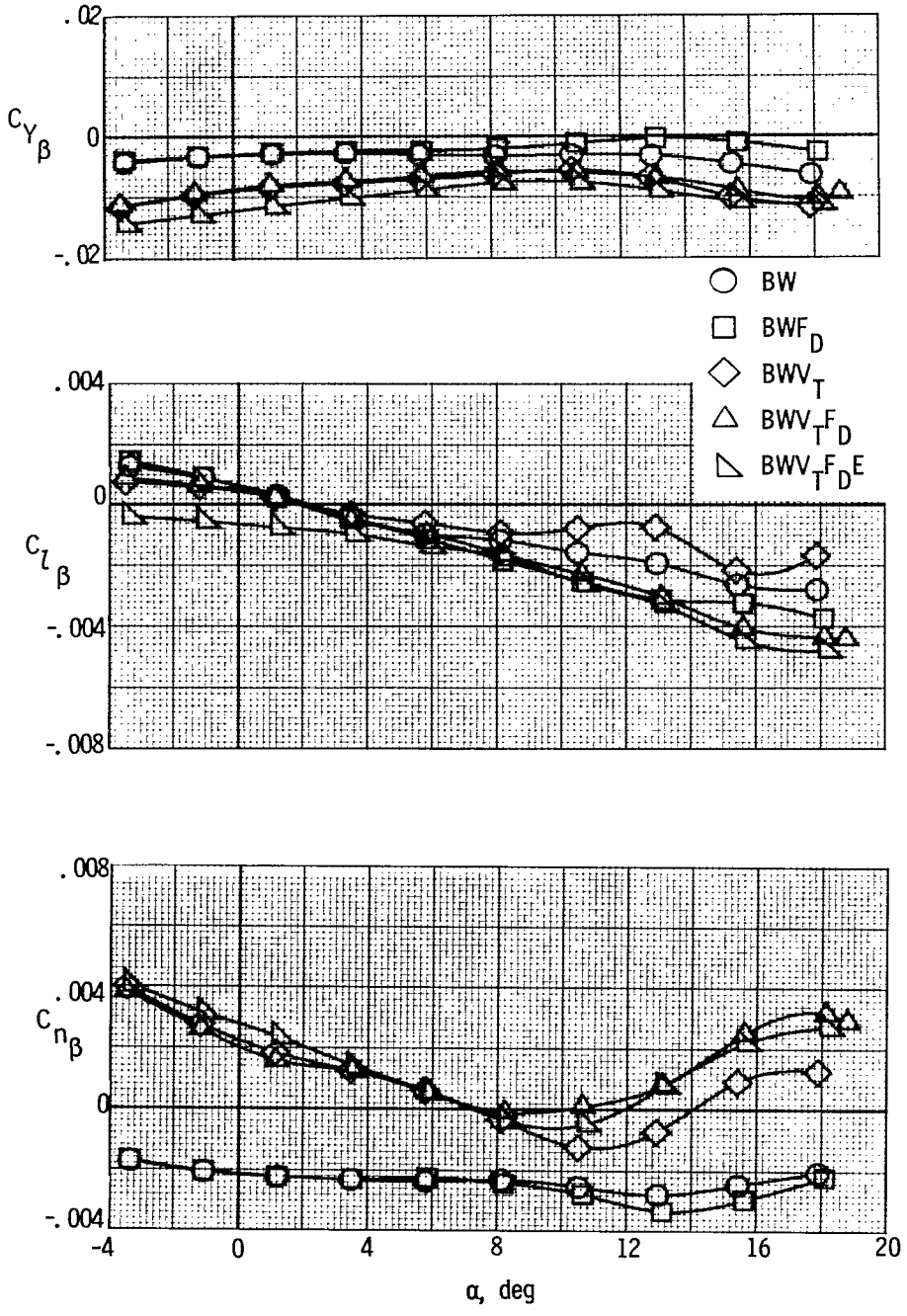

(c) M = 0.95.

Figure 11.- Continued.

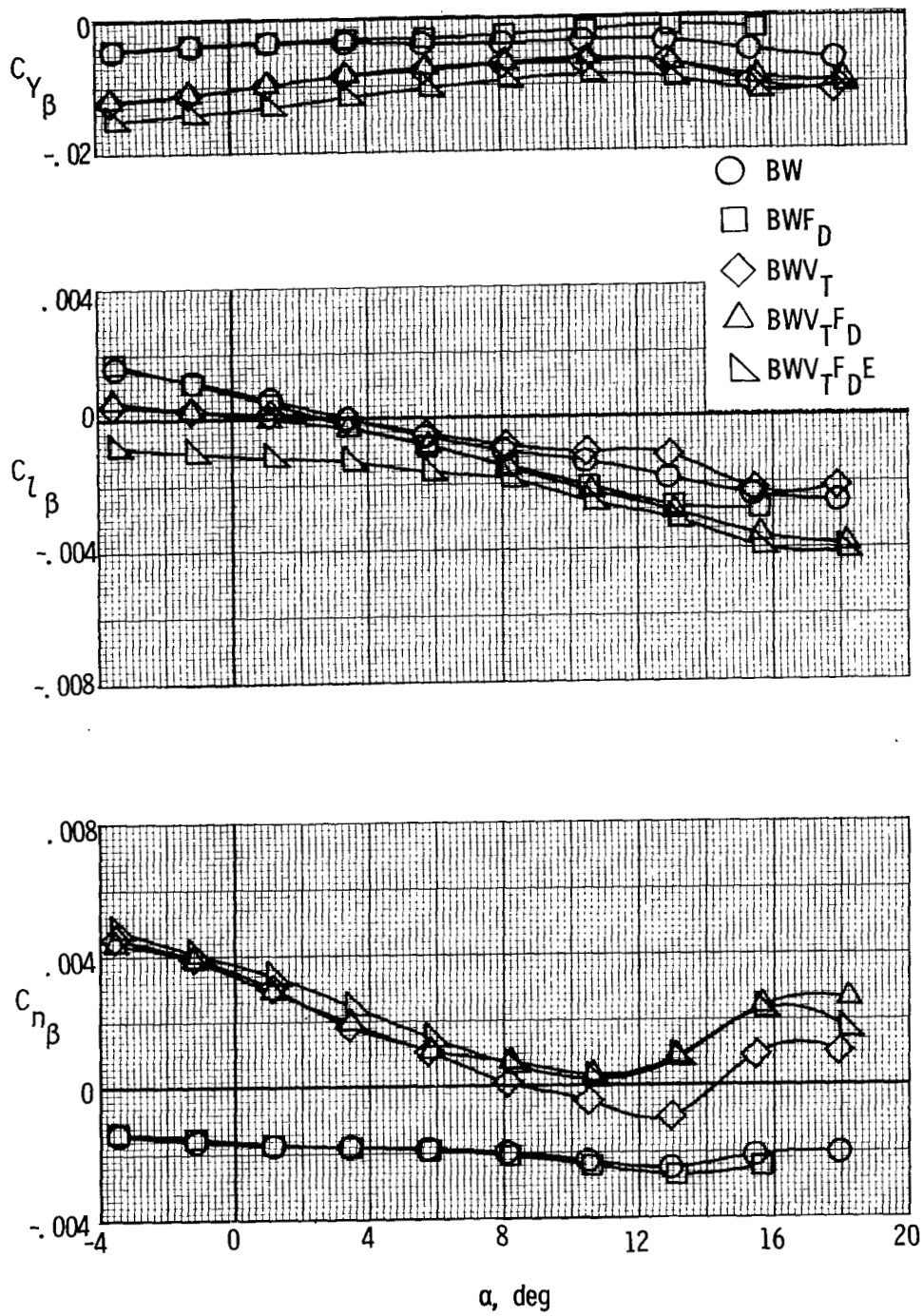

(d) M = 0.98.

Figure 11.- Continued.

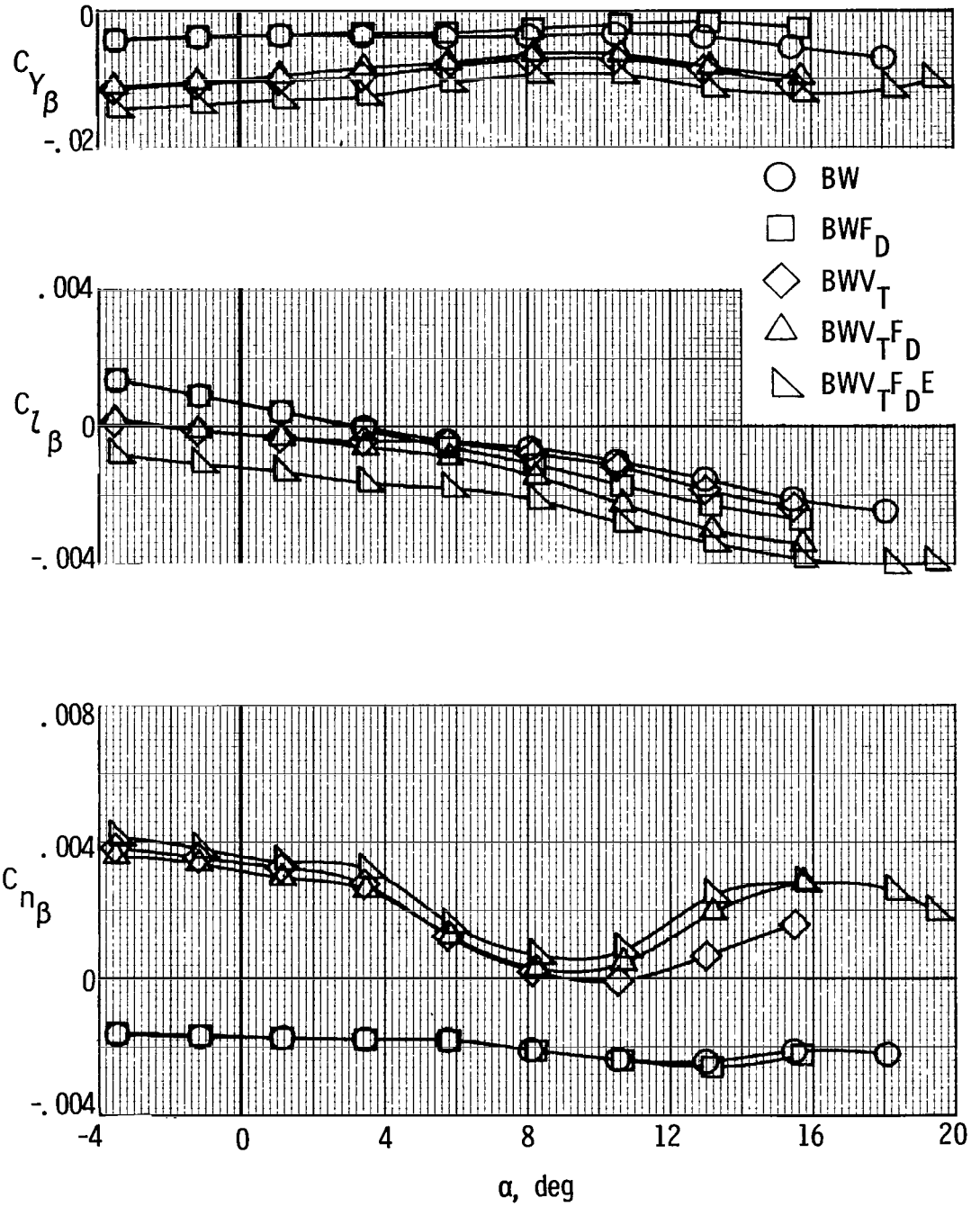

(e) M = 1.10.

Figure 11.- Continued.

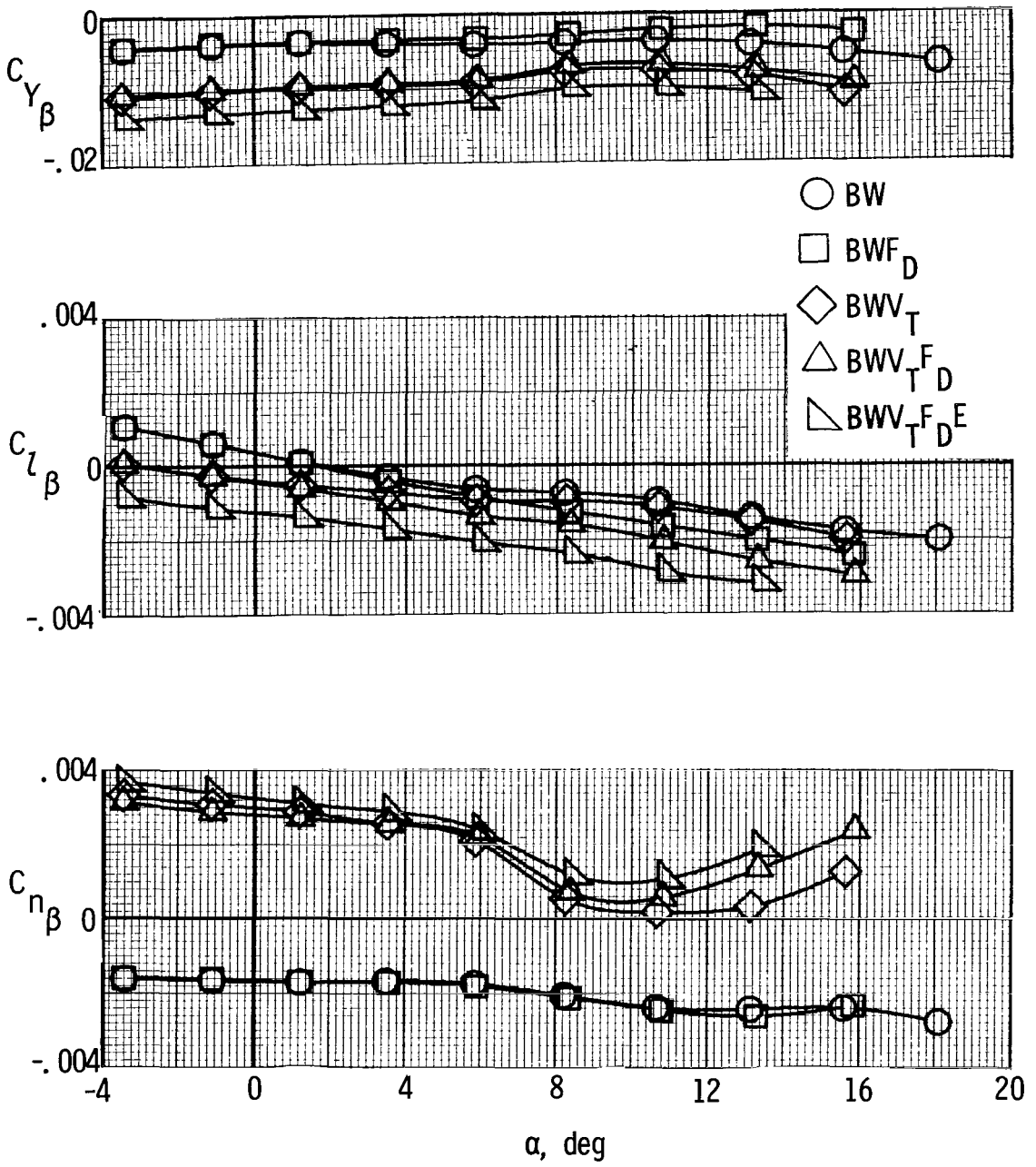

(f) M = 1.20.

Figure 11.- Concluded.

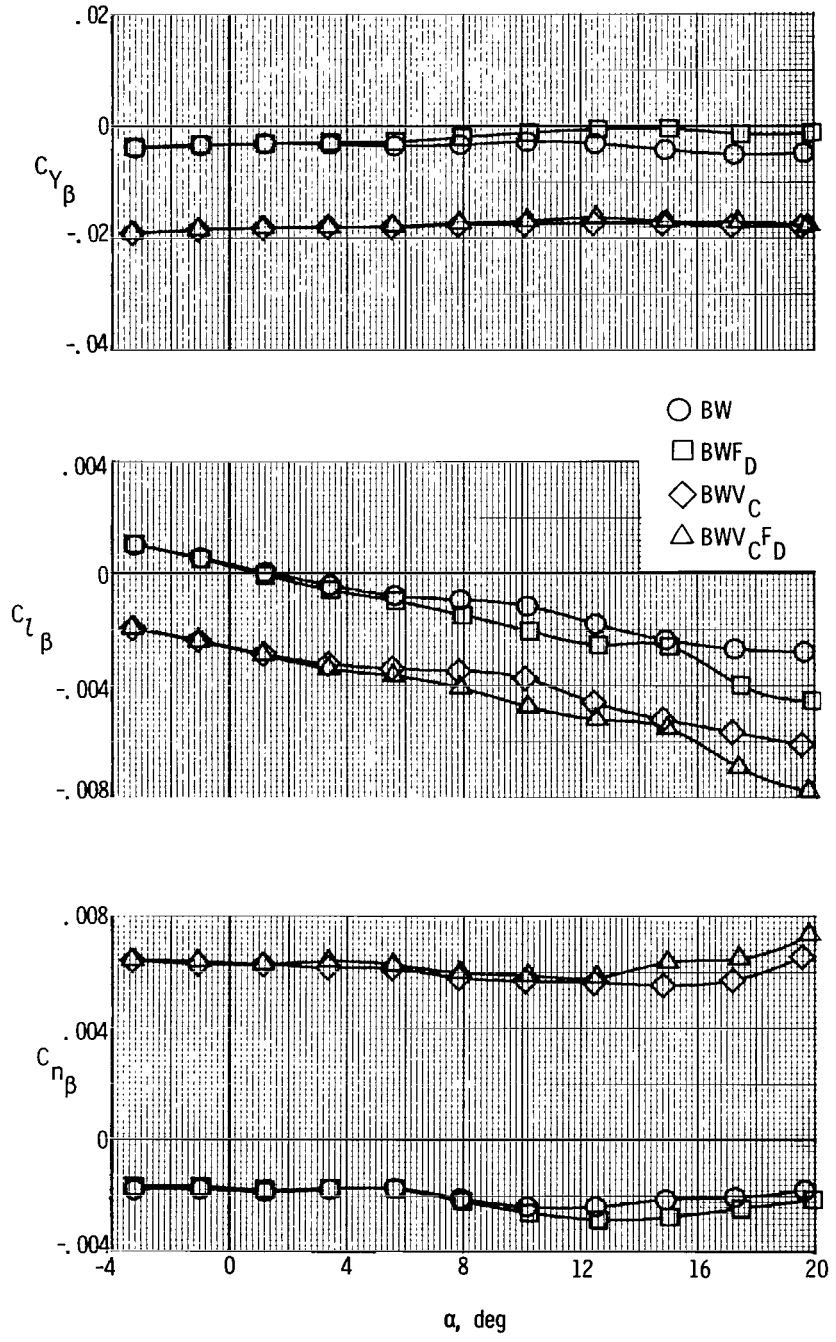

(a) M = 0.80.

Figure 12.- Lateral-directional stability characteristics of the body-wing configuration alone and with various forward delta wing and center-tail components.

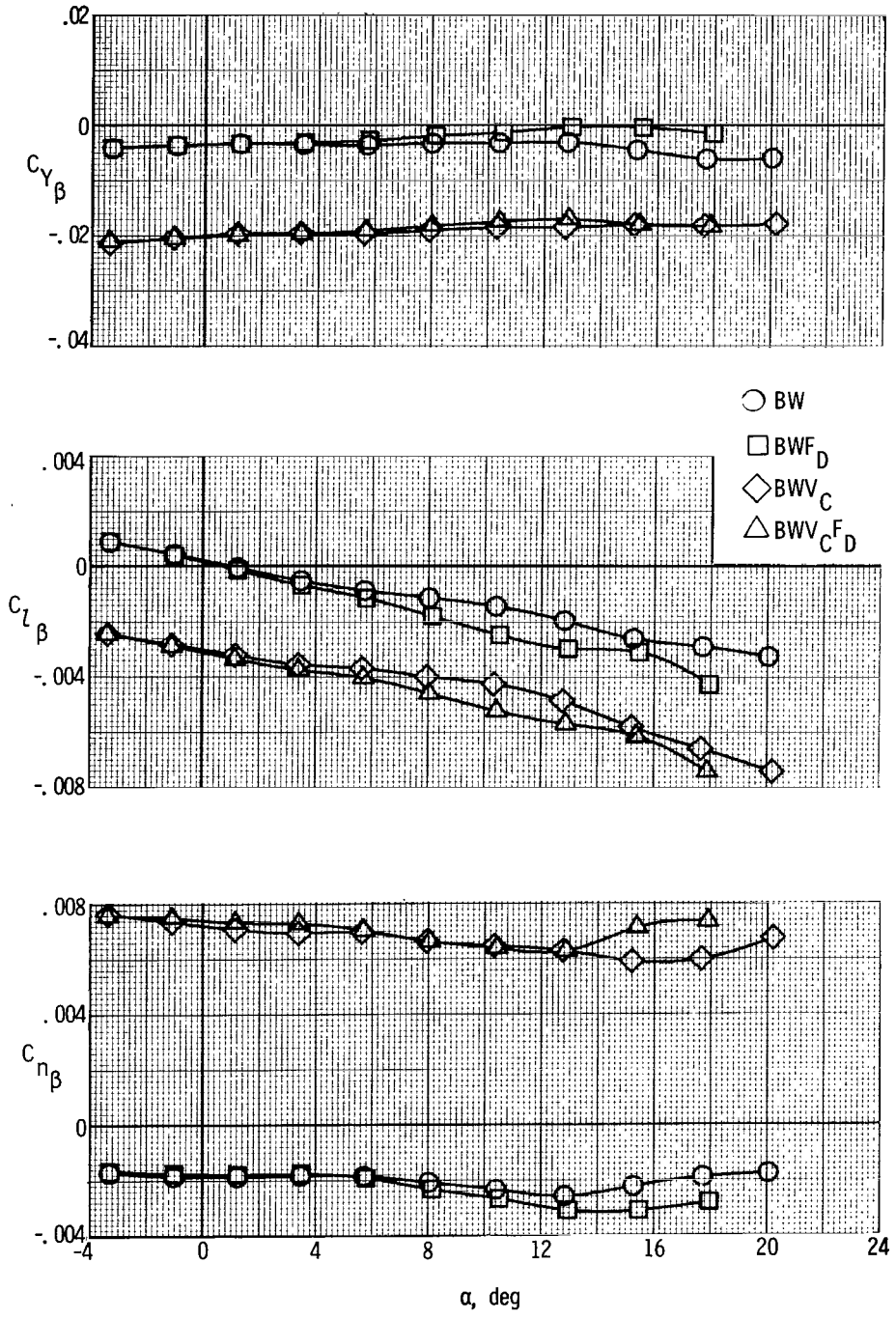

(b) M = 0.90.

Figure 12.- Continued.

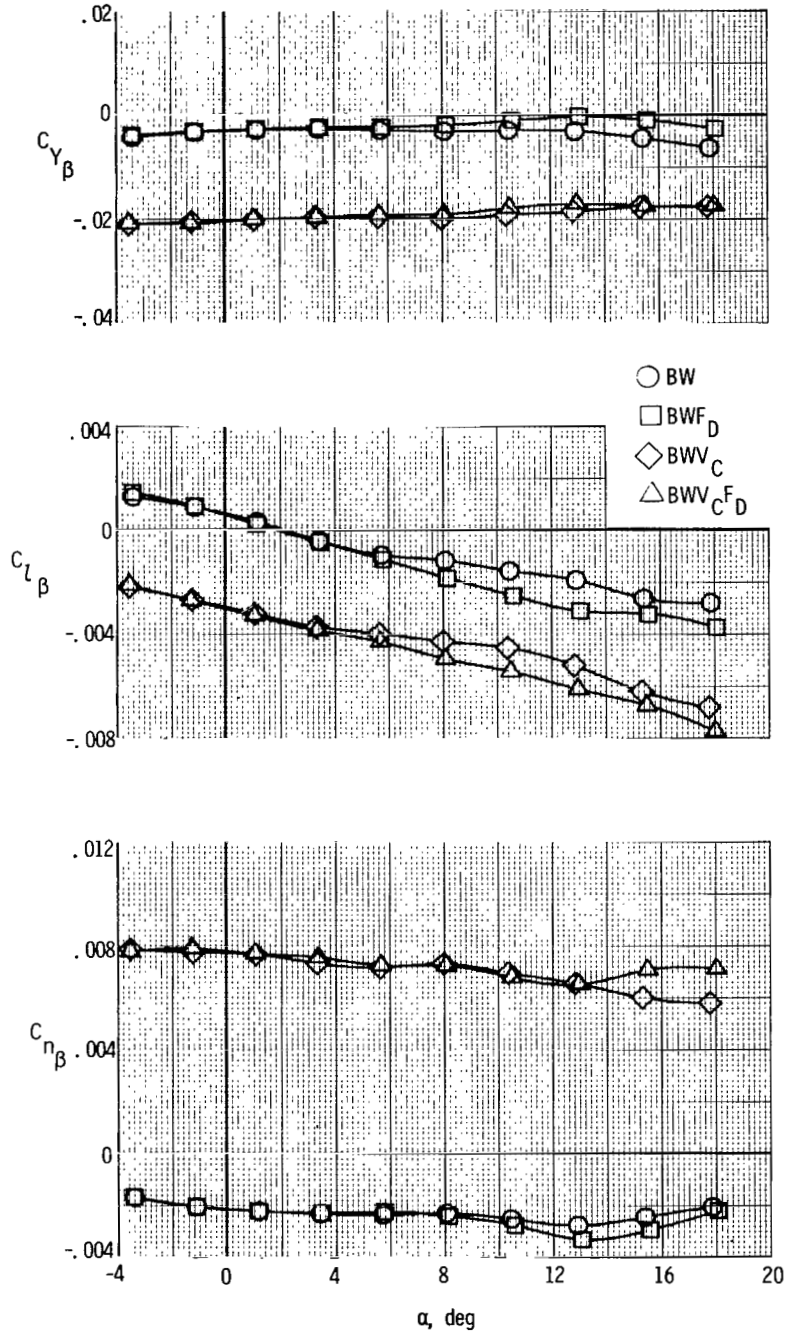

(c) M = 0.95.

Figure 12.- Continued.

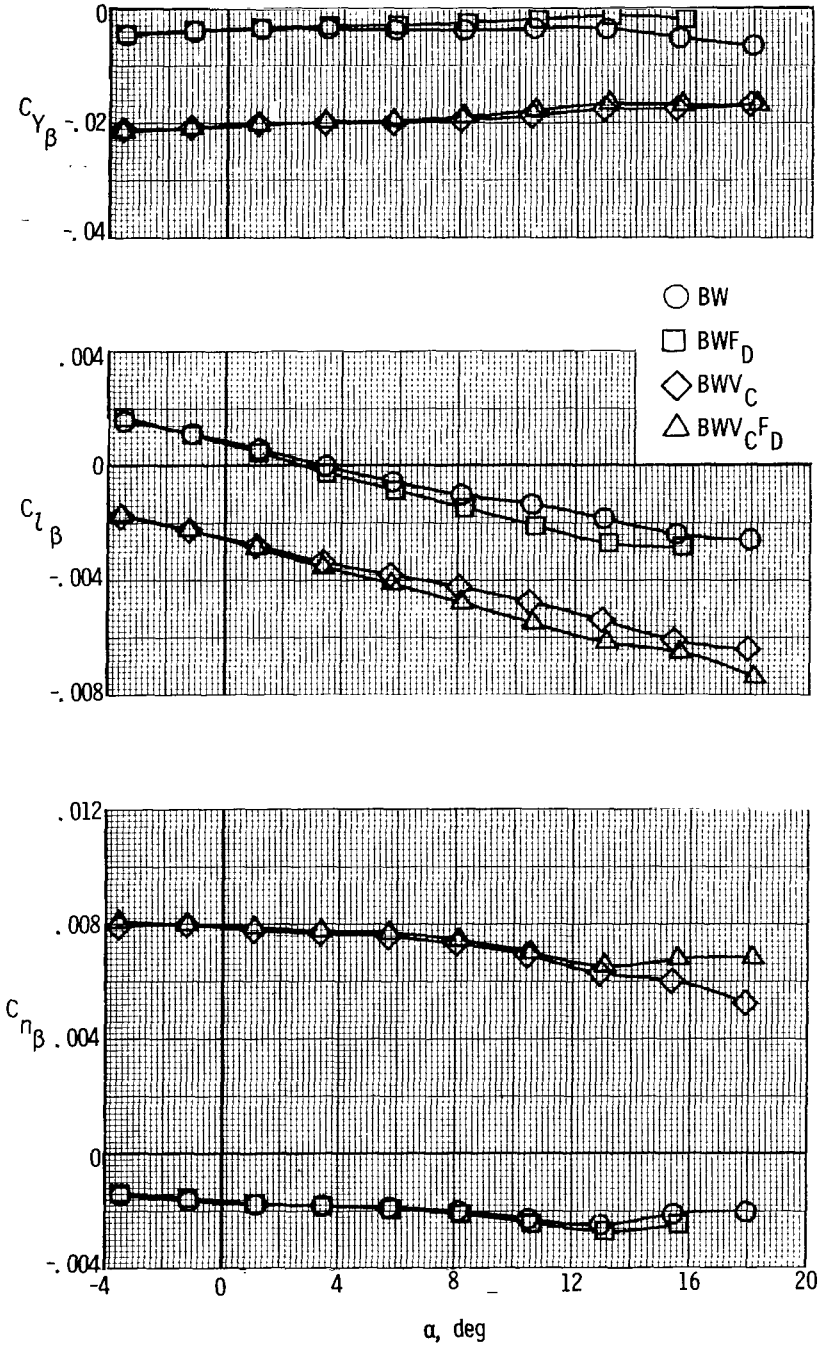

(d) M = 0.98.

Figure 12.- Continued.

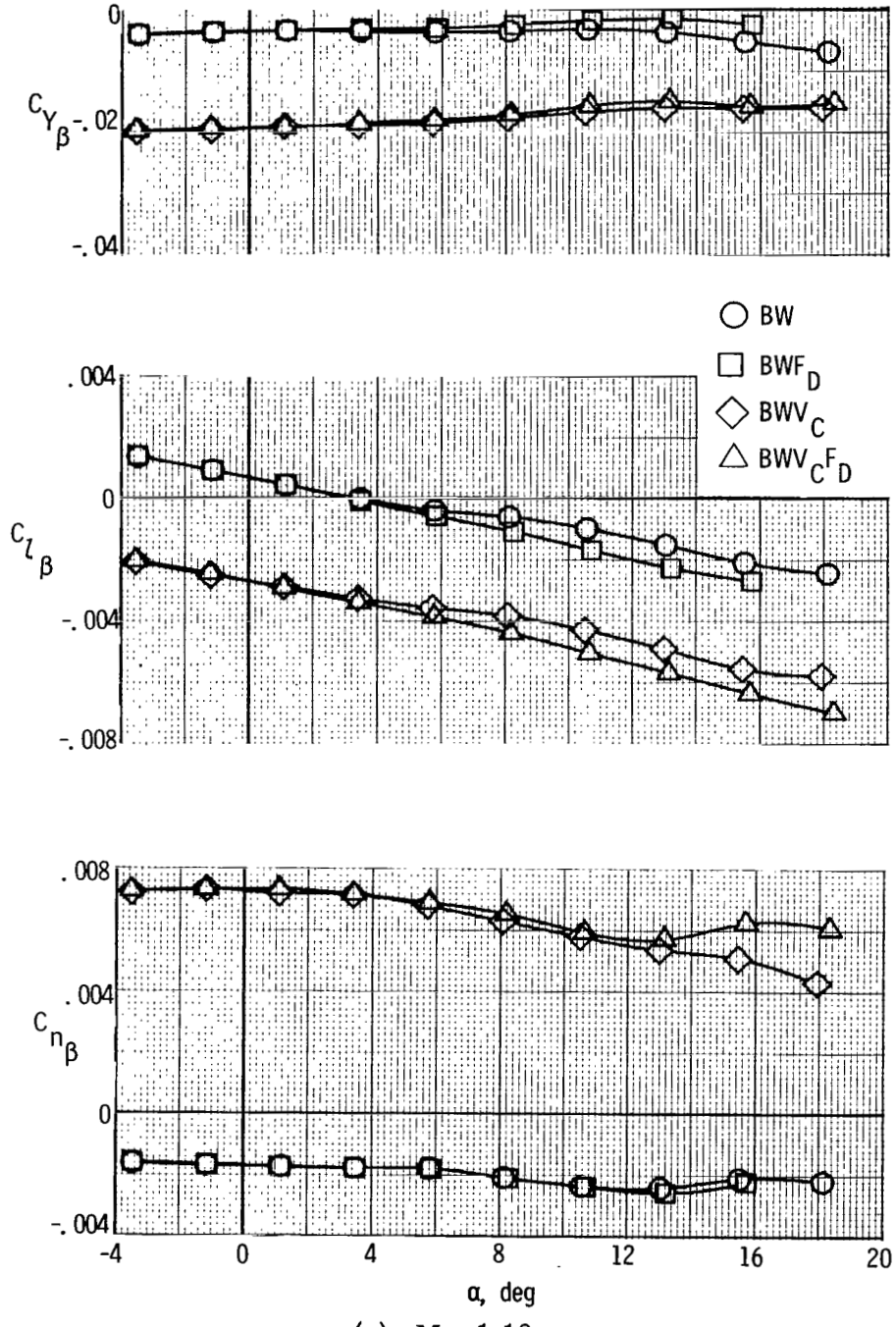

(e) M = 1.10.

Figure 12.- Continued.

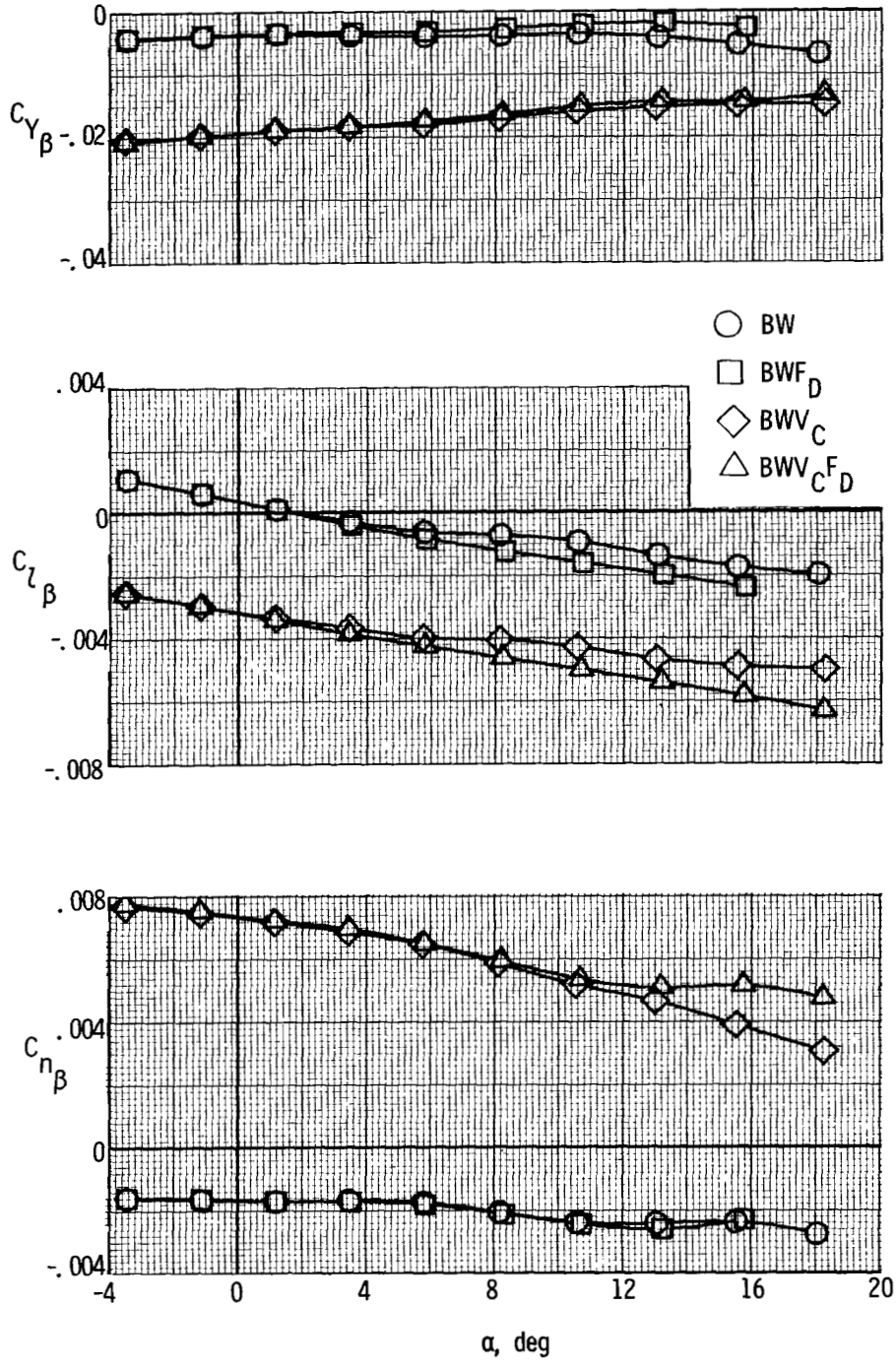

(f) M = 1.20.

Figure 12.- Concluded.

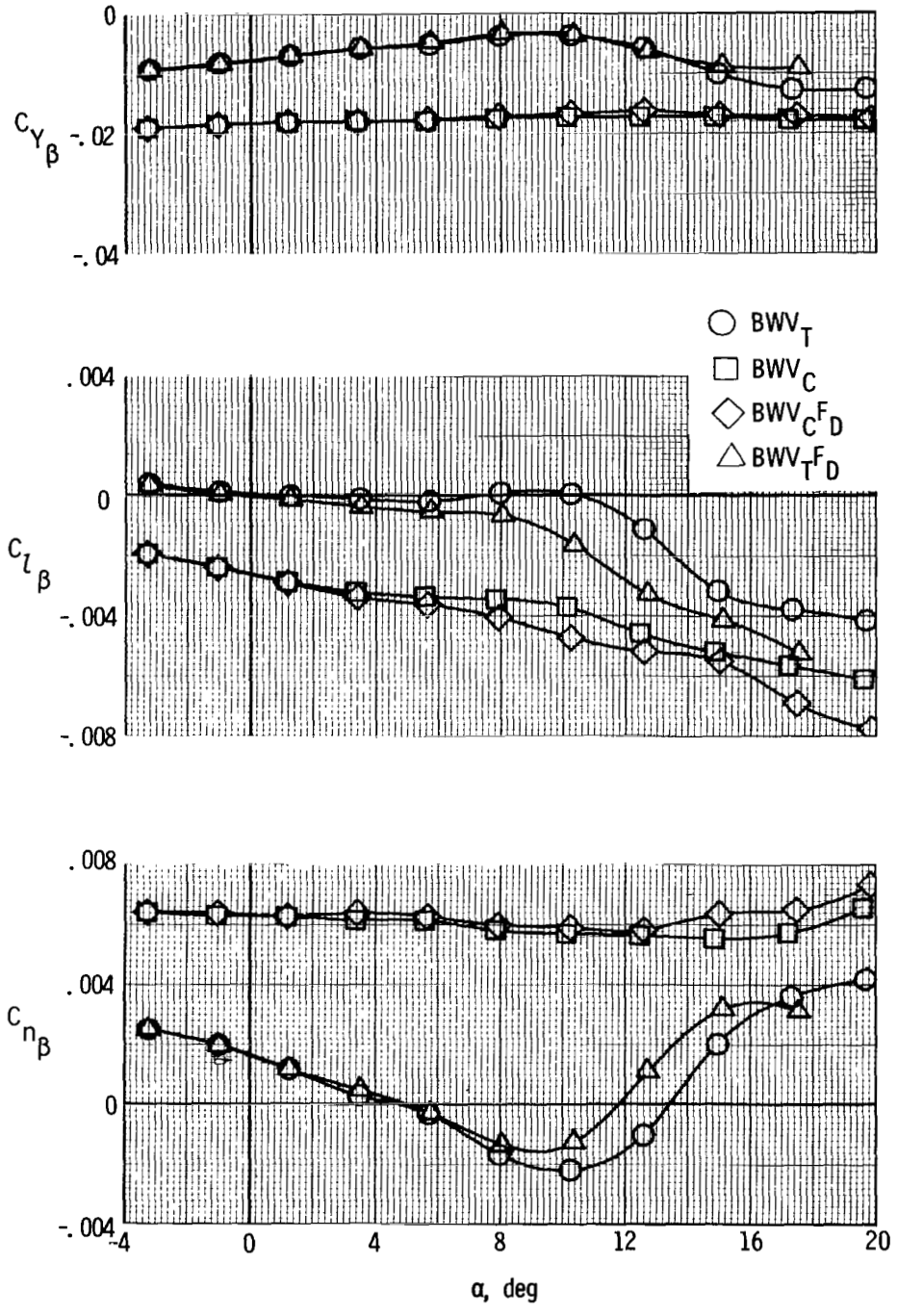

(a) M = 0.80.

Figure 13.- Comparison of the lateral-directional stability characteristics of tip-fin and center-tail configurations.

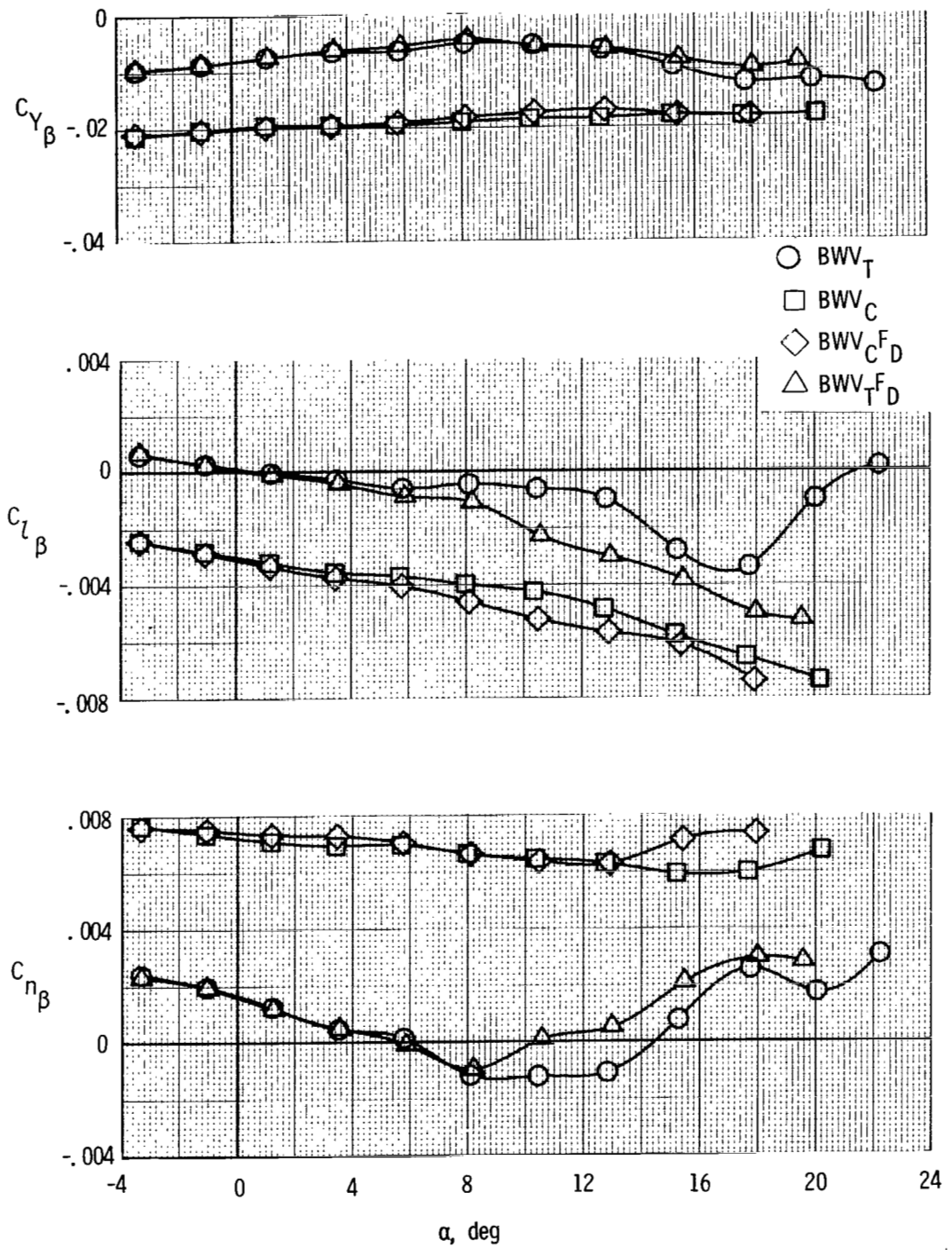

(b) M = 0.90.

Figure 13.- Continued.

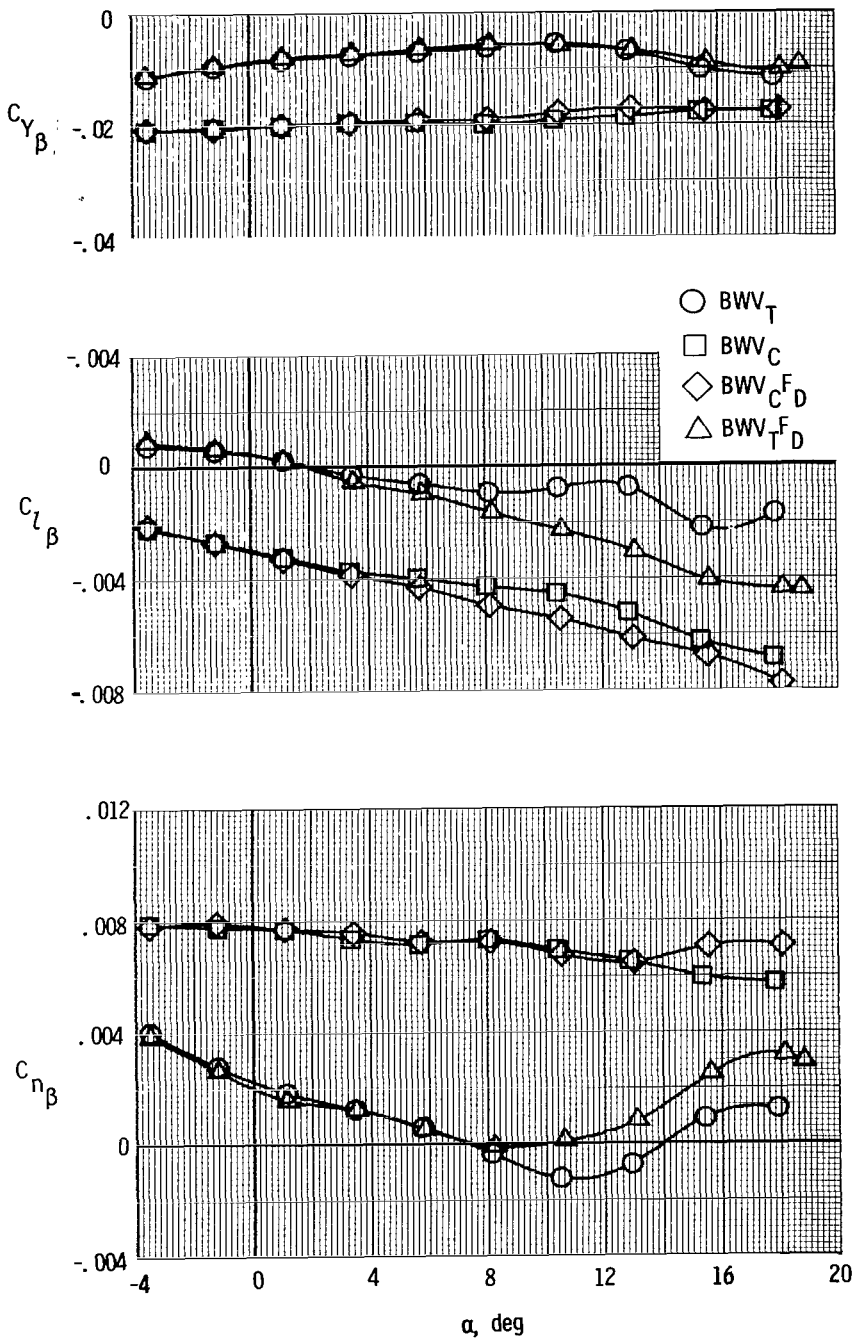

(c) M = 0.95.

Figure 13.- Continued.

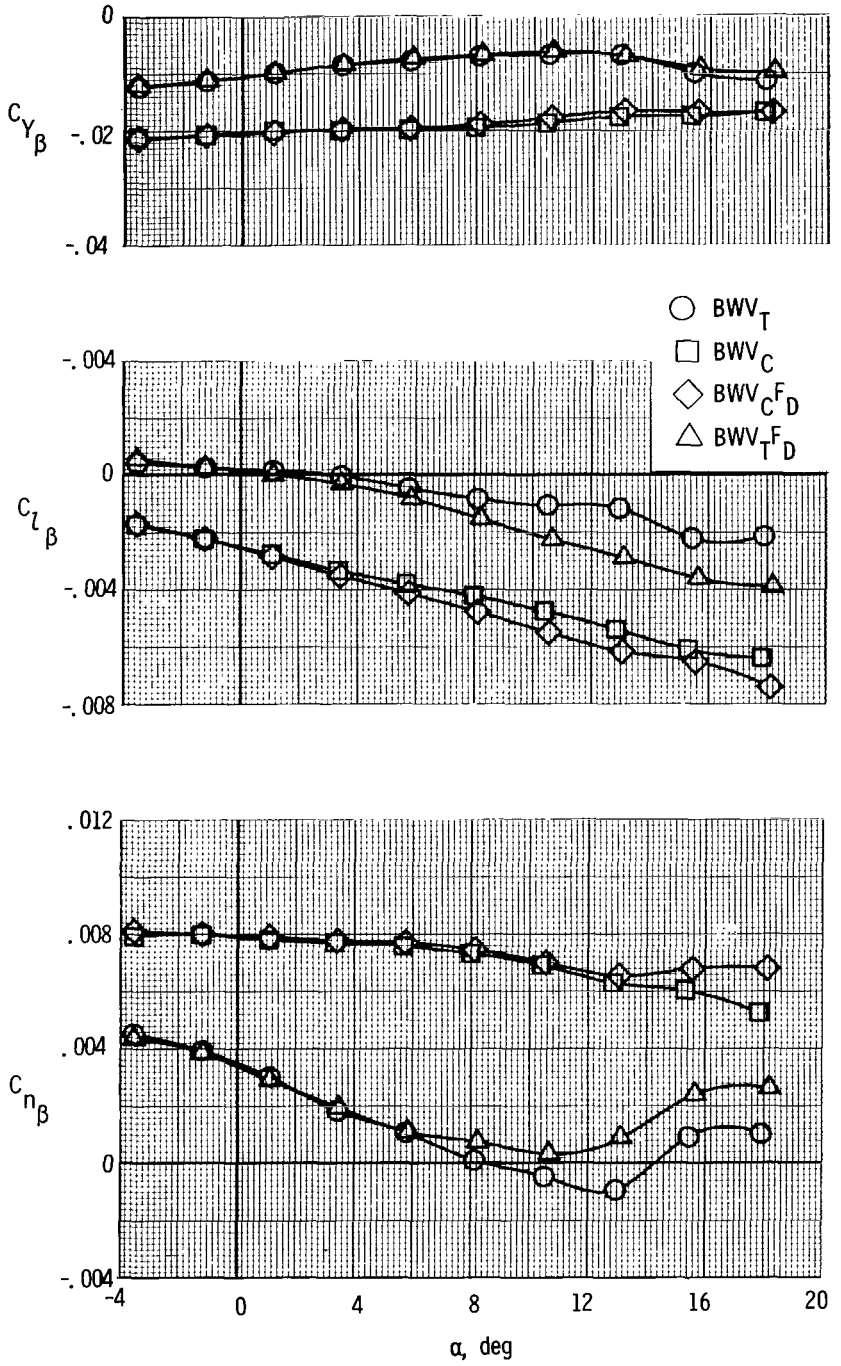

(d) M = 0.98.

Figure 13.- Continued.

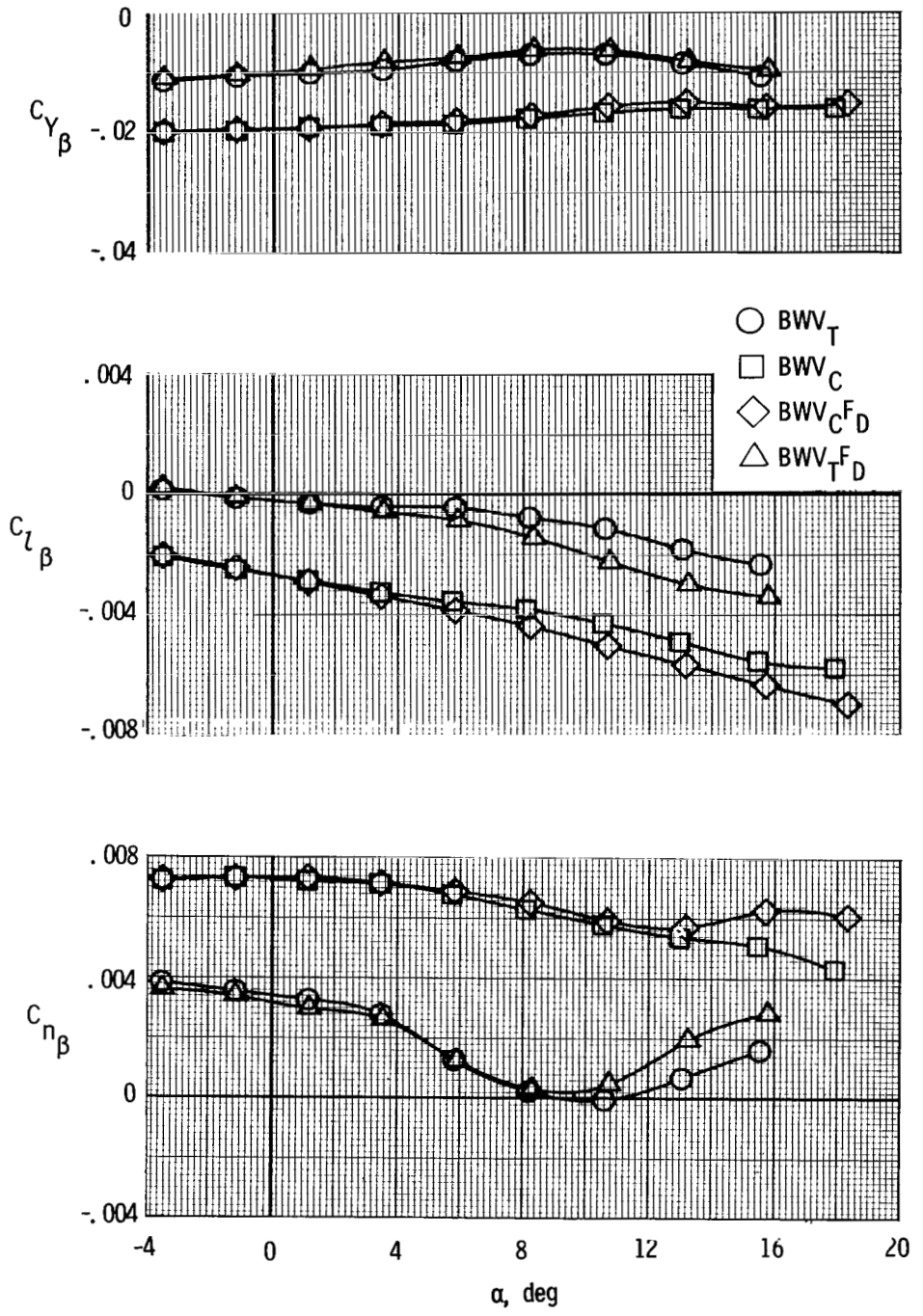

(e) M = 1.10.

Figure 13.- Continued.

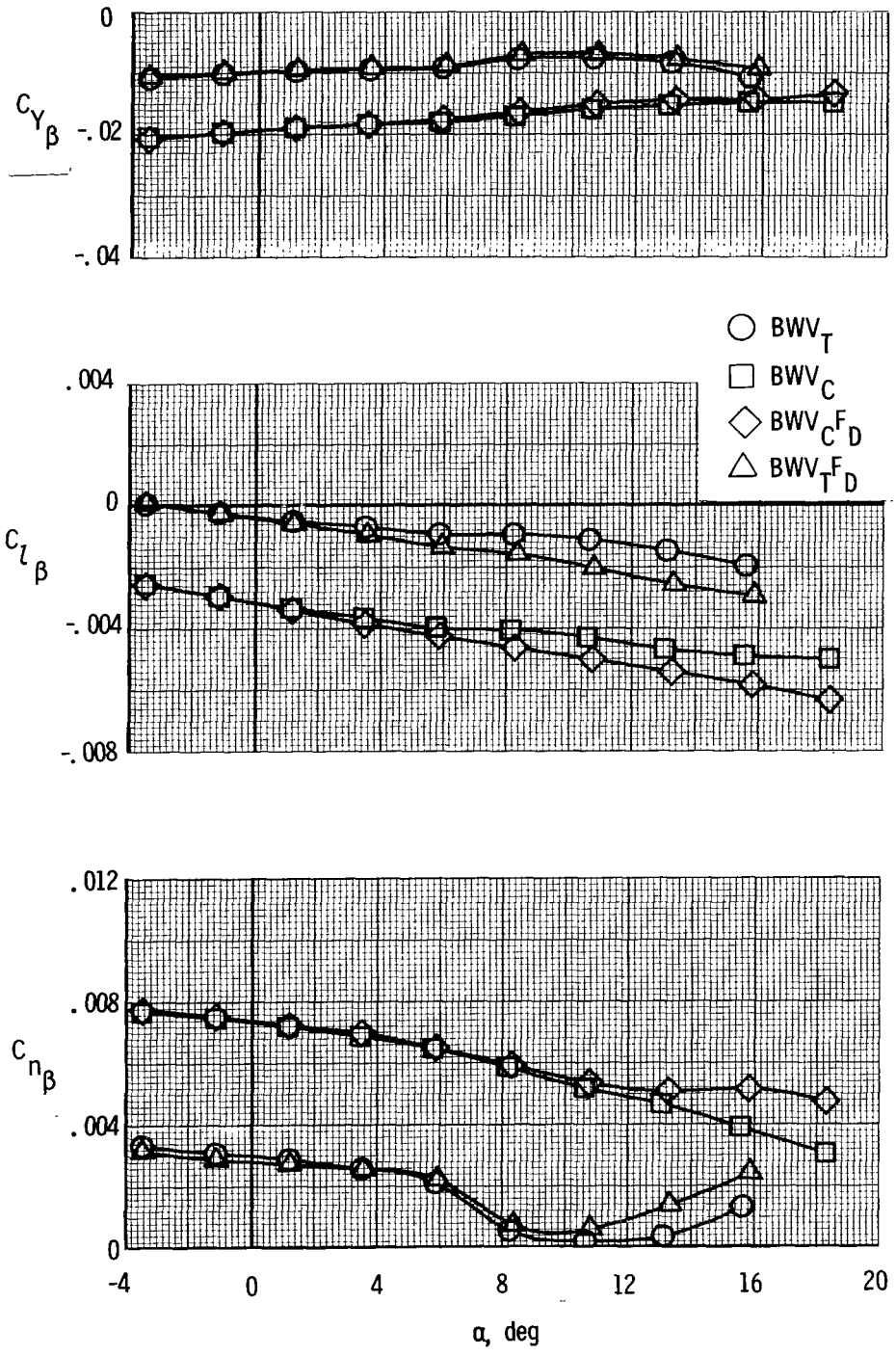

(f) M = 1.20.

Figure 13.- Concluded.

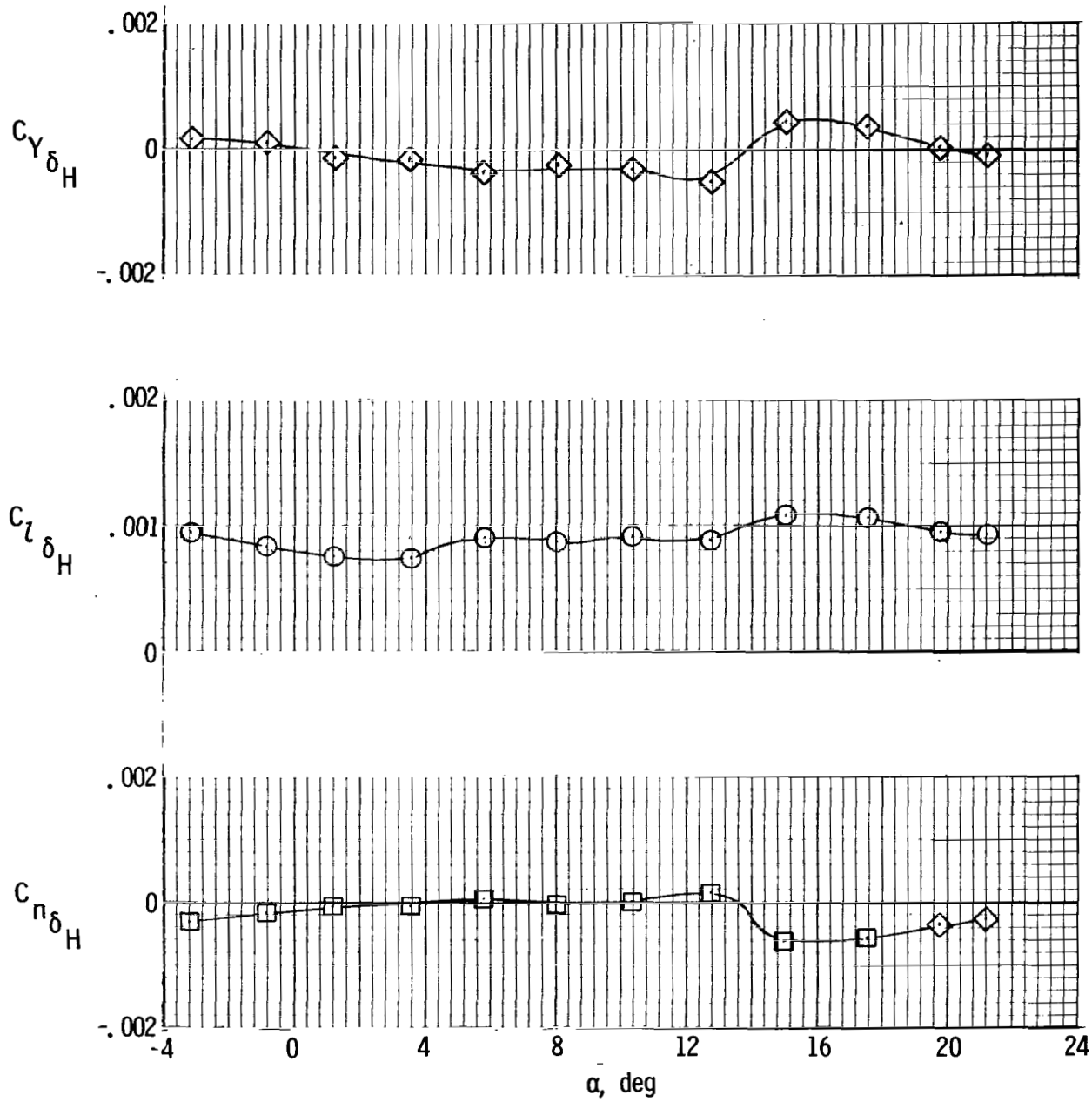

(a) M = 0.80.

Figure 14.- Roll control of configuration BWV_TF_DE.

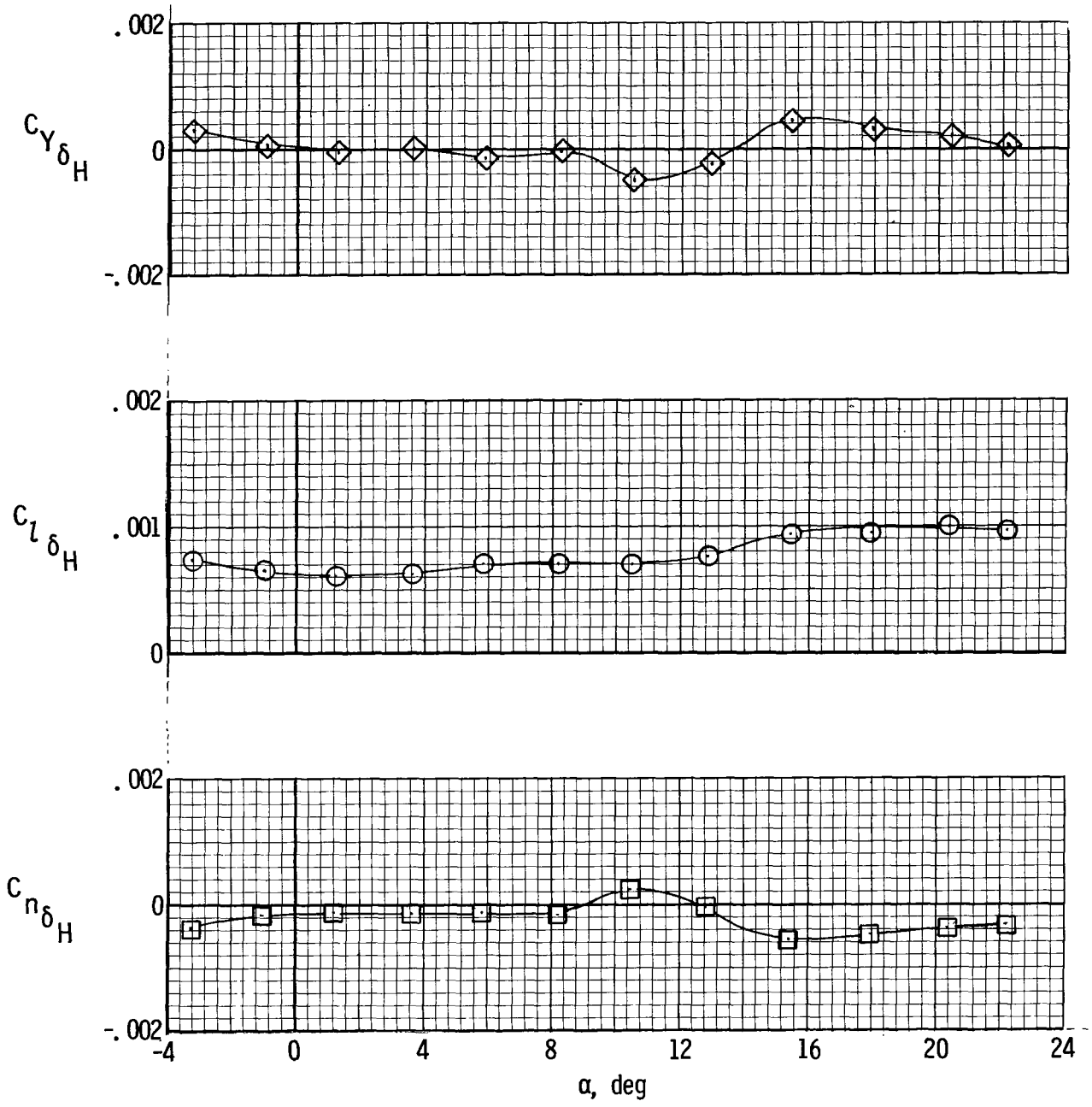

(b) M = 0.90.

Figure 14.- Continued.

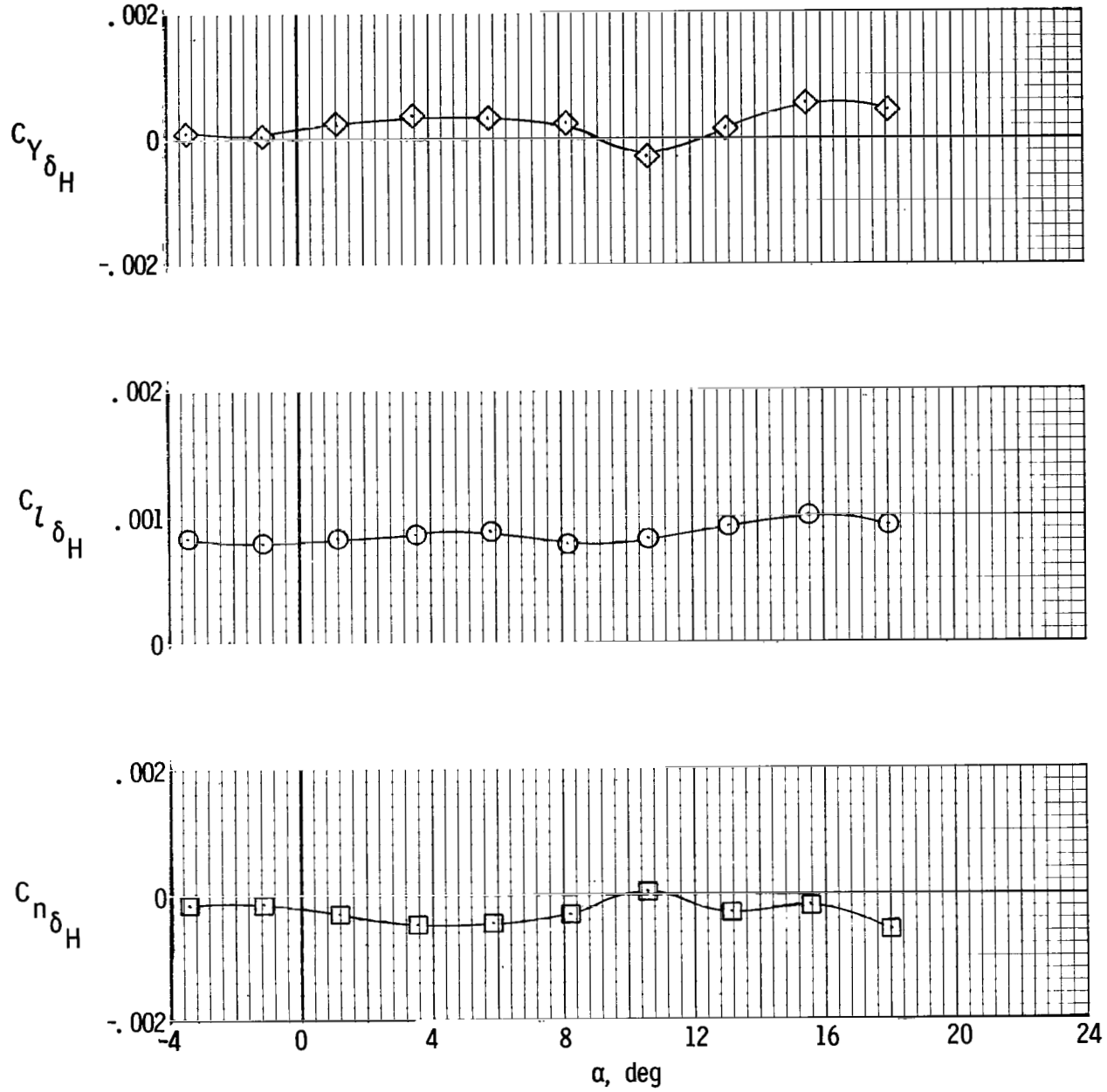

(c) M = 0.95.

Figure 14.- Continued.

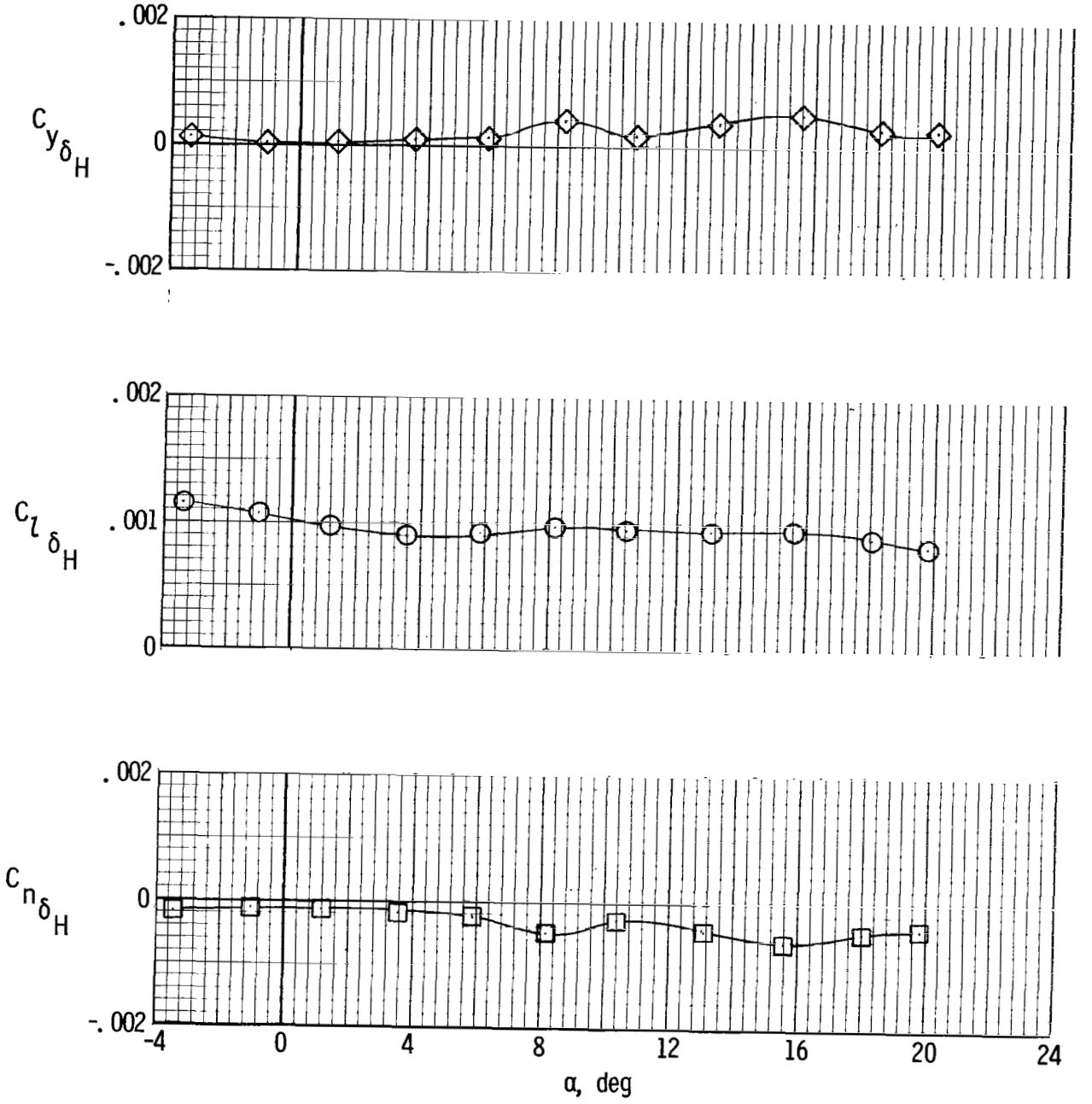

(d) M = 0.98.

Figure 14.- Continued.

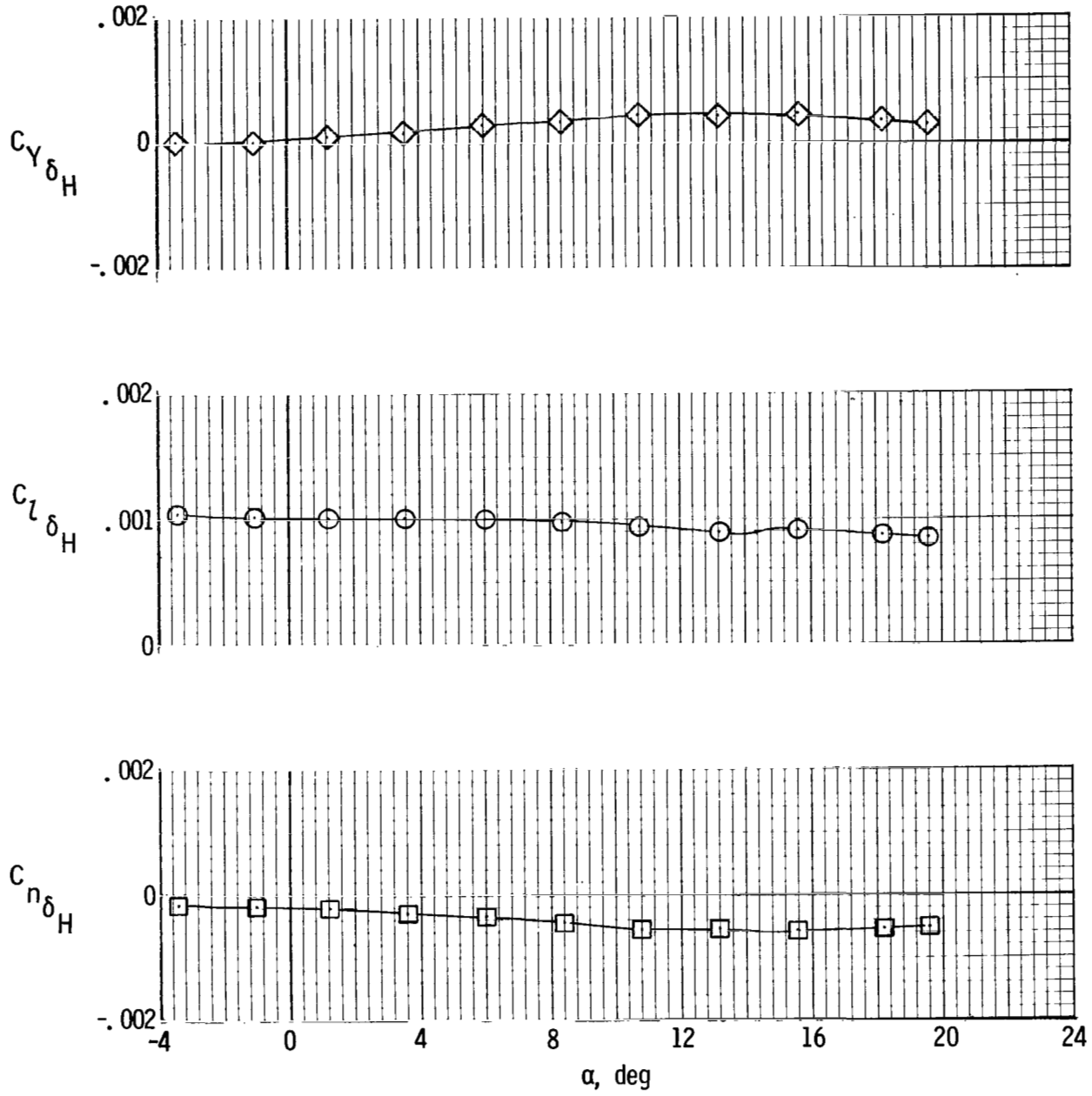

(e) M = 1.10.

Figure 14.- Continued.

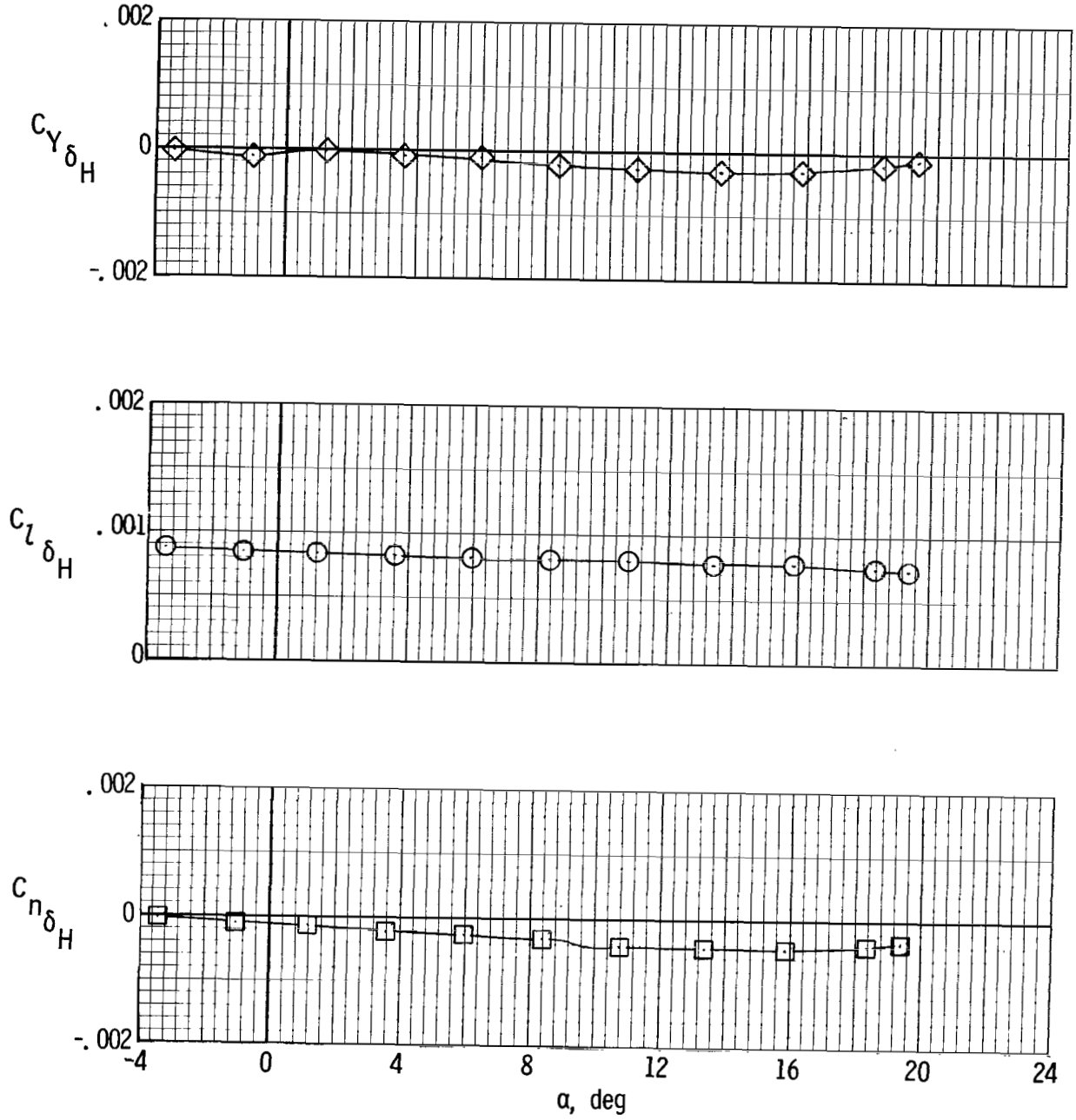

(f) M = 1.20.

Figure 14.- Concluded.

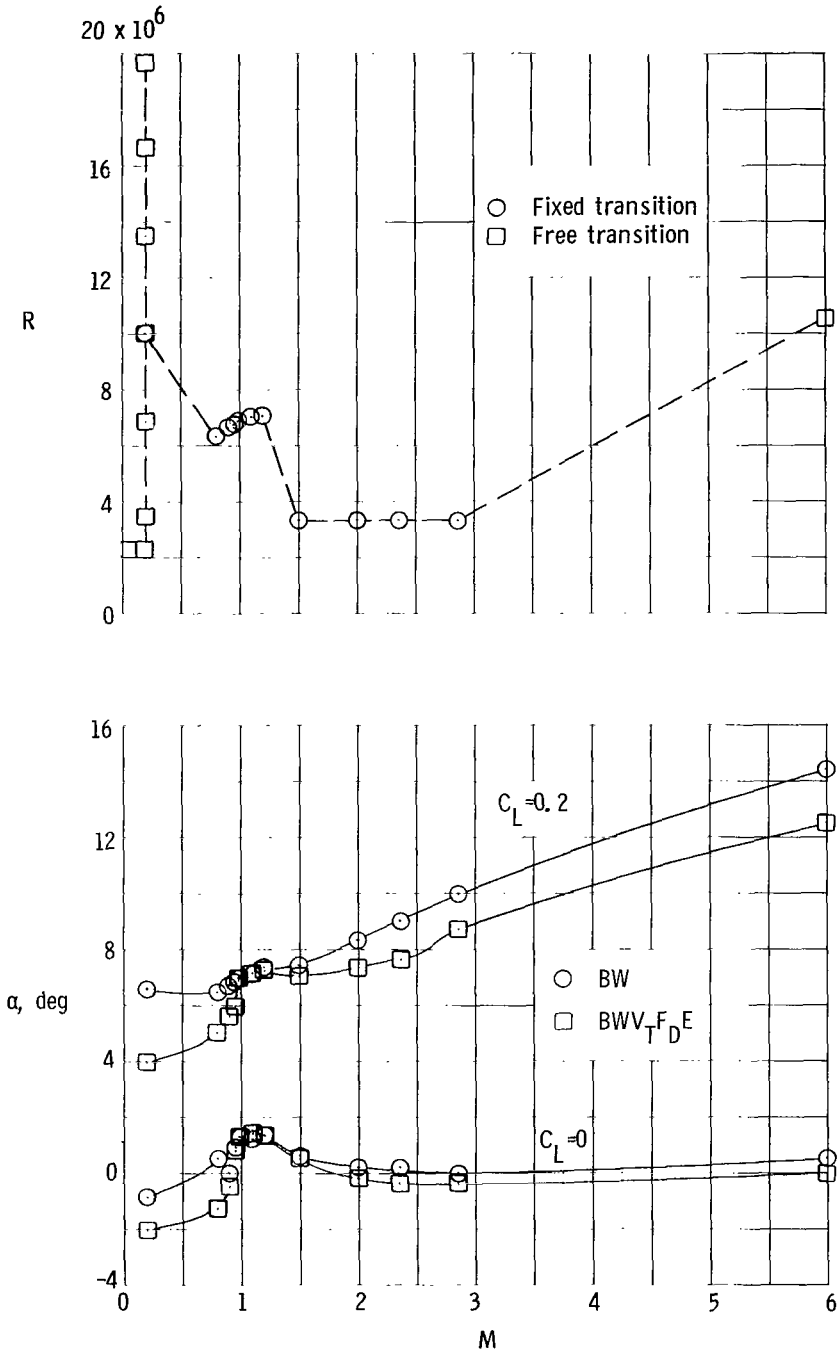

Figure 15.- Variation of test Reynolds number and angle of attack with Mach number for lift coefficients of 0 and 0.2.

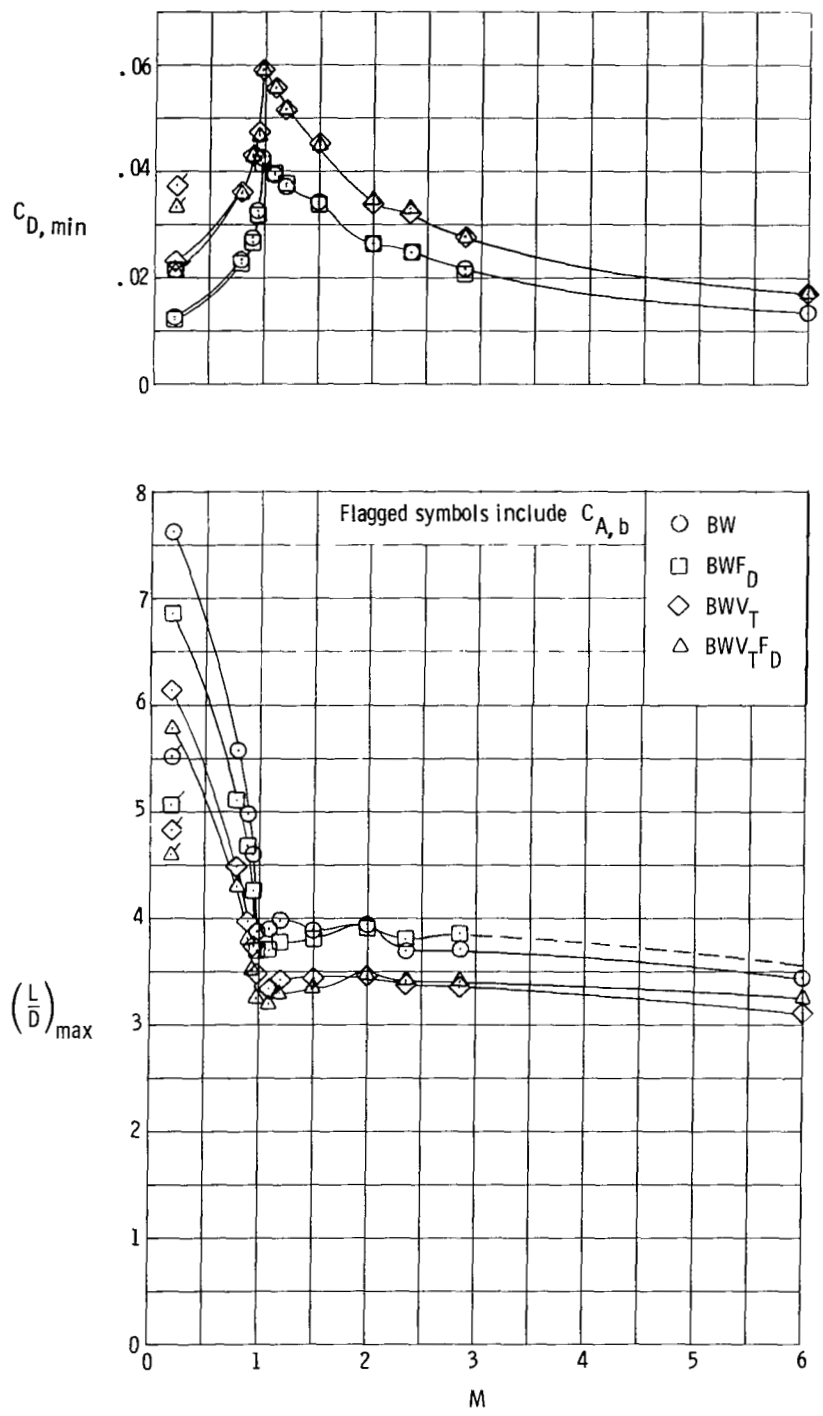

Figure 16.- Variation of minimum drag and maximum lift-drag ratio with Mach number on component buildup of tip-fin models.

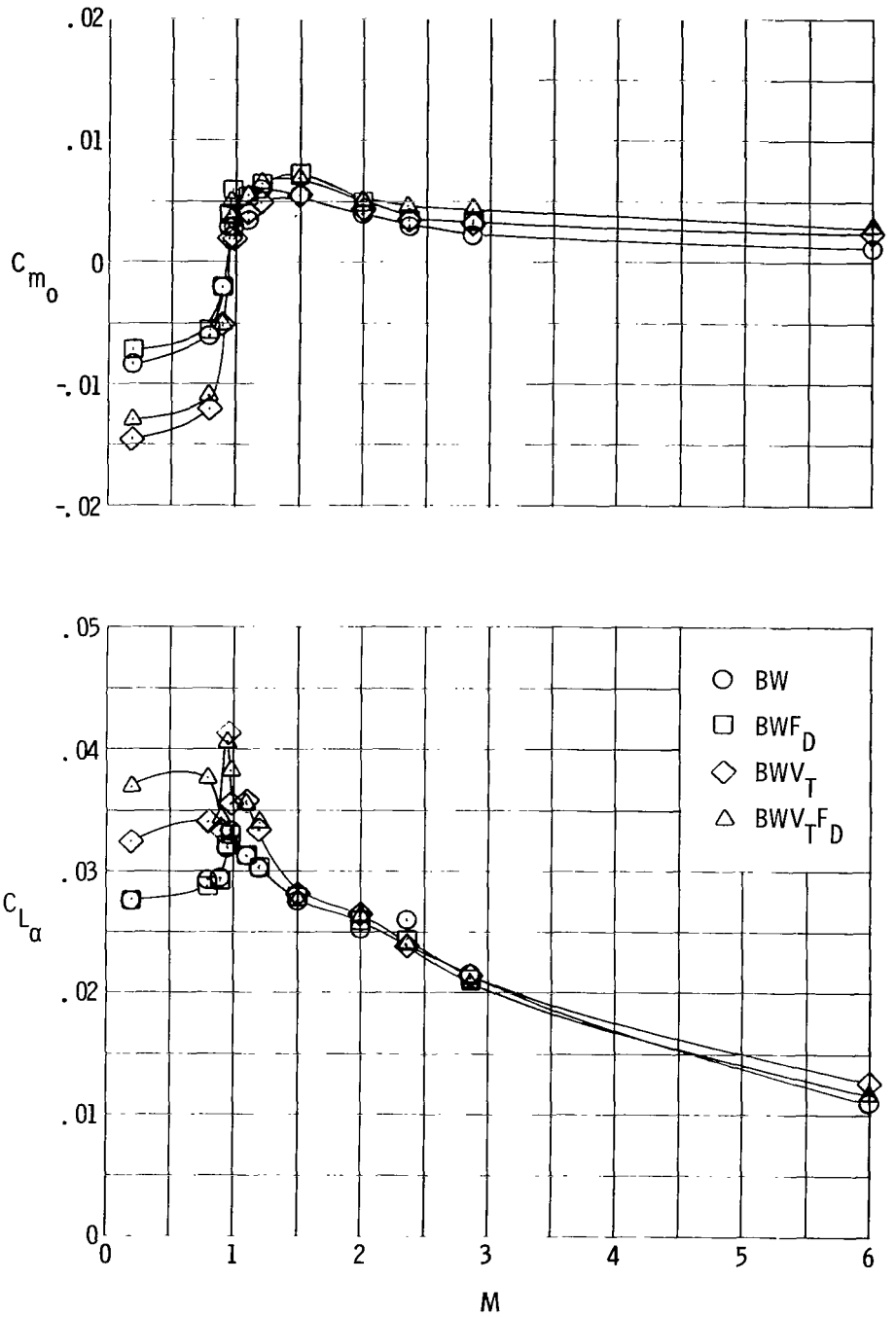

Figure 17.- Variation of values of pitching-moment coefficient with Mach number at zero lift and slope of lift curve at zero lift on component buildup of tip-fin models.

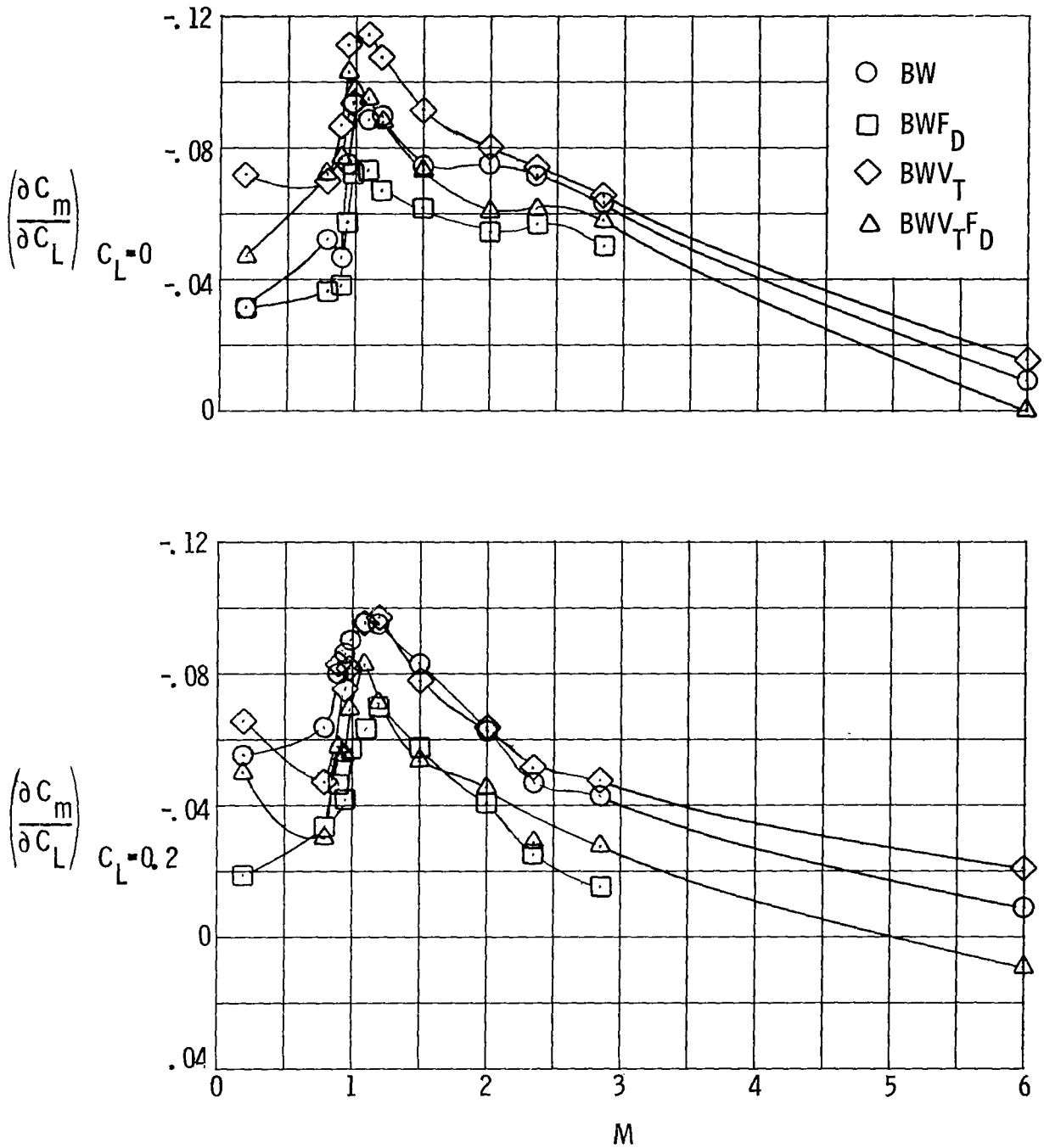

Figure 18.- Variation of longitudinal stability with Mach number at lift coefficients of 0 and 0.2 on component buildup of tip-fin models.

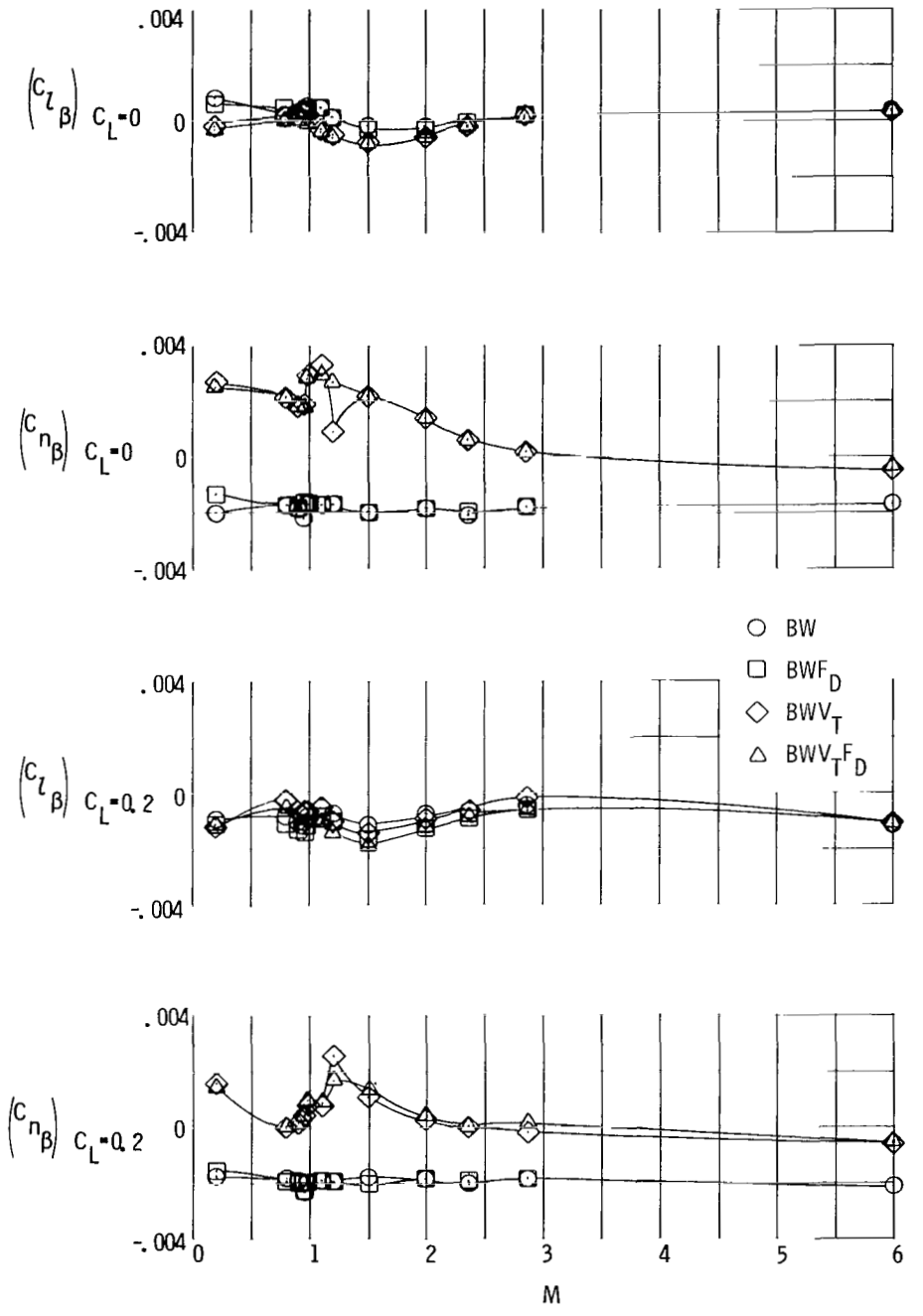

Figure 19.- Variation of lateral-directional stability with Mach number at lift coefficients of 0 and 0.2 on component buildup of tip-fin models.

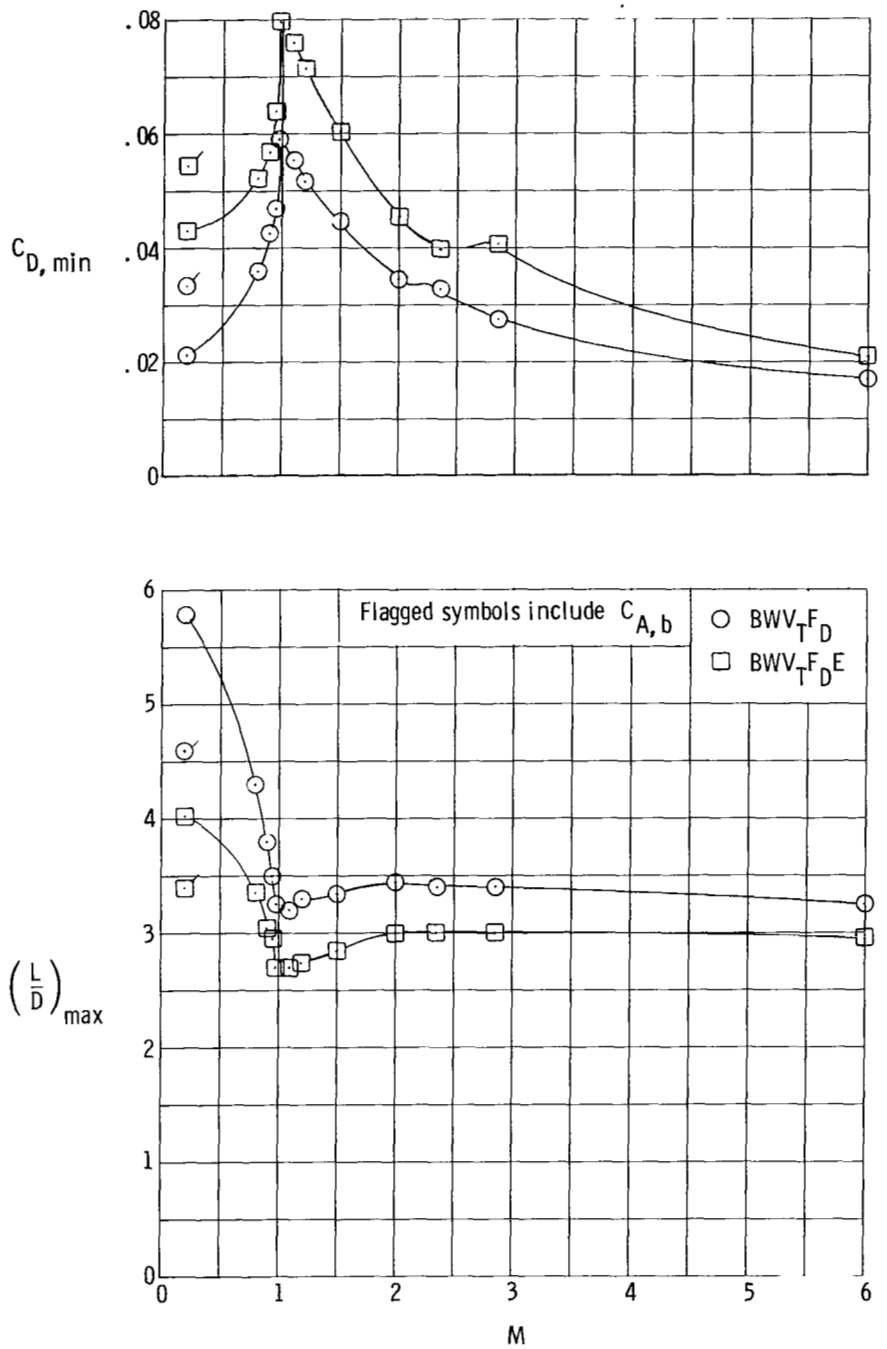

Figure 20.- Variation of minimum drag and maximum lift-drag ratio with Mach number on complete configuration with and without engine.

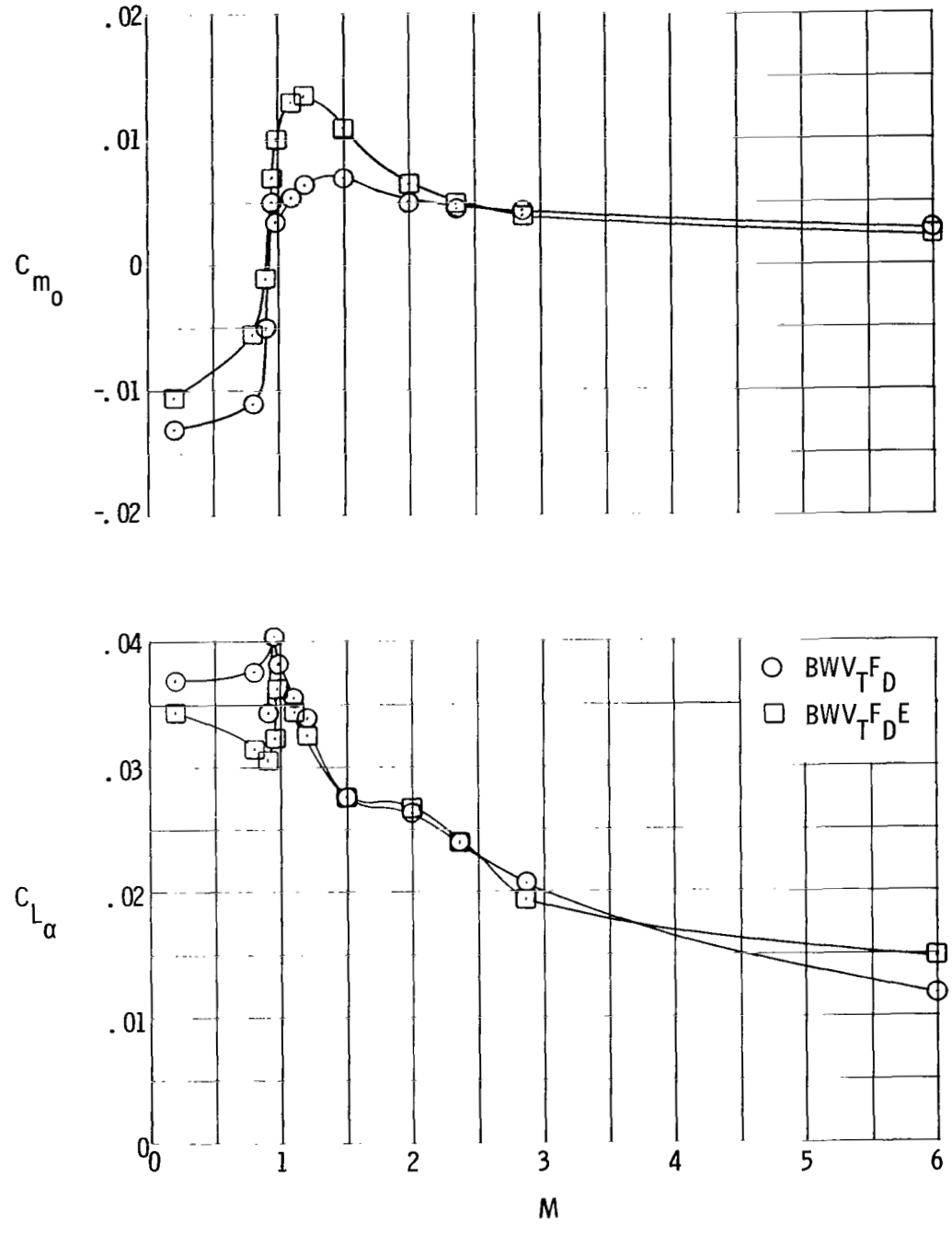

Figure 21.- Variation of values of pitching-moment coefficient with Mach number at zero lift and slope of lift curve at zero lift on complete configuration with and without engine.

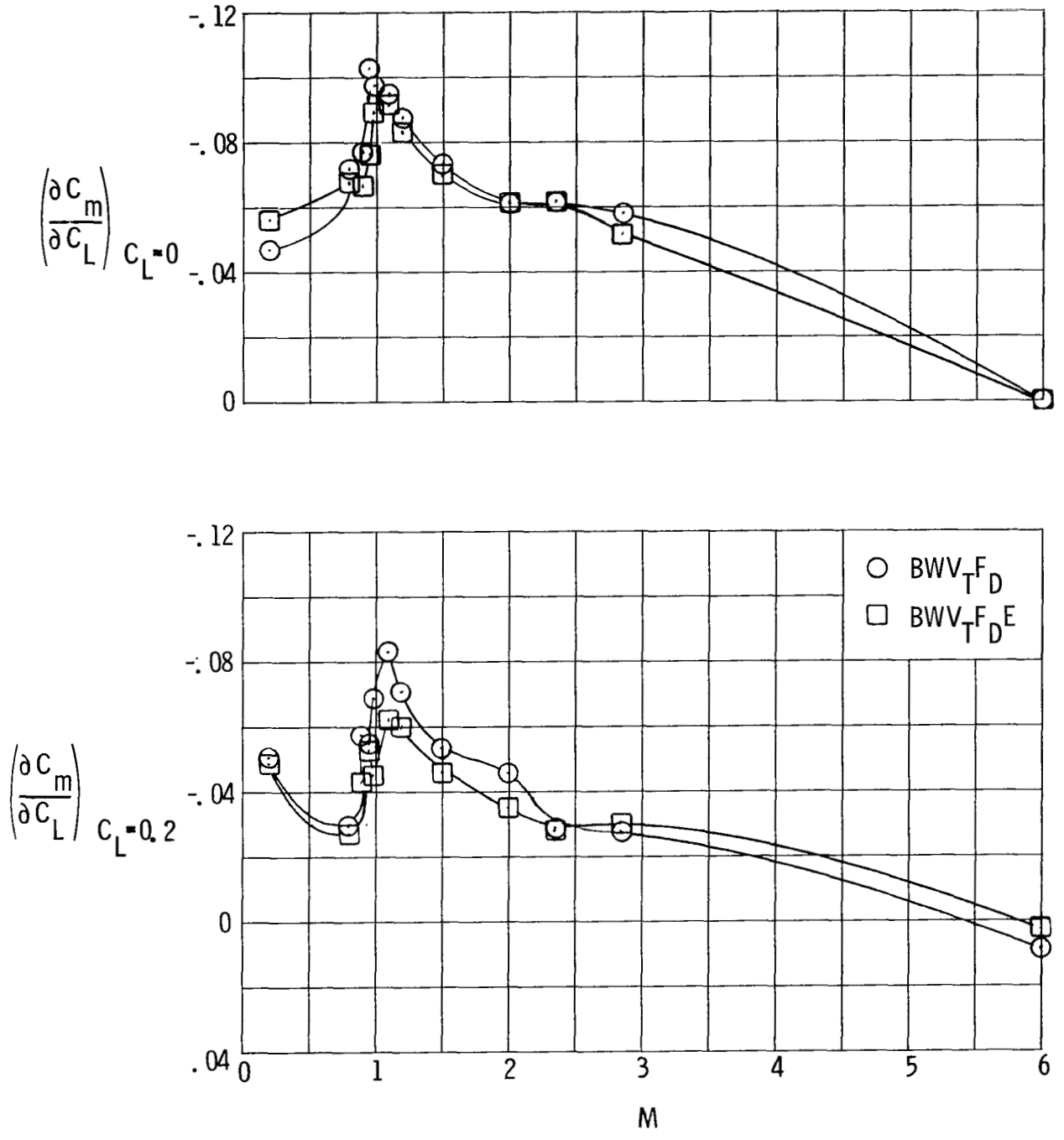

Figure 22.- Variation of longitudinal stability with Mach number at lift coefficients of 0 and 0.2 on complete configuration with and without engine.

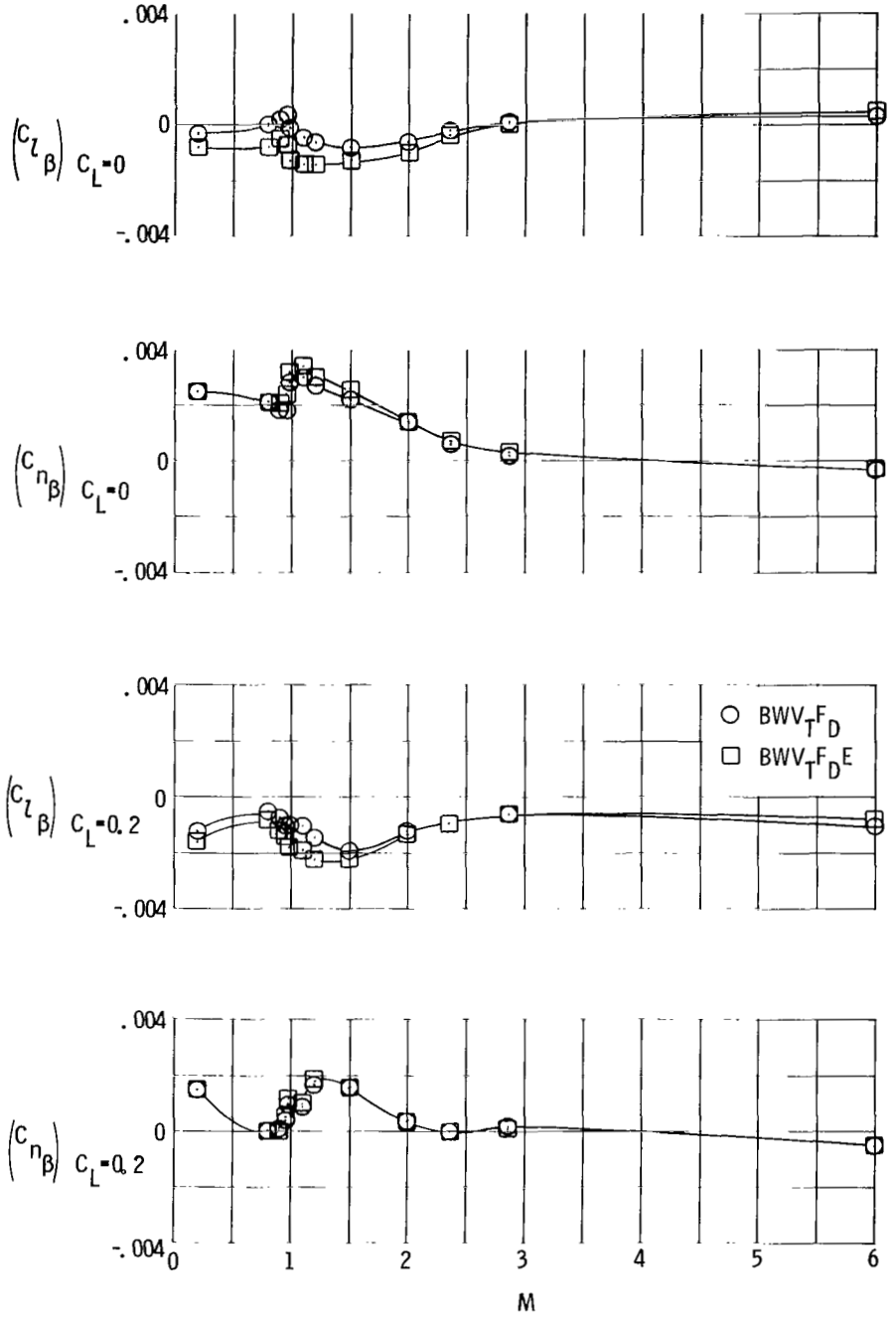

Figure 23.- Variation of lateral-directional stability with Mach number on complete configuration with and without engine.

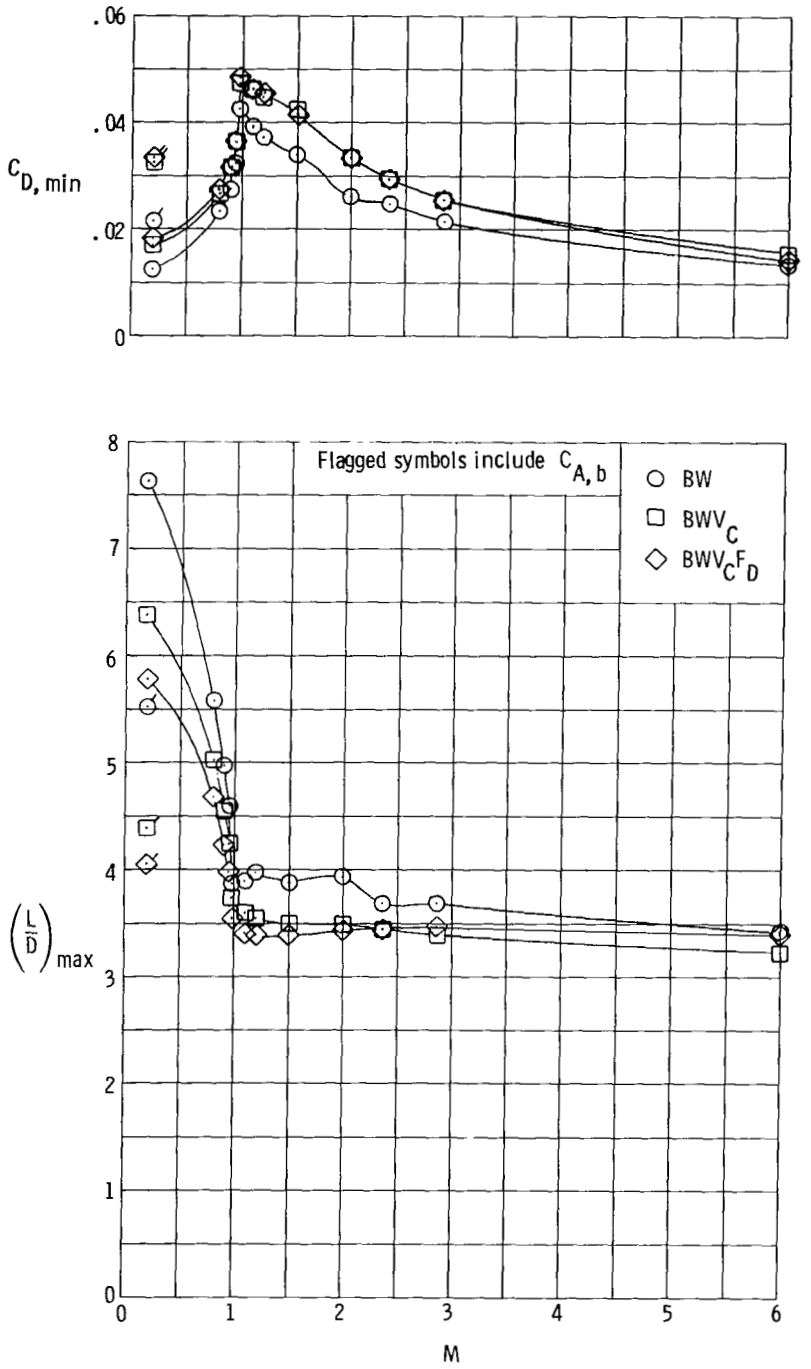

Figure 24.- Variation of minimum drag and maximum lift-drag ratio with Mach number on component buildup of center-tail models.

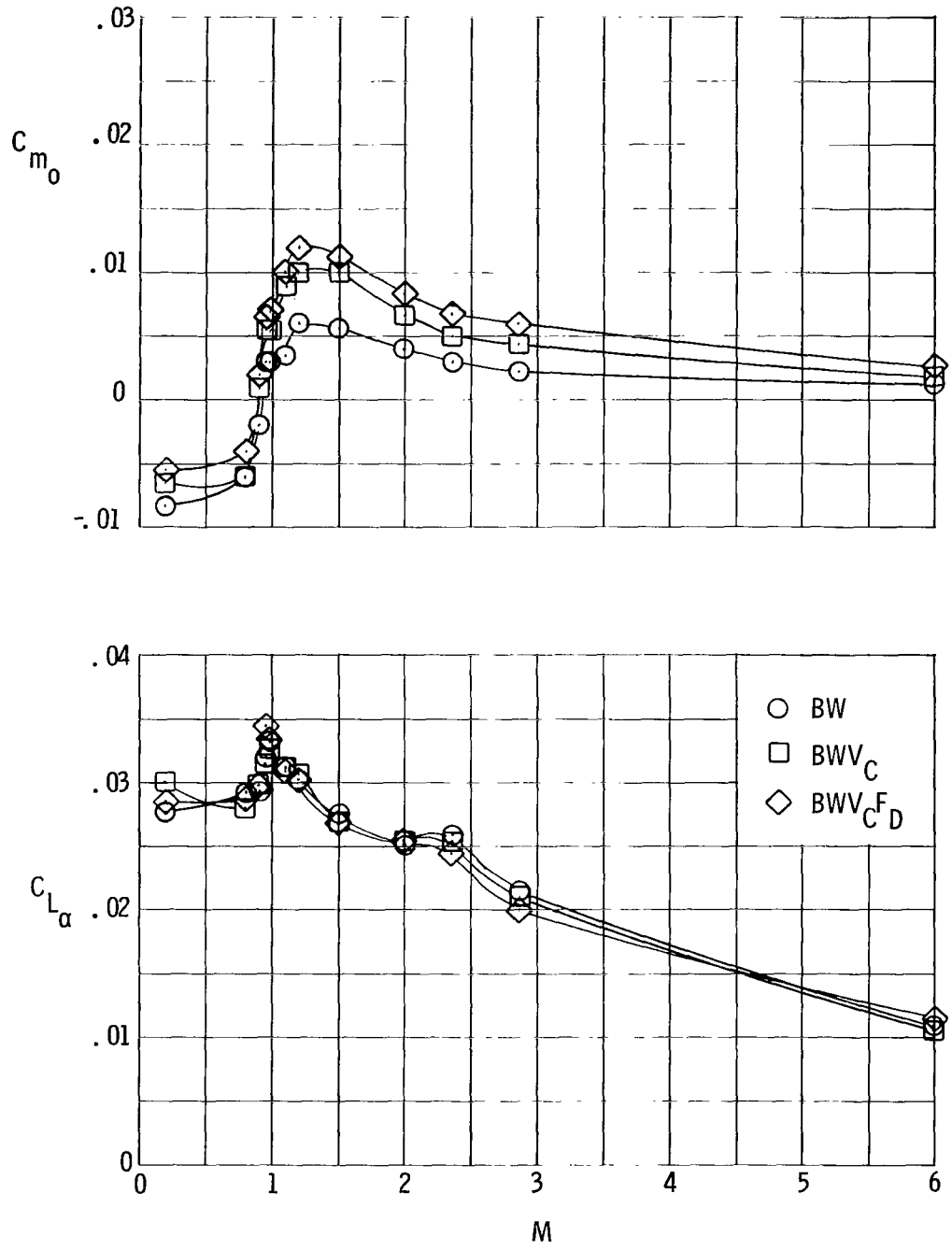

Figure 25.- Variation of values of pitching-moment coefficient with Mach number at zero lift and slope of lift curve at zero lift on component buildup of center-tail models.

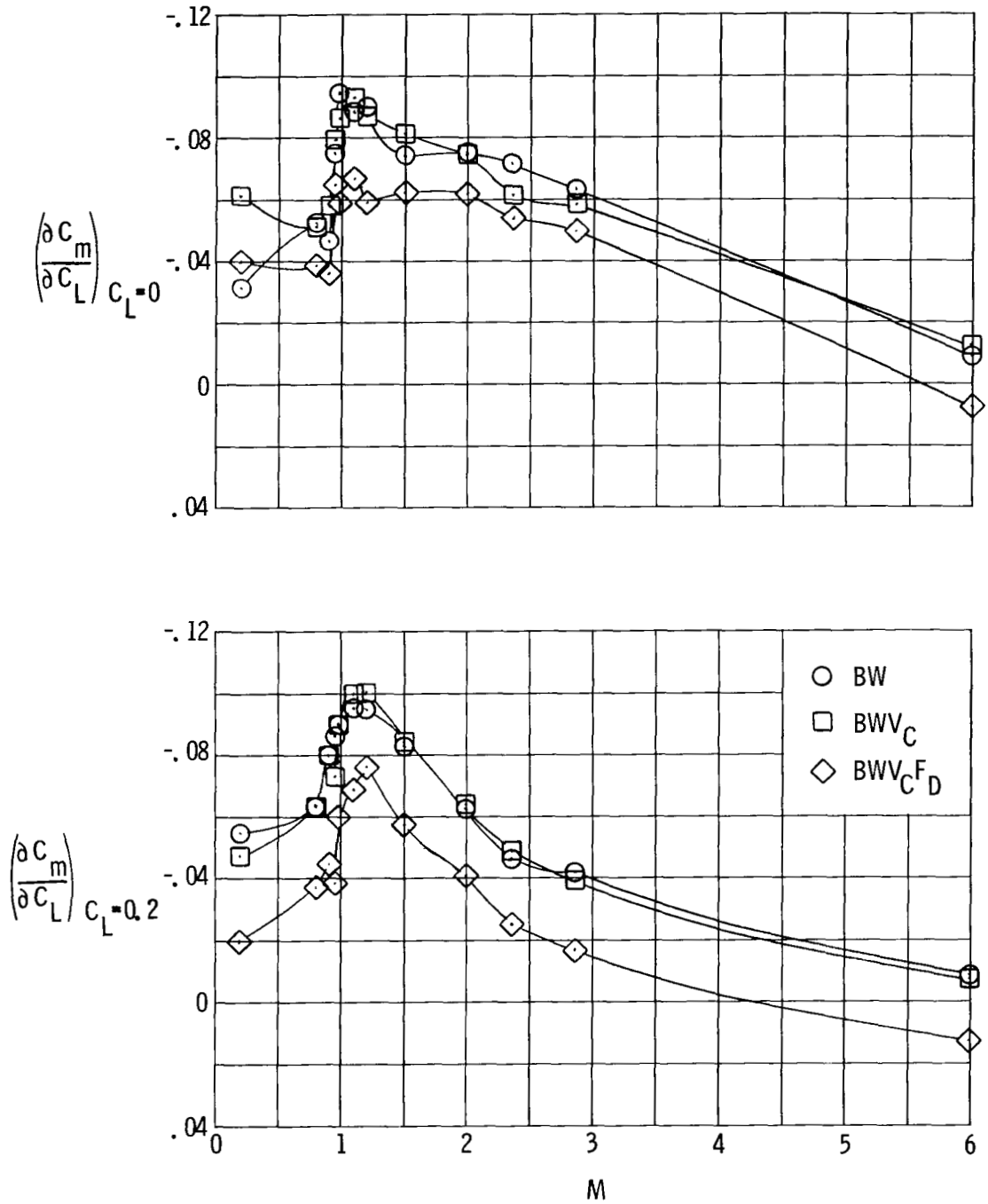

Figure 26.- Variation of longitudinal stability with Mach number at lift coefficients of 0 and 0.2 on component buildup of center-tail models.

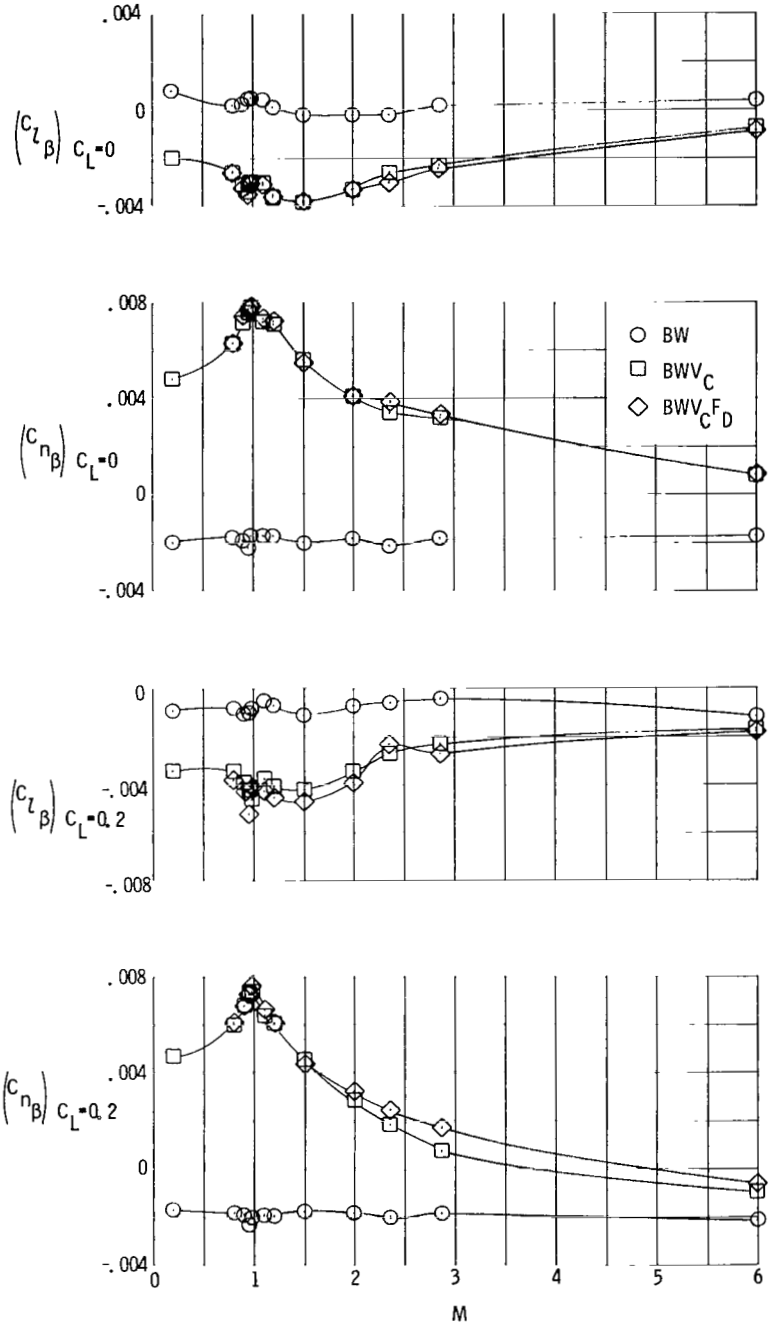

Figure 27.- Variation of lateral-directional stability with Mach number on component buildup of center-tail models.

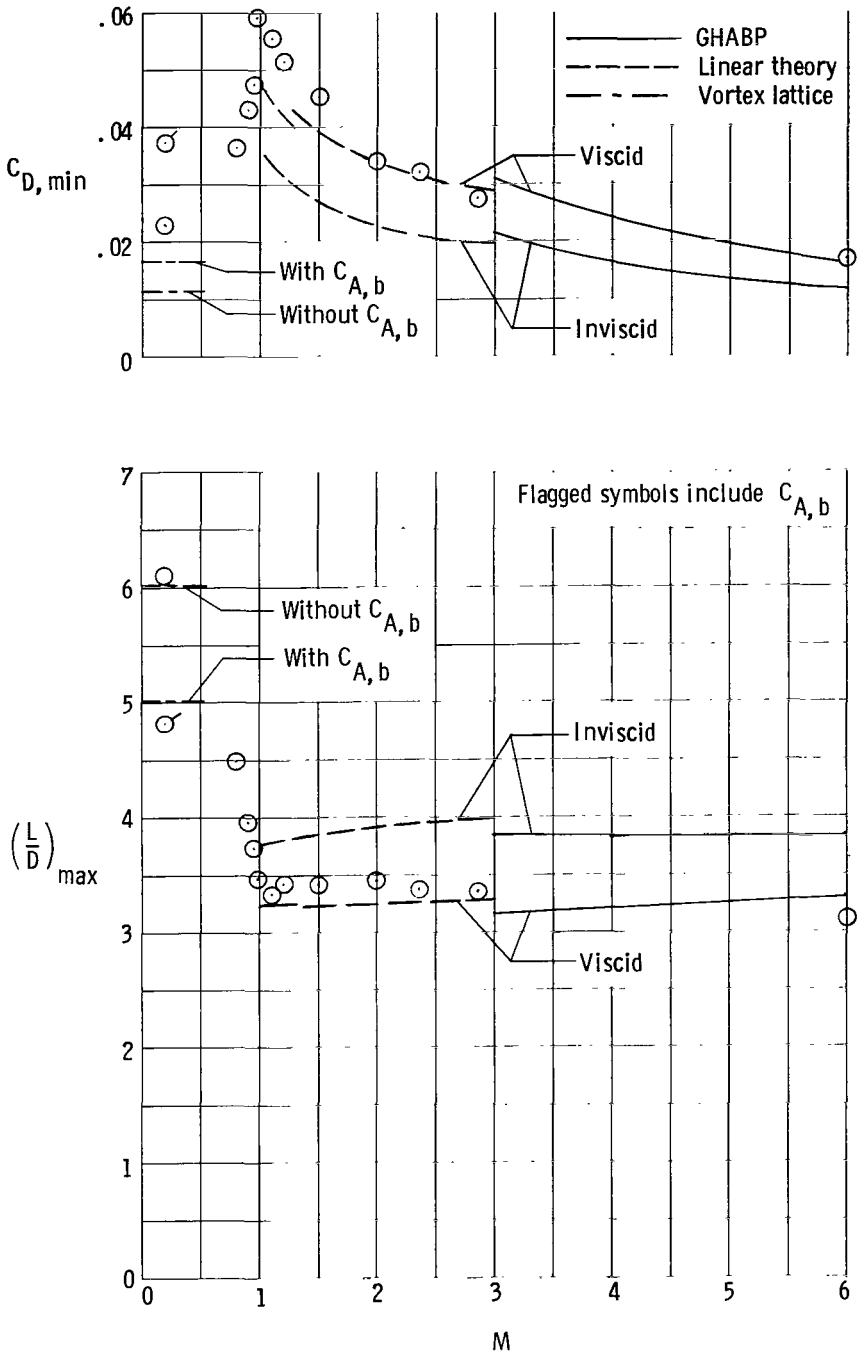

Figure 28.- Comparison of theoretical estimates of minimum drag coefficient and maximum lift-drag ratio with experimental data at M = 0.20 to 6.0 for WBV_T configuration.

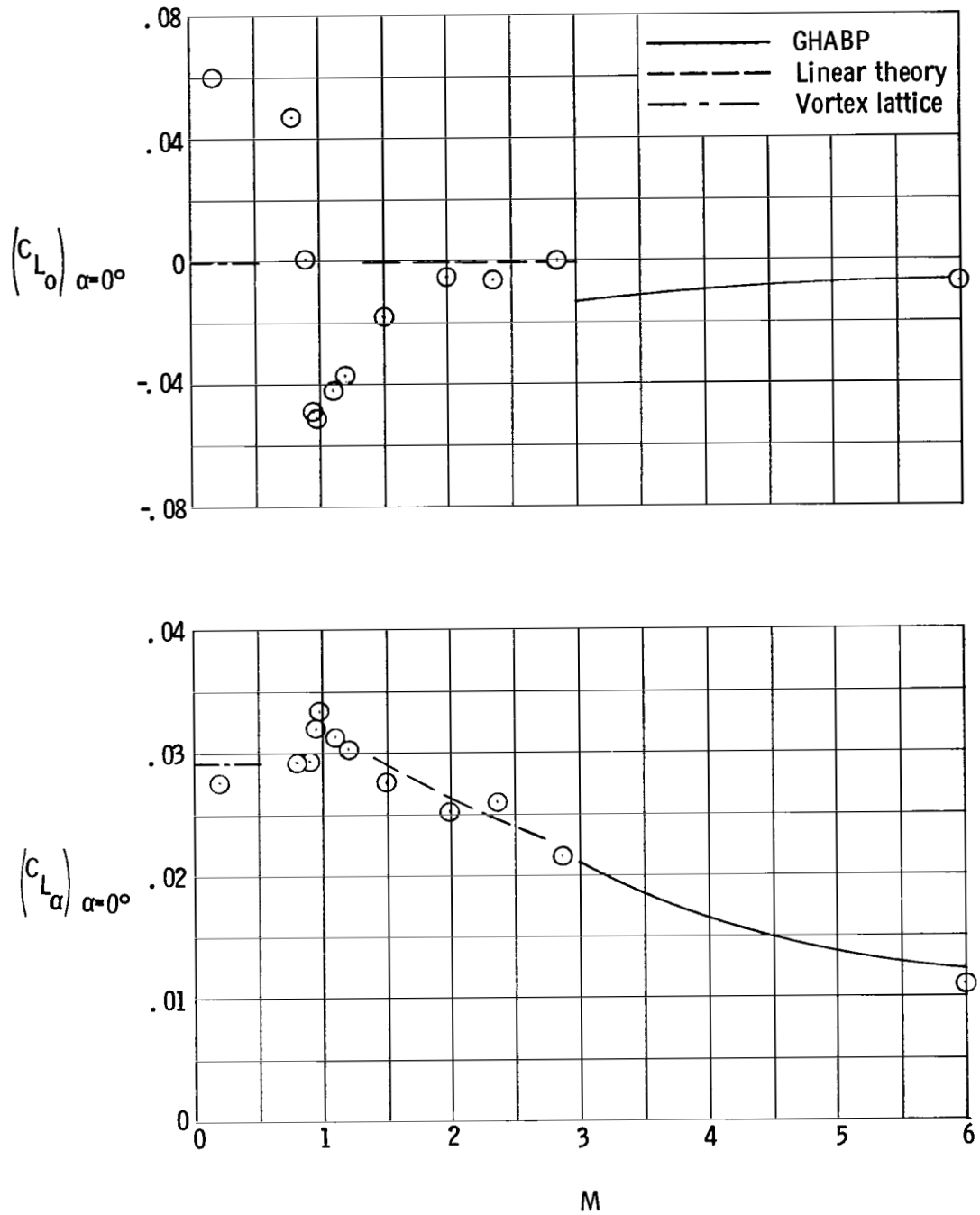

Figure 29.- Comparison of theoretical estimates of lift coefficient and lift-curve slope at $\alpha = 0^{o}$ with experimental data at M = 0.20 to 6.0 for WBV_T configuration.

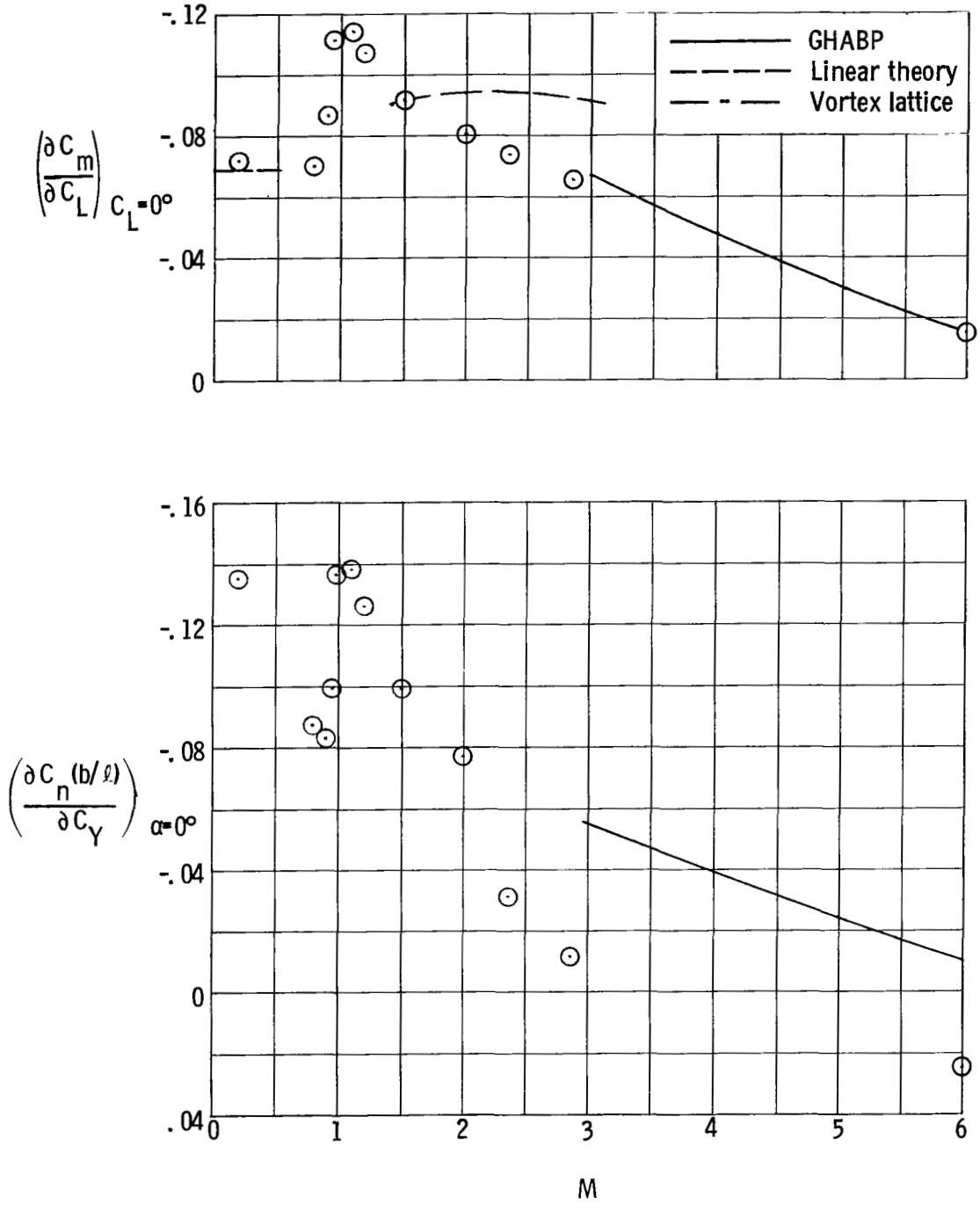

Figure 30.- Comparison of theoretical estimates of static longitudinal and directional stability at M = 0.20 to 6.0 for WBV_T configuration.

1. Report No.	2. Government Accession No.	3. Recipient's Catalog No.
NASA TP-1552		

4. Title and Subtitle	5. Report Date
AERODYNAMIC CHARACTERISTICS OF A HYPERSONIC RESEARCH AIRPLANE CONCEPT HAVING A 70° SWEPT DOUBLE-DELTA WING AT MACH NUMBERS FROM 0.80 TO 1.20, WITH SUMMARY OF DATA FROM 0.20 TO 6.0	December 1979
	6. Performing Organization Code

7. Author(s)	8. Performing Organization Report No.
Jim A. Penland, James B. Hallissy, and James L. Dillon	L-13158
	10. Work Unit No. 505-11-33-01

9. Performing Organization Name and Address	11. Contract or Grant No.
NASA Langley Research Center Hampton, VA 23665	
	13. Type of Report and Period Covered Technical Paper

12. Sponsoring Agency Name and Address	14. Sponsoring Agency Code
National Aeronautics and Space Administration Washington, DC 20546	

15. Supplementary Notes

16. Abstract

The data of the present report are divided into three areas. The first area includes the results of a wind-tunnel investigation of the static longitudinal, lateral, and directional stability characteristics of a hypersonic research airplane concept having a 70° swept double-delta wing. The force tests were conducted in the Langley 8-foot transonic pressure tunnel for Mach numbers from 0.80 to 1.20, for a Reynolds number (based on fuselage length) range of 6.30×10^6 to 7.03×10^6, at angles of attack from about -4° to 23°, and at angles of sideslip of 0° and 5°. The configuration variables included the wing planform, tip fins, the center vertical tail, and scramjet engine modules. The second area is a summary of the variations of the more important aerodynamic parameters with Mach number for Mach numbers from 0.20 to 6.0. The third area is a state-of-the-art example of theoretically predicting performance parameters and static longitudinal and directional stability over the Mach number range.

17. Key Words (Suggested by Author(s))	18. Distribution Statement
Hypersonic aircraft Transonic stability and control Lift Computational aerodynamics	Unclassified – Unlimited Subject Category 02

19. Security Classif. (of this report)	20. Security Classif. (of this page)	21. No. of Pages	22. Price*
Unclassified	Unclassified	144	$7.25

*For sale by the National Technical Information Service, Springfield, Virginia 22161

NASA-Langley, 1979

2 1 1U,A, 111079 S00903DS
DEPT OF THE AIR FORCE
AF WEAPONS LABORATORY
ATTN: TECHNICAL LIBRARY (SUL)
KIRTLAND AFB NM 87117

S